An Experimental Investigation of the Vibrational Comfort of Child Safety Seats

Joseph A. Giacomin

A thesis submitted for the Degree of Doctor of Philosophy

December 2002

Department of Mechanical Engineering

The University of Sheffield

Summary

The research of this thesis was performed to understand the vibrational dynamics of stage 0&1 child safety seats and of the children who occupy them. Since no previous vibration data for small children or child seats was found, the investigation took the form of experiments designed to shed light on the behaviour of the system consisting of child, child seat, vehicle safety belt and vehicle seat. To provide a background for interpreting the results a literature review was performed of child seat characteristics, of human whole-body response and of primate whole-body response. An industrial test procedure for measuring the vibration isolation properties of vehicular seats is also presented as an illustration of the concepts involved.

A whole-body vibration bench for testing children in the vertical direction was built and apparent mass and absorbed power functions were measured for 8 children of age less than 24 months and mass less than 13 kg. An algorithm was developed for identifying the parameter values of a single degree of freedom mass-spring-damper model of the seated body using Differential Evolution optimisation. The parameter values were determined for each child and compared to those of adults and primates. This thesis also presents the results of modal testing of 2 child seat units and of operational deflection shape testing of 1 unit in an automobile under 3 loading conditions (empty, sandbag or child). In-vehicle transmissibility measurements were also performed in the vertical direction for 10 children and child seats using 9 automobiles. The floor-to-human transmissibilities were determined for each child and driver when passing over a reference road surface at both 20 and 40 km/h.

Except for the damping ratio, all child mechanical response parameters were found to differ with respect to those of adults or primates, with the differences being greater with respect to adults. The first resonance frequency of children was found to be located at 8.5 Hz as opposed to 4.0 Hz for adults, raising questions regarding the applicability of standards such as ISO 2631 towards the evaluation of child vibrational comfort. The child seats were found to have higher transmissibilities on average than the vehicular seats occupied by adults. A characteristic low frequency rigid body rocking motion was noted at 1.8 Hz as were multiple flexible body resonances starting from frequencies as low as 15 Hz. Areas of possible improvement and topics for further research have been identified.

Contents

List of Illustrations

List of Tables

Chapter 1

Why Study Child Safety Seats ?

1.1 Some Crash Safety Facts

Since the 1950s numerous technical innovations have enhanced vehicle crash safety. According to Hendey and Votey (1994) seat belts were first introduced in the United States by Ford and Chrysler as early as 1955 and were in widespread use by 1964. Federal Law made lap and shoulder belts a requirement of all automobiles sold in the U.S.A. by 1968, and by 1974 the familiar three-point design became an industry standard. In the 1980s and 1990s the gradual introduction in most markets of new technologies such as deformable body structures, side impact bars, self-fastening belts, pyrotechnic belt pretensioners, driver and passenger airbags, side airbags and side curtains have greatly helped to reduce the number of highway deaths and injuries. The increasing effectiveness of vehicle passive safety systems can be noted from the accident statistics of Figure 1.1 compiled by the U.S. National Safety Council which show a steady decline in the accident death rate over the years, despite a dramatic rise in vehicle use.

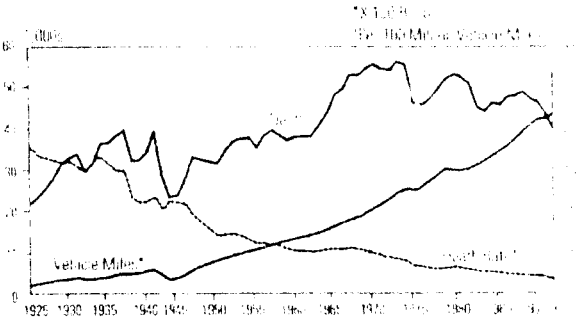

Figure 1.1 Vehicle use and accident fatality statistics compiled by the U.S. National Safety Council (reproduced from Hendey and Votey 1994)

It is today almost universally accepted that the single most important factor in reducing traffic injuries and fatalities is the use of seat belts. According to the U.S. National Highway Traffic Safety Administration (NHTSA) in 1998:

- the average U.S. national safety belt use rate was 70 percent.
- vehicle safety belts were credited with saving the lives of 11,088 passenger vehicle occupants over age 4.
- vehicle safety belts were estimated to reduce the risk of fatal injury by 45 percent and the risk of moderate to critical injuries by 50 percent.
- average in-patient costs for crash victims who did not use safety belts were 50 percent higher than for victims who were belted.

1.2 Crash Safety and Children

It was recognised at an early date that vehicular restraint systems would not, on their own, be able to adequately protect children due to the difference in size with respect to the adult target population. According to Melvin et. al. (1978) surveys of automobile crashes involving children performed during the early 1970s identified several disturbing facts. A first problem was the low usage rate of child restraint systems, often as little as 5% of the reported road accidents. Another problem was that in as many as 50% of the cases the child restraints were improperly installed, in terms of either positioning or belt tension. A final problem at that time was the high incidence of child head or facial injuries due to contact with hard or intrusive vehicle interior structures during the crash event. Though the Federal Motor Vehicle Safety Standard 201 required soft padding for several interior structures such as the

dashboard, surveys showed that children were impacting with other vehicle structures beyond those covered in the safety standard.

Growing concern regarding child safety led a number of researchers such as Von Wimmersperg and Czernakowski (1976) to study the biomechanics of small children during deceleration so as to design devices to protect them. Child Restraint Systems were in widespread use in the North American market by the early 1980s and child safety seat laws have been in effect in all 50 U.S. states since 1985 (Uphold et al. 1991). Also by 1985 the child restraint systems were beginning to appear which were suitable for the special needs of orthopaedic patients such as those described by Stout et al. (1992).

Today child restraint systems are required by law in numerous vehicle markets including the European market and their use is widespread. Having introduced the systems, current research aims to provide improved child restraint devices and to encourage parents to make more careful use of the available systems. The importance of child restraint systems is emphasised by the NHTSA statistics for the year 1998 which show that:

- 140 children died in vehicle crashes in the United States and more than 200,000 were injured.
- injuries sustained in car crashes were the leading cause of death in children over 1 year old.
- 51 percent of children younger than age five who died in passenger vehicle crashes were unbelted.
- adult safety belt use was found to be the best predictor of child occupant restraint use. A driver who was buckled up was 3 times more likely to restrain a child passenger than one who was not.

Fortunately, the NHTSA statistics for the year 2001 showed that today more than 90% of children in the United States are transported in approved child safety seats. There is still, however, great concern about child restraint system usage by the parents. According to recent statistics published by the National Safe Kids Campaign (2001) based on more than 17,500 checkup events performed in the U.S.A., more than 85 percent of parents misused their child seat with an average of two installation errors per seat. The most frequent errors were found to be the safety belt

not holding the seat tightly in place (63% of cases), the child harness straps not snug (33% of cases) and the harness straps not routed correctly (20% of cases). Studies performed in the United Kingdom have revealed similar findings. A survey of 36 cases by Rainford et. Al. (1993) found that the areas of greatest concern were slack in the harness (occurred in 68% of the seats surveyed), incorrect height of the shoulder straps (occurred in 64% of the seats surveyed) and too much movement of the child seat (occurred in 56% of the seats surveyed).

1.3 Types of Child Safety Seat

According to the U.S. NHTSA Dictionary of Child Safety Seat Terms (2001) a child safety seat is defined as *"a crash tested device that is specially designed to provide infant/child crash protection. A general term for all sorts of devices including those that are vests or car beds rather than seats"*. The NHTSA defines four basic categories of child restraint system. The first is the *infant-only restraint*, a device designed for use only by a baby (usually weighing less than 17-22 pounds) in a semi-reclined, rear-facing position. The second is the *rear-facing infant seat* which is a type of restraint system that is specifically meant for use by children from birth up to approximately 20 pounds (9 kg), used in the rear-facing mode only. The third is the *forward-facing child restraint* intended for use only in the forward-facing position for a child at least age one and from 20 pounds up to 40 pounds (9 to 18 kg) while the final category is the *convertible child safety seat/restraint* which can be used in more than one mode, usually rear-facing for infants and forward-facing for toddlers.

Since accident statistics show that the majority of motor vehicle crashes are frontal impacts, infants are considered safest when facing the rear (Arbogast et al. 2001). In a frontal crash the back of a rear-facing child safety seat supports the child's head, neck and back. The American Academy of Pediatrics recommends that children ride facing the rear of the vehicle until they reach both 1 year of age and 20 lb (Winston and Durbin 1999). This guideline is based on the observation that children in the specific age group are characterised by incomplete vertebral ossification and excessive ligamentous laxity which put them at risk of spinal cord injury. Despite the recommendations to use *infant-only restraints, rear-facing infant seats* and *convertible child safety seat/restraint* in the rear-facing mode, and despite this suggested usage being clearly outlined in the product literature provided with all

seats at the time of purchase, a recent study performed by the group Partners for Child Safety showed that 30% of children less than 1 year of age were facing forward at the time of their accident. Parents expressed concern that their infants were uncomfortable in the rear-facing position and that they could not see their children while driving. Arbogast et. Al. (2001) make the point that while child comfort is an important issue, safety should be the overriding concern. This issue will be revisited later in this thesis because the current research was driven by the author's belief that child seats can provide BOTH safety AND comfort without a loss of either performance characteristic.

Figure 1.2 presents two child safety seats sold under the Mothercare ® brand name which can be considered typical examples of rear-facing and forward-facing designs. The seats are fixed in place by means of the vehicle's safety belts. In the case of rear-facing seats the products found in commerce can be divided into two general categories: those which pass the belt over the legs of the child and those which pass the belt through the lower seat base. In both designs the vehicle safety belt is first passed behind the backrest section of the child seat so as to provide the necessary support to resist overturning moments during vehicle deceleration. The designs then differ in the return path of the belt. In the first case, installation requires the user to return the belt over the child's legs through slots in the sides of the frame in the region between the waist and knees before buckling to the vehicle. In the second case the belt is passed through slots in the lower half of the seat frame (as shown in the example of Figure 1.2a before buckling to the vehicle.

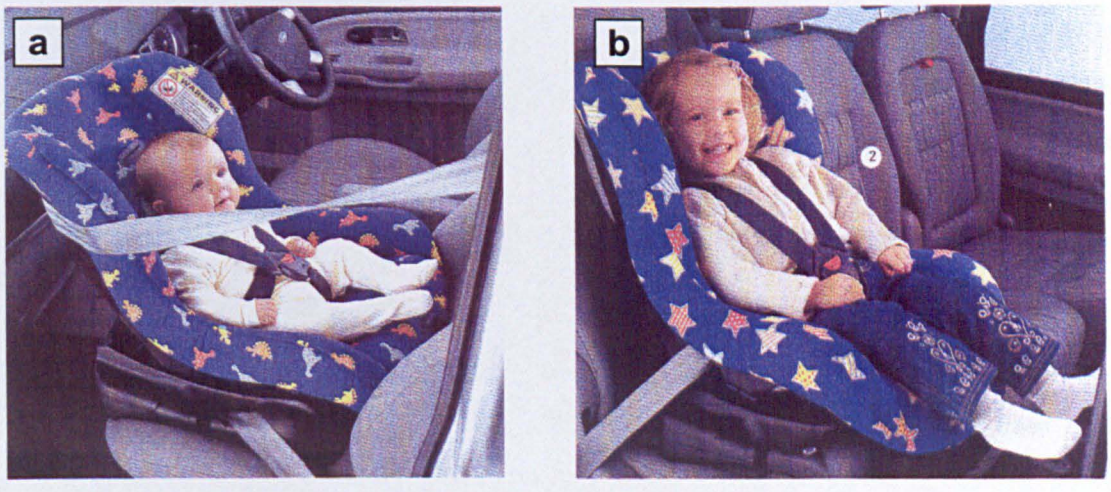

Figure 1.2 Child safety seat installation: rearward facing (a) and forward facing (b) (reproduced from Mothercare ® Catalogue 2002)

In response to the numerous research studies which have evidenced a high percentage of child injuries caused by faulty installation by untrained parents, a new and simplified system of child seat fixation has been introduced in 2001 model year automobiles in the U.S.A. and is required by law from model year 2002. The LATCH (Lower Anchors and Tethers for Children) system consists of specific anchor points at the vehicle floor below the seat and at one or more points behind the backrest. The LATCH system is a hybrid ISOFIX system (Bell et al. 1994) and thus represents a simplification of the ISOFIX concept initially researched in Sweden (Pedder et al. 1994). By providing easy to reach strong points specifically for child seat fixation, and by avoiding the use of the vehicle's safety belts, the latch system is expected to facilitate child seat installation and thus reduce the risk of injury due to faulty installation. An example of a LATCH system as described in the recent NHTSA specification is presented below as Figure 1.3.

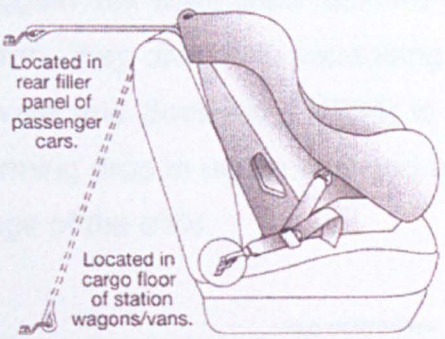

Figure 1.3 LATCH system of installation for child safety seats (reproduced from NHTSA website 2001)

A final safety product for use with children is the *belt-positioning booster seat*. Research by DeSantis-Klinich et al. (1994) found that the smallest child who can safely travel restrained by only a standard vehicular 3-point belt has a sitting height of 74 cm, a standing height of 148 cm and a weight of 37 kg. Smaller or heavier children cannot be safely decelerated by means of only the vehicle belts. Belt-positioning booster seats have thus been developed for transporting children who are too large for a child safety seat and too small or heavy for the vehicle belt system. Booster seats are of two basic types, the *high-back booster seat* and the *backless (or low-back) booster seat*. Booster seats raise the child upwards such that the lap and shoulder belts fit properly. Figure 1.4 presents an example of a belt-positioning booster seat sold under the Mothercare ® brand name.

Figure 1.4 Belt-positioning booster seat (reproduced from Mothercare ® 2002 catalogue)

Booster seats have recently become the target of efforts to increase child restraint use by the general public. Awareness campaigns have been launched because of research findings which suggest that while child restraint usage rates are high in the case of the smallest children, they drop with increasing size and age. Figure 1.5 published by Johnston, Rivara and Soderberg (1994) is typical of recent statistical surveys, and shows an alarming drop in usage rate and a corresponding increase in injury rate with increasing age of the child.

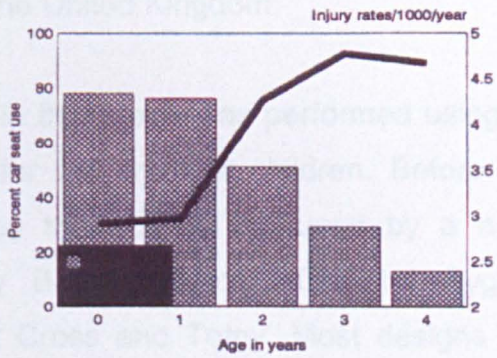

Figure 1.5 Percentages of children in a car seat at the time of a crash compared to car crash injury rates for all US children in 1990 (reproduced from Johnston, Rivara and Soderberg 1994)

As a final comment regarding all types of child seat, recent research by Glass, Segui-Gomez and Graham (2000) has found statistically significant evidence supporting the hypothesis that positioning the restraint system on the rear seat of the vehicle reduces the risk of child fatality in a crash.

1.4 Stage 0&1 Child Safety Seats

Due to the anthropometric changes (Pheasant 1988 and Tilley 1993) typical of early life a range of restraint products is provided for children from birth to the time when he or she is large enough to make direct use of vehicle seat belts. The standard system of nomenclature defining the age and weight limits of products used in the United Kingdom is presented below.

Stage	Installation	Child Weight	Child Age
0	Rearward facing	0 - 13 kg	0 - 15 months
0 & 1	rearward facing / forward facing	1 - 18 kg	0 - 4 years
1	forward facing	9 - 18 kg	9 months – 4 years
2	forward facing	15 - 25 kg	4 – 6 years
3	forward facing	22 – 36 kg	6 – 11 years

Table 1.1 System of stages used to define age and weight limits for child safety seats in the United Kingdom

The research described in this thesis was performed using stage 0&1 products, the restraint systems used for the smallest children. Before performing any tests 30 seats were inspected by the author, produced by a number of manufacturers including: Brittax, Baby Boss, Concord, Cosatto, Cygnet, Elecktrolux-Klippan, Klippan, Kwik Fit, Silver Cross and Tomy. Most designs were characterised by a plastic or Styrofoam basket covered in either cotton or polyester cloth. The seats normally had a lining under the covering cloth which consisted of polypropylene or some other suitable material, and normally included polyester wadding to soften the otherwise hard contact that would occur between the child and the plastic cage. Of the seats surveyed only 3 provided an additional foam pad which covered both the buttock and back areas. A further seat had a small area of foam padding covering the region in the immediate vicinity of the child's head. All seats indicated compliance with either standard ECE R44/02 or ECE R44/03.

1.5 The Issue of Vibrational Comfort

Inspection of stage 0&1 child restraint systems is sufficient to note the absence of design details that are required if the maximum possible level of child comfort were to be guaranteed. For example, the majority of the currently available restraint systems lack passages to facilitate the movement of air through the seat. This is in contrast to vehicular primary seating systems which in almost all cases use porous materials such as polyurethane foam and perforated frames to enhance the transport of heat and humidity away from the body. Several recent automobiles go as far as to offer seats which are equipped with cooling blowers which move fresh air to the regions of contact with the human body.

Upon first inspection the author also formed the opinion that numerous features which might improve the vibrational performance of child restraints were also lacking. For example, the majority of child restraints are fixed to the vehicle chassis by means of the vehicle's belts and few if any restraints offer pretensioner systems for removing the slack in the belt system. The result is a situation characterised by ample rigid body movements of the restraint system, even at low vibration amplitudes. A further observation was that only 5 of the 30 seats surveyed provided foam padding between the wadding and the seat frame. This is in contrast to the situation with vehicle primary systems where large amounts of money have been spent and numerous investigations performed to quantify the ability of polyurethane foams and other elastic materials to isolate drivers from vibrational disturbances. Research studies such as those of Cunningham et al. (1994), Ebe (1994) and Yu-Hallada et al. (1998) show the importance of optimising the elastic interface.

A thorough literature survey by the author produced no known publications on the subject of child body vibrational behaviour or of child seat vibrational behaviour. This situation is in great contrast to that for the drivers and passengers supported by vehicle primary seating systems. The themes of adult whole-body vibration response, seat dynamics, foam dynamics and of vehicle suspension dynamics have each been the subject of several hundred research papers over the last 100 years. Whereas the knowledge of the adult human body is sufficient to permit manufacturers to define standard tests of seated vibrational comfort using various specialised devices such

as vibrational mannequins, the complete lack of information makes defining a vibrational test methodology for child restraint systems an impossibility.

The research described in this thesis was motivated by the author's belief that BOTH crash safety AND vibrational comfort can be simultaneously achieved for child restraint systems. The objective of the research was to identify the basic mechanisms influencing the dynamics of the system composed of child, child seat, vehicle seat and vehicle belts and to gather and analyse enough experimental data to support the definition of a test methodology and of future numerical models. Some of the questions which required answering were the following:

- *What are the vibrational characteristics of the seated child body ? Are the resonance frequencies, resonant amplitudes and energy dissipation properties similar to those of adults ?*

- *If the child vibrational response were different from that of adults how would it affect the use of the currently accepted methodologies for quantifying subjectively perceived vibrational comfort ?*

- *What are the vibration characteristics of child restraints as an individual unit ? And how are these modified by installation in the vehicle ?*

- *What vibration levels and floor-to-child transmissibilities occur in current child restraint systems ? And how much can these characteristics vary from design to design ?*

- *How do the vibrational characteristics of current child seats compare to those of the vehicle primary seating systems used by adults ?*

It is the author's hope that after reading this thesis the reader will feel that some of the above listed issues have been clarified.

Chapter 2

Review of the Mechanical Response to Whole-body Vibration and its Modelling

2.1 Introduction

The purpose of this chapter is to provide an introduction to the mechanical response to whole-body vibration with emphasis on studies performed relative to the seated posture. Since the experimental measurements presented later in this thesis are the first examples of vibration tests performed for small children and for child seats it is important to judge them against the body of existing knowledge for adult humans and for primates. Towards this purpose more than 300 books and scientific papers treating whole-body vibration have been reviewed and are listed in the bibliography. This chapter is an extract in which a work is described if it satisfies at least one of the following three criteria: 1) it represented an innovation in testing or modelling when presented, 2) the data contained is particularly useful or 3) it introduced a new interpretation of a whole-body response. This chapter is subdivided according to the engineering approach taken. For example, transmissibility measurements are the

subject of one section while driving point measurements of mechanical impedance or apparent mass are the subject of another. Within each section the order of presentation of the studies was taken to be chronological as the author feels that much can be learned from the order in which the technical achievements progress. The figures and tables have been left in their original form both to speed compilation and to help the reader to appreciate the level of technology available at the time. It is hoped that the material can serve as an overview for anyone interested in the field of human vibration.

2.2 Whole-Body Vibration

The term whole-body vibration refers to macroscopic body movements of the type which arise when a person is subjected to vibration in one of the following typical ways: when standing on a vibrating surface, when lying supine on a vibrating surface or when sitting on a vibrating surface. Due to the need to compare measurements a system of reference axis needs to be carefully defined. The system used today in most whole-body vibration standards is shown below.

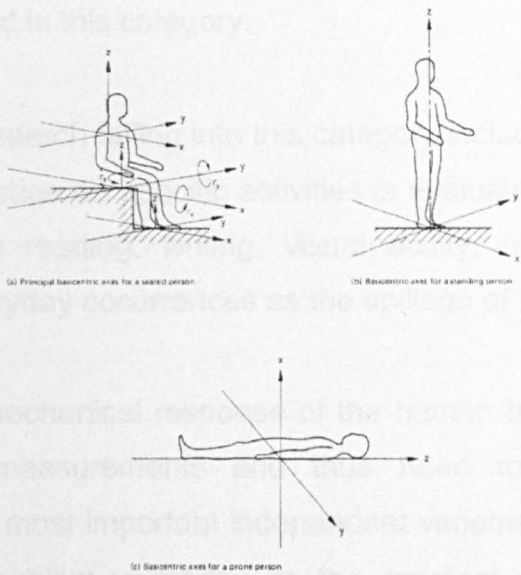

Figure 2.1 System of reference axis defined in BS 6841 for measuring whole-body vibration (reproduced from British Standards Institution 1987)

The frequencies normally considered when investigating whole-body vibration are those corresponding to long wavelengths, capable of inducing a simultaneous response of several body parts. Vibrations capable of inducing such responses are usually limited to frequencies below 100 Hz. While vibration studies have been

performed in this range of frequencies for a wide variety of reasons, the declared objectives can broadly be categorised as one of the following:

Mechanical response: these investigations have quantified the response to vibration in terms of force, movement or energy. Many of these studies have been purely experimental, some have led to the development of models, and a few have specifically addressed only the theoretical issues behind model development.

Subjective response: these studies have measured the subjective response to vibration, meaning the mapping from mechanical to perceived stimuli. These studies have been mostly experimental, though some theoretical work exists treating only the basis for the psychophysical relationships involved.

Health effects: a variety of investigations have attempted to determine the forces and motions occurring internally to the body, the fatigue and rupture laws governing body structures and the incidence of such loadings in the workplace. Also, epidemiological investigations of the trends in the health statistics for populations exposed to vibration can be included in this category.

Activity interference: research falling into this category includes a variety of studies in which the effect of vibration on specific activities is evaluated. Examples include the effects of vibration on reading, writing, visual acuity, hand tool usage, control actuation and such everyday occurrences as the spillage of drinks.

When measuring the mechanical response of the human body several independent variables affect the measurements and thus need to be controlled by the investigator. The single most important independent variable is the test subject. Most studies point to inter-subject variability as the greatest single contributor to the variance observed in experimental data sets. The physical characteristics of the subjects, the ability to perform tests using also a control group and use of a sample size sufficient to permit statistical significance testing are all factors which influence the reliability and generalisability of the results. For seated subjects a second impendent parameter that is normally controlled is the state of foot support. The feet can either be supported by a non-moving platform, supported on a platform which moves with the seat surface, or supported by a platform which moves independently

of the seat surface. The method of support has been shown by several authors (for example Griffin 1990) to affect driving point measurements of the human body. A third independent parameter which requires consideration is the sitting posture, where sitting posture is taken to mean the angular relations between the various body parts and the state of muscle tension (relaxed or erect). A fourth independent parameter is the vibration excitation defined by its type, frequency content and level. Ample evidence exists to show that the body responds nonlinearly to vibration thus leading to the necessity to clearly state the vibrational input used.

Numerous scientific measurement methods are employed in the field of whole-body vibration research. Medical, physiological, psychological and ethical constraints make the measurement of whole-body mechanical parameters and response properties challenging. Since intrusive measurements of muscle loading, joint loading, inter-abdominal pressure, intervertebral disk pressures or bone movement are difficult to perform outside the clinical setting, only a relatively small number of studies have used these methods. A greater number of studies have measured electromyographic (EMG) activity via surface electrodes as evidence of muscle participation and loading during vibrational response, and a similar number have measured response to vibration by means of electrocardiagrams (EKG) or oxygen uptake (VO_2). The vast majority of studies found in the literature have been based, however, on external engineering measurements of motion or force. Engineering measurements of the body and the models developed from them are the subject of this chapter. The chapter is subdivided according to the methods involved, the sections being: transmissibility, driving point impedance or apparent mass, absorbed power, mechanical modelling, model uniqueness and whole-body research performed using primates.

2.3 Transmissibility Measurements

The most frequently performed whole-body measurement has been the transmissibility from a support surface to some output point of interest on the body. Since accelerometers are the mostly commonly used sensors the transmissibility is normally expressed in terms of the measured acceleration as

$$H(j\omega) = \frac{a_{out}(j\omega)}{a_{in}(j\omega)} \quad (2.1)$$

where *a* is the measured acceleration at the reference points, ω is the frequency and $j = \sqrt{-1}$. The acceleration at the input is usually measured by an accelerometer placed on the moving support while the acceleration at the output is measured by one attached to the body by means of an appropriate device. For measurements at spinal vertebra the output accelerometer can be either attached to a pin and carrier which is medically inserted into the spinous process of the vertebra or it can be glued to the skin by means of a bioadhesive or tape. In the case of skin attachment, the transfer function of the tissue and skin is compensated for in the signal processing (see Kitazaki and Griffin 1995 for examples). For measurements at the pelvis, legs, abdomen, shoulder, neck or head appropriate mechanical carriers are used which are strapped tightly to the body by means of elastic bands or belts.

Of the possible output locations, the head has been by far the most popular since it is the location of the brain, the vestibular organs and the vision apparatus. Head motion is usually measured by a sensor attached either to a firmly strapped-on helmet (bicycle helmet being common) or by a set of accelerometers attached to a bite-bar. A bite-bar (see Griffin 1990 for details) consists of a dental mould which is held firmly between the teeth from which extends one or more rods carrying accelerometers. Sensor layouts of either 6 or 10 accelerometers have been used on bite-bars to measure the full six degrees of freedom of head motion.

Probably the earliest known reports of whole-body transmissibility measurements were a group of papers published in Germany in the autumn of 1939 and spring of 1940. It appears that the first to reach publication was a study by E.A. Von Müller whose title, translated into English, was "The effects of vertical sinusoidal vibration on sitting and standing persons". In the study the transmission of vibration to the hips and head of 3 individuals was measured in both the sitting and the standing postures using a vibrating platform and specially built displacement sensors. Numerous features of the human response as we now understand it were already discussed in this early work. Figure 2.2 presents a curve of vibration amplitude measured at the head for 2 sitting subjects for frequencies from 1 to 10 Hz showed that one (C-SI)

had a resonant response at both 4 and 8 Hz. These two frequencies are the principal externally measurable whole-body resonances of the adult human body in the sitting posture and have been studied in great detail in the years since Mueller's investigation. Figure 2.3 presents Mueller's floor-to-head displacement data for one standing subject at two different input amplitudes in three postures: straight knees (ST1), bent knees (ST2) and standing on toes with bent knees (ST3). He correctly hypothesised the changes brought about by different postures and correctly identified that bending the knees reduced the transmission of vibration to the upper body. The shape of the response curves was seen to change with excitation amplitude, a feature which was correctly interpreted to be caused by nonlinear behaviour of the body. Notable also in Muller's study was the range of measurements reported, from subjective response to pulmonary ventilation to heart rate to energy consumption and skin surface temperature. Pulmonary ventilation, for example, was found to increase greatly at frequencies from 5 to 6 Hz due to diaphragm movement induced by the resonant response of the upper body.

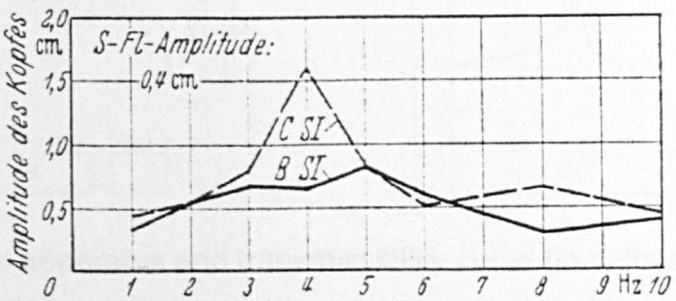

Figure 2.2 Head displacement measured for two seated subjects using sinusoidal vibration of fixed amplitude (reproduced from Mueller 1939)

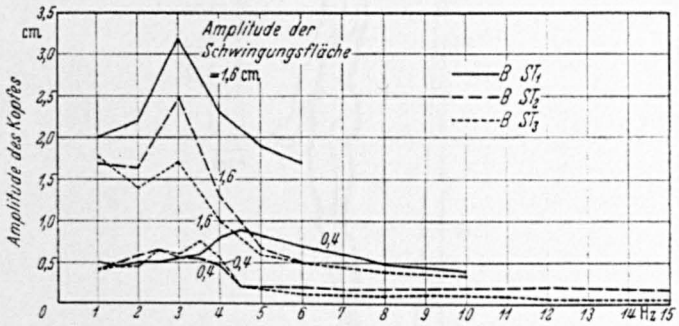

Figure 2.3 Head displacement measured for 1 standing subject in 3 postures using 1.6 cm (upper curves) and 0.4 cm (lower curves) sinusoidal excitation (reproduced from Mueller 1939)

Another study from the autumn of 1939 was by Georg Von Bekèsy who described the functional principles of the skin mechanoreceptors and presented perhaps the world's first tactile perception threshold curve. Also presented was a transmissibility curve measured for a preloaded spinal segment containing 6 cervical vertebra (Figure 2.4). The measured axial transmissibility showed a peak at 250 Hz which was taken to be the first resonance frequency of the spine. Another innovation was the use of piezoelectric microphone elements mounted on a rubber backing for measuring the vibrations of the body surface. With these devices Von Bekèsy performed transmissibility tests for a single standing subject for two cases: exposure by means of a moving floor and exposure by means of a moving handle. His graphical representation (Figure 2.5) of the results showed the today familiar concepts of vibration attenuation with distance from the energy source and across body articulations.

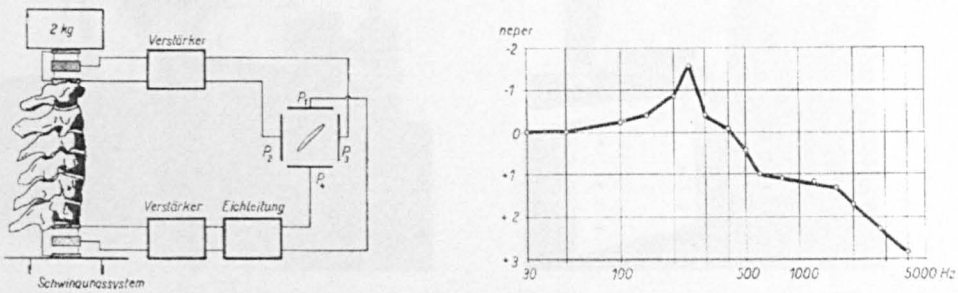

Figure 2.4 Test apparatus and transmissibility curve (in units of Bels) measured for a segment of the cervical spine (reproduced from Von Bekèsy 1939)

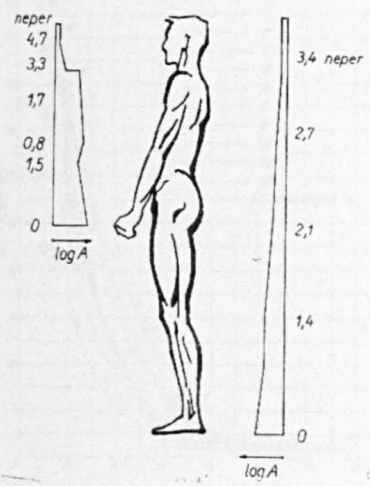

Figure 2.5 Attenuation of vibration (in units of Bels) across the body with increasing distance from the source (reproduced from Von Bekèsy 1939)

A 1940 paper by Coermann presented an electrodynamic exciter system (Figure 2.6) and coil sensors designed for human whole-body vibration testing. Measurements of vibration induced fatigue and vibration induced reduction in visual acuity were presented. As shown in Figure 2.7 seat-to-head transmissibility was presented for 10 sitting and 1 standing subject over the frequency range from 15 to 140 Hz. Coermann noted that the vibration attenuation increased with increasing frequency and that the response was linear over the range of vibration amplitudes tested. Another characteristic of Coermann's study which renders it typical of later research was the impossibility of performing tests at low frequencies (below 15 Hz in Coermann's case) using the electrodynamic shaker system. To this day many tabulations of whole-body response begin from some minimum frequency such as 1, 2 or 5 Hz due to the physical limitations of the exciter system or measurement instrumentation used.

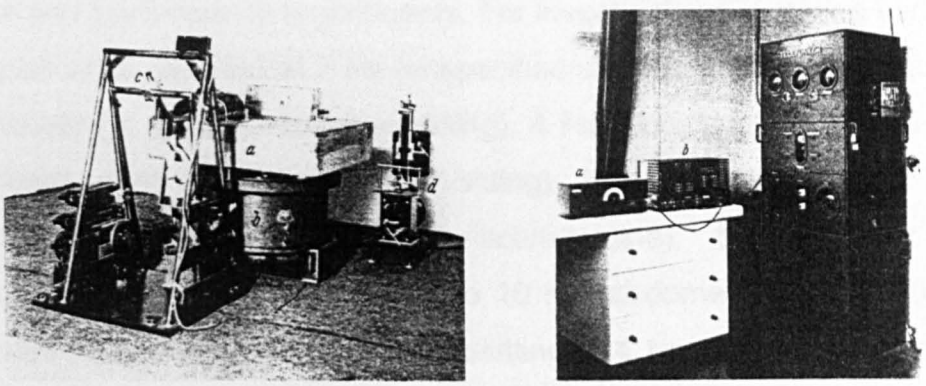

Figure 2.6 Electrodynamic exciter, test platform, signal generator, preamplifier and power amplifier used by Coermann (reproduced from Coermann 1940)

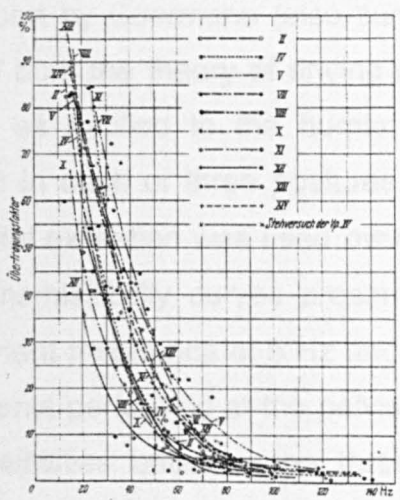

Figure 2.7 Vertical seat-to-head transmissibility for 10 seated and 1 standing (stehversuch) subjects (reproduced from Coermann 1940)

In 1957 as part of a research effort investigating the physiological problems of aircraft ejection Lantham measured vertical vibration for individuals seated without a backrest. Three accelerometers were used, one attached to the vibrating platform, one to a tightly strapped-on waist belt and the third was stitched to a tight fitting leather flying helmet. Sinusoidal vibration was applied at frequencies from 2 to 20 Hz and amplitudes from 0.375 inch to 0.15 inch. Transmissibility curves were produced by taking the ratio of peak output acceleration to peak input acceleration from seat to hip, from seat to head and from hip to head. All three curves had resonance peaks at 5, 10 and 20 Hz corresponding to damping factors of 0.25, 0.4 and 0.5 respectively.

In 1959 Guignard published a comprehensive review of 129 references from the then existing literature. In tables he summarised the known body resonances, subjective reactions and performance impairments. For investigations involving vertical vibration resonances were reported at 2 Hz (unspecified/standing), 3 Hz (body/supine), 3 to 5 Hz (trunk/sitting), 4 Hz (unspecified/sitting), 4 Hz (body/supine), 4 to 5 Hz (pectoral girdle/sitting), 4 to 7 Hz (unspecified/sitting), 5 Hz (trunk/sitting), 5 Hz (pectoral girdle/sitting), 5.6 Hz (abdominal viscera/supine), 5 to 8 Hz (abdominal viscera/supine), 6 Hz (trunk/sitting), 6 to 10 Hz (abdomen/unspecified), 8 to 10 Hz (abdominal viscera/sitting), 12 Hz (trunk/sitting), 14 Hz (vertebral column/sitting), 16 to 30 Hz (soft parts of face/unspecified), 17 to 20 Hz (head/sitting) and 25 Hz (head/sitting).

An influential 1961 ASD report by Coermann (also summarised in 1962 in Human Factors) developed in detail both the theory of driving point mechanical impedance and that of transmissibility as applied to the human body. Eight subjects were exposed to vertical vibration in each of three postures: sitting erect, sitting relaxed and standing erect. Sinusoidal excitation was used over the frequency range from 1 to 20 Hz. Seat-to-head transmissibility curves presented for one of the subjects (Figure 2.8) showed a dominant resonance at 5 Hz and a secondary resonance at 9 Hz. Acceleration measurements performed at the pelvis and neck also permitted the calculation of the transmissibilities between the three body locations. From the analysis of the results Coermann concluded that the 5 Hz resonance was due to both pelvic and spinal motion while the secondary resonance at 9 Hz was due to motion

of only the pelvis. He also observed that further harmonics of the two resonances were too highly damped to be noticed in the externally measured transmissibilities.

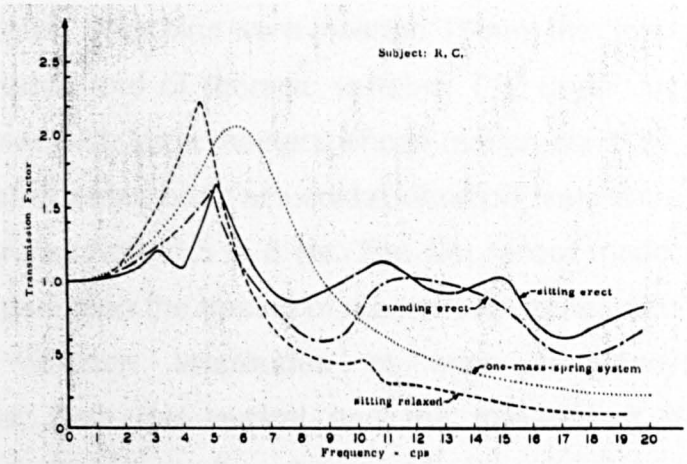

Figure 2.8 Seat-to-head transmissibility curves for one subject in three sitting postures (reproduced from Coermann 1961)

A 1963 paper by Hodgson, Lissner and Patrick investigating the effects of aircraft ejection described the results from measurements performed on three seated cadavers using accelerations of up to 18g and rates of change of the acceleration (jerk) of up to 2,600 g per second. Accelerometers were fixed rigidly to the vertical acceleration platform, to the iliac crest of the pelvis, to the sternum and to the skull. As illustrated in Figure 2.9 the oscillatory behaviour of the acceleration time histories suggested resonant behaviour with a frequency of 27.5 Hz and an average damping ratio of 0.17. These early results showed that body stiffness is much greater, and body damping much lower, under high acceleration conditions.

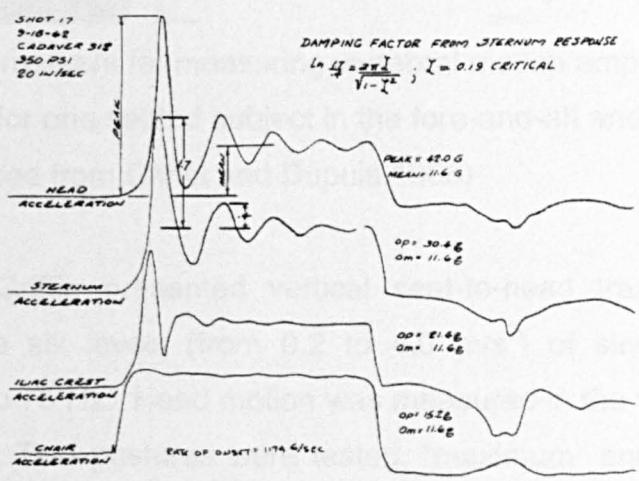

Figure 2.9 Acceleration time history from one vertical acceleration table test (reproduced from Hodgson et. al. 1963)

A 1966 study by Christ and Dupuis presented an innovative technique for measuring whole-body response. Wire pins were inserted 15 mm into the spinous processes of each lumbar vertebra and of thoracic vertebra T12 under local anaesthesia. The ends were equipped with large markers whose motion could be recorded using a 35 mm camera. Seated whole-body sinusoidal vibration tests were performed with one subject at frequencies from 0.5 to 8 Hz. The film record made against a calibration background grid permitted the tracing of marker trajectories and the determination of the maximum vibration amplitudes at each frequency. Seat-to-vertebrae transmissibility for both the vertical and the fore-and-aft directions showed a resonance at 4 Hz. Fore-and-aft motion was found to be a factor of two lower than vertical motion for all vertebrae. As part of the investigation random vibration tests were performed using several suspension seats. It was shown that a well designed suspension seat could lower the vertical displacement amplitude of the cervical and lumbar vertebra by 49% and 53% respectively.

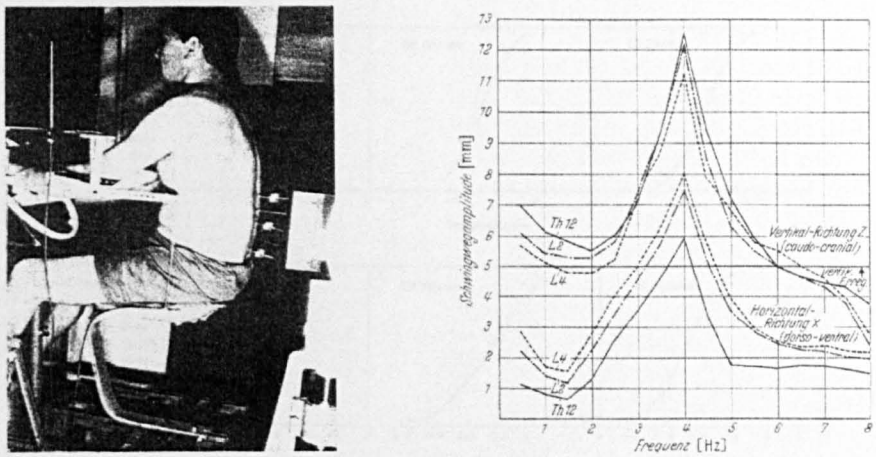

Figure 2.10 Pins and markers for measuring vertebral motion amplitudes for L4, L2 and T12 for one seated subject in the fore-and-aft and vertical directions (reproduced from Christ and Dupuis 1966)

A 1975 study by Griffin presented vertical seat-to-head transmissibility for 12 subjects exposed to six levels (from 0.2 to 4.0 m/s^2) of sinusoidal vibration at frequencies from 7 to 75 Hz. Head motion was measured in the vertical, fore-and-aft and pitch directions. Two postures were tested, “maximum” and “minimum”, which the subjects chose themselves so as to either maximise or minimise the sensation of vibration at the head. The study was one of the first to specifically address the issue

of inter and intra subject variability. Significant differences were found between the two sitting postures and across individual subjects. Differences in sitting posture were hypothesised by Griffin to be the greatest cause of variability between the transmissibilities reported in previous studies.

A 1978 study by Griffin and Whitham analysed the individual variability of both mechanical and subjective seated response for 112 subjects subdivided into three groups: 56 men, 28 women and 28 children. For the mechanical evaluations seat-to-head transmissibility was measured using two sinusoidal signals: 4 and 16 Hz at 1.0 m/s^2 r.m.s. amplitude. As shown in Figure 2.11 the transmissibility values for the group were found to be normally distributed. Statistically significant correlations with the anthropometric parameters of the subjects were found (particularly a negative correlation with height and weight) but the size of these effects was small. In fact, a conclusion drawn by the authors was that "it is clear from the correlation coefficients that it is not possible to make a usefully accurate prediction of the response of an individual from a knowledge of his age, sex or size".

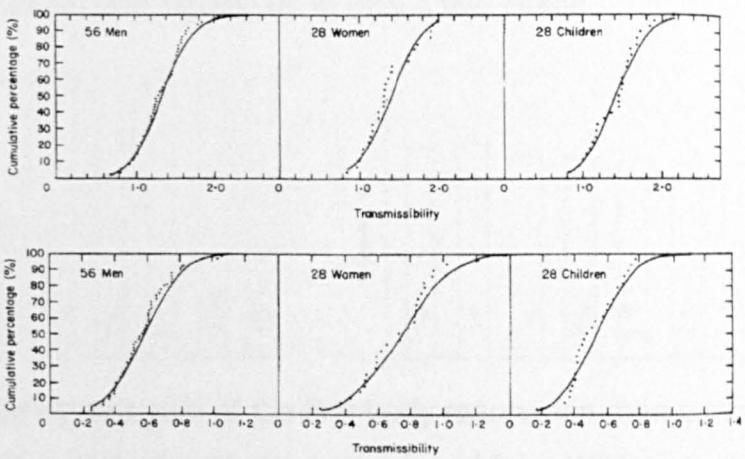

Figure 2.11 Cumulative seat-to-head transmissibility at 4 Hz (top) and 16 Hz (bottom) for three groups of subjects (reproduced from Griffin and Whitham 1978)

A 1978 study by Mertens described the nonlinear properties of the upright seated human body when exposed to vibration in the presence of increased gravity. The tests were performed in a rotating centrifuge first described by Vogt (1968). Nine subjects were exposed to sinusoidal vibration in the frequency range from 2 to 20 Hz with fixed r.m.s. acceleration amplitude of 0.4g. The gravity loading was varied from +1g to +4g in steps of 1g. Both driving point impedance and seat-to-head transmissibility were measured. The main peak of the impedance curves of all

subjects was found to vary with gravity loading, taking the values: 5 Hz at +1g, 11 Hz at +2g, 12 Hz at +3g and 13 Hz at +4g. The dominant seat-to-head resonance frequency was found to change with gravity loading: 5 Hz at +1g, 10 Hz at +2g, 11 Hz at +3g and 13 Hz at +4g. No significant differences were found between the results of the male and female test subjects.

A 1982 study by Wilder, Woodworth, Frymoyer and Pope investigated the effect of sitting posture on seat-to-head transmissibility and on the EMG activity measured at the right erector spinae and external oblique muscles at L3 level. An accelerometer was attached to the vibrating support while another was attached to a tightly strapped-on hockey helmet. Single and swept sine tests were performed over the range from 0 to 20 Hz for 45 subjects in the vertical direction. Several sitting postures were tested with the legs unsupported. As shown in Figures 2.12 and 2.13 posture was found to effect both the frequency value and the transmissibility gain of the two principal human body resonances, with more pronounced effects on the first than on the second resonance. Differences in the average results for males and females were found to be small, and significant in only a few cases.

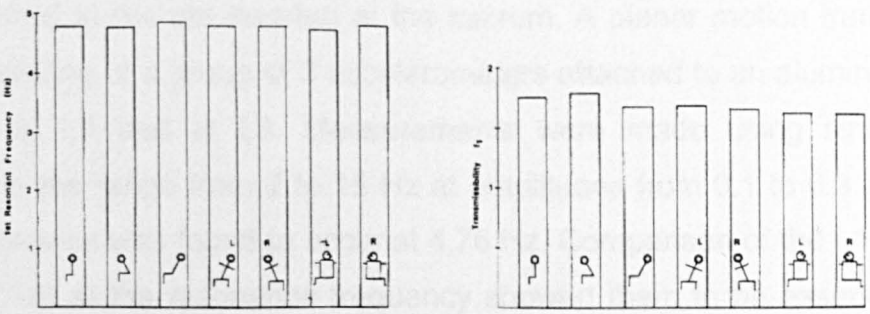

Figure 2.12 Frequency and gain of the first body resonance measured for 45 subjects in various seated postures (reproduced from Wilder et. al. 1982)

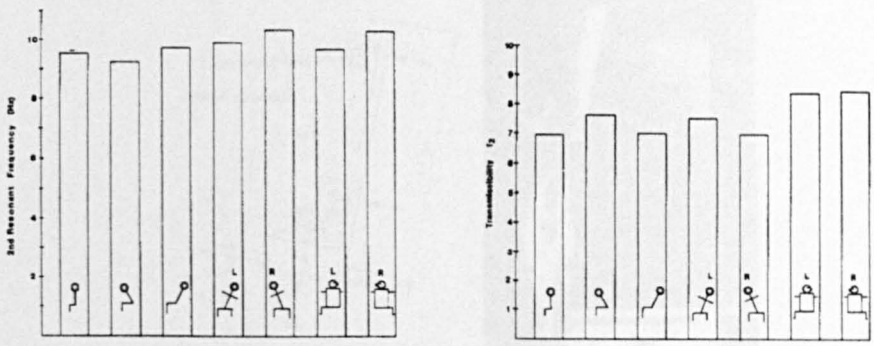

Figure 2.13 Frequency and gain of the second body resonance measured for 45 subjects in various seated postures (reproduced from Wilder et. al. 1982)

In 1985 a study by Hagena et. al. presented the results of in-vivo vertical transmissibility measurements performed for 11 subjects in the sitting and standing positions. Kirschner-wires (K wires) were inserted into the sacrum and into the spinous processes of the L1, L4, L5, T6 and C7 vertebrae, permitting direct measurement of spinal response. Vertically orientated accelerometers were attached to each K-wire and to the support surface. Transmissibility curves were determined from the support to each vertebra and from the sacrum to each vertebra. Transmissibility peaks were found at 4, 13 and 19 Hz. Based on the observed vertebral movements the principal resonance at 4 Hz was suggested to be due to motion of the entire body while the secondary resonance at 13 Hz was suggested to correspond mostly to motion of the spinal column. The 19 Hz transmissibility peak was ascribed to a local response of the head. The transmissibilities for the seated and the standing postures were found to present only small differences.

A 1986 paper by Panjabi et. al. presented in-vivo experiments of 5 seated subjects. A threaded 2.4 mm diameter Kirschner wire (K-wire) was used to fix accelerometers to the sacrum and to the spinous processes of L1 and L3. A single accelerometer was attached to the pin inserted at the sacrum. A planar motion transducer (Figure 2.14) consisting of a group of 3 accelerometers attached to an aluminium fixture was mounted at L1 and at L3. Measurements were made using sinusoidal vertical vibration in the range from 2 to 15 Hz at amplitudes from 0.1 to 0.3 g. The principal body resonance was found to occur at 4.76 Hz. Comparison of the L1 and L3 signals (Figure 2.15) at the resonance frequency showed them to be essentially the same, suggesting high stiffness in the lumbar region.

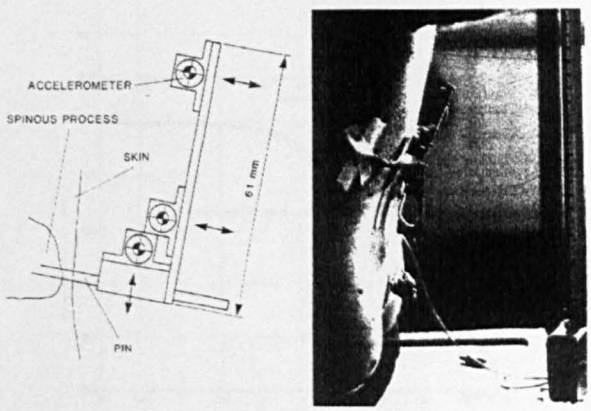

Figure 2.14 Three-accelerometer planer motion transducer (left) and in-vivo installation at L1 and L3 (right) (reproduced from Panjabi et. al. 1986)

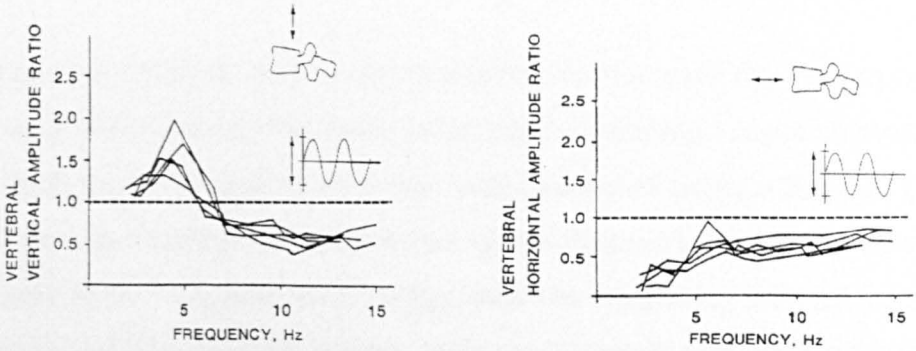

Figure 2.15 Vertical and fore-and-aft transmissibility measured at L1 and L3 (reproduced from Panjabi et. al. 1986)

1987 saw the publication of *International Standards Organisation 7962 (1987): Vibration and shock – Mechanical transmissibility of the human body*. The standard summarised (Figure 2.16) the then existing literature treating seat-to-head and floor-to-head transmissibility over the range from 0.5 to 31.5 Hz. The tabulated values represented an average taken over several studies which had used different sensors, postures and measurement points at the head. A mass-spring-damper model was provided to simplify response computation. Despite the possible shortcomings of such an averaging method the standard remained in publication in its original form until amalgamated into the 2001 revision of *International Standards Organisation 5982 Mechanical vibration and shock – range of idealised values to characterise seated-body biodynamic response under vertical vibration*.

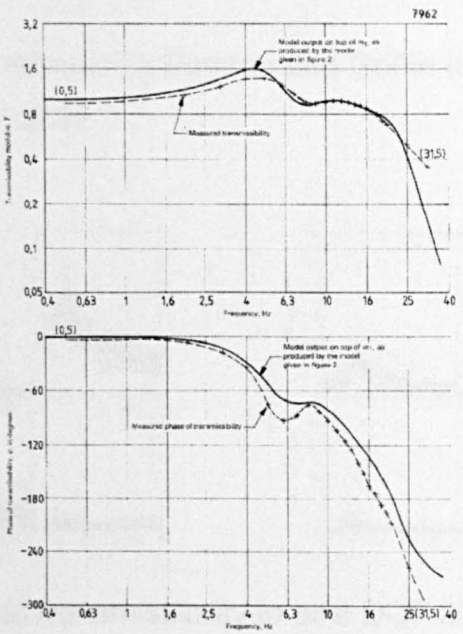

Figure 2.16 Modulus and phase curves for vertical seat-to-head and floor-to-head transmissibility from ISO 7962 (reproduced from ISO 7962:1987 (E))

A 1988 paper by Paddan and Griffin presented transmissibility curves measured for all 6 degrees of freedom at the head using vertical vibration input by means of a rigid seat and backrest unit. Head movement was measured using a bite-bar (Figure 2.17) carrying 6 accelerometers. The vibration signal was a Gaussian random signal with r.m.s. amplitude of 1.75 m/s^2 and energy over the frequency interval from 0.2 to 31.5 Hz. Two sitting postures were tested: back-on-backrest and back-off-backrest. Intra-subject variability was evaluated by means of tests with one subject using 7 bite-bar masses and 5 bite-bar grips. Changes in seat-to-head transmissibility as a function of both increasing sensor mass and grip strength were found to be small. Inter-subject variability was evaluated using 12 subjects (Figure 2.18) and was found to be the largest source of variance. The principal body resonance was found to be at 7 Hz for most subjects, with some showing evidence of a second peak in the region from 10 to 14 Hz. Head motion was found to occur mostly in the fore-and-aft, vertical and pitch axis (the mid-sagittal plane). The back-on-backrest posture was found to increase the magnitude of head vibration in most cases.

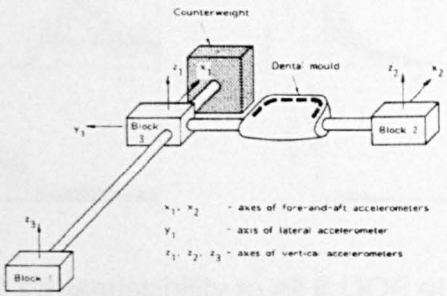

Figure 2.17 Bite-bar developed by Paddan and Griffin (reproduced from Paddan and Griffin 1988)

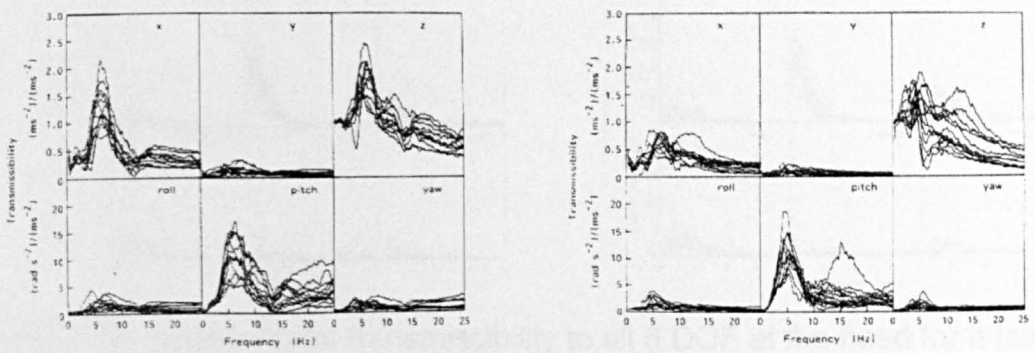

Figure 2.18 Seat-to-head transmissibility to all 6 DOF at the head from a vertical vibration input in the back-on- backrest (left) and back-off- backrest (right) postures (reproduced from Paddan and Griffin 1988)

A second 1988 paper by Paddan and Griffin presented seat-to-head transmissibilities for 12 subjects using fore-and-aft and lateral vibration at the seat. The same rigid seat and test method was used, but the Gaussian random signal was defined over the range from 0.2 to 16 Hz. For tests using fore-and-aft input vibration (Figure 2.19), resonances were found with the back-on-backrest posture at 1.5 and 8 Hz in the fore-and-aft direction, at 6.5 Hz in the vertical direction and at 7.5 Hz along the pitch axis. For tests in the same direction performed in the back-off-backrest posture only a 2 Hz peak was found in the fore-and-aft response of the head and only a 4 Hz resonance was found in the vertical and pitch directions. With lateral vibration input (Figure 2.20) resonances were found at 2 Hz for both postures. The differences between the transmissibilities for the two postures were small and in most cases not statistically significant. The authors concluded that use of a backrest had a large effect on the fore-and-aft response but only a small effect on the lateral response.

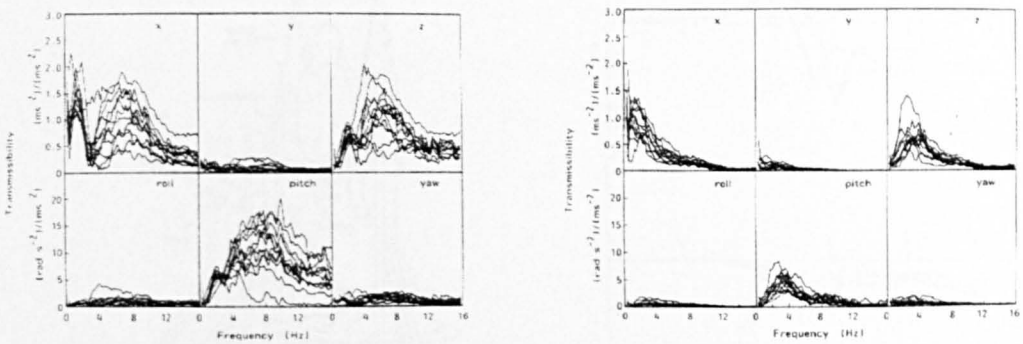

Figure 2.19 Seat-to-head transmissibility to all 6 DOF at the head for a fore-and-aft vibration input in the back-on-backrest (left) and back-off- backrest (right) postures (reproduced from Paddan and Griffin 1988)

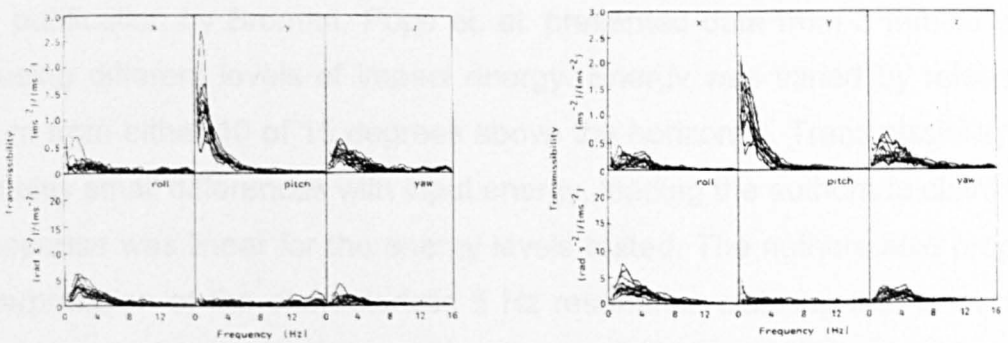

Figure 2.20 Seat-to-head transmissibility to all 6 DOF at the head for a lateral vibration input in the back-on-backrest (left) and back-off- backrest (right) postures (reproduced from Paddan and Griffin 1988)

A 1989 study by Pope, Broman et. al. avoided the need for a complex shaker system by using instead a calibrated impact pendulum which struck a suspended platform. The pendulum delivered 3.9 joules of energy to the platform on which the subject was seated and produced a flat vibration spectrum from 2 to 30 Hz. An accelerometer was placed on the seat, a second on a threaded 10 mm K-wire inserted into the spinous process of the L3 vertebra and a third was placed on a bite-bar held in the mouth. Transmissibilities were measured for three female subjects. A principal resonance was found at 5 Hz and a second in the region from 8 to 16 Hz. Soft foam materials placed under the subjects were found to lower the frequency and increase the gain of the first resonance. The same materials were found to reduce the gain of the second resonance, a behaviour which the authors suggested might be due to the deformed foam pads resisting the pelvic rotation associated with the second resonance.

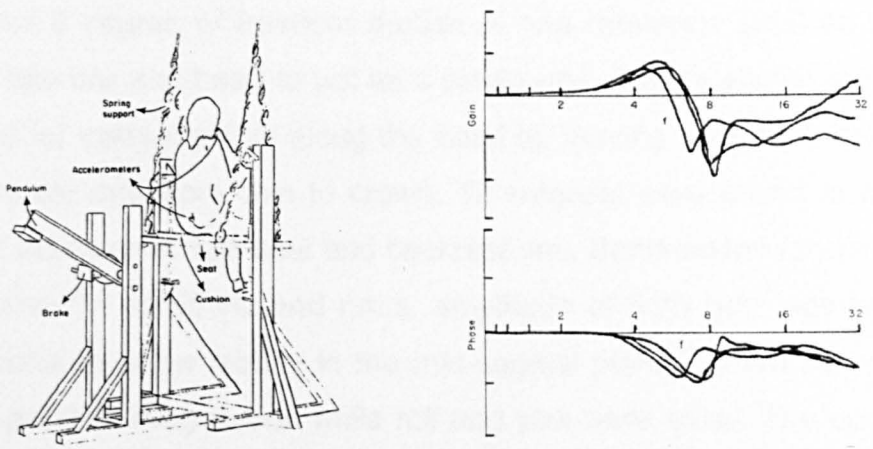

Figure 2.21 Impact apparatus and transmissibilities measured for 3 female subjects sitting in a relaxed posture (reproduced from Pope et. al. 1989)

A 1991 publication by Broman, Pope et. al. presented data from 3 female subjects tested using different levels of impact energy. Energy was varied by releasing the pendulum from either 10 of 15 degrees above the horizontal. Transmissibility results showed only small differences with input energy, leading the authors to claim that the body response was linear for the energy levels tested. The authors also proposed a new interpretation of the characteristic 5 Hz resonance claiming that is was due to compression of the buttocks tissue combined with rotational spinal motion.

A 1991 study by Pope et. al. measured the relative motion between lumbar vertebrae in the mid-sagittal plane by means of a transducer consisting of pins inserted into the

spinous processes of adjacent vertebrae and linkages carrying accelerometers. The geometry of the linkage transducer permitted direct measurement of the relative axial translation, anterior-posterior shear and rotation. Three seated female subjects were tested. Motion across lumbar vertebrae L4 and L5 was measured for two subjects while motion across L3 and L4 was studied for the third. Input vibration at frequencies of 5 and 8 Hz at amplitudes from 0.5 to 1.5 m/s^2 was used. Relative motions were found to be greater at 5 Hz than at 8 Hz, and axial displacement was larger than shear. Axial displacements ranged from 0.05 to 1.07 mm, shear displacements ranged from 0.01 to 0.35 mm and sagittal rotations ranged from 0.0 to 0.4 degrees.

A 1992 study by Paddan and Griffin investigated the effect of the measurement position at the head on seat-to-head transmissibility. 6 accelerometers were used to measure the full 6 degree of freedom motion of one reference point on a bite-bar. Assuming the bite-bar and head to act as a single unit, 3 translational motions were then calculated for various points along the head by moving from back to front, from left ear to right ear and from chin to crown. 12 subjects were tested in the vertical direction while sitting on a rigid seat and backrest unit. Band-limited random vibration with content from 0.1 to 50 Hz and r.m.s. amplitude of 1.75 m/s^2 was used. Head motion was found to occur mostly in the mid-sagittal plane. Of the three rotations, pitch had the greatest magnitudes while roll and yaw were small. The consequence of this movement pattern was to render the vertical transmissibility highly sensitive to the location of the measurement point along the fore-and-aft axis of the head and to render the fore-and-aft transmissibility highly sensitive to the location of the measurement point along the vertical axis from chin to crown. The head was found to exhibit resonances at 3 and 6 Hz for all subjects in the fore-and-aft direction and at 5 Hz for all subjects in the vertical direction.

A 1998 study by El-Khatib et. al. measured the vertical accelerations at the seat, at the five lumbar vertebra and at the sternum for seven cadaveric subjects exposed to 1.5 m/s^2 r.m.s. random vibration in the frequency band from 0.8 to 25 Hz. The use of such subjects permitted rigid mounting of the accelerometers to the anterior face of the vertebral bodies. The main body resonance was found to occur at an average value of 6.3 Hz while the second was found from 10 to 15 Hz. Posture had an important effect on seat-to-head transmissibility with 10-14% differences in resonant

amplitude occurring between some postures. Inter-subject variability was found to be the largest effect with large changes occurring in the transmissibility functions from one subject to the next. The main result was the finding that the transmission of vertical vibration was nearly constant throughout the lumbar spine, accelerations from L1 to L5 being approximately equal under all conditions tested. Also, the use of a lumbar support was found to not greatly affect transmissibility to the lumbar spine.

Two papers published in 2000 by Nishiyama et. al. presented measurements from the seat to points on the human body for 11 subjects. Swept sine and random signals were used in the frequency range from 2 to 20 Hz. The subjects were seated in an automobile-like device consisting of seat, steering wheel and pedals which was vibrated in the vertical direction (Figure 2.22). The effect of arm position, and thus of steering wheel location, on transmissibility was measured (Figure 2.23). Four arm positions were tested: 90, 120, 150 and 180 degrees. The authors concluded that arm angle had a statistically significant effect on the motion of the upper arm, lower arm, thigh and shin. Head, chest and hip motion were largely unaffected.

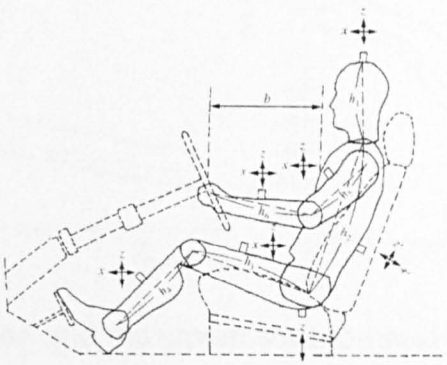

Figure 2.22 Test arrangement and accelerometer locations used by Nishiyama et. al. (reproduced from Nishiyama et. al. 2000)

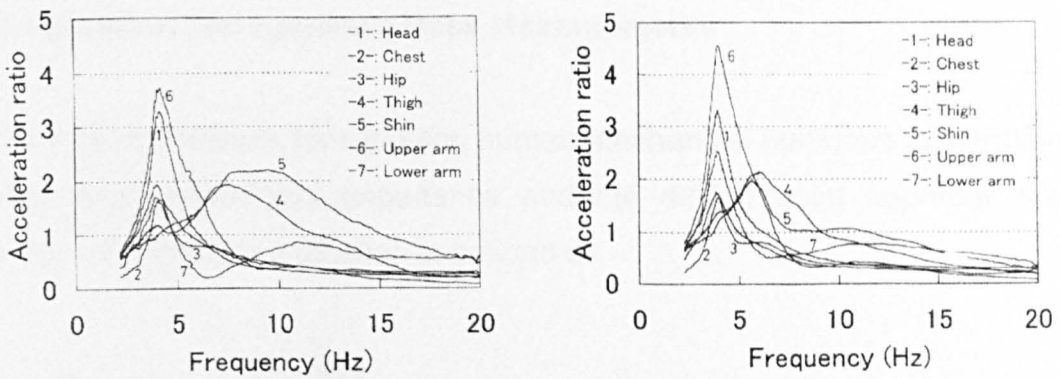

Figure 2.23 Transmissibility to 7 body locations for arm positions of 90 degrees (left) and 180 degrees (right) (reproduced from Nishiyama et. al. 2000)

2001 saw the publication of a thoroughly revised edition of International Standards Organisation standard 5982, now titled *"Mechanical vibration and shock - range of idealised values to characterise seated-body biodynamic response under vertical vibration"*. While the 1981 edition of the standard provided only driving point mechanical impedance data, the 2001 edition replaced ISO 7962 by presenting seat-to-head transmissibility data as well (Figure 2.24). Minimum, mean and maximum transmissibility curves are provided which are stated to be representative of (a) a posture described as erect seated without backrest support, with feet supported and vibrated, (b) subject mass in the range from 49 to 93 kg and (c) unweighted sinusoidal or random input acceleration amplitudes between 0.5 and 3.0 m/s^2 with the predominance of frequencies within the range from 0.5 to 20 Hz. A three degree of freedom mass-spring-damper model was also provided in the standard and the movement of the upper mass m_2 is stated to be "tentatively" representing the head.

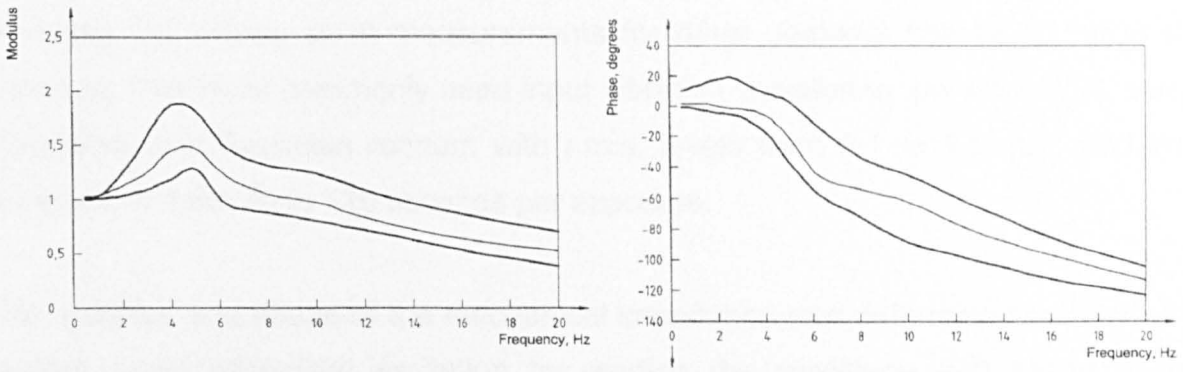

Figure 2.24 Minimum, mean and maximum seat-to-head transmissibility values for the seated body under vertical vibration (reproduced from ISO 5982:2001 (E))

2.4 Impedance and Apparent Mass Measurements

Two common methods for reporting human mechanical response to vibration are the driving point mechanical impedance and the driving point apparent mass. The mechanical impedance function is defined as

$$Z(j\omega) = \frac{F(j\omega)}{v(j\omega)} \tag{2.2}$$

where F is the input force measured at the driving point, v is the response velocity measured at the driving point, ω is the frequency of oscillation and $j = \sqrt{-1}$. The driving point apparent mass function is defined as

$$M(j\omega) = \frac{F(j\omega)}{a(j\omega)} = \frac{Z(j\omega)}{j\omega} \qquad (2.3)$$

where a is the driving point acceleration. These measurements are normally performed using a platform which is rigid over the frequency interval of interest, attached to a vibration exciter by means of one or more force transducers. Platform motion is measured using a displacement transducer or acceleration sensor fixed at some convenient point along the surface. The test subject is typically seated or standing, but driving point measurements for other postures can be found in the literature. The most commonly used input vibration waveforms are sinusoidal, swept sinusoidal and Gaussian random with r.m.s. levels from 0.1 to 1.5 m/s^2 and time durations of from 30 to 120 seconds per exposure.

The modulus and phase of the mechanical impedance was determined in most early studies using sinusoidal excitation by reading the amplitude and phase values directly from an oscillograph or oscilloscope. More recently it has become common to use random excitation and to perform Fourier analysis on the acquired time histories using an FFT analyser. The ratio of force to either velocity or acceleration is normally determined using a spectral estimator, either H_1, H_2 or H_v, which assumes random measurement error on either the input signal, the output signal or both signals respectively (see chapter 3 for details).

Probably the earliest known reporting of human whole-body driving point mechanical impedance was published by Von Bekèsy in 1939. The shape of the impedance curve for a single standing subject (Figure 2.25) showed a response peak at 10 Hz. Von Bekèsy concluded from this that the human body did not act as a pure mass when vibrated.

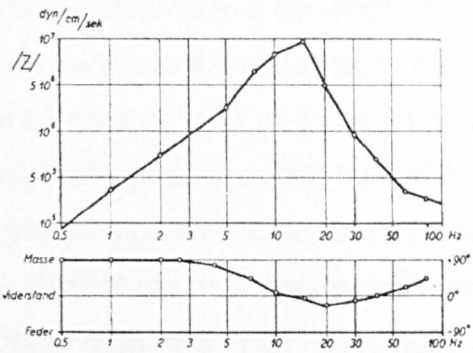

Figure 2.25 Vertical direction driving point mechanical impedance curve for a single standing subject (reproduced from Von Bekèsy 1939)

A 1957 paper by Dieckmann presented various whole-body measurements for the sitting and the standing postures. Among the material was a comparison of the driving point mechanical impedance curve measured for one standing subject to that for a rigid mass (Figure 2.26). As with Von Bekèsy, Dieckmann noted that "the shape of the impedance curve of the human body shows that in relation to impressed vibrations the human body cannot be looked upon as a simple mass". The author also noted peaks at 5 Hz and 12 Hz suggesting the presence of two body resonances.

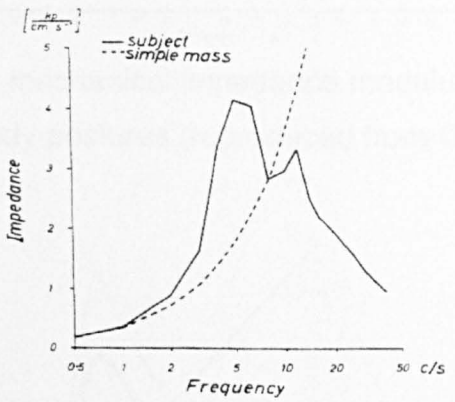

Figure 2.26 Mechanical impedance measured for a standing subject and for a rigid mass (reproduced from Dieckmann 1957)

An influential 1961 ASD report by Coermann (published also in 1962 in Human Factors) developed in detail the theory of mechanical impedance as applied to the human body and discussed in detail the experimental arrangements. Eight subjects were exposed to sinusoidal vertical vibration in each of three postures: sitting erect, sitting relaxed and standing erect. Sinusoidal excitation was used over the frequency range from 1 to 20 Hz. Coermann observed that the seated or standing human body

acted as a rigid mass for frequencies up to 2 Hz after which resonant dynamics could be found. The location of the peaks in the impedance modulus curves were found to change both as a function of posture and of input excitation level. Results for one subject showed that the dominant peak changed from 6.3, to 5.2 to 5.9 when moving from the sitting erect, to the sitting relaxed to the standing posture (Figure 2.27). Tests performed using one subject at r.m.s. acceleration amplitudes from 0.1 to 0.5 g showed that the whole-body response was nonlinear, but that changes in the impedance modulus and phase were within a range of about 10%. Coermann fitted a one degree of freedom mass-spring-damper model to the data (Figure 2.28) and found damping ratios from 0.57 to 0.74 depending on the posture.

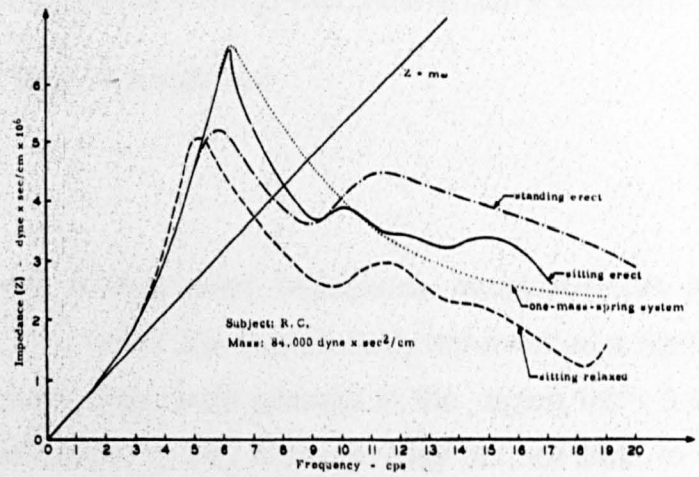

Figure 2.27 Driving point mechanical impedance modulus measured for one subject in several body postures (reproduced from Coermann 1961)

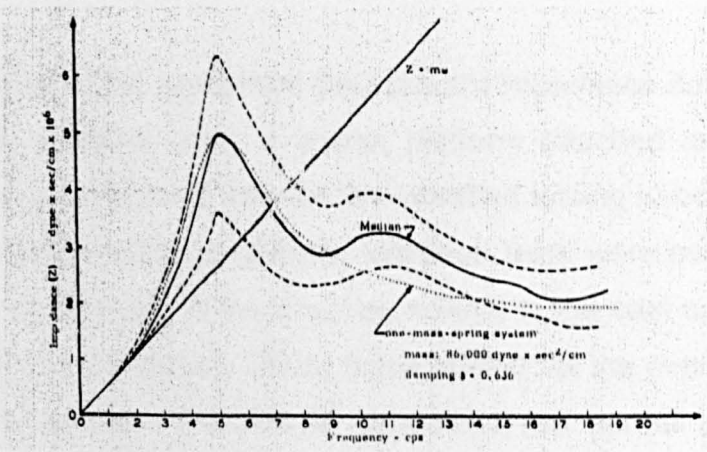

Figure 2.28 Median, 20th percentile and 80th percentile impedance modulus curves for 8 subjects sitting erect (reproduced from Coermann 1961)

A 1966 paper by Weis and Primiano developed an expression for the movement of the human centre of gravity given the measured driving point mechanical impedance and support surface acceleration.

$$S_m = \frac{Z(\omega) S_s(\omega)}{j\omega M_m} \tag{2.4}$$

where:

S_m is the Fourier Transform of the person's centre of mass displacement

S_s is the Fourier Transform of the displacement of the support surface

$Z(\omega)$ is the measured driving point mechanical impedance

M_m is the mass of the person

$j = \sqrt{-1}$.

Also presented were driving point impedance measurements from two subjects which were used to show that the human body behaved as a rigid mass up to 2 Hz, that one or more resonance were present in the region from 5 to 12 Hz and that impedance dropped above 15 Hz. Although they did not state to which frequencies they were referring, the authors concluded that there was 3 to 5 dB of amplification of the centre of mass motion at certain resonance frequencies and that the damping factor appeared to be in the range from 0.3 to 0.4.

A 1968 paper by Vogt et. al. presented driving point impedance data measured for a group of ten male subjects using a shaker platform attached to a centrifuge. By rotating in a circle the centrifuge allowed the vibration testing to be performed under different constant acceleration conditions. Vibration tests were performed at gravity loadings of +1g, +2g and +3g in the direction normal to the seat surface (generating compressive forces on the spine). Under these conditions the overall stiffness of the body was found to increase from 69×10^6 dyne/cm under normal gravity to 164×10^6 dyne/cm under 3g acceleration. The change in stiffness caused the first impedance peak to move from 5 Hz under normal acceleration to 7 Hz under +2g acceleration to 8 Hz at +3g. The damping coefficient was found to be relatively constant at a value of 0.575 across all experiments.

A 1968 paper by Vykukal described mechanical impedance tests performed for 4 subjects using a man-carrying device (Figure 2.29) and centrifuge. The subjects were constrained to sit in the semi-supine position typical of the early space vehicles. Impedance measurements were made using sinusoidal inputs of 0.4 g r.m.s. amplitude at frequencies from 2.5 to 20 Hz, coupled with constant acceleration loadings of +1g, +2.5g and +4g from the centrifuge (Figure 2.30). The author concluded that increased gravity conditions caused the body to show increased stiffness, reduced damping and higher transmission of energy to the internal organs.

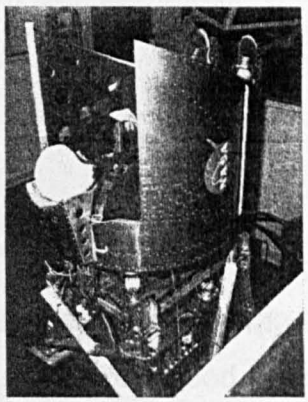

Figure 2.29 NASA Ames man-carrying vibration device used in centrifuge tests (reproduced from Vykukal 1968)

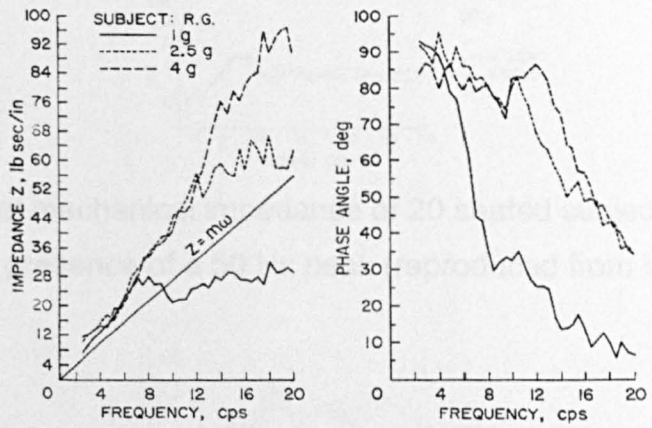

Figure 2.30 Impedance modulus and phase for one subject tested at three levels of constant acceleration in a centrifuge (reproduced from Vykukal 1968)

A 1975 paper by Miwa presented vertical driving point mechanical impedance for subjects in a variety of postures over the frequency range from 3 to 200 Hz. The postures included kneeling, sitting with various leg supports, sitting semi-supine, sitting stooped, sitting cross legged, standing, standing knees bent, standing on

heels, standing on toes, standing on one leg, standing with knees completely bent, standing on knees, back only on table, abdomen only on table, head only on table and various tests of the legs and hand-arm system. Sinusoidal excitation was applied using amplitudes of 0.1 or 0.3 g r.m.s.. The results showed that increasing the excitation amplitude lowered both the frequency and the modulus of the impedance peaks. Impedance peaks were found for the kneeling posture at 6 and 15 Hz, for the sitting posture at 6.5, 16 and 50 Hz, for the standing posture at 7, 18 and 55 Hz and for semi-supine sitting at 4, 7.5, 18 and 50 Hz.

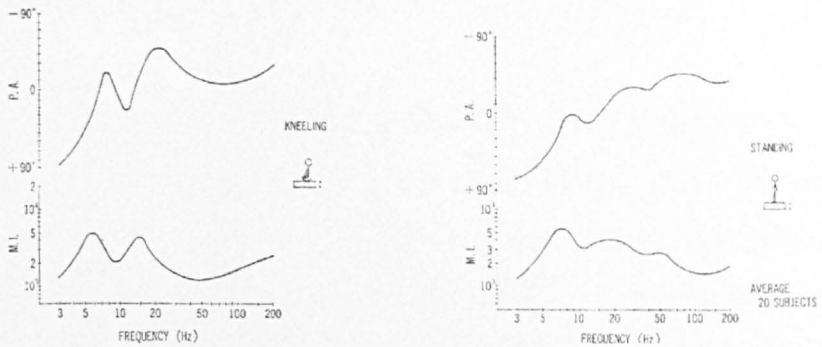

Figure 2.31 Vertical mechanical impedance averaged over 20 subjects for the kneeling and standing postures (reproduced from Miwa 1975)

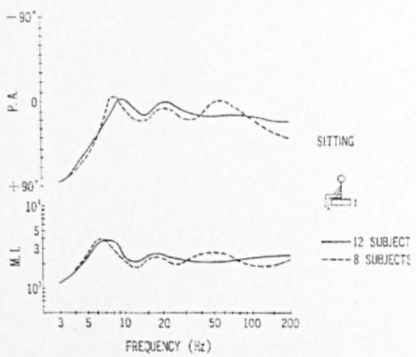

Figure 2.32 Vertical mechanical impedance of 20 seated subjects subdivided according to the presence of a 50 Hz peak (reproduced from Miwa 1975)

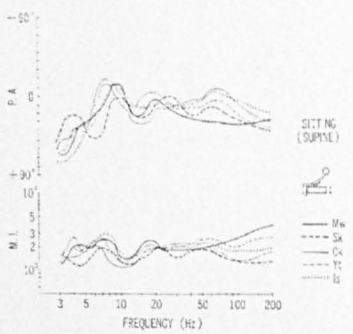

Figure 2.33 Vertical mechanical impedance for 5 subjects in the semi-supine sitting posture (reproduced from Miwa 1975)

A 1978 paper by Sandover suggested the potential superiority of apparent mass measurements over impedance measurements when investigating whole-body dynamic response. Apparent mass functions were determined for the seated posture in the vertical direction using random vibration over the frequency interval from 0.5 to 25 Hz. Results obtained using acceleration input signals having various spectral distributions at r.m.s. levels of either 1 or 2 m/s^2 were found to be similar leading the author to state that whole-body response could be considered linear, to a first approximation, for applications such as transport systems. The peak apparent mass and transmissibility values found in this study were at 4.5 Hz.

In 1981 the International Standards Organisation published *Standard 5982 (1981): Vibration and shock – Mechanical driving point impedance of the human body*. It was a summary of the then existing literature for driving point mechanical impedance of the body in the vertical direction for the seated, standing and supine postures. Modulus and phase were presented in both tabular and graphical (Figure 2.34) form for the interval 0.5 to 31.5 Hz. To simplify calculation a mass-spring-damper model was also specified. The standard remained in use until revised in 2001.

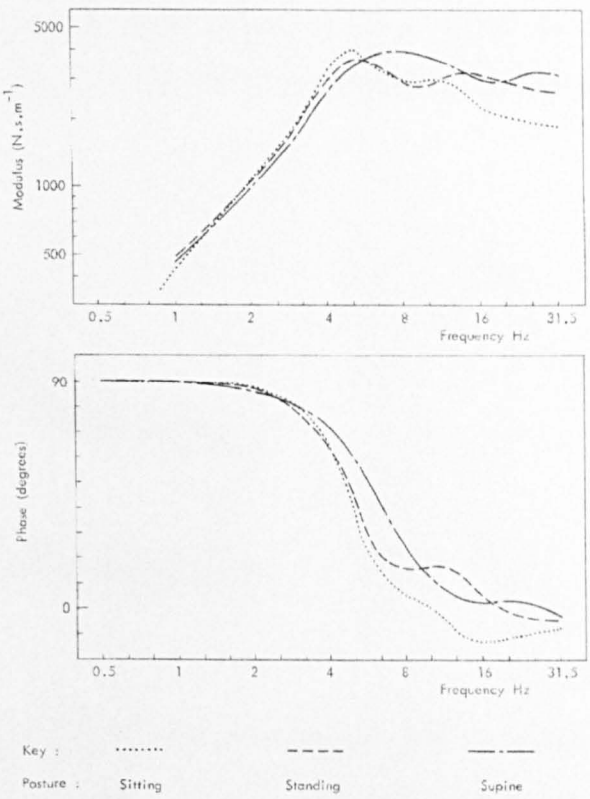

Figure 2.34 Modulus and phase curves specified in ISO 5982:1981 (reproduced from Griffin 1990)

A 1989 study by Fairley and Griffin investigated the effects of subject anthropometry, gender, sitting posture and response linearity. Vertical apparent mass was measured for a group of 60 people composed of 12 children, 24 women and 24 men. Gaussian random acceleration signals were used which covered the frequency interval from 0.25 to 20 Hz and had an r.m.s. amplitude of 1.0 m/s^2. The average frequency of the main peak was found to be 6 Hz at 0.25 m/s^2 acceleration, decreasing to 4 Hz at 2.0 m/s^2. Repeat testing of the same individual showed that the apparent mass varied by less than 10% from test to test. The effect of foot support was found to be large. For the moving footrest the apparent mass values at low frequencies tended towards the static mass supported by the seat, but for the fixed footrest the values varied as a function of the height from ground and the static stiffness of the lower body. The lower the footrest the lower the apparent mass values at frequencies below the first resonance. A correlation analysis between the static mass normalised apparent mass values and the anthropometric data of the subjects showed some statistically significant relationships but the changes were small. The frequency and amplitude of the first peak were affected by both body weight and sitting height. Subject age had a large effect on the normalised apparent mass at 20 Hz, but not at 10 Hz. Fairley and Griffin defined a mean normalised apparent mass curve describing the 60 subjects (Figure 2.35) and provided an associated three mass lumped parameter model.

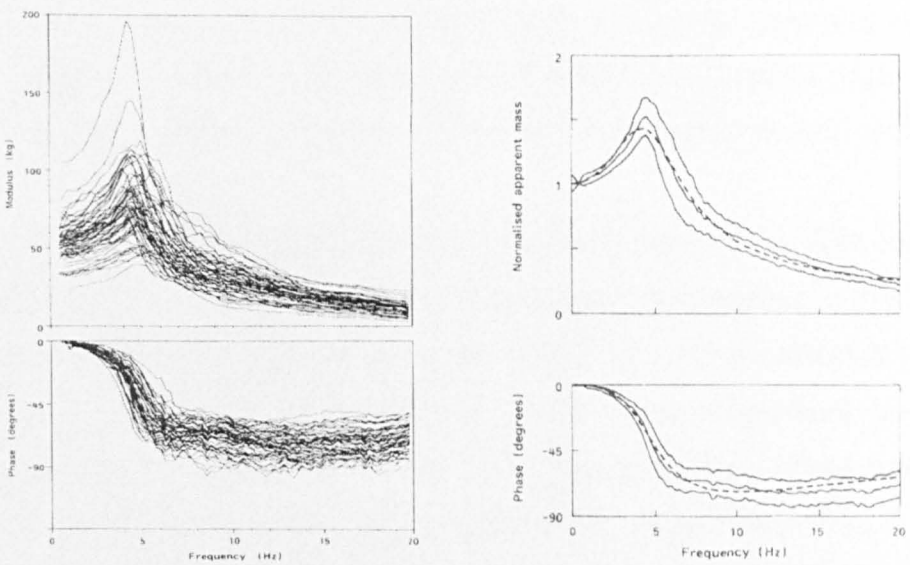

Figure 2.35 Apparent mass of 60 test subjects and normalised mean and one standard deviation curves (reproduced from Fairley and Griffin 1989)

A further paper in 1990 by Fairley and Griffin presented apparent mass results for 8 seated subjects tested in the fore-and-aft and lateral directions (Figure 2.36). Two postures were tested, "with-a-backrest" and "without-a-backrest", using 0.25 to 20 Hz random vibration at levels from 0.5 to 2.0 m/s^2 r.m.s.. With no backrest both the fore-and-aft and lateral directions showed a peak at 0.7 Hz and a second, smaller, peak in the region from 1.5 to 3 Hz. With a backrest a single peak was found at 3.5 Hz for the fore-and-aft direction and at about 1.5 Hz for the lateral direction. The effect of the backrest was found to be most pronounced in the fore-and-aft direction. Muscle tension was found to influence the apparent mass in either direction.

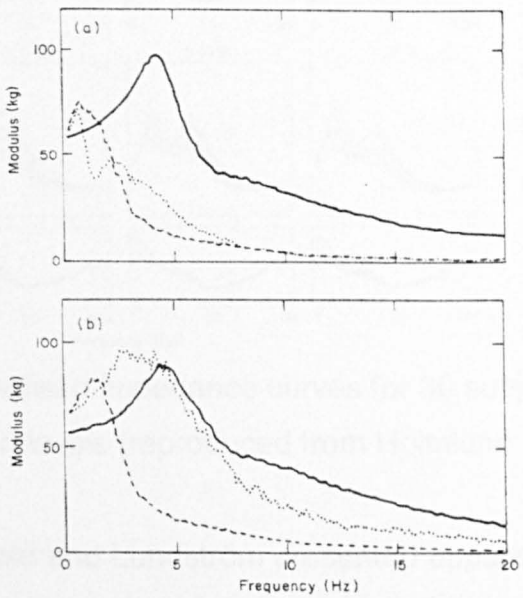

Figure 2.36 Mean apparent mass of 8 subjects with a backrest (top) and without a backrest (bottom) in the fore-and-aft (dotted line), lateral (dashed line) and vertical (solid line) directions (reproduced from Fairley and Griffin 1990)

A 1998 paper by Holmlund and Lunström presented impedance data for 15 female and 15 male seated subjects tested under sinusoidal acceleration in the fore-and-aft and the lateral directions. Frequencies from 1 to 80 Hz and amplitudes from 0.25 to 1.4 m/s^2 r.m.s. were used. All impedance values were normalised by the seated mass of the subjects (Figure 2.37). For both directions the curves were found to increase with frequency until reaching a peak in the region from 2 to 5 Hz. For the lateral direction a second peak was found for most subjects from 5 to 7 Hz. The authors observed that the peak at 4 Hz would separate into two peaks at about 3 and 6 Hz at low test amplitudes and in relaxed postures. ANOVA tests showed significant gender-based variability while a Wilcoxon test showed a significant dependency on

sitting posture. An important conclusion drawn by the authors was that the impedance curves for the fore-and-aft and the lateral directions were sufficiently different to support the development of separate evaluation methods for each axis.

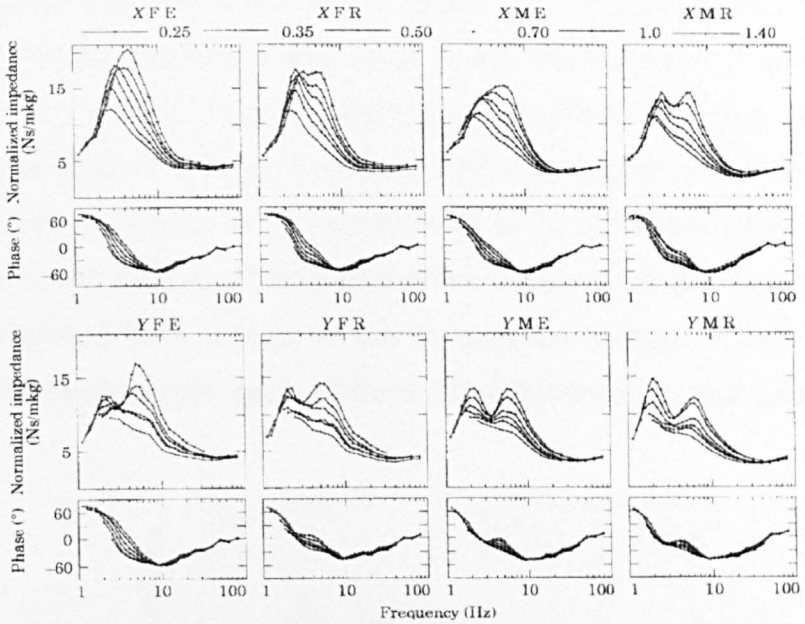

Figure 2.37 Mean normalised impedance curves for 30 subjects tested at six acceleration levels (reproduced from Holmlund and Lundström 1998)

A 1999 paper by Mansfield and Lundström presented apparent mass data for 5 male and 15 female subjects exposed to random vibration in the frequency range from 1.5 to 20 Hz at three amplitudes: 0.25, 0.5 and 1.0 m/s^2. The novelty of this investigation was the testing of the principle that vibrational disturbances can be summed across different axis by linear superposition. Superposition of vibrations acting at different measurement points and along different axis is an assumption of all existing standards. The authors measured the apparent mass of their seated subjects using a rig which permitted the orientation of the seat and subject to be varied with respect to the vibration exciter. Measurements were performed for angles of 0, 22.5, 45, 67.5 and 90 degrees to the mid-sagittal plane. Two response peaks were found for all subjects. The first was at 3 Hz at low levels of vibration, decreasing to 2 Hz at high levels. The second peak at 5 Hz and changed little with amplitude. The frequency of the first peak decreased as the direction changed from 0 degrees (fore-and-aft direction) to 90 degrees (lateral direction). By combining measurements of force and acceleration made along two orthogonal directions and comparing the result to direct

measurement along the axis it was found that the principle of superposition did not hold for horizontal whole-body vibration.

A 2000 paper by Holmlund, Lunström and Lindberg presented vertical seated impedance measured for a group of 15 males and 15 females (Figure 2.38). Sinusoidal excitation was used in the interval from 2 to 100 Hz at amplitudes from 0.5 to 1.4 m/s^2. The impedance was found to increase up to a first maximum in the range from 4 to 6 Hz. For most subjects second and third maxima were found in the ranges from 8 to 12 Hz and from 50 to 70 Hz respectively. Female subjects generally produced a more distinct and often higher peak at the second maxima. The authors compared their results to the impedance curves of ISO 5982 and noted important differences which were attributed to differences in test conditions used.

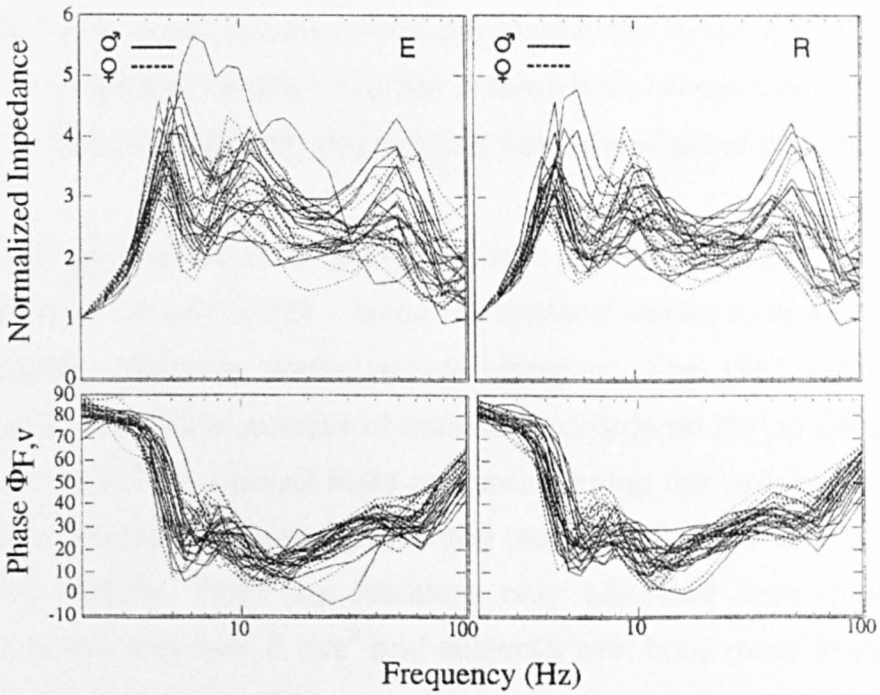

Figure 2.38 Vertical mass normalised impedance for 30 subjects in erect and relaxed postures under sinusoidal 1.0 m/s^2 acceleration (reproduced from Holmlund, Lundström and Lindberg 2000)

A 2000 paper by Mansfield and Griffin analysed the nonlinear response of the body. Vertical apparent mass and seat-to-body transmissibility was presented for 12 subjects tested at 6 magnitudes of random vibration from 0.25 to 2.5 m/s^2 (Figure 2.39). Transmissibility was determined from the seat to the upper and lower abdominal wall, to L3, to the superior iliac spine and to the iliac crest. The peak in the

average apparent mass function calculated across the group was found to decrease from 5.4 to 4.2 Hz from the lowest to the highest vibration amplitude tested. This softening system behaviour was also found in the average transmissibility results, with resonant peaks moving to lower frequencies as the amplitude increased.

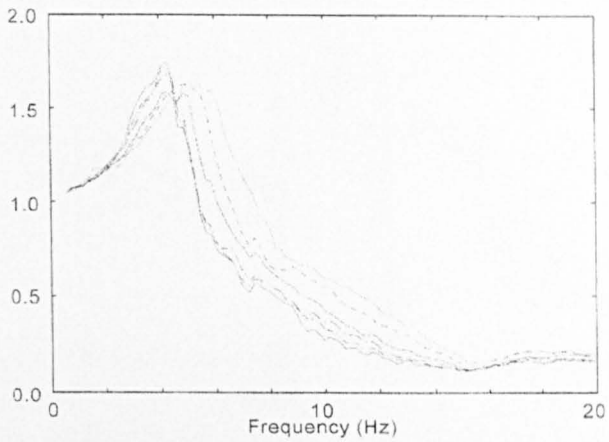

Figure 2.39 Median normalised vertical apparent mass for 12 subjects at 6 amplitudes of random vibration. Curves ordered from lowest amplitude (dotted line) to highest (solid line) (reproduced from Mansfield and Griffin 2000)

2001 saw the publication of a revised edition of ISO standard 5982, now titled *"Mechanical vibration and shock - range of idealised values to characterise seated-body biodynamic response under vertical vibration"*. The 1981 edition had been criticised due to the limited number of data sets considered during development and due to use of data from several body postures. During the revision great care was taken to clarify the body posture represented (seated), the data sets considered and the statistical validity. From the literature only tabulated data generated using acceleration levels less than 5 m/s^2 and subject's with body mass in the range from 49 to 93 kg was used. The ISO committee defined minimum, maximum and mean curves of mechanical impedance (Figure 2.40), apparent mass (Figure 2.41) and seat-to-head transmissibility. A mass-spring-damper model was also provided to facilitate calculation. The mean and limit curves were stated to be representative of (a) a posture described as erect seated without backrest support, with feet supported and vibrated, (b) subject mass in the range from 49 to 93 kg and (c) unweighted sinusoidal or random input acceleration amplitudes between 0.5 and 3.0 m/s^2 with the predominance of frequencies within the range from 0.5 to 20 Hz. The standard suggests the use of the mean values for developing mechanical surrogates for

applications such as seat testing. The tabulated data and model are claimed to be representative of the exposures which occur when driving vehicles such as agricultural tractors, earth moving equipment and fork-lift trucks. The standard warns against applying the data to automobiles since the specified impedance is not wholly representative of the vibration amplitudes and sitting postures found in cars.

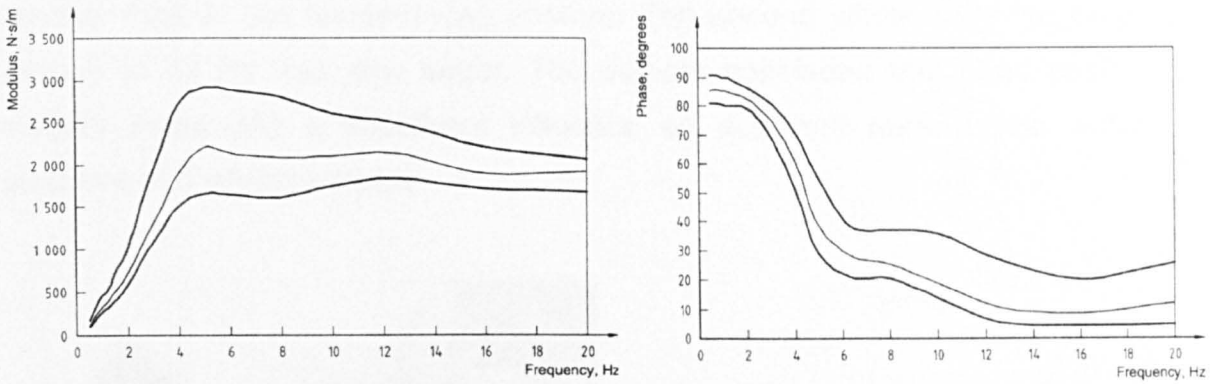

Figure 2.40 Minimum, maximum and mean impedance curves for the seated body under vertical vibration (reproduced from ISO 5982:2001 (E))

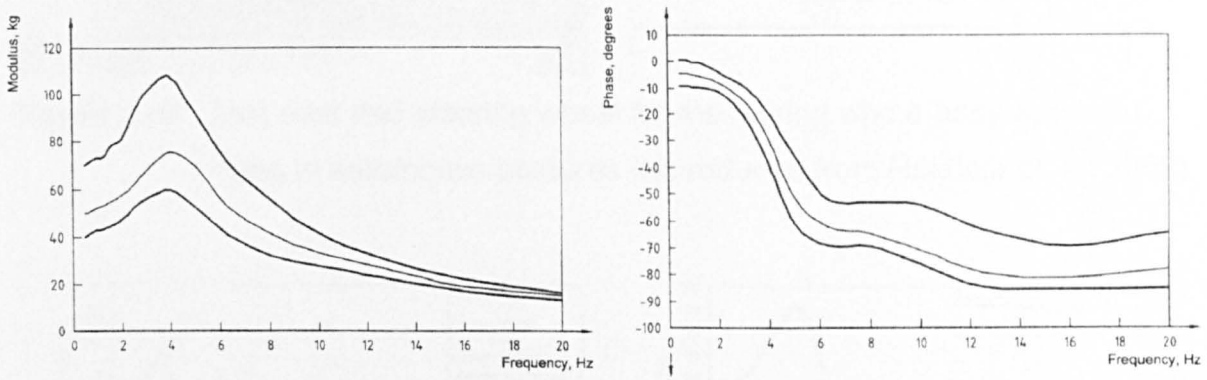

Figure 2.41 Minimum, maximum and mean apparent mass curves for the seated body under vertical vibration (reproduced from ISO 5982:2001 (E))

A 2002 paper by Rakheja, Stiharu and Boileau presented seated vertical apparent mass functions for 24 subjects using sitting postures and vibration amplitudes typical of automobiles. The objective was to quantify the differences that such conditions cause with respect to the simplified postures used in most tests reported in the literature. A rigid seat with vertical support surface inclined at 13 degrees to the horizontal and with included backrest angle of 101 degrees was used, along with an automobile steering wheel set at a column angle of 23 degrees (Figure 2.42). The acceleration signals were 0.5 to 40 Hz Gaussian vibration at 0.25, 0.5 and 1.0 m/s^2 and a road signal measured over a rough surface which had an r.m.s. amplitude of 1.07 m/s^2. Considerable variation was found with respect to the standard postures.

For the hands-in-lap sitting posture the apparent mass peaks were found to be in the region from 6.5 to 8.6 Hz, considerably higher than the 4.5 to 5 Hz most often reported in the literature. Body response in this posture was found to be significantly different from the data of ISO 5982 (see Figure 2.43). For the hands-on-steering-wheel posture the magnitude of the apparent mass peak tended to be considerably smaller than in the hands-on-lap posture. The second whole-body response peak from 8 to 12 Hz was also larger. The authors concluded that hand position and subject mass had a significant influence on apparent mass under automotive postures and vibration levels.

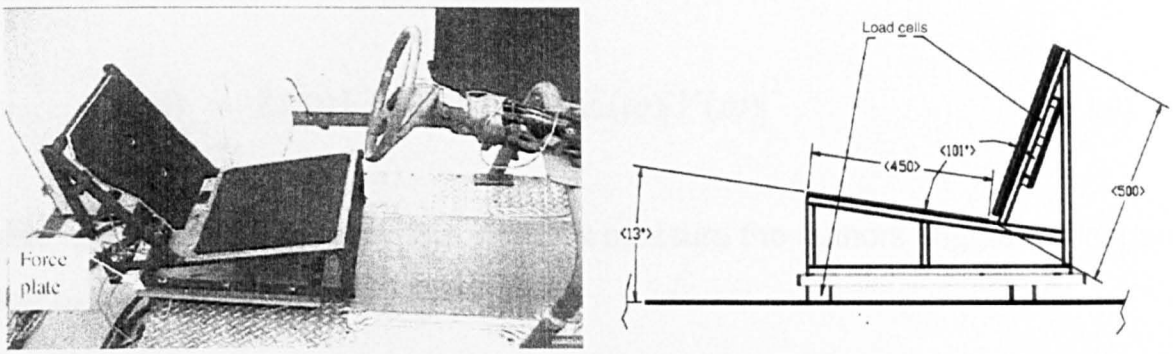

Figure 2.42 Test seat and steering wheel for measuring whole-body apparent mass in automotive postures (reproduced from Rakheja et. al. 2002)

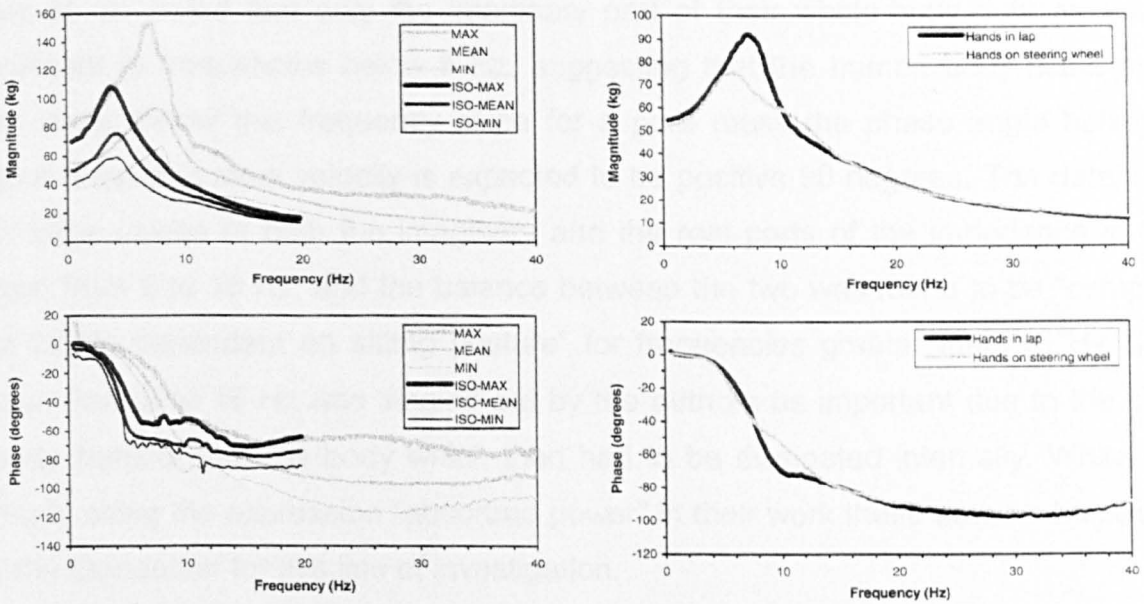

Figure 2.43 Average apparent mass for automotive postures. Comparison of results from hands-in-lap to ISO 5982 (left) and to those from hands-on-wheel (right) (reproduced from Rakheja et. al. 2002)

2.5 Absorbed Power Measurements

A 1964 paper by Weis, Neville, Clarke and Brinkley discussed the theoretical framework and the possible use of driving point mechanical impedance when studying human dynamic response. Since the two quantities used to determine impedance are also the quantities defining power

$$P(\omega) = F(\omega)V(\omega) \tag{2.5}$$

the expression for the power was rearranged in terms of impedance

$$P(\omega) = Z(\omega)V(\omega)V(\omega) = Z(\omega)\left|V(\omega)\right|^2 \tag{2.6}$$

and since impedance $Z(\omega)$ is a complex measure the authors suggested inspecting the real and imaginary parts individually

$$Z_{\mathrm{Re}}(\omega) = \left|Z(\omega)\right|\cos\angle Z(\omega) \text{ and } Z_{\mathrm{Im}}(\omega) = \left|Z(\omega)\right|\sin\angle Z(\omega) \tag{2.7}$$

Weis et. al. noted that only the imaginary part of their whole-body data sets was significant at frequencies below 5 Hz, suggesting that the human body acted as a pure mass below this frequency since for a pure mass the phase angle between output force and input velocity is expected to be positive 90 degrees. The data sets had large values of both the imaginary and the real parts of the impedance in the region from 5 to 15 Hz, and the balance between the two was found to be "complex and highly dependent on sitting posture" for frequencies greater than 15 Hz. The region from 5 to 15 Hz was singled out by the authors as important due to the high energy transfer into the body which then had to be dissipated internally. While not actually using the expression "absorbed power" in their work these authors helped to lay the foundation for this line of investigation.

An influential 1968 paper by Lee and Pradko presented the results of what the authors described as "extensive testing" of seated human subjects. They tabulated impedance modulus, impedance phase angle and absorbed power for the frequency

interval from 0 to 12 Hz. Results for all three axis of seated whole-body vibration were presented as well as vertical absorbed power for the feet alone. Lee and Pradko suggested the superiority of the absorbed power method due to absorbed power being a physically interpretable quantity and because, being a scalar, it could be easily summed along different axis.

A 1998 paper by Lundström, Holmlund and Lindberg presented absorbed power for 15 males and 15 females tested using sinusoidal vibration from 2 to 100 Hz at r.m.s. amplitudes from 0.5 to 1.4 m/s^2. As shown in Figure 2.44 the absorbed power increased with frequency until 4 to 6 Hz after which it decreased. The frequency of maximum absorbed power decreased with increasing amplitude and when changing from an erect to a relaxed posture. The absorbed power was found to increase with the square of the input acceleration amplitude and proportionally with subject mass. To facilitate comparisons between subjects of different size the authors chose mass to normalise their data. After normalisation the curves were found to be nearly identical to the 1968 Lee and Pradko results. A further point developed by the authors was the different frequency dependence of their average absorbed power curves with respect to the frequency weighting curves of ISO 2631-1 (1997) based on subjective response data. The authors proposed that if absorbed power were found to be predictive of damage to biological tissue then the ISO curves were overestimating the damage potential at frequencies below 6 Hz while underestimating the damage potential for frequencies greater than 6 Hz.

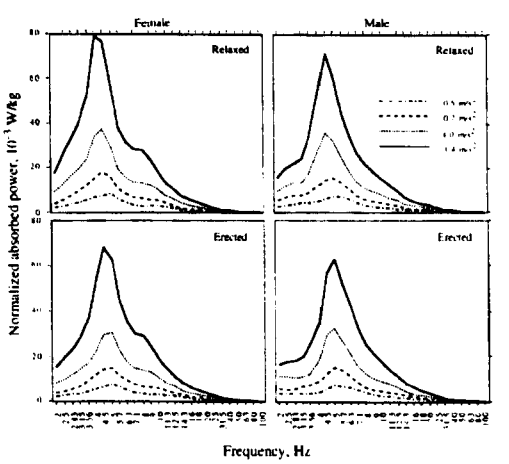

Figure 2.44 Mean normalised absorbed power for 15 females and 15 males at 5 acceleration amplitudes (reproduced from Lundström, Holmlund and Lindberg 1989)

A second 1998 paper by Lundström and Holmlund presented absorbed power measurements for the same group of 15 male and 15 female subjects, but in all three vibration axis (Figure 2.45). Sinusoidal vibration was used at frequencies from 1 to 80 Hz and r.m.s. amplitudes from 0.25 to 1.4 m/s^2. Absorbed power was found to increase with frequency up to a peak from 4 to 6 Hz for vertical vibration and to increase up to 3 Hz for fore-and-aft and lateral vibration. ANOVA testing suggested that females absorbed more power per kilogram than males. The authors again noted the different conclusions that would be drawn about the same vibration exposure by use of the ISO 2631 frequency weightings or by a line of constant absorbed power.

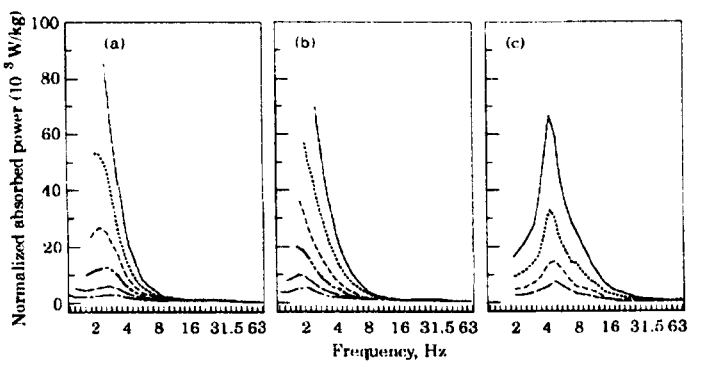

Figure 2.45 Mean normalised absorbed power for the x (a), y (b), and z (c) directions at six acceleration amplitudes for 30 subjects in 2 postures (reproduced from Lundström and Holmlund 1998)

A 1998 paper by Mansfield and Griffin presented seated absorbed power curves for 12 male subjects measured using random excitation in the interval from 0.2 to 20 Hz at r.m.s. acceleration amplitudes from 0.25 to 2.5 m/s^2. The authors noted that it was convenient to determine the absorbed power from the cross spectrum between the velocity and force as

$$P_{abs}(\omega) = P_{\mathrm{Re}}(\omega) = \left|G_{xy}(\omega)\right| \cos(\theta(\omega)) \qquad (2.8)$$

Since absorbed power was found to increase in proportion to the square of the acceleration (see Figure 2.46) the authors chose acceleration to normalise their data, which had the added advantage of compensating any variations due to differences in the acceleration of the test signal from frequency to frequency (see Figure 2.47). The frequency of maximum absorbed power was found to be 5 Hz, with decay gradients

of –12 dB/octave either side of the peak. This frequency was lower, and the absorbed power greater, at higher vibration amplitudes. The authors compared their results to those of both Lee and Pradko (1968) and Lundström et. al. (1998) and concluded that there was a remarkable similarity between the data sets. Like Lundström et. al. they compared their findings to the frequency weighting curves specified in ISO 2631 and BS 6841. Unlike the previous authors, however, they concluded that the differences suggested that "the absorbed power is unlikely to yield good general predictions of the discomfort or risks of injury from whole-body vertical vibration".

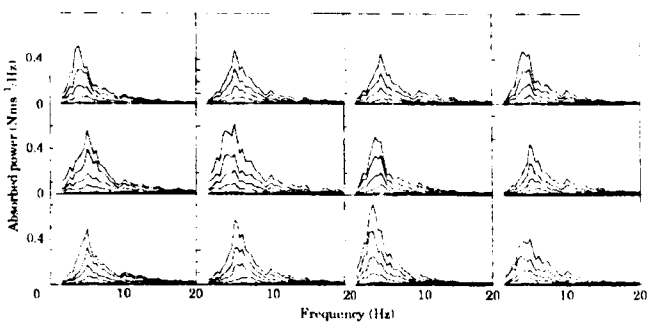

Figure 2.46 Absorbed power of 12 subjects tested at 6 acceleration amplitudes (reproduced from Mansfield and Griffin)

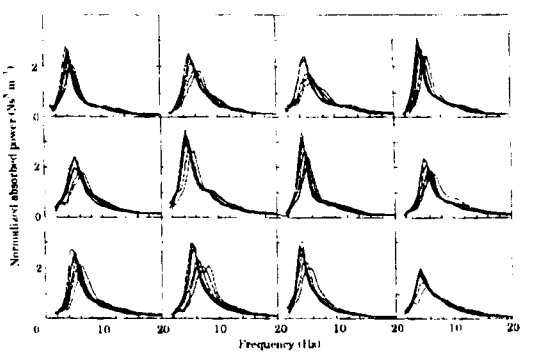

Figure 2.47 Normalised absorbed power of 12 subjects tested at 6 acceleration amplitudes (reproduced from Mansfield and Griffin)

A 2001 paper by Mansfield, Holmlund and Lunström presented vertical direction apparent mass and absorbed power for 24 subjects exposed to 15 vibration conditions. The input acceleration signals were of 5 types and were scaled to three r.m.s. amplitudes: 0.5, 1.0 and 1.5 m/s^2. The five types were random, repeated equally spaced shocks, repeated unequally spaced shocks, random background with equally spaced shocks and random background with unequally spaced shocks. The objective was to identify any systematic differences measured for shocks as opposed

to continuous vibration. The shape of the absorbed power curves changed little with excitation type or amplitude, but the frequency value of the absorbed power peak in the region from 4 to 7 Hz was found to drop with increasing input amplitude. For individual subjects the total absorbed power, calculated as the integral of the absorbed power curve from 3 to 20 Hz, showed statistically significant increases for shock signals with respect to continuous vibration.

2.6 Modelling the Mechanical Response of the Human Body to Vibration

The human body has traditionally been modelled for vibrational purposes as consisting of a finite number of elements each with its own mass, stiffness and damping properties. Such models can serve one of two basic purposes: (1) to represent the input impedance of the body to a sufficient degree to permit its simulation in the testing of objects such as seats and (2) to represent the inner structures and dynamic mechanisms of the body to a sufficient extent to aid the understanding of human motion and of the potentially damaging effects of vibration on tissue and organs. This section presents the most significant examples of the two model types.

Early attempts at modelling the dynamic behaviour of the seated body were driven by the need to better understand aircraft ejection. Three of the first four pilots who tested ejector seats during WWII suffered spinal injury. An understanding of human body dynamics and tolerance limits was needed. The earliest recorded use of a dynamic model of the body was made at this time by Siegfried Ruff (Ruff 1950) whose model treated the body as a rigid mass which is accelerated during ejection. Spinal injuries such as vertebral ruptures were considered to occur after what Ruff termed a "rupture path". He assumed an acceleration ramp law of the form

$$a = C\,t^{m} \tag{2.9}$$

and also assumed that rupture of body structures such as the spinal vertebrae or soft tissue was characterised by a physiological "rupture distance". By double integrating ejection acceleration data from the tests in which the three pilots suffered spinal injury Ruff was able to estimate the "rupture distance" and then tabulate maximum

tolerable values of C, t and m. Ruff's acceleration tolerance curve was the basis for ejector seat design of many years subsequent to his work.

In 1957 Lantham presented a paper in which experimental data from vertical vibration tests in the range from 2 to 20 Hz was used to develop a lumped parameter model consisting of a mass for the head (18 lb), a mass for the torso and equipment (135 lb) and a mass for the seat (119 lb) connected by springs and dampers. The spring and damper values produced natural frequencies of the three subsystems of 5, 10 and 20 Hz and damping factors 0.25, 0.4 and 0.5 respectively. The model was constructed and analysed using an analogue computer. Simulations were used to choose between several possible seat stiffness values and helped to establish upper limits for maximum peak ejection acceleration (25g) and rate (300 g/s).

In 1958 Hess and Lombard modelled the spinal column as a continuous elastic beam. The assumption was made that the movements of the upper body were mostly along the axis of the spine, thus rendering the problem one-dimensional. The body was treated as a homogenous elastic rod, specified by three parameters: length, density and elastic coefficient. One end of the rod was free while the other was subjected to the prescribed acceleration of the seat. An analogue computer was used to simulate the system and ejection data from 17 test subjects was used to determined average model parameters by a process of matching the simulator output to the experimental head acceleration data. The average model had a wave travel time (from seat surface to head) of 0.025 seconds.

In 1961 Payne developed an influential set of one and two degree of freedom mass-spring and mass-spring-damper models of the body. He presented detailed analytical development of the impact dynamics of several combinations of human body posture and seat restraint. Experimental data relative to the human spine was gathered from the available sources of the period to produce composite tolerance envelopes, and these envelopes were used as the basis for estimating the parameter values of two degree of freedom mass-spring and mass-spring-damper models of the spine and torso. The natural frequencies of the model were 1.87 and 44.24 Hz which were called the "visceral mode" and the "spinal mode". Payne's analytical developments served as the basis for much later research including the well known Dynamic Response Index (DRI) model developed by the same author

In 1966 Liu and Murray presented an aircraft ejection model in which the spine was again treated as a uniform elastic beam but which, this time, had at the top a rigid mass representing the head. The authors obtained a closed form solution for the stresses developed in the case of an acceleration pulse applied to the hip. Their formulation was the first attempt at answering the question of where and when the maximal axial stresses occur along the spinal column.

A 1966 study by Toth was the first to present a model in which individual vertebra were considered as separately moving objects. Though the model still treated spinal motion as being purely axial, eight mass elements representing pelvis through to T11 were connected together by nonlinear springs and dampers. A spring was also used to represent the stiffness of the soft tissue between the rigid seat surface and the pelvis. A trapezoidal pulse taking 0.005 seconds to linearly reach a peak value of 60g then remain constant for 0.005 seconds was applied. The resulting forces acting at each vertebra were compared to their known failure strengths and it was determined that L1 would be the first to rupture.

In 1968 Terry and Roberts improved the continuous rod model of Hess and Lombard by representing the spine as a uniform Maxwell-type medium without a terminal mass. A Maxwell constitutive equation was used of the form

$$\dot{\varepsilon} = \frac{1}{E}\dot{\sigma} + \frac{1}{\eta}\sigma \qquad (2.10)$$

where ε represents the strain, σ the stress, E the Young's modulus, η the dynamic viscosity of the damping and the dot denotes differentiation with respect to time. It was combined with the equation of motion of a one-dimensional wave in a uniform rod to develop the governing partial differential equations. A computer program determined the optimal Young's modulus and Poisson ratio by comparing the model predicted output to experimental head acceleration data from ramp tests with cadavers (Figure 2.48). The best fits were obtained for data sets with low maximum acceleration values. The authors noted the change in the response frequency and damping with changing acceleration level and suggested that the equations might be improved by making the viscosity a function of the strain rate. The natural frequency

of the ejection models was found to be 12 Hz, higher than the natural frequency of models developed for low acceleration environments.

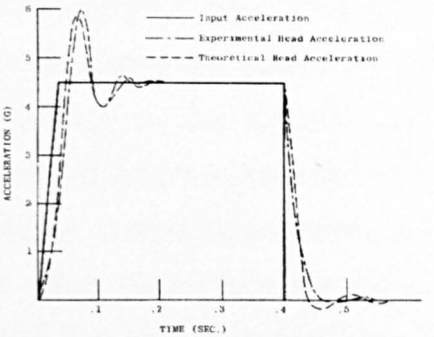

Figure 2.48 Best fit model response and experimental head acceleration from a low acceleration ramp test (reproduced from Terry and Roberts 1968)

A 1970 paper by G.R. Hopkins presented two nonlinear lumped parameter models of the seated body under vertical vibration. The first, which the author called the "nonlinear geometry model", used abdominal springs which did not rigidly couple the movement of the abdominal mass to that of the upper and lower body. Hopkins argued that when the visceral mass moved towards the head it compressed the lungs but did not put tension on the abdominal wall or pelvis. Likewise, when it moved downward it compressed lower structures but did not pull the diaphragm. The second model included the pumping action of the lungs which push air in and out through an orifice following the movement of the abdominal mass. This "nonlinear dynamic" model had an additional nonlinear force-displacement relationship added to the equations of motion to represent the air flow through the orifice. Appropriate choice of model parameters was shown to lead to driving point mechanical impedance values which approximated experimental data sets from the literature.

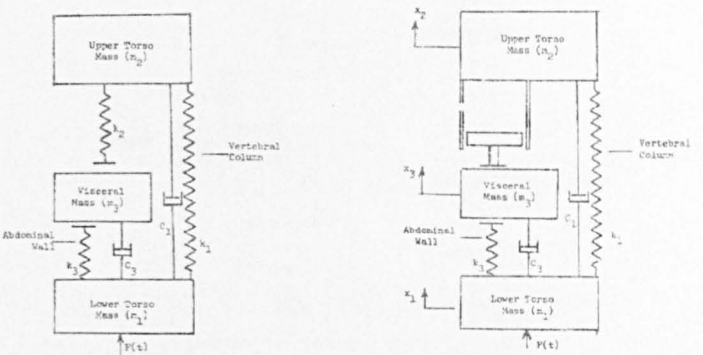

Figure 2.49 Nonlinear geometry model (left) and nonlinear dynamic model (right) developed by Hopkins (reproduced from Hopkins 1970)

In 1971 Orne and Liu developed a detailed model of the lumbar and thoracic spine. Each vertebra was modelled as a 3 degree of freedom rigid body connected to adjacent vertebra by means of springs which represented the axial, shear and bending resistance of the intervertebral discs. The elements were positioned such that their initial configuration simulated the seated curvature of the spine, and each rigid body was loaded dynamically by the eccentric inertial properties of the local organs and tissue. A trapezoidal ejection pulse with finite rise time and peak value of 10 g was used in all simulations. Computations were performed for 100 msec, thus avoiding the need to model active neuromuscular loops which have time constants varying from 100 to 200 msec. The results showed that 10 g was sufficient to reach injurious stress levels in the lumbar spine and that the presence of harnesses or other constraints against spinal bending helped to reduce the risk of injury.

1971 also saw the publication of a report by Payne and Band which described the 4 degree of freedom model of the seated body shown in Figure 2.50. The 4 masses represented the head-neck, thorax-spine, viscera and buttocks-pelvis. Two variations of the model were developed; in the first the masses were connected by linear springs and dampers while in the second the thorax-spine and buttocks-pelvis springs were taken to be nonlinear and were modelled using polynomial force-deflection curves. 35 linear models were constructed and simulated using an analogue computer, and several parameter sets were found to accurately reproduce experimental impedance curves. Payne and Band also developed nonlinear equations for the thorax-spine and buttocks-pelvis springs in order to correctly represent the changes in system dynamics that occur for different input amplitudes and under different constant acceleration loadings.

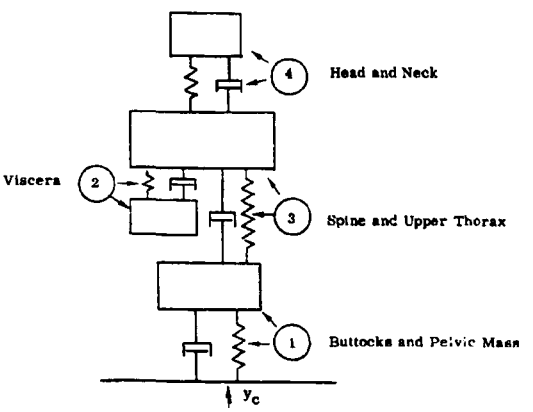

Figure 2.50 Four degree of freedom lumped parameter model of the seated human body (reproduced from Payne and Band 1971)

In 1974 Prasad and King developed a lumped parameter model of the spine which included for the first time the transmission of force through the articular facets. Each of the 24 vertebra was taken to have three degrees of freedom in the mid-sagittal plane (two translations and one rotation). The model parameters were estimated from results found in the literature and from cadaveric sections, and the model output was validated against vehicle crash impacts with three cadaveric subjects. The importance of facet load transmission was established as was the role of initial spinal curvature at the time of deceleration onset.

A 1974 paper by Muksian and Nash presented the 7 degree of freedom lumped parameter model of the seated body shown in Figure 2.51. Cubic spring and cubic damping elements were defined in addition to the usual linear units. Coulomb friction was also simulated between the torso mass and back by means of signum functions. Parameter values were estimated from literature data. Since the model was nonlinear the response was determined by means of time domain integration. Seat-to-head transmissibility calculated from the steady state response was compared to results from the experimental studies by Goldman and Von Gierke (1960) and by Pradko et. Al. (1967). Muksian and Nash observed the impossibility of reproducing the experimental data over the complete frequency range investigated (1 to 30 Hz) using a fixed set of parameter values. Matching of the experimental data required the use of different damping coefficients for frequencies above and below 8 Hz. This change was interpreted by the authors to suggest system nonlinearity and changes in voluntary and involuntary muscle response between 5 and 9 Hz.

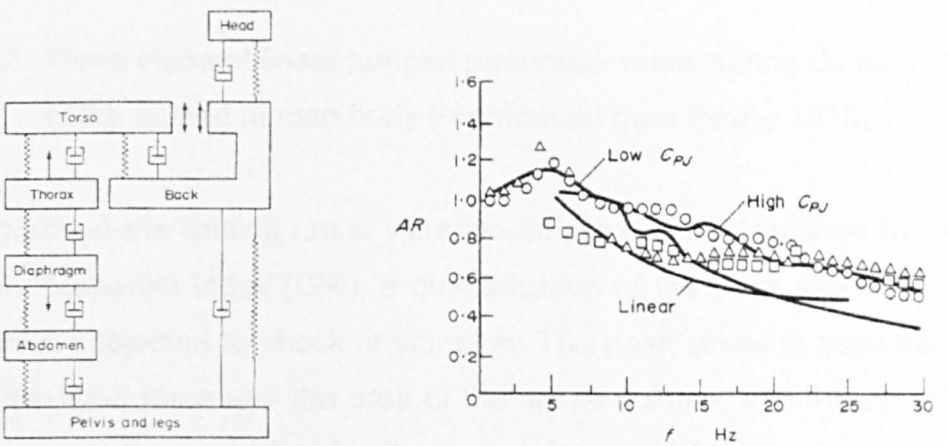

Figure 2.51 Nonlinear model of the seated body and comparison of predicted seat-to-head transmissibility to experimentally measured data sets (reproduced from Muksian and Nash 1974)

The problem of fixed parameters values was partially addressed by a study reported in 1976 by Belytschko, Schwer and Schultz. A 3 dimensional model of the head and spine was developed and an incremental stiffness method was used to deal with nonlinear behaviour when oscillating at large movement amplitudes. An important result of the study was the suggestion that the 5 Hz peak normally found in experimentally determined impedance functions could not be caused by an axial resonance of the spine. It was proposed, instead, to be a movement consisting of seat and buttock interaction, of spinal flexure and of axial response of the viscera.

In 1978 Payne presented a method which has gained wide acceptance for estimating human vibration tolerances limits and ride quality. The method uses a mass-spring-damper model of the seated body (see Figure 2.52) consisting of three elements: one for "body vibration", one for "visceral movements" and one for "spinal movements". The spinal model is defined by a natural frequency of 8.42 Hz and by a damping ratio of 0.224. The visceral model is defined by a natural frequency of 4.0 Hz and by a damping ratio of 0.4 and the body vibration model is defined by a natural frequency of again 8.42 Hz but by a damping ratio of 1.0.

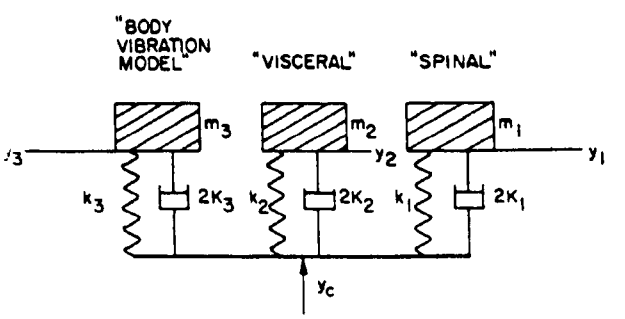

Figure 2.52 Three element linear lumped parameter mass-spring-damper model of the seated human body (reproduced from Payne 1978)

In Payne's method the limiting r.m.s. vibration amplitude is determined by means of the Dynamic Response Index (DRI), a quantification of the peak stress occurring in the spine when subjected to shock or vibration. The peak stress is assumed to be a function of the input force and the area of the spinal column, and the spinal column area is assumed to be proportional to the mass of the subject

$$peak\ stress = \frac{peak\ force}{area} \propto \frac{peak\ force}{subject\ mass} \tag{2.11}$$

Given these assumptions it is possible to express the peak stress in the spring as

$$peak\ stress \propto \frac{k}{m}\delta_{\max} = \omega_n^{\ 2}\,\delta_{\max} \tag{2.12}$$

Thus for a given input the maximum deflection $\delta_{\max}$ is determined and the value $\omega_n^{\ 2}\,\delta_{\max}$ is the dynamic response index (DRI). Correlation tables then provide the incidences of spinal fracture as a function of DRI. An important innovation of Payne's 1978 paper was the establishment of a framework for using DRI for evaluating comfort. For each degree of freedom a Vibration Ride Ratio was defined as

$$VRR = \frac{\ddot{y}_n}{g}\,r.m.s. \tag{2.13}$$

and the Vibration Ride Quality Index (VRQI) is defined as the highest value among the three systems. The limits proposed were 0.5 VRQI for "severe less than 1 hour", 0.2 VRQI for "tolerable, less than 1 hour", 0.2 VRQI for "long-term severe" and 0.1 VRQI for "long-term tolerable".

An influential 1978 paper by Belytschko, Schwer and Privitzer presented the three dimensional finite element model of the human spine, torso and head shown in Figure 2.53. The model, developed for the purpose of studying aircraft ejection, used anatomically correct representations of the skeletal segments (vertebrae, pelvis, head and ribs) with interconnecting deformable elements and hydrodynamic elements for the abdominal cavity and viscera. Linear spring and beam elements were used for the elastic deformable elements and hydrodynamic elements governed by pressure-volume laws were used for the tissue. The model was used to investigate spinal loadings for several ejection profiles and was used for evaluating the effect of head eccentric mass (as produced by flight helmets) and shoulder harness use.

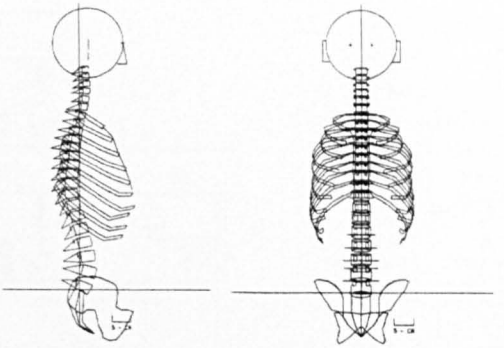

Figure 2.53 Three dimensional model of the human spine developed for use in aircraft ejection studies (reproduced from Belytschko et. al. 1978)

1981 saw the publication of *International Standards Organisation 5982 (1981): Vibration and shock – Mechanical driving point impedance of the human body*. Alongside tabulated vertical impedance values for the seated, standing and supine postures, the standard also specified mass-spring-damper models for use in the frequency range from 0.5 to 31.5 Hz. A separate model was provided for each posture. Of note was the use of a 3 degree of freedom model for the supine posture as opposed to two degree of freedom representations for sitting and standing. The standard remained in publication until revised in 2001.

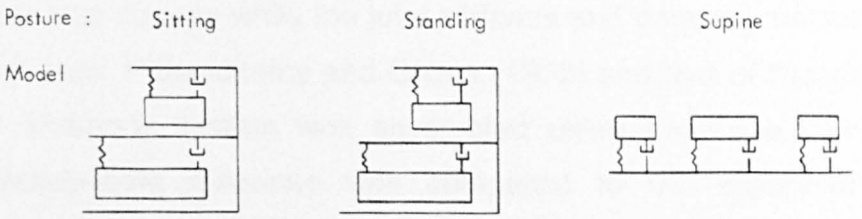

Figure 2.54 Vertical driving point impedance models for the sitting, standing and supine postures from ISO 5982 (reproduced from Griffin 1990)

1987 saw the publication of *ISO Standard 7962 (1987): Vibration and shock – Mechanical transmissibility of the human body*. The standard was intended as a summary of the existing literature on seat-to-head and floor-to-head transmissibility. Besides tabulated modulus and phase data, the standard also provided a 4 degree of freedom mass-spring-damper model of the body (Figure 2.55). The movement of mass m_1 representing the head was suggested for use in calculating seat-to-head and floor-to-head transmissibility. ISO standard 7962 remained in publication until amalgamated into the 2001 revision of ISO 5982.

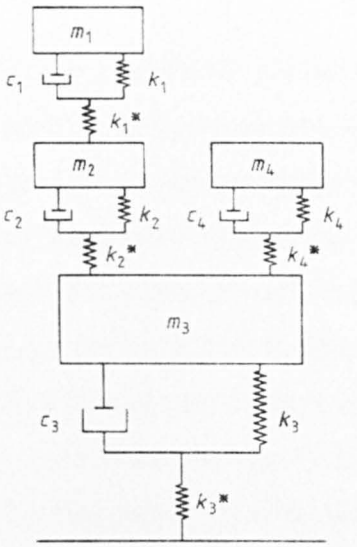

Model parameters	
m_1	8,24 kg
m_2	8,05 kg
m_3	44,85 kg
m_4	13,86 kg
k_1	22×10^8 N·m^{-1}
k_2	$20,13 \times 10^4$ N·m^{-1}
k_3	$88,56 \times 10^3$ N·m^{-1}
k_4	$36,47 \times 10^3$ N·m^{-1}
k_1^*	36×10^7 N·m^{-1}
k_2^*	65×10^9 N·m^{-1}
k_3^*	$52,34 \times 10^4$ N·m^{-1}
k_4^*	$69,30 \times 10^3$ N·m^{-1}
c_1	748,1 N·s·m^{-1}
c_2	578,0 N·s·m^{-1}
c_3	2 964,0 N·s·m^{-1}
c_4	901,8 N·s·m^{-1}

c dynamic viscosity
k, k^* spring rate
m mass

Figure 2.55 Four degree of freedom mass-spring-damper model specified in ISO standard 7962 for calculating z axis seat-to-head or floor-to-head transmissibility (reproduced from ISO 7962:1987 (E))

Two 1987 papers by Amirouche presented the first application of multibody dynamic techniques to the modelling of whole-body vibration. The body was subdivided into 13 rigid and flexible segments, each having 6 degrees of freedom, interconnected by spherical, revolute or slider joints. The geometry of each segment was based on the Hybrid III crash test dummy while the joint stiffness and damping values were based on the work of Patil, Palanichamy and Ghista (1978) and that of Muksian and Nash (1974). The multibody system was assembled using Kane's equations and the computed steady-state response was compared to the experimental data of Coermann (1962) and of Panjabi et. al. (1986). The 5 Hz main resonance frequency was found to be predicted. The modelling of the damping forces was identified by the author as the most important area requiring further development.

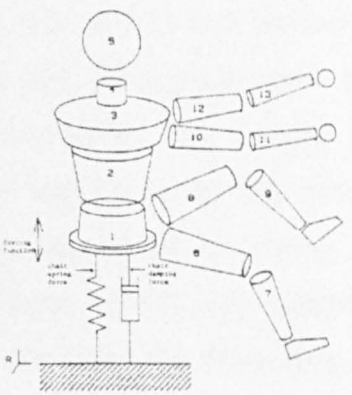

Figure 2.56 Multibody model of the seated body (reproduced from Amirouche 1987)

A 1989 paper by Fairly and Griffin presented vertical apparent mass measured from 1 to 20 Hz for a group of 60 people consisting of 12 children, 24 women and 24 men. A mean normalised curve was produced which described the 60 subjects as was a three-mass lumped parameter model (see Figure 2.57). In the model m_1 was taken to represent the part of the upper body which moves relative to the seat platform, m_2 the mass of the body and legs that moves with the seat platform and m_3 the mass of the legs that is supported by and moves with the footrest. The values were chosen to be 45.6 kg for m_1, 6.0 kg for m_2 and 11.5 kg for m_3. Spring stiffness K_B was chosen to provide a natural frequency for the upper body of 5.0 Hz and the damping value C_B was taken to be 1360 Ns/m (a damping ratio of 0.475). The lower components were varied to cover the possible thigh stiffness values of the individuals tested. K_T was taken to be 0, 500, 1000 or 2000 N/m while C_T was determined from K_T such that the damping ratio for the lower body was kept constant at 0.5.

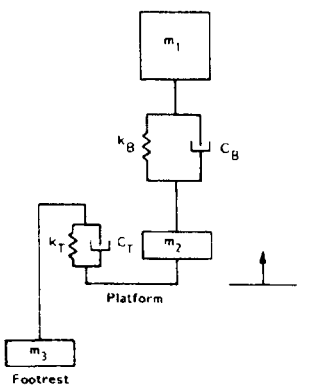

Figure 2.57 Lumped parameter model of the seated body based on apparent mass tests of 60 subjects (reproduced from Fairley and Griffin 1989)

A 1996 paper by Broman et al. presented a linear 2 dimensional mass-spring-damper model of the lumbar spine, pelvis and buttocks. The innovation with respect to previous research was the use of sagittal plane lumbar rotations in addition to fore-and-aft and vertical movements. The model was used to determine the transmission of vibration from seat to L3 in the sitting posture and was validated against experimental data measured at L3 using accelerometers fixed to pins inserted into the spinous process. While only partially matching the experimental data, the results highlighted the need for modelling sagittal plane rotations of the lumbar spine.

A 1997 paper by Kitazaki and Griffin described a 2 dimensional finite element model of the seated body derived from the 1978 work of Belytschko and Privitzer. The model consisted of 134 elements and 87 master degrees of freedom. Mass and inertia properties were derived from the work of Belytschko while spring constants and modal damping ratios were adjusted based on an experimental data published by Kitazaki and Griffin (1998). 7 modes of vibration were found in the frequency interval from 0 to 10 Hz. The main resonance at 5 Hz consisted of a motion in which the head, spinal column and pelvis moved as a single unit, shearing and axially deforming the tissue of the buttocks. The second principal resonance was found to be a rotational mode of the pelvis. The authors noted that a shift in the frequency of the first resonance could only be achieved by changing the axial stiffness of the buttocks tissue. It was therefore suggested that the change in vibration response seen in experimental data sets for different sitting postures could be attributed to the change in buttock stiffness caused by modifications in the contact area with the seat.

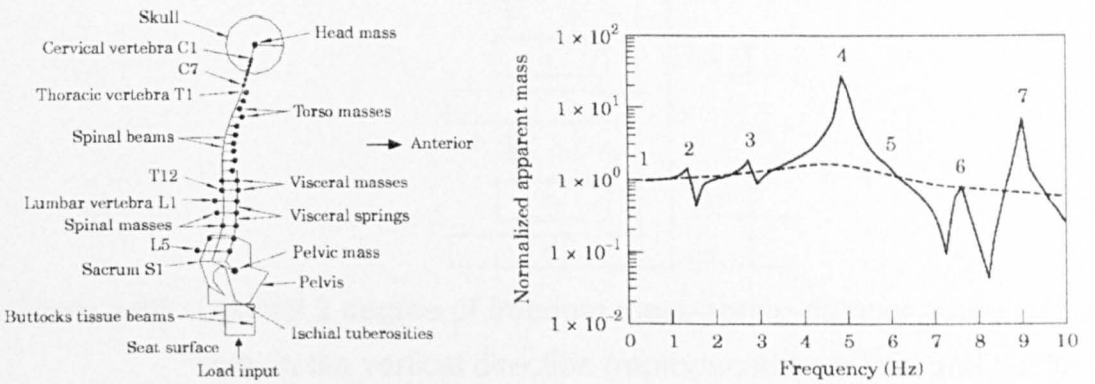

Figure 2.58 Two dimensional model of the seated body and vertical apparent mass calculated without damping and for modal damping ratios from 0.2 to 0.5 (Kitazaki and Griffin 1997)

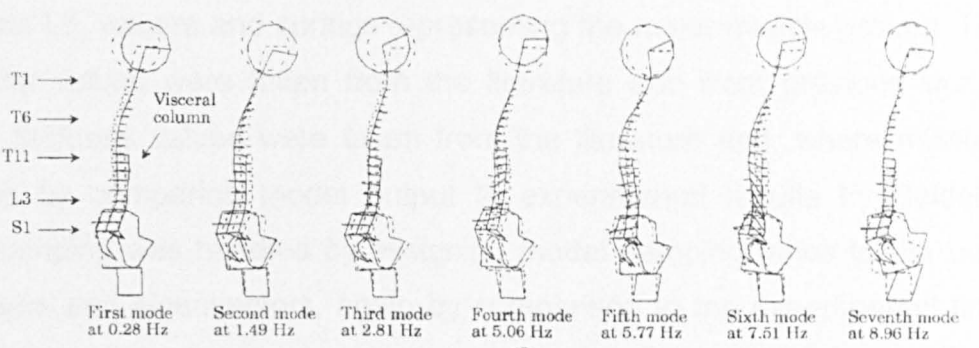

Figure 2.59 First 7 natural frequencies and mode shapes for the two dimensional model of the seated body (Kitazaki and Griffin 1997)

A 1998 paper by Wei and Griffin described a reanalysis of the apparent mass data originally described in the 1989 paper by Fairley and Griffin. The objective was to establish the best mass-spring-damper representation of a seated adult in the vertical direction for use in applications such as seat testing. Two single degree of freedom models and two dual degree of freedom models were fit to the experimental data using either the magnitude of the apparent mass, or the phase, or both in combination. Fits were performed to the data of each of the 60 individuals of the original experimental programme. A two degree of freedom model with structural support (Figure 2.60) was found to be the best representation. The model representing the collective average of all 60 individuals had the parameters K_1=35,007 N/m, C_1=815 Ns/m, K_2=33,254 N/m, C_2=484 Ns/m, M=5.6 kg, M_1=36.2 kg, M_2=8.9 kg and total mass (sum of M_1, M_2 and M_3) equal to 50.7 kg.

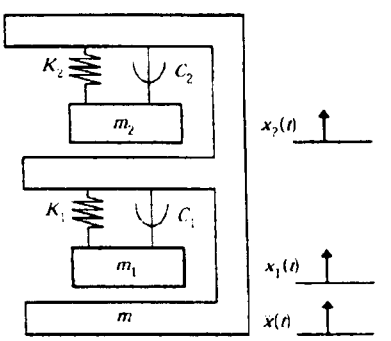

Figure 2.60 Optimal 2 degree of freedom mass-spring-damper model of the seated body in the vertical direction (reproduced from Wei and Griffin 1998)

A 1998 paper by Pankoke, Buck and Woelfel presented a two dimensional linear lumped parameter model of the seated body (Figure 2.61). The model included the head, torso, arms, legs, pelvis and a detailed lumbar region consisting of vertebra L3, L4 and L5, viscera and springs representing the major muscle groups. The mass and inertia values were taken from the literature and from previous work by the authors. Stiffness values were taken from the literature and, where missing, were estimated by comparing model output to experimental results by Seidel (Seidel 1995). Damping was handled by assigning modal damping ratios to the undamped eigenvalues and eigenvectors, again by comparison to the experimental findings of Seidel. Subject height and mass could be accommodated in a simple way by means of global changes to the mass and inertia values assigned to the model elements. Modal analysis found 8 natural frequencies in the range from 0 to 20 Hz. Modal

damping ratios were found to be from 5 to 35 percent critical depending on the mode, with the two main externally measurable modes at 4.7 and 7.8 Hz having values of 26 and 20 percent respectively. Good agreement between the model predicted output and the experimental vertical impedance and seat-to-head transmissibility data was found in the range from 0 to 6 Hz.

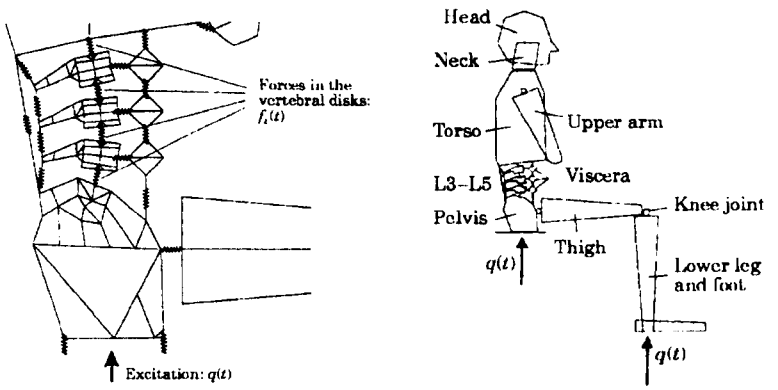

Figure 2.61 Two dimensional linear lumped parameter model of the seated body (reproduced from Pankoke, Buck and Woelfel 1998)

A 1999 paper by Mansfield and Lunström described the development of a model for representing the apparent mass of the seated body in the fore-and-aft and lateral directions. Since the apparent mass of the human body in the horizontal directions has peaks at 0.7, 2 and 5 Hz, a three degree of freedom mass-spring-damper model was considered appropriate. Six models, each having three degrees of freedom, were fit to 4 apparent mass data sets taken from the literature. A parallel three-mass system was found to provide the best fit across all the data sets attempted.

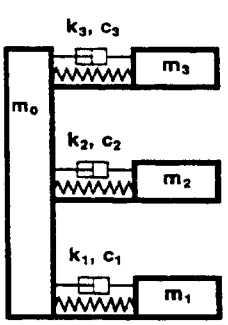

Figure 2.62 Mass-spring-damper model for the fore-and-aft and lateral directions (reproduced from Mansfield and Lunström 1999)

A 2001 report by Denninger and Besnault described the redevelopment of the Lizee et. al. (1998) Finite Element crash test human body model for use in seat vibration studies. A linearised version was developed and the parameters were adjusted by

direct comparison to the 1989 experimental vertical apparent mass and seat-to-head transmissibilities published by Fairley and Griffin. Modal analysis found 12 modes of vibration in the frequency interval from 0 to 16 Hz. Frequency response simulation confirmed that the highest externally measured seat-to-head transmissibility values were at 4.8 and 12.7 Hz (see Figure 2.63). Modal damping ratios of 1% produced apparent mass and seat-to-head transmissibility functions which contained evident peaks associated with each of the natural frequencies of the model. Use of more biologically realistic modal damping ratio such as 20% critical obscured the smaller modes, leaving only the two familiar externally measurable resonances at 4.8 and 12.7 Hz.

Figure 2.63 First nine natural frequencies of the finite element model of Denninger and Besnault (reproduced from Denninger and Besnault 2001)

The year 2001 saw the publication of a thoroughly revised edition of ISO standard 5982, now titled *"Mechanical vibration and shock - range of idealised values to characterise seated-body biodynamic response under vertical vibration"*. The new edition defined minimum, maximum and mean curves of idealised driving point mechanical impedance, apparent mass and seat-to-head transmissibility A three degree of freedom mass-spring-damper model was provided to represent the driving point mechanical impedance and apparent mass of the body in the seated posture.

The model was stated to be representative of (a) a posture described as erect seated without backrest support, with feet supported and vibrated, (b) subject mass in the range from 49 to 93 kg and (c) unweighted sinusoidal or random input acceleration amplitudes between 0.5 and 3.0 m/s^2 with the predominance of frequencies within the range from 0.5 to 20 Hz. While specifying the model for use in representing the driving point properties of the body, ISO 5982 states that mass m_2 can be *tentatively* used for determining seat-to-head transmissibility.

Table B.1 — Values for the parameters of the model (body mass of 75 kg)

Parameter	Mass kg				Stiffness N/m			Damping coefficient N·s/m		
	m_0	m_1	m_2	m_3	k_1	k_2	k_3	c_1	c_2	c_3
Value	2	6	2	45	$9{,}99 \times 10^3$	$3{,}44 \times 10^4$	$3{,}62 \times 10^4$	387	234	$1{,}39 \times 10^3$

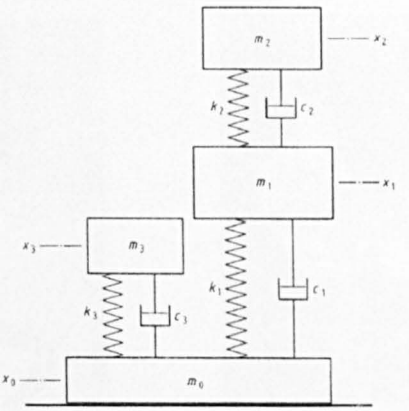

Figure 2.64 Vertical mass-spring-damper model of the seated human body specified by ISO standard 5982 (reproduced from ISO 5982:2001 (E))

2.7 Studies Involving Primates

In an effort to find a convenient surrogate for use in scientific investigations of whole-body vibration several researchers have studied the vibration response properties of primates. The anatomical and cognitive characteristics of these creatures provide many similarities to humans. This section describes the most influential studies found in the literature.

A 1971 paper by Broderson and Von Gierke described a test apparatus (Figure 2.65) for measuring the driving point mechanical impedance of Rhesus monkeys and presented data for two subjects weighing 14.5 and 17 lbs. Both swept sine and stationary sine testing were performed. The impedance curves of both animals were

similar to those of humans and had large peaks at frequencies in the region from 6 to 8 Hz. Stroboscopic examination suggested a large abdomen response at 6 Hz and a large spine (back) response at 8 Hz. The authors evaluated the effect of test duration by measuring responses at the beginning and end of a 1 hour exposure period. The average mechanical impedance was found to drop with vibration exposure, with most of the change occurring in the first 10 minutes of the test due to muscle fatigue. The authors suggested that this implied that short test times would be expected to mask the response of any body systems which are readily suppressed by tightening of the muscles. Broderson and Von Gierke concluded their paper by presenting a two-mass single degree of freedom linear model of their 14.5 pound test subject (Figure 2.66).

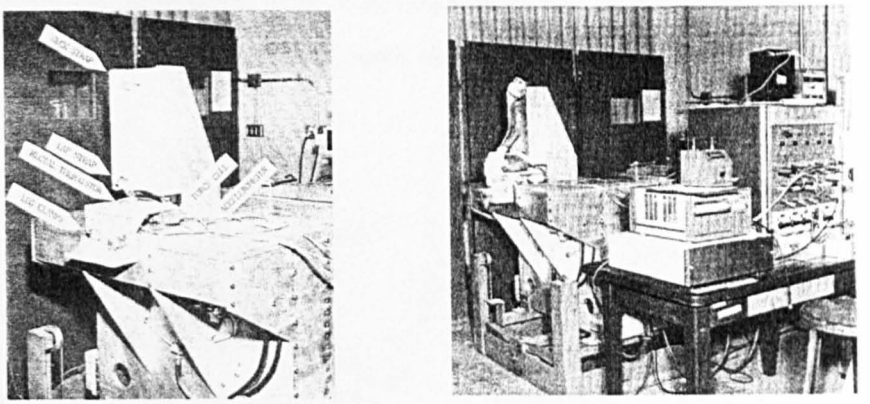

Figure 2.65 Two views of the experimental apparatus developed for testing Rhesus monkeys (reproduced from Broderson and Von Gierke 1971)

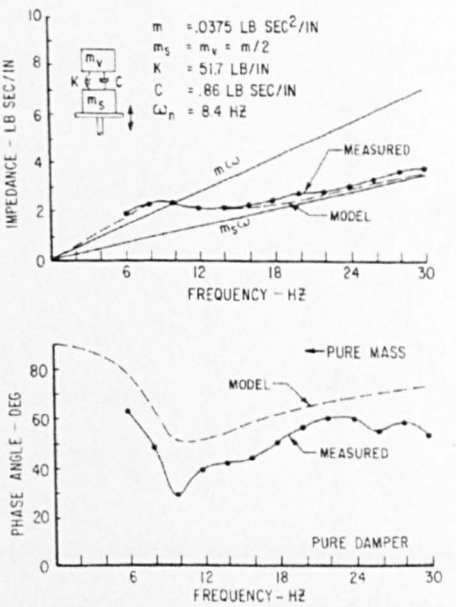

Figure 2.66 Impedance of a 14.5 lb Rhesus monkey and of its single degree of freedom model (reproduced from Broderson and Von Gierke 1971)

A 1976 paper by Edwards, Lafferty and Knapp presented driving point mechanical impedance from tests of 6 Rhesus monkeys and 18 dogs in a sitting posture. The tests were performed using sinusoidal excitation in the range from 2 to 30 Hz at peak amplitudes of 0.5 and 1.0 g. The impedance modulus data was normalised by the animal's body weight. A single degree of freedom model (see Figure 2.67) of the type used previously by Broderson and Von Gierke was fit to each animal at each frequency, obtaining individual mass, spring and damper coefficients for each frequency. Plots of the parameters versus frequency showed that all values changed with frequency, suggesting that the single degree of freedom model was insufficient to represent the measured dynamics. The impedance curves and model parameters were found to differ between the monkeys and the dogs, with the dogs generally showing higher stiffness values but lower damping coefficients (Figure 2.68).

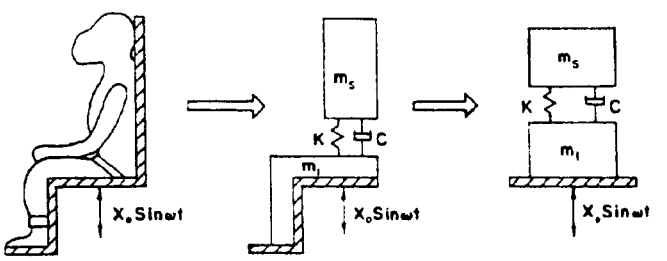

Figure 2.67 One degree of mass-spring-damper model used by Edwards et. al. (reproduced from Edwards et. al. 1976)

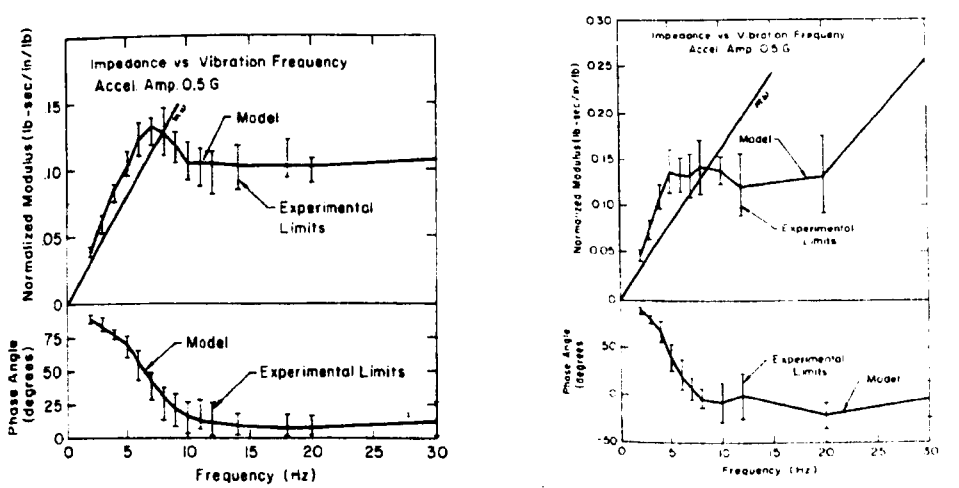

Figure 2.68 Driving point mechanical impedance curves for a group of Rhesus monkeys (left) and a group of dogs (right) in the seated posture (reproduced from Edwards et. al. 1976)

A 1982 paper by Quandieu and Pellieux presented a surgical implantation technique for fixing miniature accelerometers directly to the lumbar vertebra in primates and for running the associated wiring harnesses to the scalp where connection could be made to the data acquisition system. The accelerometers were attached by means of clips to the anterior surface of the L4, L5, L6 and L7 vertebrae, in an area clear of muscle tissue so as to not affect the animal's normal movement. Eleven baboons underwent the surgery which lasted 10 hours on average. All the animals were sufficiently healthy to be exposed to vibration 6 days postoperatively. Seated vibration tests performed using a restraining chair showed high coherency for all vertebral channels up to frequencies in excess of 80 Hz. The anaesthetised baboons were tested under 0.1 g r.m.s. vertical acceleration at frequencies from 0 to 100 Hz. The main resonance was found at 16 Hz, higher than for humans.

A 1985 study by Slonim measured the whole-body characteristics of a group of primates consisting of 4 Rhesus monkeys (Macaca mulatta) and three baboons (Papio papio). The Rhesus monkeys were 7 to 8 years in age while the baboons were 4 to 5 years in age. All primates were males and were of similar size with masses in the range from 8 to 17 kg. Each animal underwent surgical implantation of two vertically aligned accelerometers, one at L5 and the other at T3, along with necessary wiring and connectors. Four days after surgery each animal was exposed to vertical sinusoidal vibration in the seated posture at frequencies in the range from 4 to 50 Hz at two acceleration levels, 0.177 and 0.283 g r.m.s.. Impedance curves, seat-to-L5, seat-to-T3 and L5-to-T3 transmissibility were determined for each animal each day for four consecutive days. Average impedance modulus showed peaks for the Rhesus monkeys at 8, 20 and 35 Hz while the average curves for the baboons showed peaks at 7, 18 and 40 Hz (see Figure 2.69). Seat-to-T3 transmissibility showed a dominant resonance in the range from 6 to 12 Hz for the Rhesus monkeys and 5 to 10 Hz for the baboons (see Figure 2.70). Impedance and transmissibility results obtained with the two different test amplitudes were similar, leading Slonim to state that the response of the primates was approximately linear over the range tested. Least squares regression was used to determine the parameters of a Broderson-Von Gierke primate model for each animal. Slonim discussed the degree of similarity found between the two primates and concluded by stating that "the Rhesus monkey appears to be as good a model as the more expensive and less

available baboon in evaluating the effects of biomechanical stress on the body with the aim of extrapolating the results to humans".

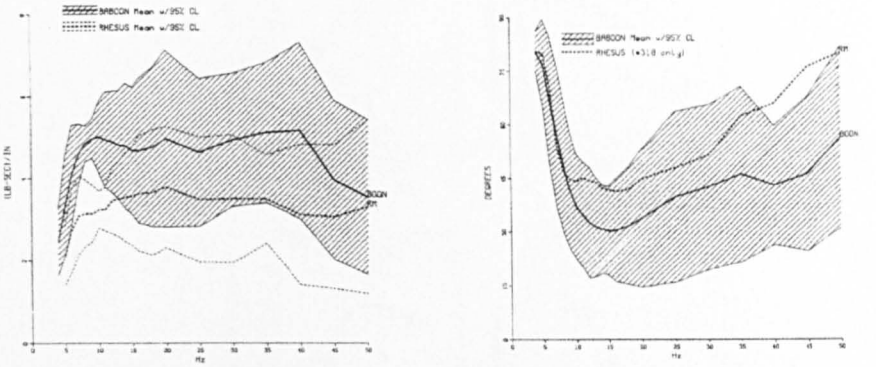

Figure 2.69 Average and 95 percentile driving point impedance modulus and phase for the Rhesus and baboon primates (reproduced from Slonim 1985)

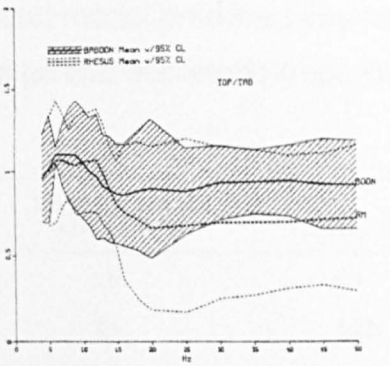

Figure 2.70 Average and 95th percentile seat-to-T3 transmissibility for the Rhesus and baboon primates (reproduced from Slonim 1985)

A 1992 paper by Smith presented impedance data and mass-spring-damper models for four Mucaca Mulatta Rhesus monkeys. A device for accommodating the sedated animals in a sitting posture incorporated load cells for measuring the transmitted forces and an accelerometer for measuring the imparted motion. Sinusoidal vibration tests were performed at 13 frequencies from 3 to 20 Hz using a peak acceleration level of 0.5 g. A total of 84 tests were performed, 24 of which were repeated tests performed at fixed intervals over a two week period in order to evaluate intra-subject variability. The impedance curves (Figure 2.71) were found to show only a single peak at 10 Hz for all tests. The damping factor was found to be about 0.47 in all cases. A two-mass single degree of freedom model was fit to the data of each animal and the results were compared to the previous studies by Broderson and Von Gierke (1971), Slonim (1985) and Smith (1991) as shown in Table 2.1.

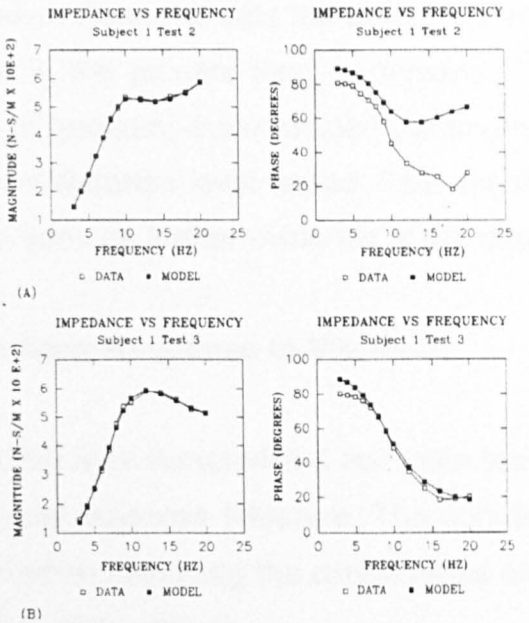

Figure 2.71 Experimental and model predicted impedance curves for one rhesus monkey tested on two occasions (reproduced from Smith 1992)

	Broderson and von Gierke (1971)	Slonim (1985)	Smith (1991)
Peak g	1.0	0.4	0.5
Natural frequency (undamped, Hz)	8.4	9.22*	10.24
Stiffness coeff. (10^{-3} N m^{-1})	9.054	25.304 ± 12.73	15.190 ± 5.80
Damping coeff. (10^{-3} N s m^{-1})	0.1506	0.4496 ± 0.1396	0.2317 ± 0.1224
Total mass (kg)	6.574	7.534 ± 2.803	6.672 ± 0.604
Mass ratio (R)	1.0	≈0	0.988
Damping factor	0.309	0.515	0.472
S.E.E (10^{-2} N s m^{-1})	—	0.245†	0.060

Table 2.1 Optimal model parameter values obtained for Rhesus monkeys (reproduced from Smith 1992)

A 1994 study by Smith and Kazarian investigated the effects of acceleration amplitude on the impedance curves of three Rhesus monkeys. Smith's 1992 apparatus was used for testing the sedated animals in the vertical direction. Sinusoidal signals at 13 frequencies from 3 to 20 Hz were again used but this time two r.m.s. amplitudes, 0.69 and 3.37 m/s^2, were attempted. The impedance curves for the three animals had a main peak in the region from 9 to 14 Hz which was described as motion of the upper torso. A secondary peak was found for the lower amplitude tests at about 5 Hz, which was described as being due to the dynamics of the legs. Significant decreases occurred in the frequency of the primary impedance

peak with increasing acceleration amplitude, establishing that the vibration response of the animal was nonlinear. From the data the authors concluded that the degree of nonlinearity was greater in the primate than in humans. The authors presented a three mass, two degree of freedom, linear lumped parameter model of the primate fit to the data from each acceleration level tested. The variation in parameter values with input amplitude was seen as further evidence of the degree of nonlinearity.

2.8 Summary of Whole-body Response to Vibration

The intention of this section is to summarise a few main features which emerge from the whole-body mechanical response literature. The concepts described here were taken into consideration when designing the experiments and interpreting the results described in later chapters of this thesis.

Average Mechanical Properties: Due to the statistical variance associated with human measurements most studies have averaged data for several subjects or several experimental conditions. While not without drawbacks, most studies average the experimentally measured response curves or the fitted model parameters.

Inter-Subject Variability: Most research points to inter-subject variability as the most important of the independent test parameters. This variability makes it difficult to identify physical phenomena from tests of only a single subject. Most studies have been performed using 6 to 15 subjects. Several have used test groups of 60 or more individuals when the objective has been to determine the statistical distribution of the response data.

Intra-Subject Variability: Most research suggests that whole-body measurements will vary for the same individual from test to test due to variation in physical constitution, posture, muscle tension or nervous state. Intra-subject variability of a response variable has been shown to normally be within +/- 10% for frequencies up to 20 Hz. All findings suggest that intra-subject variability is smaller than inter-subject variability.

Whole-Body Frequency Response Functions: Human response to vibration has most often be quantified by means of driving point mechanical impedance, apparent mass

and transmissibility. Transmissibilities along the same vibrational axis have been measured as have transmissibilities in which the output and input quantities are aligned along different axis. For transmissibility functions most authors have consistently referred to peaks as "resonances". For the human testing application the use of this term is preferred to that of "natural frequency" since biological tissue is highly damped. Many authors also use the term "resonance" for peaks in the measured impedance and apparent mass functions. This is in error, as a peak in a ratio of force to motion is an anti-resonance.

Linearity: Most whole-body vibration studies point to the fact that the human body is characterised by a highly nonlinear response. The degree of nonlinearity is most evident in the case of high strain rates or high dynamic loadings such as ejection testing and centrifuge testing. Under these conditions body resonances can change by as much as 4 to 5 Hz from their nominal values. Many studies have shown, however, that for low strain rates and low dynamic loadings such as those of road transport the response of the body can be treated, to a first approximation, as linear.

Normalisation: In human testing the size and mass of the individual greatly affect several of the engineering measurements involved. The engineering measurements involving force (mechanical impedance, apparent mass and absorbed power) are regularly normalised by the static mass of the test subject. Mass normalisation reduces the inter-subject variability of the data and facilitates the comparison of response properties.

Frequencies and Amplitudes of Whole-Body Vibration: Due to the highly dissipative nature of the body and to the inertia values of its component parts, high frequency energy does not easily propagate to regions distant from the source of excitation. For this reason the frequency range associated with the concept of whole-body vibration is normally taken to be from 0 to 100 Hz, with most studies involving seats actually being limited to the range 0 to 20 Hz. Based on the intended application and the ethical considerations involved, whole-body testing is normally performed using acceleration amplitudes in the range from 0.25 to 2 m/s^2 with maximum test amplitudes reaching 5 m/s^2 in some applications.

Whole-Body Resonance Frequencies Measured Under Vertical Vibration: The research surveyed in this chapter suggests the existence of several large, externally measurable, whole-body resonances for adult humans. Transmissibilities measured in the vertical direction for the seated posture normally show a dominant peak in the region from 4 to 6 Hz while a second peak is normally found from 8 to 16 Hz. The first appears to consist of vertical and fore-and-aft movement of the trunk over the elasticity of the buttocks tissue. The second appears to involve mostly trunk movement caused by spinal bending and pelvic rotation. Various and complex movements of the head with respect to the trunk have been reported. The range of frequencies of these reports is from 20 to 40 Hz, with the movement and frequency of resonance being highly dependent on the test conditions.

Whole-Body Resonance Frequencies Measured Under Horizontal Vibration: The number of studies treating the horizontal directions (fore-and-aft or lateral) are far fewer than the vertical. Nevertheless, the research surveyed in this chapter suggests the existence of several large, externally measurable, whole-body resonances for adult humans. From transmissibility measurements in the horizontal direction for the seated posture resonances have been systematically reported in the region from 0.7 to 4 Hz. At least one, but more likely two resonance movements occur for average adults in the region around 1 Hz. Reports of 3 to 4 Hz movements appear to occur mostly at high amplitudes due to energy transfer between the fore-and-aft and the vertical directions.

Whole-Body Anti-Resonance Frequencies Measured Under Vertical Vibration: Driving point mechanical impedance or apparent mass functions measured for seated adults under vertical vibration normally show a first dominant peak from 4 to 6 Hz and a second smaller peak from 8 to 15 Hz.

Whole-Body Anti-Resonance Frequencies Measured Under Horizontal Vibration: Driving point mechanical impedance or apparent mass functions measured for seated adults under horizontal vibration normally show a first, and dominant, peak in the region from 2 to 5 Hz and a second, smaller, peak from 5 to 7 Hz.

Damping: The human body has been found in all studies to be highly damped, with damping ratios normally in the range from 0.25 to 0.6 for the main, externally

measurable resonance responses. Numerical models of the body have shown that numerous whole-body resonances, other than the two main externally measurable resonances, emerge when damping levels are lowered below 5 to 10 percent critical. This suggests that the damping levels involved make it impossible to identify many important vibration behaviours from external measurements

Whole-Body Vibration Models: At least two categories of whole-body vibration model are in common use. The first can be described as an impedance, or loading, model which represents the effect of the body on other engineering structures such as seats. These models typically consist of linear mass-spring-damper systems, but a few nonlinear lumped parameter systems can also be found in the literature. The second model type can be described as a human response model, which represents in detail the biological components contributing to the whole-body response. Such models are used to gain an understanding of the dynamic mechanisms of the body and are today most often developed using the multi-body or finite element methods. In the early literature mass-spring-damper models often served in both roles.

2.9 Vibration Testing Methodologies for Vehicle Seating Systems

Before proceeding in this thesis to describe the whole-body vibration research and the seat vibration tests performed for children, it is useful to briefly describe the testing of vehicular primary seating systems and to provide an example of a typical industrial procedure. While not a systematic review of the subject, the material serves to identify some of the concepts commonly encountered when attempting to characterise the vibrational properties of vehicle seats. The material is useful for evaluating the possible problems that may be encountered when trying to define future vibration testing standards for child safety seats.

The vibration isolation properties of seats have been the subject of numerous investigations since the first studies of human response to vibration in the 1940s. Seating systems are recognised as playing a fundamental role in providing both comfort and health effects protection to humans. The importance of the system has lead to numerous investigations of adult whole-body response and of the effect of seat design parameters on vibration transmissibility. The research studies have lead to the development of testing procedures which are today in common use. Standards

such as *BS 30326-1 (1994) Mechanical vibration – Laboratory method for evaluating vehicle seat vibration* or *ISO 10326-1 (1992)* of the same name specify procedures for testing the vertical vibration isolation properties of a seat. Sensor characteristics (floor accelerometer and SAE pad), the method of loading the seat (a 5^{th} percentile and a 95 percentile human subject), a criteria for choosing the vibration input (mission signal), the appropriate frequency weighting to use to represent human response and a method for summarising the test results (S.E.A.T. index) are all specified. These standards are used for testing the seats of agricultural tractors, off-road vehicles, heavy lorries and numerous other forms of transport.

Due to the development costs involved all major vehicle manufacturers and seat system manufacturers also have individual in-house vibration testing methods. These methods are conceptually similar to general standards such as BS 30326-1 and ISO 10326-1. For example, human test subjects are widely used to provide a representative impedance loading on seats during testing. Methods define a fixed number of subjects for testing each seat, varying from 1 or 2 to as many 15 in some cases. Since both the test subjects and the seats themselves can show signs of nonlinearity it is currently considered important to test seats using vibration signals which are representative of the operating conditions encountered in the vehicle. Industrial test methods are normally based on the use of one or more mission signals which correspond to selected road inputs. One approach to mission signal selection used by several vehicle manufacturers is to assign a specific road surface from the testing centre to each standard driving condition identified from marketing surveys. For example, city driving might be assigned a pave' test surface, country driving might be assigned a test track with broken asphalt segments and highway driving might be assigned a smooth asphalt surface. Examples of the frequency spectra of typical mission signals for city, country and highway driving are presented in Figure 2.72. The response of a seat to a battery of different signals is expected to provide a global evaluation of the ability of the seat to isolate its occupants from the vibrations expected in the vehicle. A separate vibration test is normally performed for each condition and the set of test results can either be analysed directly or the individual results can be averaged together, each result weighted by either the number of kilometres or the average amount of time the average driver is expected to travel over the road surface in a given year.

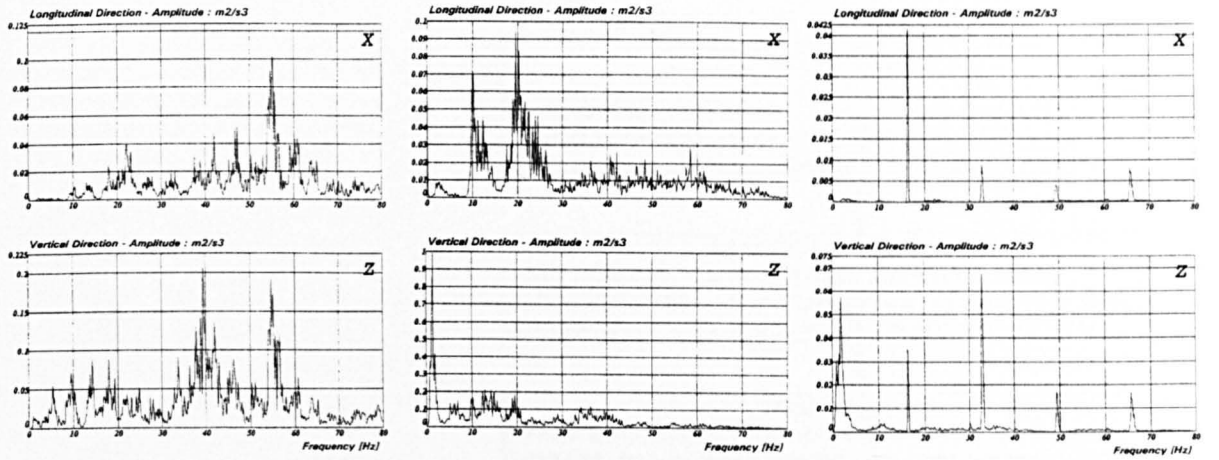

Figure 2.72 Acceleration power spectral densities of 3 mission signals in the fore-and-aft (X) and vertical (Z) directions for city (left), country (centre) and motorway driving (right). (reproduced from Giacomin and Bracco 1995)

Another component that is common to current industrial seat testing procedures is the use of a simple method for summarising the overall frequency response of the seat in a given direction by means of a single number. Most methods quantify seat vibration isolation by means of the Seat Effective Amplitude Transmissibility (Griffin 1990). The S.E.A.T. index is defined as

$$S.E.A.T.[\%] = \frac{\int_0^T W^2(\omega) G_{YY}(\omega)\, d\omega}{\int_0^T W^2(\omega) G_{XX}(\omega)\, d\omega} [100] \qquad (2.14)$$

where $G_{XX}(\omega)$ is the acceleration power spectral density of the input vibration signal at the bench surface at the base of the seat, $G_{YY}(\omega)$ is the acceleration power spectral density measured by means of an SAE pad at the interface between seat and human occupant, $W^2(\omega)$ is the appropriate frequency weighting for the vibration direction in question, ω is a frequency and T is the time duration of the test signal. The S.E.A.T. index applies the appropriate frequency weighting at both the seat input and output measurement points, then integrates both signals and takes the ratio of the two. The result is a single number which represents the ratio of the vibrational disturbance felt on the seat to that which would have been felt if the seat were perfectly rigid over the frequency range considered.

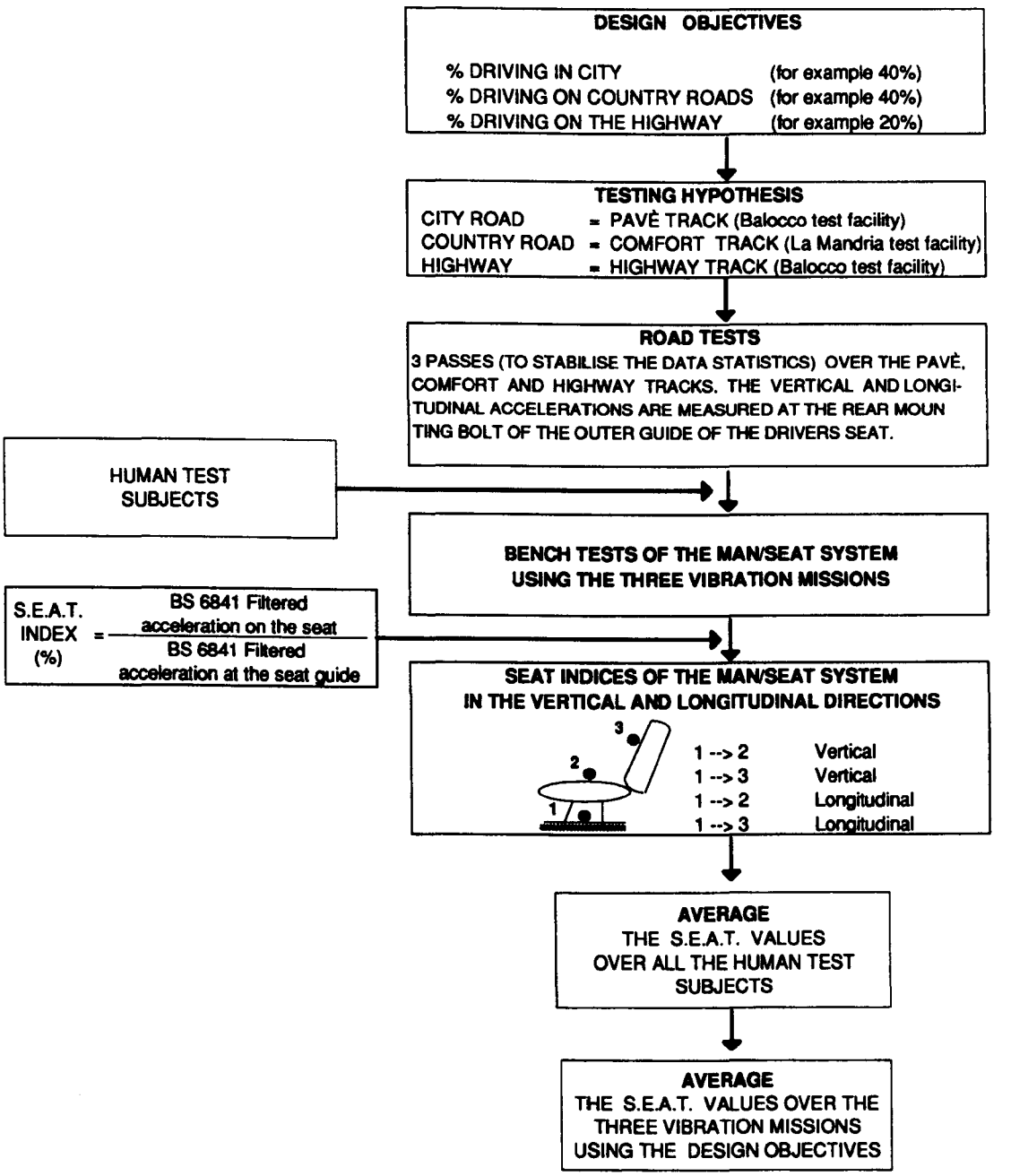

Figure 2.73 A two-axis vibrational comfort testing procedure used for automobile seats (reproduced from Giacomin and Bracco 1995)

Figure 2.73 provides a typical two-axis industrial vibrational comfort testing procedure for automobile seats, first described in 1995 by Giacomin and Bracco. Marketing data for the target automobile was used to determine the percentages of city, country and highway driving for the vehicle. Each driving scenario was then assigned a specific test surface from the company proving grounds over which the target vehicle was tested to determine the acceleration signals to apply at the base of the seat in the laboratory. Laboratory tests with 12 subjects measured the accelerations at the

base of the seat and at the human interfaces (using SAE pads) at the cushion and backrest in both the vertical and fore-and-aft directions. S.E.A.T. values were determined for each human interface in each direct for each mission. A final weighted average S.E.A.T. value was determined using the kilometric driving percentages associated with the mission signals, again from marketing statistics.

The sequence of operations described above can be considered representative of the industrial seat testing methods in current use. Future experimental procedures for measuring the vibration isolation properties of child safety seats will, due to the similarity in physical principles involved, be based on similar techniques. An awareness of current vehicle seta testing methodology may be useful when judging the motivations for, and the importance of, the tests described in this thesis.

Chapter 3

Measurement of the Whole-Body Vibration Response of Small Children

3.1 Introduction

For mechanically coupled person-machine systems the role of the human body in determining the overall dynamic response is greatly dependent on the ratio of body mass to machine mass. The dynamic forces contributed by the human element of the system are normally only considered during machine design when they are large enough to represent a sizable percentage to total sum of forces. In the case of automobiles, which have typical mass values from 700 to 1800 kg, the inertia and stiffness forces contributed by a typical adult human with mass in the range from 50 to 110 kg are relatively small. The mass ratio (human mass divided by machine mass) in this case varies from 3 to 15 percent. For such vehicles chassis design and seat design progress largely in parallel since neglecting the human body does not greatly affect the accuracy of ride and handling predictions. For smaller vehicles such

as mopeds, scooters and motorcycles the machine mass is in the range from 45 to 360 kg implying mass ratios from 14 to 245 percent. In this case human body forces cannot be neglected, rather, they may be the fundamental forces in the case of the lightest machines.

For child seats which have their own "suspension system" consisting of vehicle seat stiffness and safety belt tension the mass ratio is even less favourable than for 2 wheeled vehicles. Stage 0&1 seats have masses which are within the range from 1 to 4 kg and are used by child occupants with masses ranging from 1 to 18 kg. The resulting mass ratios of 25 to 1800 percent suggest that any analysis of the coupled system must start with an understanding of the human response properties involved.

From the review of the human vibration literature no response data or models were found for small children. It was therefore decided to follow the example of investigations performed for adult humans and primates by testing children to determine their apparent mass and absorbed power properties. Such tests require the simultaneous measurement of driving point force and movement. Since for land transport the vertical axis is normally the direction of highest vibration, it was decided to investigate the behaviour of the child body along that axis. Apparent mass and absorbed power results for adults suggest that the frequency range of seated whole-body response can be taken to be approximately 0 to 20 Hz. Given the lack of knowledge regarding the dynamic behaviour of children, however, it was decided to test frequencies up to at least 30 Hz. Consideration of the intended application also suggested that the children be tested in a posture that can be considered typical of stage 0&1 seats.

A test facility was needed to achieve the above requirements. Essential elements of the device would be a vibration exciter, vibration platform, rigid seat, force and motion sensors and appropriate control and acquisition systems. As with other investigations involving humans the design of the hardware, software and laboratory protocol were heavily influenced by health, safety and ethical considerations. Besides considering the best practice which emerges from the scientific literature it was also possible to evaluate choices against the general guidelines provided by British Standard 7085 "*Safety Aspects of Experiments in Which People are Exposed*

to Mechanical Vibration and Shock" of 1989. The standard, which is currently the only one of similar scope available from national or international standardisation bodies, provides guidelines regarding the hardware, software, protocol and reporting aspects of human vibration testing. Appendix A provides a systematic comparison between the BS7085 recommended practice and the characteristics of the facility developed for testing children. Specific safety concerns are discussed in the text that follows when the choice of test facility characteristics has been effected.

This chapter describes the test facility and test protocol developed for performing whole-body vibration measurements of children under 20 kg in mass in the seated posture. Apparent mass curves, mass-spring-damper models and absorbed power curves are presented for 8 children tested over the frequency range from 1 to 45 Hz. The apparent mass and absorbed power characteristics of the children are compared to those found in the research literature for adults. The chapter concludes by analysing the allometric relationship between body mass and vibration response for primates, children and adults, and discusses the implications of the findings.

3.2 Child Vibration Testing Facility

3.2.1 Choice of Vibration Exciter, Control System and Sensors

The choice of vibration exciter and vibration control system was made with the primary objective of providing a safe environment for the children who would be tested. BS7085 identifies two primary risk factors in human testing (a) use of mechanical vibration or shock that is too severe in terms of magnitude or duration and (b) failure to exclude from testing a subject who is medically unfit. Minimisation of the risks inherent in point (a) suggested the use of the smallest possible excitation system capable of imparting to a child of mass in the expected range from 2 to 18 kilograms a vibration similar to what occurs in vehicles. A Ling Dynamic Systems (LDS) V406 permanent magnet shaker and accompanying PA100E electronic power amplifier were chosen. With natural convective cooling the unit was rated at a maximum peak sine force of 98 N and a maximum random force (measured in accordance to ISO5344) of 38 N. With the expectation that the combined moving mass of the system (test subject, rigid seat, vibration platform, bearings, shaker coil

and sensors) would be at least 20 kg, the V406 would be incapable of imparting accelerations greater than 5 m/s^2 to the child. More than any other factor, the limited force production capability of the exciter provided the fundamental safety guarantee.

Also specified in BS7085 are recommended characteristics for human testing control systems. A three level control strategy is suggested in which an *input monitor* maintains the calculated control signals within specified movement or force values, a *platen motion monitor* maintains hardware motion or force within pre-established limits independently of controller output, and a *system monitor* continuously assesses the function and state of the various components, initiating a shutdown procedure if any individual element shows signs of malfunction. In an attempt to match the complex and independent safety functions of the three monitors the vibration control system chosen was the Endurance Monitor (EMON) software system (LMS International 1999) coupled to a DIFA SCADASII electronic frontend unit. The SCADAS II frontend contained 4 output channels, 12 input channels, A/D and D/A converters and a hardware DSP chip implementing Fourier and correlation functions. The EMON software permitted the setting of numerical limits on the test force and acceleration in accordance with the *input monitor* principle. These limits were set to the lowest values compatible with the research requirements which were 2.0 m/s^2 peak acceleration and 100 N peak transmitted force. The principle of *platen motion monitor* was partially fulfilled by the use of a DIFA SCADAS Shutdown Control Unit which incorporated both a large manual emergency shutdown button accessible to the test operator and an emergency soft-stop condenser circuit for bringing the exciter to rest in the case of power or sensor failures. The principle of *system monitor* was partially fulfilled by the use of the PA100E electronic power amplifier which incorporated a core overheating and an overvoltage interrupt which shut down the voltage supply in the event of a failure condition.

Calculation of apparent mass or absorbed power requires the simultaneous acquisition of the input acceleration acting on the human body and the response force produced. The acceleration was measured by means of a micro-strain-gauge ENTRAN EGAS-FT-25 accelerometer fixed to the lower surface of a rigid seat. The accelerometer (S/N 981344) was rated to a maximum acceleration of 25 g, had a sensitivity of 3.66 mV/g with 15 volts supply and had a natural frequency of 730 Hz.

As in the work of Coermann (1961) the force transmitted to the rigid seat was measured by means of three transducers placed at the apexes of a triangle. The three load cells were micro-strain-gauge ENTRAN type ELH-TC11-500s (S/N 98017, 98018 and 98019) rated as linear to 500 N and having sensitivities of 0.17, 0.16 and 0.16 mV/N with 15 volts supply. Maximum rated loading to failure was 1000 N. The relationships between the control software, the vibration excitor, the sensors and the data acquisition system are presented in the schematic diagram of Figure 3.1 below.

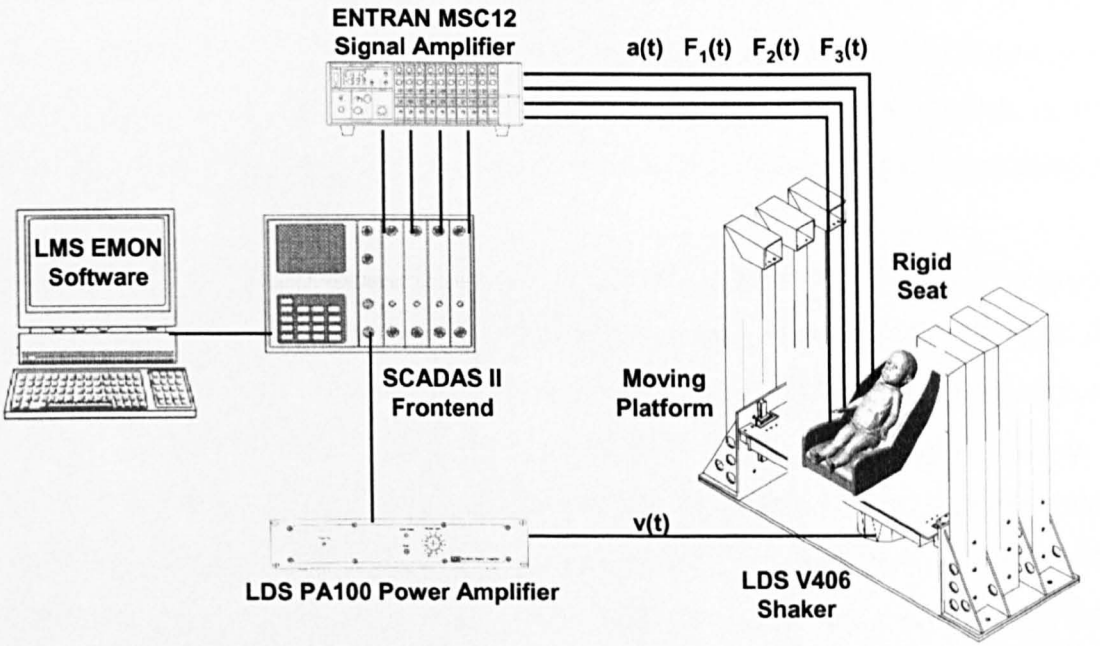

Figure 3.1 Schematic diagram of the child vibration testing facility.

3.2.2 Vibration Platform and Suspension System Design

By their physical nature electrodynamic exciters such as the V406 are unable to maintain constant force preloads for extended periods of time. These devices often incorporate an internal spring, or spider, of sufficiently large resistance to maintain the moving coil in its neutral position (at zero displacement) under gravity loading. The internal spring is insufficient, however, to maintain positioning under loads such as the 18 to 25 kg of the rigid seat and child. A platform and additional external suspension system was therefore required.

The design of the vibration platform was based on three requirements: (1) that the moving mass be sufficiently small to permit the shaker to achieve the required test accelerations, (2) that the platform area be sufficiently large to avoid the child reaching with hands or feet any bench components when sitting restrained and (3) that the platform area be sufficiently large to permit future mounting of commercial child safety seats. Based on these considerations an aluminium platform assembly was designed which was 760 mm long by 405 mm wide. The linear bearings chosen were AccuGlide CG-20CE PB units manufactured by Thomson Industries. The units had friction coefficients between 0.002 and 0.003 and yaw and pitch moment capacity of 125 Nm. Bearing preloading was achieved by means of a sliding wedge block mounted on one side of the platform. By sliding half of the block vertically downwards using adjustment screws various static force levels could be achieved.

Static load support was achieved using a suspension system consisting of a group of linear springs connecting the vibrating platform to support towers on each side of the rig. The deflected length of the linear springs had to be made adjustable since the load acting on the platform changed significantly from test to test due to the difference in mass between children. If left uncompensated, this would have pushed the shaker head away from its neutral position leading to a reduction of the maximum achievable test amplitude. The number of springs used also had to be made adjustable so that suspension stiffness could be varied with mass loading. Stiffness adjustment permitted the natural frequency of the system to be kept below 1 Hz, avoiding the frequency range of the intended measurements.

Provision was made for a maximum of 16 equal springs whose deflected length could be adjusted by means of screws and washers. Each had an undeflected length of 290mm and stiffness of 90 N/mm. A calibration table containing the recommended number of springs for use with each loading was produced such that the natural frequency of the moving mass (child, rigid seat, platform, coil and sensors) could be kept below 1 Hz. The overall design of the vibration platform is illustrated in Figures 3.2 to 3.4.

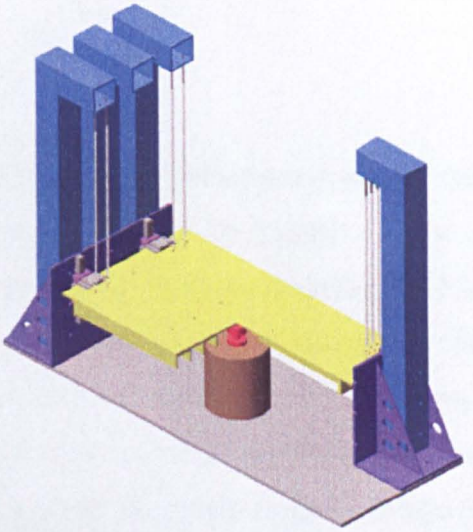

Figure 3.2 Shaker, vibration platform and platform suspension system.

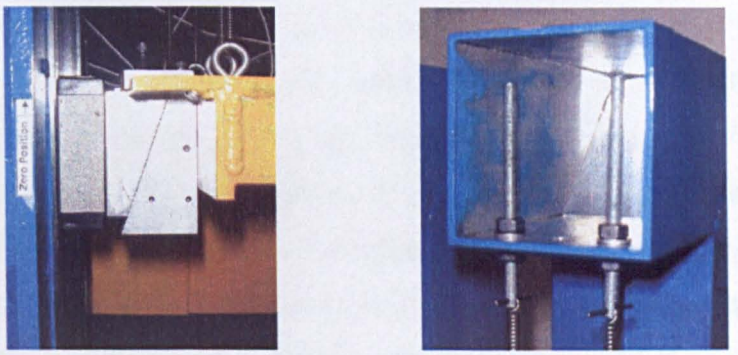

Figure 3.3 Platform suspension features: sliding wedge block for preloading the bearings (left) and tensioning rods for positioning the platform (right).

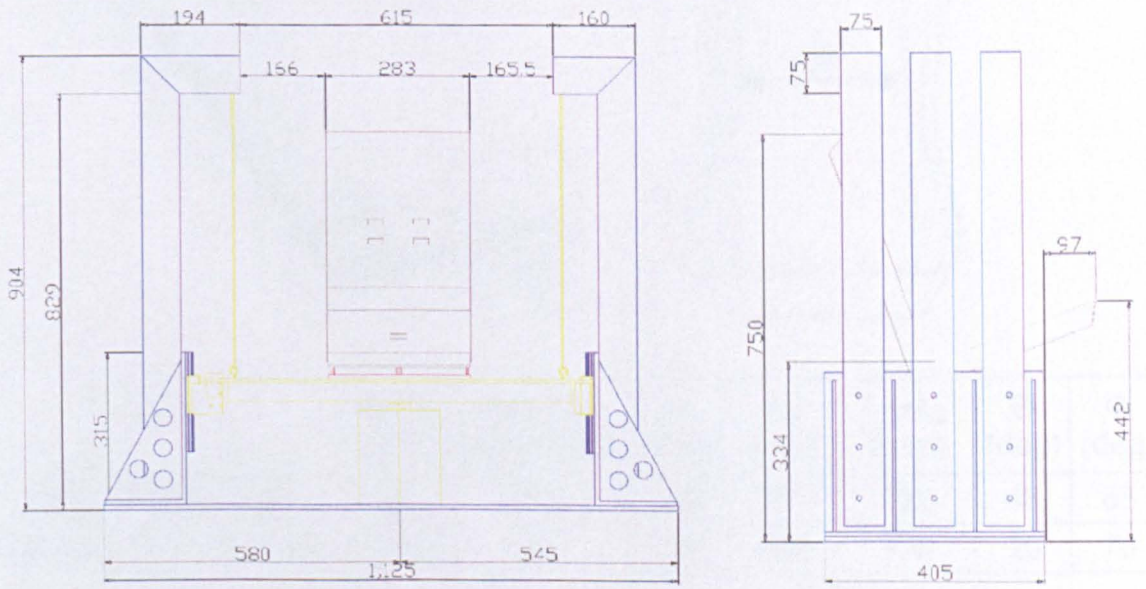

Figure 3.4 Front and side views of child test rig showing the principal dimensions.

3.2.3 Rigid Seat Design

The geometry of the rigid seat was determined based on child anthropometric data and geometric data from commercial seats. Tilley (1993) provides average anthropometric measurements for humans starting from age 2 months. For children of 9 to 11 months of age the average total length of the supine body is 730 mm, while the average buttock-to-head distance is 480 mm and the total width (inter-acromion distance) is 208 mm. For commercial child seats four parameters were chosen to define the sitting posture: lower section length (L_1), backrest section length (L_2), included angle between the two sections (Φ) and the seat angle with respect to the horizontal (Θ). While the first three parameters are independent, the seat angle with respect to the horizontal varies as a function of the shape of the vehicle seat and the tension applied through the belts. In order to facilitate comparisons measurements were performed on a flat horizontal surface. Two stage 0&1 child seats were taken to be representative of the most common designs and were measured. The smaller of the two was a Britax Rock-A-Bye while the larger was the Mothercare Rock 'n' Go. Each product had a geometry which was typical of a class of similar stage 0&1 seats found in stores. In particular, the Mothercare product used a plastic frame which appeared to be an outsourced component common to several manufacturers. The postural parameters for the two seats are presented below.

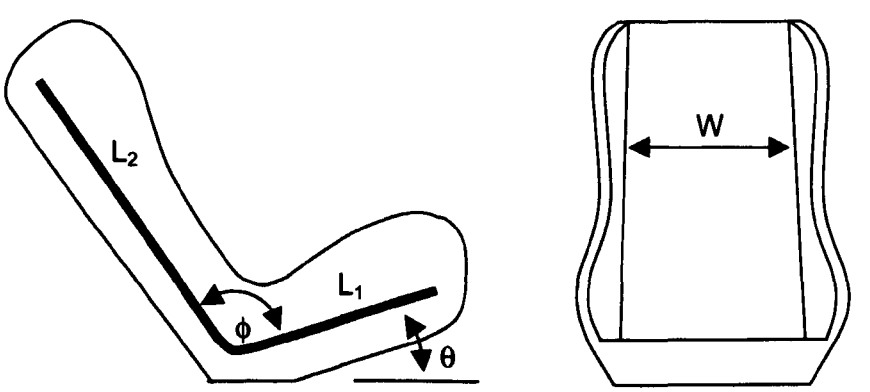

Seat	Mass (kg)	Internal Width (mm)	L_1 (mm)	L_2 (mm)	L_1+L_2 (mm)	Θ (deg)	Φ (deg)
Britax Rock-A-Bye	2.5	240	270	450	720	43	85
Mothercare Rock 'n' Go	2.8	280	290	440	730	20	70

Table 3.1 Sitting posture parameters for two stage 0&1 child seats.

Based on the anthropmetric and geometric data a seat basket was designed which had a lower section length (L_1) of 300 mm, a backrest section length (L_2) of 450 mm and a width of 280 mm. An included angle Φ of 90 degrees was chosen and a somewhat vertical posture of 20 degrees with respect to the horizontal (Θ) was used for the lower section (see Figure 3.5). The basket was fabricated of 1.5 mm thick aluminium sheet which was cut to pattern, bent into shape and spot welded at points along the joining lines. A base section to support the basket and to provide a mounting surface for the sensors was machined out of solid aluminium stock. The base section was 146 mm long, 65 mm at its highest point and 280 mm wide. The basket and base section were spot welded together at several points to form the rigid seat. Lateral drilling into the base section was used to remove material until a mass of exactly 3.0 kilograms was achieved for the complete unit. Natural frequencies estimated for the unit using simplified models suggested a first resonance greater than 170 Hz.

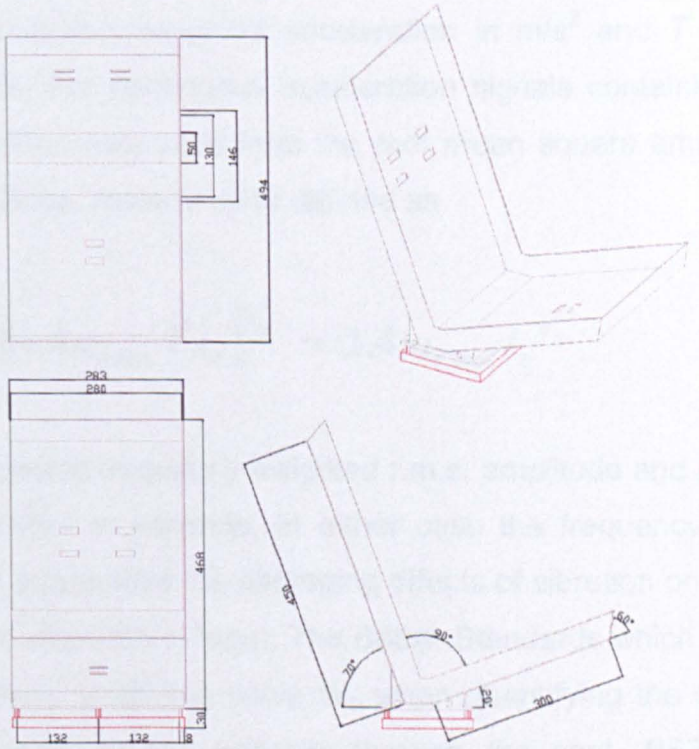

Figure 3.5 Four views of the rigid seat used for measuring child apparent mass.

In line with the safety guidelines of BS7085, and in order to minimise child movement during testing, the rigid seat was equipped with restraining belts from a Mothercare

Rock 'n' Go product. Mounting holes of approximately the same size as in the Rock 'n' Go were perforated into the lower and upper sections of the rigid seat at approximately the same location. The belts were fastened in the same manner by passing them through the holes and by blocking them from behind using the plastic clips moulded into the terminus of each belt.

3.2.4 Choice of Acceleration Test Signals

The principal requirement of human vibration testing is to keep the total energy of the exposure to a minimum. All recent vibration standards such as BS 7085 specify that vibration exposure should be measured in terms of the *Vibration Dose Value (VDV)*

$$VDV = \left[\int_0^T a^4(t)\,dt\right]^{1/4} \qquad (3.1)$$

where *a(t)* is the frequency-weighted acceleration in m/s^2 and *T* is the period of exposure in seconds. For continuous acceleration signals containing few transient events the VDV is often estimated from the root mean square amplitude using the *estimated vibration Dose Value (eVDV)* defined as

$$eVDV = \left[(1.4\,a_{r.m.s.})^4 t_o\right]^{1/4} = 1.4\,a_{r.m.s.}\,t_o^{1/4} \qquad (3.2)$$

where $a_{r.m.s.}$ is the overall frequency weighted r.m.s. amplitude and t_o is the length of the exposure measured in seconds. In either case the frequency-weighting curve (Figure 3.6) used to summarise the damaging effects of vibration on the human body varies with point and direction of input. The British Standards which treat whole-body vibration use frequency weighting curve W_b when quantifying the effects of vertical direction vibration input to the buttocks through the seat. BS7085 specifies a frequency weighted VDV value of 15 $m/s^{1.75}$ as the health and safety action level above which a medical officer should be present for all tests. Table 3.2 presents the frequency weighted r.m.s. values which produce 15 $m/s^{1.75}$ VDV for various lengths of exposure. To facilitate comparison with acceleration values from fields other than

human testing the table also presents the unweighted acceleration amplitude of harmonic excitation at three different frequencies which produces 15 $m/s^{1.75}$ VDV exposure. The unweighted amplitudes were determined using the asymptotic approximation values of the W_b filter to remove the effect of the weighting. The amplitudes provided in the table suggest that for exposures lasting a few minutes unweighted r.m.s. levels should generally be kept below about 3 m/s^2 .

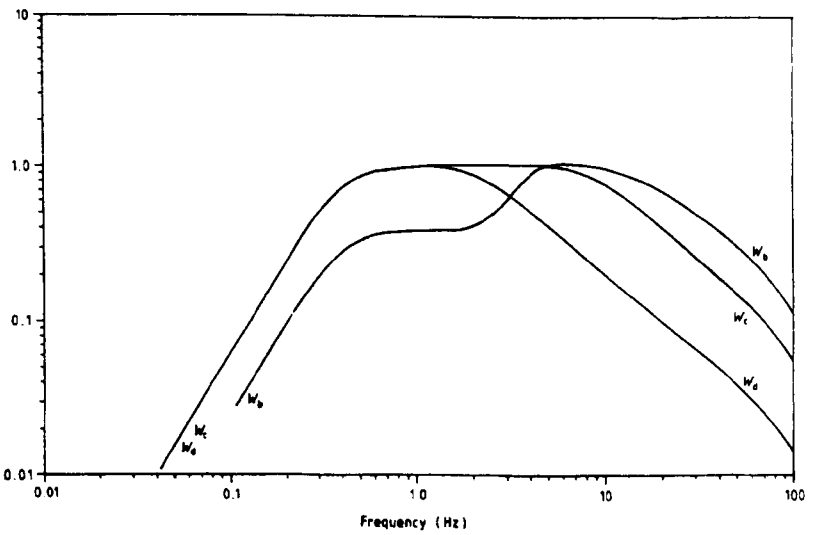

Figure 3.6 Frequency-weightings specified in BS7085 (reproduced from BS 7085)

Exposure Duration	Weighted r.m.s. Acceleration	Unweighted r.m.s. Acceleration of a 1.0 Hz Sine Wave	Unweighted r.m.s. Acceleration of a 10 Hz Sine Wave	Unweighted r.m.s. Acceleration of a 50 Hz Sine Wave
1 second	10.71	26.8	10.7	33.5
4 seconds	7.57	19.0	7.6	23.6
16 seconds	5.36	13.4	5.3	16.7
1 min	3.84	9.6	3.8	12.0
2 min	3.24	8.1	3.2	10.1
4 min	2.72	6.8	2.7	8.5
16 min	1.92	4.8	1.9	6.0
1 hour	1.38	3.5	1.4	4.3
4 hour	0.98	2.4	0.9	3.0
8 hour	0.82	2.1	0.8	2.6

Table 3.2 Weighted and unweighted r.m.s. acceleration amplitudes producing 15 $m/s^{1.75}$ VDV. All values in m/s^2.

Considering the road vehicles in which child seats are transported recent research by Paddan and Griffin (2002) presented frequency weighted acceleration values measured at the seat of 100 vehicles over characteristic, but unspecified, surfaces. Among the vehicles were 25 automobiles. The vertical W_b weighted acceleration was reported for the seat cushion interface with the driver in the vertical direction. The measurements for automobiles spanned a range from 0.25 to 0.61 m/s^2 weighted r.m.s., with a median value of 0.37. The corresponding eVDV values for a 2 minute exposure are from 1.16 to 2.82 with a median value of 1.71. This suggests that vertical vibration at the seat cushion of road vehicles on relatively smooth roads is a factor of 9 lower, on average, than the health and safety action level. Additional useful information is found in *British Standard 6841 Measurement and Evaluation of Human Exposure to Whole-Body Mechanical Vibration and Repeated Shock* of 1987 which provides a discomfort scale based on the use of frequency weighted r.m.s. acceleration amplitudes. The scale, presented in Table 3.3 below, suggests that the vibration levels reported by Paddan and Griffin for the seat interface of automobiles are no more than "a little uncomfortable".

Frequency Weighted r.m.s. Acceleration Amplitude at the Human Interface	**Subjective Discomfort**
Less than 0.315 m/s^2	Not uncomfortable
0.315 to 0.63 m/s^2	A little uncomfortable
0.5 to 1.0 m/s^2	Fairly uncomfortable
0.8 to 1.6 m/s^2	Uncomfortable
1.25 to 2.5 m/s^2	Very uncomfortable
Greater than 2 m/s^2	Extremely uncomfortable

Table 3.3 Frequency weighted acceleration amplitudes corresponding to various levels of subjective discomfort.

Considering the need to render the vibration test as rapid as possible to lower the total exposure it was decided to follow the example of several previous researchers such as Sandover (1978), Fairley and Griffin (1990) and Mansfield and Griffin (1998) who performed measurements using band-limited Gaussian random excitation. This excitation has the ability to measure system response over a given frequency interval

with a single test thus reducing the amount of time the child is requested to sit in the test device and reducing the total exposure. For the child tests a band-limited Gaussian white noise acceleration signal was defined from 1 to 50 Hz using a sampling rate of 200 Hz. Preliminary testing showed that the unweighted input r.m.s. acceleration at the platform needed to be greater than 0.6 m/s^2 to overcome friction in the bearings and to provide a good signal-to-noise ratio. Two drive signals were therefore chosen which had r.m.s. voltage levels of 1400 and 1800 mV corresponding to actuated r.m.s. acceleration levels of approximately 0.8 and 1.2 m/s^2 at the platform and seat. Applying W_b frequency weighting to the platform acceleration resulted in weighted r.m.s. values of approximately 0.52 m/s^2 using the 1400mV signal and 0.75 m/s^2 for the 1800 mV signal. Test signal length for both signals was chosen to be 2 minutes, which lead to VDV values of 10 and 14 $m/s^{1.75}$ respectively. While the frequency weighted r.m.s. levels of 0.52 and 0.75 m/s^2 were somewhat higher than the average levels reported by Paddan and Griffin, the test signals can nonetheless be considered similar to the vibrational environment present in vehicles.

3.2.5 Child Test Bench Calibration and Commissioning

The test rig was calibrated as a complete unit using rigid masses in the place of the child occupant. Four steel blocks, each of length 25 cm and width 7.5 cm, were cut to various thicknesses to provide total masses of 1.8, 3.8, 7.8 and 15.8 kilograms. An assembly consisting of two threaded rods and two cross members weighting a total of 0.2 kg was used to fasten the masses to the rigid seat so as to provide a pure inertial loading on the device. Band-limited Gaussian random white noise voltage signals were input to the bench through a Finite Impulse Response Filter (FIR) filter designed to compensate the low force output of the V406 at frequencies below 10 Hz. While 1400 mV and 1800 mV drive signals were planned for the actual child tests, the calibration tests were performed at levels from 1000 mV to 1800 mV in steps of 200 mV. Mass loadings of 0 kg, 4 kg, 8 kg and 16 kg were used. The apparent mass modulus curves obtained for the calibration loadings contained errors of less than 2% from 2 to 35 Hz and less than 10 percent over the range from 1 to 42 Hz (see Figures 3.7 and 3.8). Apparent mass phase measured with the rigid masses was less precise. For a pure mass the acceleration input and force output should be

in phase and thus exhibit a phase angle of zero degrees. The measured phase angles increased from +1 degree to a maximum of +8 degrees at 45 Hz.

All modulus and phase curves obtained for the calibration loadings were similar. Unlike the apparent mass results presented later in this chapter for the children, the calibration data was left in its original form, thus the apparent mass modulus is the sum of the test load *and* the 3 kg mass of the rigid seat. Mass compensation was performed for all child results by subtracting 3 kilograms from the real part of the apparent mass function at each frequency. No compensation was performed for the absorbed power results since a rigid mass cannot absorb energy.

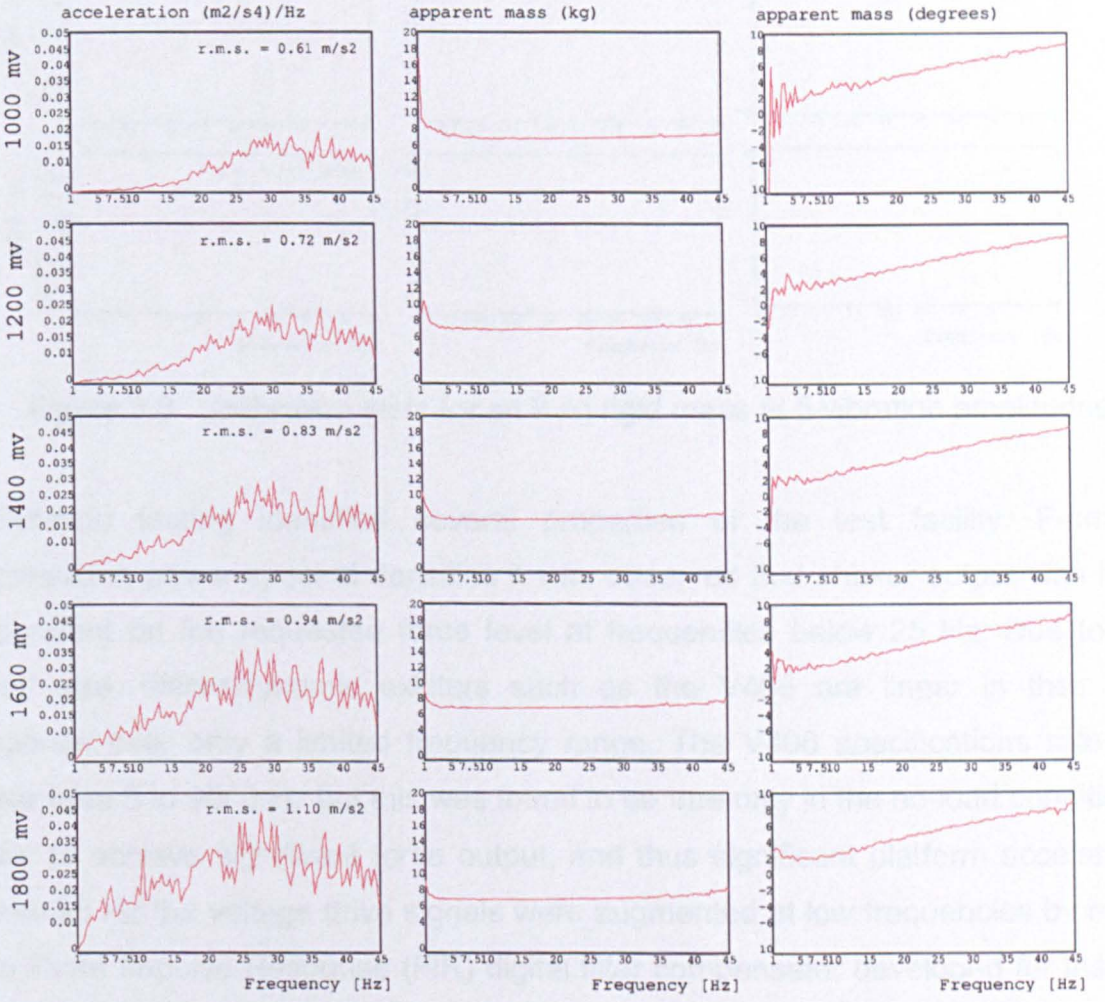

Figure 3.7 Calibration tests for a 4 kg rigid mass at 5 vibration amplitudes.

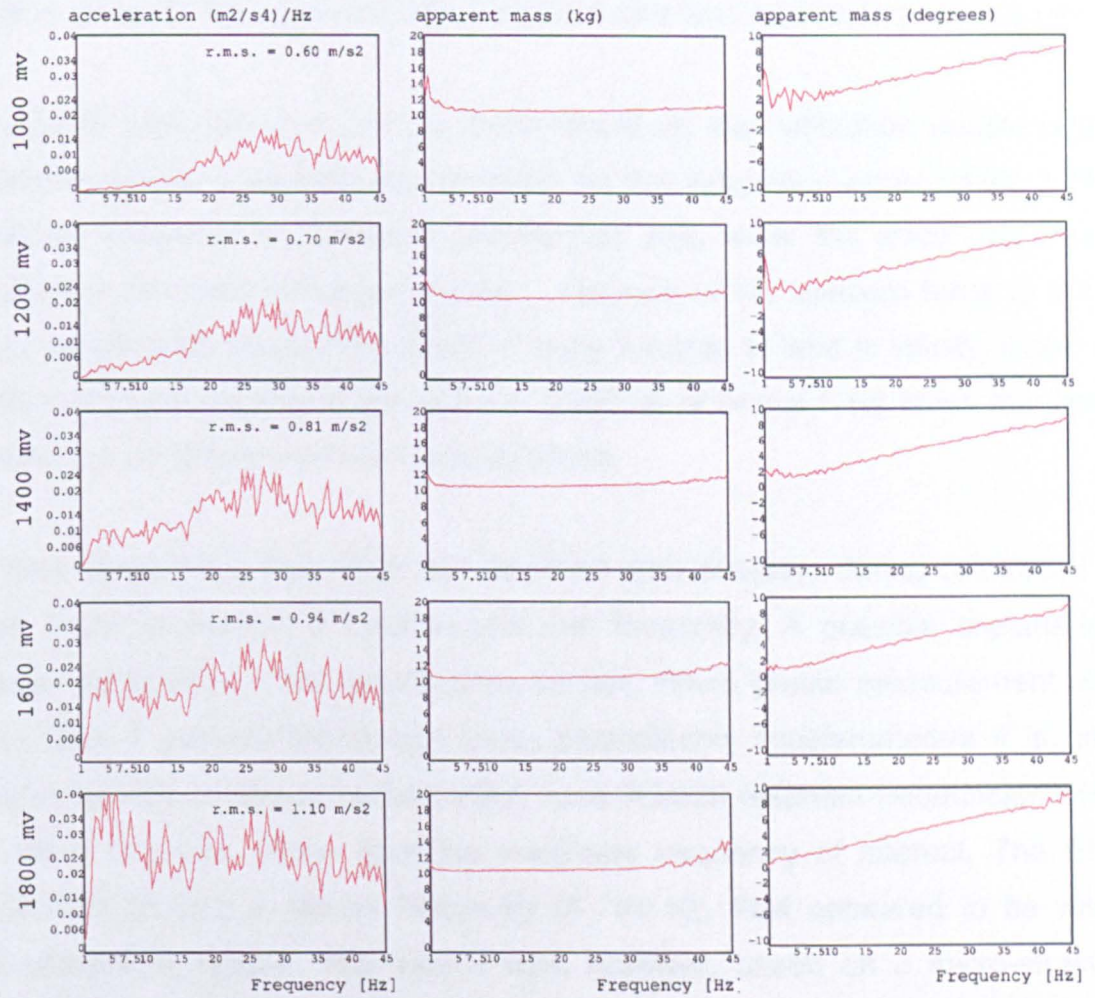

Figure 3.8 Calibration tests for an 8 kg rigid mass at 5 vibration amplitudes.

Calibration testing identified several properties of the test facility. From the acceleration power spectral densities it was observed that shaker output was highly dependent on the requested force level at frequencies below 25 Hz. Due to their small size, electrodynamic exciters such as the V406 are linear in their force response over only a limited frequency range. The V406 specifications rate it as linear from 5 to 9000 Hz but this was found to be true only in the no-load condition. In order to achieve significant force output, and thus significant platform acceleration, below 25 Hz the voltage drive signals were augmented at low frequencies by means of a Finite Impulse Response (FIR) digital filter compensator developed for the child testing application. Figures 3.7 and 3.8 show that use of the compensator filter achieved acceptably constant platform acceleration levels but that it was not possible to completely eliminate all variation with test amplitude. Fully compensated input signals would have required either the development of a compensator filter for each

child loading and each test amplitude, or the purchase of a closed loop controller, neither or which was possible within the time and cost restraints of the research.

A second comment that can be made based on the calibration results is that the modulus curves monotonically increase as the frequency approached 1 Hz. The platform acceleration amplitude approached zero while the static and movement loading of the child remained nonzero. The ratio of the nonzero force to the nearly zero acceleration caused the apparent mass function to tend to infinity. Given that no tests produced significant acceleration levels at or below 1 Hz these low frequency peaks can be considered numerical artefacts.

A third comment is that all phase response data obtained during calibration testing was found to contain a positive drift with frequency. A possible explanation was phase retardation of the acceleration sensor. When phase measurement errors of less than 1 percent are sought using piezoelectric accelerometers it is generally recommended to chose models which have internal resonant frequencies which are at least 10 times higher than the maximum frequency of interest. The ENTRAN EGAS-FT-25 had a natural frequency of 730 Hz, thus appeared to be within the recommended values. The sensor was, however, based on a micro-strain-gauge device and had a much larger internal damping value than normally found for piezoelectric units. Given the damping ratio of 0.66 specified by the manufacturer an estimate of the phase error is obtained by treating the sensor as a single degree of freedom system and determining its phase response as

$$\theta[radians] \approx Q \frac{f/f_n}{1-\left(f/f_n\right)^2} = \frac{1}{2\xi\sqrt{1-\xi^2}} \frac{f/f_n}{1-\left(f/f_n\right)^2}$$

where Q is the quality factor, ξ the damping ratio, f_n the natural frequency of the sensor and f the frequency of interest. For the EGAS-FT-25 this expression suggested a value of 3.6 degrees at 45 Hz, insufficient to explain the measurements. Considering instead the force measurement it is known that the dynamics of the structure being tested can interact with the sensor causing errors in the force signal.

McConnell (1995) derived an expression for this interaction error in the case of a sensor placed between exciter and vibrating structure. If the vibrating structure under test is treated to a first approximation as a single degree of freedom system the error ratio (ER) between the true force and the force measured by the sensor can be expressed in terms of the properties of the test object as

$$ER = \frac{1 - r^2 + j2\xi r}{1 - (1+M)r^2 + j2\xi r}$$

where r in the dimensionless frequency ratio with respect to the test object, ξ is the damping ratio of the test object and M is the ratio between the seismic mass of the sensor and the moving mass of the structure. If modulus and phase angle of the error ratio are plotted for realistic mass ratio and damping values for the child rig (M=0.01 and ξ=0.2 in Figure 3.9 below) the total phase error does not exceed 2 degrees, again insufficient to explain the measurements.

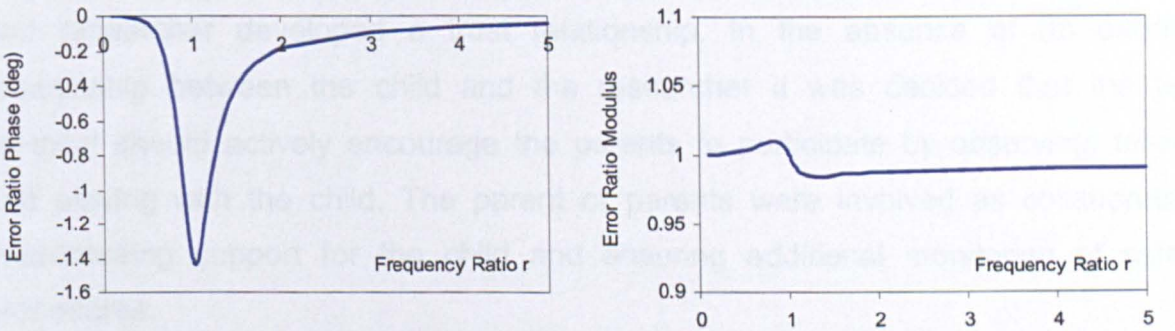

Figure 3.9 Error ratio modulus and phase for a force sensor with mass ratio of 0.01 and a structure with damping ratio 0.2.

Geometric installation errors such as accelerometer or load cell misalignment were also excluded as possible explanations since geometric errors would affect only the measured modulus, not the phase. It was therefore concluded that at least one of the sensors had a larger than specified phase error. Since phase accuracy was found to be lower than modulus accuracy, the modulus information was considered the main research finding and was taken as the basis for developments such as the mass-spring-damper models of the child body presented later in this chapter.

3.2.6 Issues Specific to Child Testing

3.2.6.1 Child Happiness

Though not clearly articulated in current ethical codes such as the code of practice of the American Psychological Association (1992), the Canadian Tri-Council Policy Statement (1998) or the code of practice of the Society for Research in Child Development (described in Berk 1997), ethical and practical considerations suggested that child happiness should be maximised during testing. Additionally, an unhappy child would be expected to move about, reducing the accuracy of the response data. In an extreme scenario a crying child would be expected to trigger a request for test interruption by the concerned parent, leading to loss of all data.

Several steps were taken to maximise child happiness during their time in the laboratory and during testing. First, *parental presence* was considered fundamental during all phases of the testing. Given the time constraints on both the researcher and the parents it was not possible to arrange preparatory sessions in which the child and researcher developed a trust relationship. In the absence of an existing relationship between the child and the researcher it was decided that the test protocol should actively encourage the parents to participate by observing, talking and playing with the child. The parent or parents were involved as collaborators guaranteeing support for the child and ensuring additional monitoring of safety procedures.

A second aspect of the test protocol aimed at ensuring child happiness was a *familiarisation period* upon entering the laboratory which gave the child and parents time to become comfortable with the laboratory environment. This period included the interval in which the aims and methods were explained to the parents, the reading and signing of the consent forms and the time taken to weigh and measure the child. Additional time was taken in some cases to read to the child and help the child play with toys that were kept on hand until the child felt comfortable with the laboratory and with the researcher.

A third feature of the test protocol aimed at ensuring child happiness was the availability of a range of *toys*. A cot mobile was purchased and installed. Numerous figures dealing with Winnie the Pooh characters were pasted to various components of the rig and surrounding laboratory. Several toys including a rattle, chime, doll, stuffed tiger and book were positioned around the bench to render the environment more child-friendly.

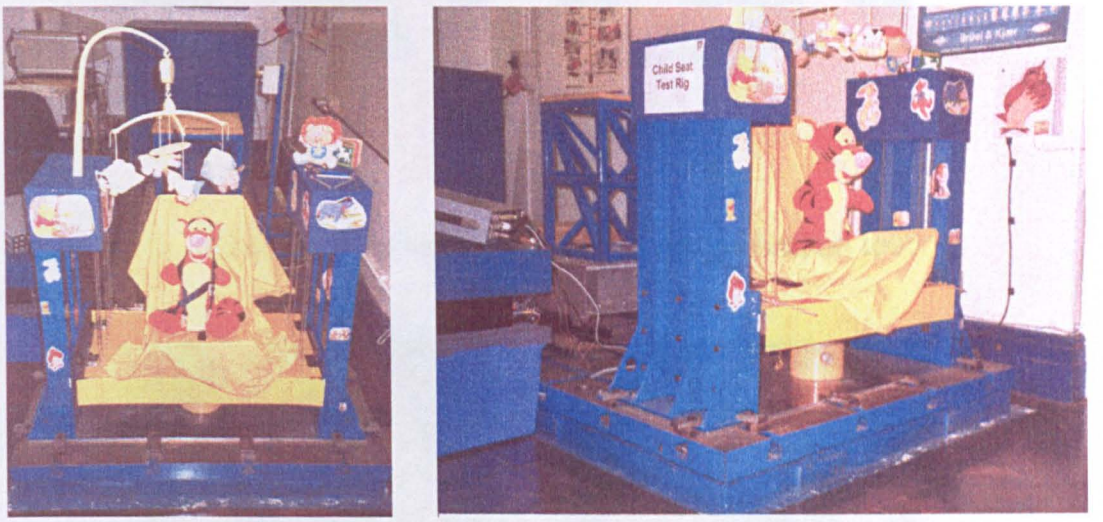

Figure 3.10 Child testing facility as seen by parents and children when entering the laboratory.

3.2.6.2 Child Movement

As early as 1961 Coermann showed that sitting posture had a significant influence on measured driving point mechanical impedance. Recent research such as the 2002 study by Mansfield and Griffin has investigated in great detail the effect of sitting posture on apparent mass, finding changes of as much as 1 Hz in the frequency of resonance and significant changes in response amplitude at and above resonance. Such findings suggested that active movement of the child, involving changes in sitting posture, should be discouraged during testing. One method of minimising child movement was the use of the safety belts which were buckled and adjusted at the start of the test session. Adjusting the belts to their normal operating tension provided an important contribution towards limiting movement. A second method used to reduce child movement was to encourage the child to play with small toys or to have an adult read to the child from a book. Play provided a distraction

which helped limit movement to small motions of the arms and upper body. During most tests both the researcher and a parent actively played with or read to the child.

Figure 3.11 Example of small movements during vibration testing.

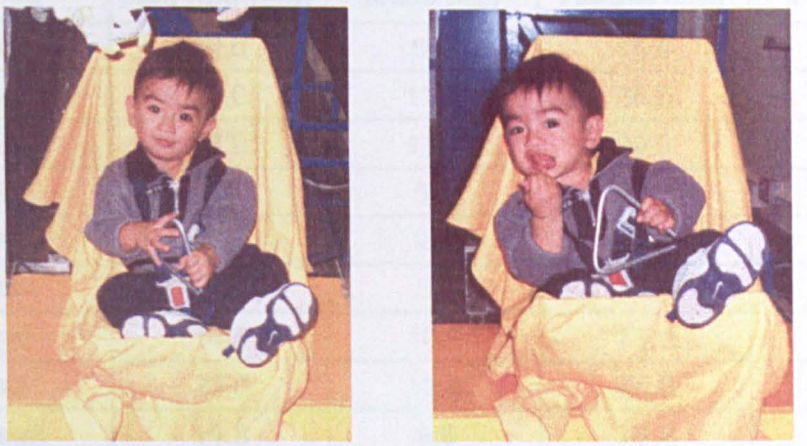

Figure 3.12 Example of large change of posture during vibration testing.

Despite all efforts the nature of children is such that some movement during the vibration exposure was inevitable. Figure 3.11 presents a typical movement consisting of motion of the upper body and arms. Such motions occurred in most tests. Figure 3.12 presents instead an example of a more significant shift in body posture with the subject leaning his upper body to his right and with one leg extended beyond the limits of the rigid seat. Postural shifts of this type were less frequent and readily identifiable in the force time histories of the three load cells. Centre of gravity motion in such cases caused the readings of at least one load cell to drop in mean value while the others increased. Apparent mass and absorbed power calculations performed using data from segments involving postural shifts showed only small differences with respect to the overall average results determined for the complete 2

minute test exposure. Since no procedure for monitoring child posture had been incorporated into the test protocol and since the differences caused by posture appeared smaller than those caused by test signal amplitude, no further reporting of child posture is provided in this thesis.

3.2.7 Test Protocol

Eight children were tested whose ages ranged from 3 to 23 months with a mean value of 11.8. Their weight ranged from 5 to 12.4 kg with a mean value of 9.5 kg while their heights ranged from 50 to 86 cm with a mean value of 73.4 as shown in Table 3.4 below..

Child	Age (months)	Mass (kg)	Height (cm)	Sex (M/F)
al	10.0	9.4	76.0	M
im	15.0	11.0	86.0	M
ja	13.0	11.4	80.0	M
ju	3.0	5.2	50.0	F
le	8.5	9.4	73.0	M
ma	7.0	8.0	66.0	F
mo	14.5	10.2	71.0	F
sa	23.0	12.4	85.0	F
Mean	**11.8**	**9.6**	**73.4**	-
Std.	**6.1**	**2.2**	**11.7**	-

Table 3.4 Test subject characteristics.

Each child was brought by a parent or parents to the test facility and a fixed procedure was followed (Table 3.5). The procedure consisted of the steps defined in Table 3.5. The protocol sought to maximise the safety of all persons involved, to minimise the vibration exposure undergone by the child and to minimise the total amount of time that the child and parents were requested to spend in the laboratory. The information describing the experiments was repeated in the same manner to all the parents using a set of verbal instructions and written consent forms. All test signals and interval times were repeated by means of an automated sequence file developed in the EMON software.

Phase	Tasks Performed and Information Obtained
Research objectives and test method (~4 minutes)	The parents were instructed regarding the research objectives and methods. A detailed verbal description of the safety features of the child testing facility was given. The type and level of acceleration signal used was stated as were the levels normally occurring in automobiles.
Reading and signing of the participation form (~2 minutes)	The parent or parents were asked to read, sign and date the participation form which repeated the main safety and test features.
Child anthropometric measurement (~2 minutes)	Supine length was measured on a table surface and weight was measured using a scale.
Play and familiarisation time (1-10 minutes)	If the child appeared unhappy with the surroundings a period of time was dedicated to play and familiarisation.
Seating and adjustment (~1 minute)	The child was placed in the rigid test seat by the parent and the belt straps were adjusted by the researcher. The cot mobile was activated and play was initiated.
Vibration exposure (~10 minutes)	The child's name and sequence number was entered by the researcher into the EMON software and the automated test procedure was invoked. One complete test sequence consisted of a 2 minute exposure using the 1400mV drive voltage signal followed by the saving of all time histories and transfer functions, followed by the 2 minute 1800 mV drive signal exposure and the saving of all 1800mV time histories and transfer functions. No more than two sequences (8 minutes of total exposure) were performed for any child on a single day.

Table 3.5 Child vibration testing protocol used with all subjects.

3.3 Apparent Mass Functions of Small Children

In this thesis the driving point frequency response function chosen for representing the response properties of children smaller that 20 kg was the apparent mass defined as

$$Apparent\ Mass(j\omega) = AM(j\omega) = \frac{F(j\omega)}{\ddot{x}(j\omega)} \qquad (3.3)$$

where $F(j\omega)$ and $\ddot{x}(j\omega)$ are the Fourier Transforms of the force and acceleration measured at the rigid seat. The apparent mass function was chosen over other representations due to the ease of interpretation (since the modulus approaches the

static mass of the subject as frequency approaches zero) and for ease of comparison to data measured for primates and adults.

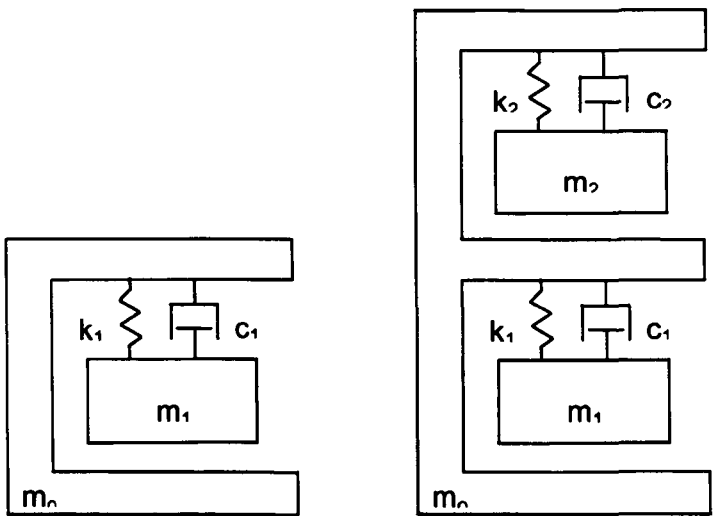

Figure 3.13 Single and dual degree of freedom models of the seated body.

Several authors have shown that single or dual degree of freedom systems (Figure 3.13) with support masses provide accurate representations of the vertical whole-body response properties of seated primates and humans. For the single degree of freedom system with support mass the expression for the driving point apparent mass can be shown to be

$$AM(j\omega) = (m_o + m_1)\left(\frac{k_1 + c_1\omega j}{k_1 - m_1\omega^2 + c_1\omega j}\right) \tag{3.4}$$

which has modulus

$$|AM(j\omega)| = \sqrt{\frac{((m_o + m_1)k_1 - m_o m_1\omega^2)^2 + ((m_o + m_1)c_1\omega)^2}{(k_1 - m_1\omega^2)^2 + (c_1\omega)^2}} \tag{3.5}$$

and phase

$$\angle AM(j\omega) = \tan^{-1}\left(\frac{(m_o + m_1)c_1\omega}{(m_o + m_1)k_1 - m_o m_1\omega^2}\right) - \tan^{-1}\left(\frac{c_1\omega}{k_1 - m_1\omega^2}\right) \tag{3.6}$$

While for the dual degree of freedom with support mass representation the expression for the driving point apparent mass can be shown to be

$$AM(j\omega) = \left(\frac{(a_3 + a_4) + (a_5 + a_6)j}{a_1 + a_2 j} \right) \tag{3.7}$$

where:

$$a_1 = k_1 k_2 - (k_1 m_2 + k_2 m_1)\omega^2 + m_1 m_2 \omega^4 - c_1 c_2 \omega^2$$
$$a_2 = (k_1 c_2 + k_2 c_1)\omega - (m_1 c_2 + m_2 c_1)\omega^3$$
$$a_3 = (m_0 + m_1 + m_2)k_1 k_2 - (m_o m_2 k_1 + m_o m_1 k_2 + m_1 m_2 k_1 + m_1 m_2 k_2)\omega^2$$
$$a_4 = m_0 m_1 m_2 \omega^4 - (m_o c_1 c_2 + m_1 c_1 c_2 + m_2 c_1 c_2)\omega^2$$
$$a_5 = (m_0 + m_1 + m_2)(k_1 c_2 + k_2 c_1)\omega$$
$$a_6 = -(m_0 m_1 c_2 + m_o m_2 c_1 + m_1 m_2 c_2 + m_1 m_2 c_1)\omega^3$$

which has a modulus of

$$|AM(j\omega)| = \sqrt{\frac{(a_3 + a_4)^2 + (a_5 + a_6)^2}{(a_1)^2 + (a_2)^2}} \tag{3.8}$$

and phase

$$\angle AM(j\omega) = \tan^{-1}\left(\frac{a_5 + a_6}{a_3 + a_4} \right) - \tan^{-1}\left(\frac{a_2}{a_1} \right) \tag{3.9}$$

Apparent mass functions were determined for each child using the experimentally acquired force and acceleration time histories. Input, output and cross power spectral densities were determined and an H_v estimate of the apparent mass function was determined. The H_v spectral estimator assumes random measurement error on both the input and output signals and is derived from the H_1 and H_2 estimators (McConnell 1995) defined by

$$H_1(\omega) = \frac{G_{xy}(\omega)}{G_{xx}(\omega)} \qquad and \qquad H_2(\omega) = \frac{G_{yy}(\omega)}{G_{yx}(\omega)}$$

Both H_1 and H_2 provide the same phase since $G_{xy}(\omega)$ and $G_{yx}(\omega)$ are complex conjugates however H_1 provides the more accurate modulus estimates at anti-resonance frequencies while H_2 provides better modulus estimates at resonance. The vector average estimator H_v is defined as the geometric mean of the two

$$H_v(\omega) = \sqrt{H_1(\omega)H_2(\omega)} \tag{3.10}$$

which due to the presence of the complex conjugates leads to only a modulus estimate (phase being taken from either H_1 or H_2) given by

$$\left|H_v(\omega)\right|^2 = \frac{G_{yy}(\omega)}{G_{xx}(\omega)} \tag{3.11}$$

Since H_v is the most frequently used estimator in cases where the measurement noise is not known a-priori it was applied in all cases analysed in this thesis. The H_v estimator was applied to the acceleration and force time histories sampled at 200 Hz. A data block size of 512 points and an overlap of 97% were used leading to a spectral resolution of 0.39 Hz between frequency lines. For the given processing parameters each 2 minute exposure produced a total of 1541 averages. A Hanning window function was used to reduce leakage and all results were plotted as power spectral densities.

Figures 3.14 and 3.15 present the apparent mass modulus and phase functions determined for each of the 8 children at the r.m.s. test amplitudes of 0.8 and 1.2 m/s^2 (1400 and 1800 mV). The response of the child body was found to be relatively linear over the range of amplitudes and frequencies considered. Upon inspection the responses suggest a single degree of freedom as commonly found for primates rather than the dual degree of freedom representation most commonly used with adult humans. Both the modulus and phase responses showed a high level of similarity across the test group. The frequency of peak response modulus (the anti-resonance frequency) occurred in a restricted interval from 5.86 to 7.42 Hz, with a mean value of 6.25 Hz for the group. An interesting observation is that the smallest

child tested, subject ju, was characterised by both the lowest apparent mass modulus and the highest damping ratio. Coherence functions for all subjects were found to be equal to approximately 1.0 over the frequency range from 1 to 45 Hz.

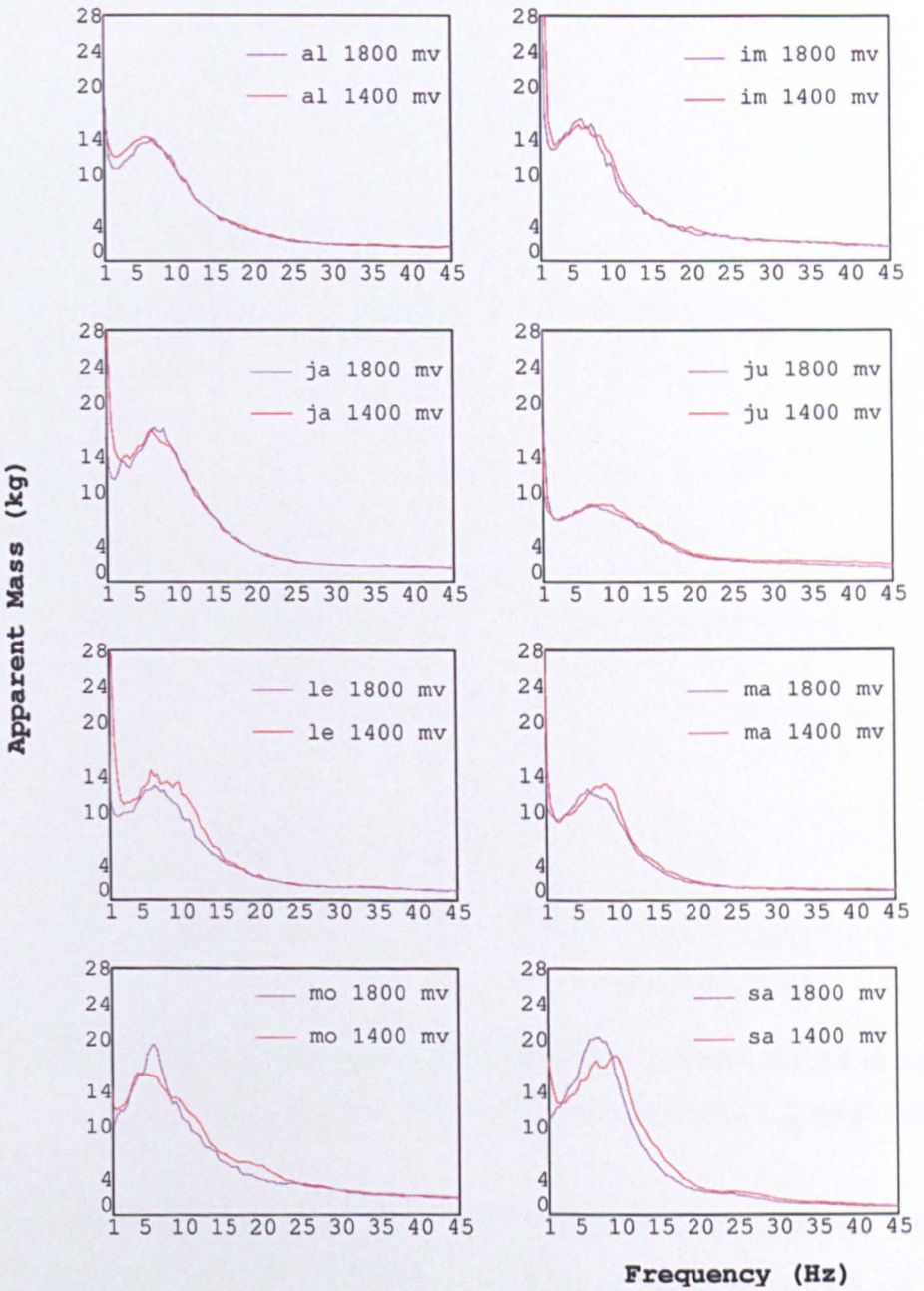

Figure 3.14 Apparent mass modulus functions for 8 children tested at r.m.s. acceleration levels of 0.8 m/s^2 (1400mV) and 1.2 m/s^2 (1800 mV).

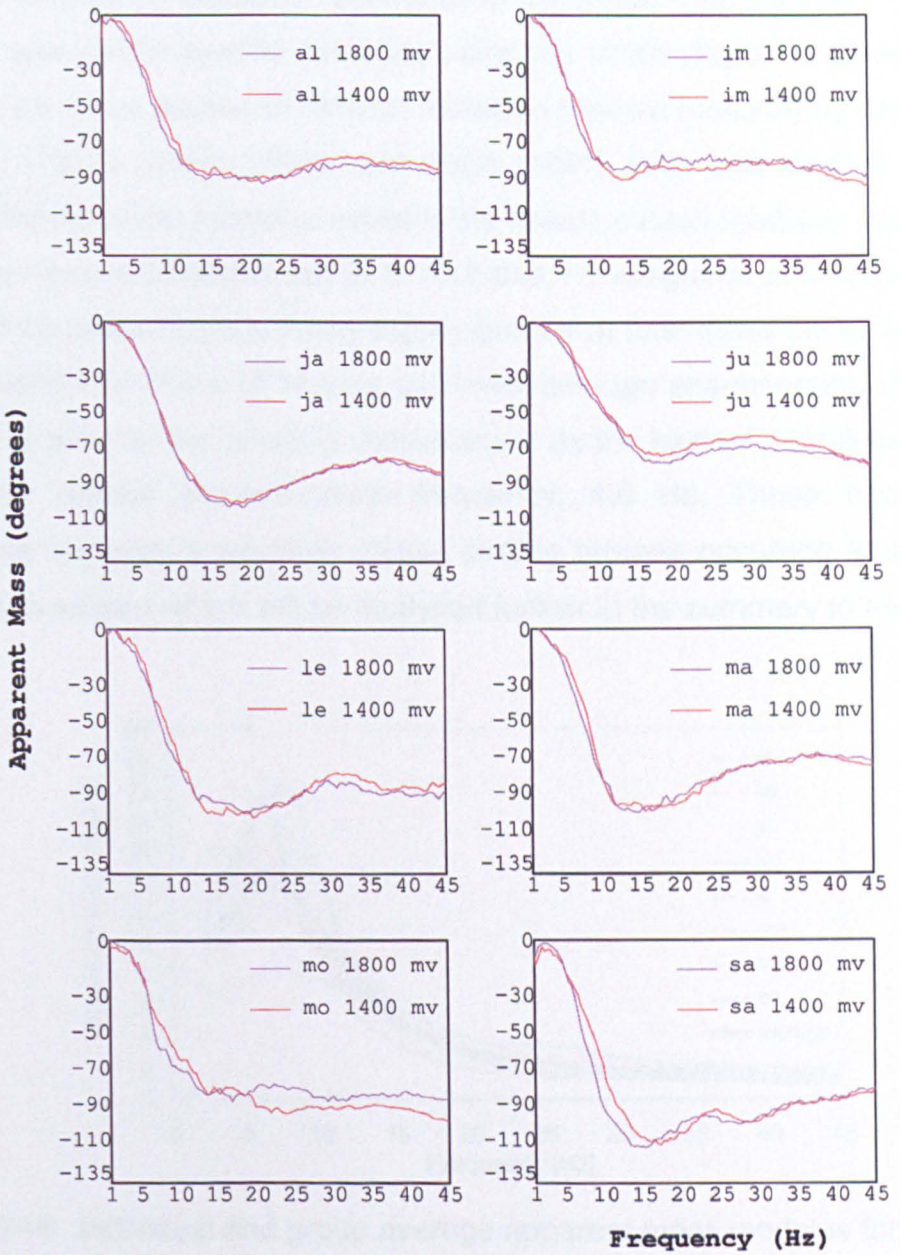

Figure 3.15 Apparent mass phase functions for 8 children tested at r.m.s. acceleration levels of 0.8 m/s^2 (1400mV) and 1.2 m/s^2 (1800 mV).

For the input vibration amplitude of 1.2 m/s^2 Figure 3.16 presents the individual apparent mass modulus curves for the 8 children of mass less than 20 kg and the group average curve. Given the single degree of freedom behaviour and the limited variation in the frequency of anti-resonance it can be seen that the average curve provides a useful representation of the behaviour of the group. Figure 3.17 compares the average apparent mass modulus curve of the children to apparent mass data reported in the literature for adult humans and for primates. The recent International Standards Organisation 5982:2001(E) defines apparent mass modulus and phase

values for erect sitting adults of total mass in the range from 49 to 93 kg. Apparent mass data was determined for primates using the single degree of freedom models reported in the three studies of Rhesus monkeys (mulata mucaca) by Broderson and Von Gierke (1971), Slonim (1985) and Smith (1991). With total masses of the order of 6 to 9 kilograms the monkeys present the lowest overall modulus values and the highest anti-resonant frequencies (8.1, 10.9 and 7.9 kilograms at frequencies of 6.5, 8.0 and 8.5 Hz respectively). Being slightly greater in total mass the children present a higher average modulus of 14.8 kg and lower average anti-resonance frequency of 6.25 Hz. The data for the adults is characterised by the highest overall modulus, 75.4 kg, and the lowest anti-resonance frequency, 4.0 Hz. These apparent mass comparisons suggests a relatively simple scaling process occurring as a function of body mass, a subject which will be analysed further in the summary to this chapter.

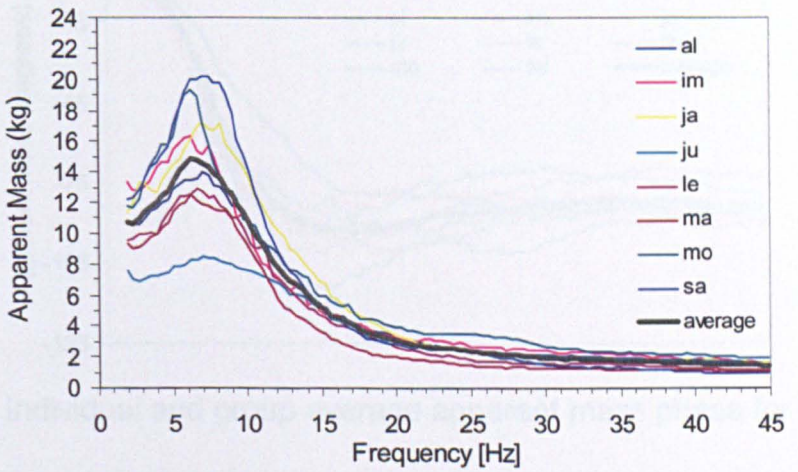

Figure 3.16 Individual and group average apparent mass modulus for 8 children.

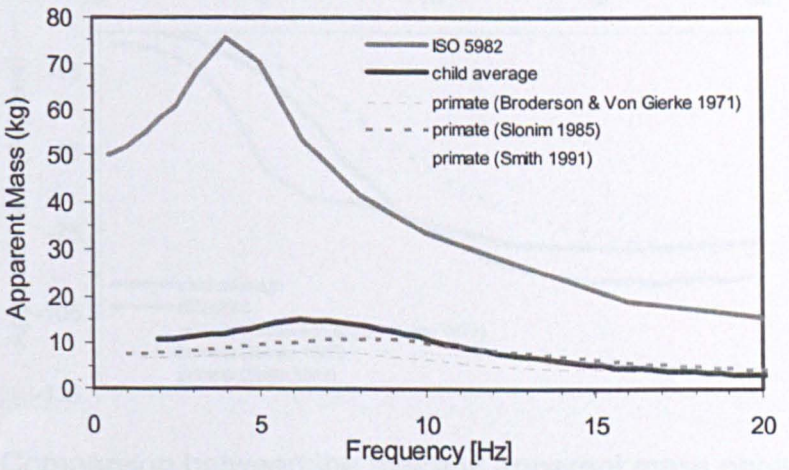

Figure 3.17 Comparison between the average apparent mass modulus found for 8 children and values reported for adults and primates.

Figure 3.18 presents the apparent mass phase angle measured for each of the 8 children and the group average curve. Again as in the case of the modulus results a strong similarity exists among the individual curves therefore the average value provides a useful representation of the entire group. Figure 3.19 compares the average phase response curve for the children to those for adult humans and primates found in the literature. More than in the case of modulus, the phase response highlight the single degree of freedom nature of the vibration response of primates and children. The phase curves defined in ISO 5982 for erect seated adults denote two distinct changes in slope, occurring at approximately 4.5 and 12 Hz, which suggest the presence of two externally measurable resonance behaviours.

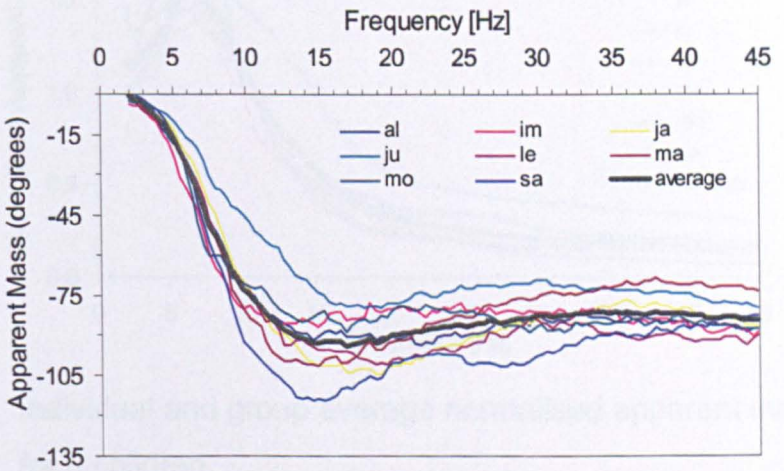

Figure 3.18 Individual and group average apparent mass phase for 8 children.

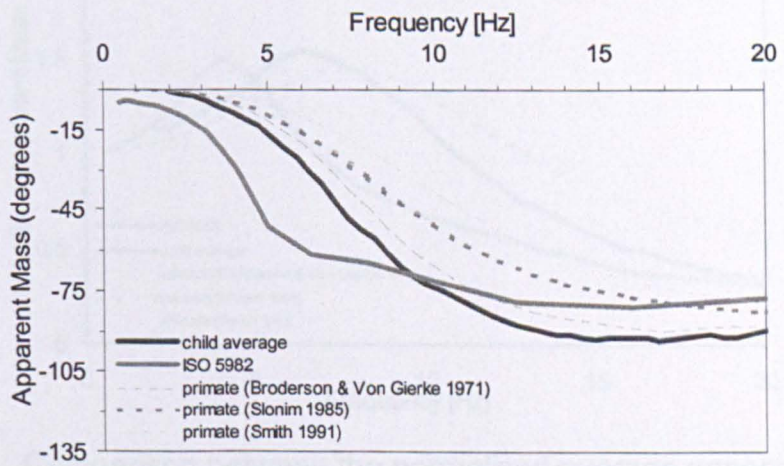

Figure 3.19 Comparison between the average apparent mass phase found for 8 children and values reported for adults and primates.

A technique used for facilitating comparisons across humans and primates of different size is to normalise the apparent mass modulus by the body mass of the individual. Figures 3.20 and 3.21 present the child, adult and primate vibration responses in mass normalised form. Using this representation the similarity between the results for the various children is even more pronounced, only the smallest child (ju of 8.0 kg) shows a substantially different behaviour. In this form it is also evident that both the children and the primates have substantially greater damping ratios than that of adult humans.

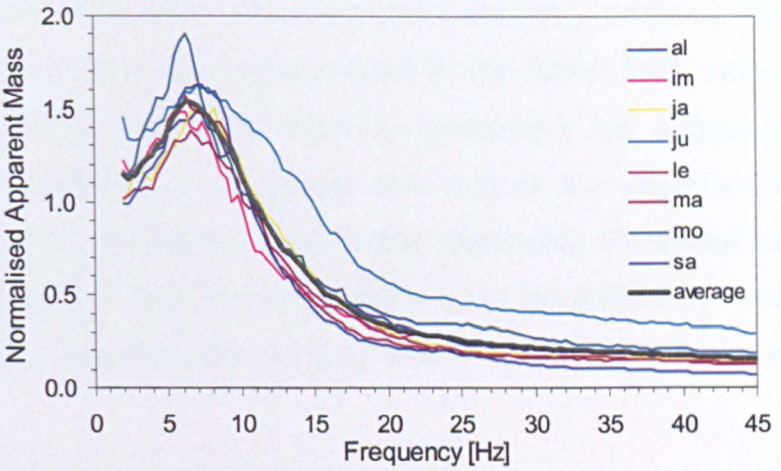

Figure 3.20 Individual and group average normalised apparent mass modulus for 8 children.

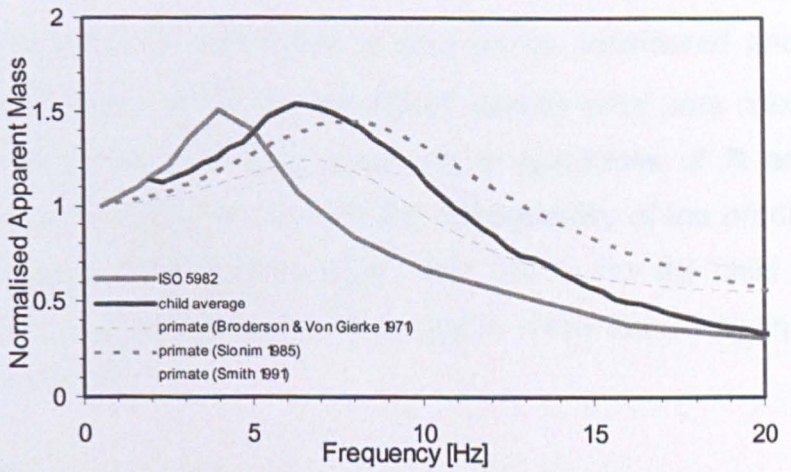

Figure 3.21 Comparison between the normalised average apparent mass modulus for 8 children and values reported for adults and primates.

3.4 Mass-Spring-Damper Models of Small Children

Economic use of human testing data requires a synthetic representation in the form of a dynamic model. As noted in the whole-body review the majority of studies performed to date for the vertical direction have summarised the human response properties by means of linear mass-spring-damper models of either one or two degrees of freedom. This approach has been adopted here in order to facilitate comparison with the existing literature.

The single degree of freedom linear lumped parameter mass-spring-damper model defined by equation 3.4 was implemented in the MATLAB® software. Parameter values were identified for each child by minimising the difference between the apparent mass modulus of the model and that of the experimental data. Phase information was not considered due to the previously discussed sensor drift. The differences between model and experiment were quantified by means of the non-normalised mean squared error (m.s.e.) which for apparent mass modulus can be expressed as

$$m.s.e = \sum_{i=1}^{N} \left(\left| AM(j\omega) \right| - \left| A\hat{M}(j\omega) \right| \right)^2 \qquad (3.12)$$

where N is the number of experimental data points considered and $A\hat{M}(\omega)$ is the apparent mass modulus of the model. Mean square error was chosen because it provides a global energy averaged measure of goodness of fit and because its minimisation has been shown to ensure the orthogonality of the prediction error with respect to the original experimental data (Allen 1971). For the child apparent mass modulus the m.s.e was calculated using a total of N=56 frequency lines covering the interval from 2 to 45 Hz.

Given a modelling error measure optimal parameter values are often identified using an algorithm which searches the parameter space for points at which the error is minimum. A variety of optimisation routines exist for locating minima, with many performing global unconstrained optimisation which potentially searches all possible

parameter values and thus all regions of parameter space. This can create difficulties in cases where the model parameters have a physical interpretation such as with the child models treated here. In such cases an unconstrained optimisation can be transformed into a constrained optimisation by means of a penalty function (Rao 1996) which increases the error measure whenever parameter values exceed a predetermined range. For the child apparent mass models a first physical restriction was that all parameter values should be positive. This was implemented by means of a penalty function which added a large fixed increase in modelling error whenever a negative parameter value was attempted.

$$penalty_1(m_0, m_1, c_1, k_1) = \begin{cases} 10{,}000 \ for \ m_0 < 0 \\ \qquad\qquad\quad m_1 < 0 \\ \qquad\qquad\quad c_1 < 0 \\ \qquad\qquad\quad k_1 < 0 \\ \\ \quad 0 \quad otherwise \end{cases} \tag{3.13}$$

A second restriction was that the individual component masses should sum to approximately the total mass of the child. The penalty function introduced in this case added a large fixed increase in error whenever the sum of the component masses m_0 and m_1 was less than 50% or more than 150% the total mass of the child in question.

$$penalty_2(m_1, m_2) = \begin{cases} 10{,}000 & for \ (m_0 + m_1) < 0.5 \ m_{child} \\ 0 & for \ 0.5 m_{child} < (m_0 + m_1) < 1.5 m_{child} \\ 10{,}000 & for \ 1.5 \ m_{child} < (m_0 + m_1) \end{cases} \tag{3.14}$$

Use of penalty functions for constraining the single degree of freedom optimisation problem lead to a total fitness function defined by the sum of the mean squared error and the possible penalties.

$$\begin{aligned} fitness(m_0, m_1, c_1, k_1) = m.s.e.(m_0, m_1, c_1, k_1) + penalty_1(m_0, m_1, c_1, k_1) \\ + penalty_2(m_0, m_1) \end{aligned} \tag{3.15}$$

The optimisation method chosen for estimating the child model parameter values was the Differential Evolution (DE) algorithm, a parallel direct search method developed for performing global optimisation over continuous parameter spaces (Storn and Price 1997). Differential Evolution is conceptually similar to Genetic Algorithm optimisation with the main difference being that all operations are performed on floating point numbers rather than on binary strings of zeros and ones. The principal motivation for the choice of Differential Evolution was its simplicity; though being one of the most robust algorithms for both linear and nonlinear optimisation it can be programmed using as few as 20 lines of code and has only three basic control parameters (*NP*, *F* and *CR*).

DE operates on a population of *NP* vectors held in a primary array, each containing a set of *D* parameter values of the problem being optimised (m_0, m_1, c_1 and k_1 in the case of the single degree child model). Based on empirical testing Price and Storn (1997) suggest a value for *NP* of 5 to 10 times the number of parameters in the individual vectors being optimised. In the first generation the values of each vector are assigned a random number, guaranteeing that the initial population spans wide regions of parameter space. For each vector of the primary array DE performs a process which leads to a final comparison between the target vector ($\boldsymbol{P}_{target}$) and a competing trial vector ($\boldsymbol{P}_{trial}$), the fitness function of the two determining which survives to take the place of the target vector in the successive generation held in the secondary array. By means of successive fitness-based selections which fill the secondary array, and swaps from the secondary to the primary array, DE attempts to transform a given starting population of parameter vectors into a final population of optimal parameter vectors.

Differential Evolution is distinguished from other direct search optimisation procedures by the biologically inspired process which produces the trial vector whose fitness is compared to that of the target vector. The first operation is the random selection of a parent vector ($\boldsymbol{P}_{parent}$) from the population of vectors of the primary array. Next, the parent vector is mutated by adding noise to its parameters. This mutation operation introduces randomness into the search, helping both to explore new areas of parameter space and to escape from local minima of the fitness function. In DE the noise added to the parent vector by the mutation process is taken

to be the scaled difference between two other vectors (P_1 and P_2) chosen randomly from the population of the primary array.

$$P_{mutated} = P_{parent} + F(P_1 - P_2) \tag{3.16}$$

where the scaling factor F is a user-supplied control parameter whose values for stability should be in the range $0 \leq F \leq 1.2$ and whose optimal values for most problems lie in the range $0.4 \leq F \leq 1.0$. With respect to using random noise of fixed variance for each parameter this process enhances the mutation since, on average, the difference between vectors from the general population provides a step size which is different for each individual parameter and which is proportional to each parameter's variance in the space. By using population-derived noise DE ensures that the parameter space will be efficiently searched in all dimensions.

The mutated parent vector and the target vector are next used in a crossover operation designed to resemble the process by which a child inherits DNA from its two parents. Crossover exchanges parameter values by means of *D-1* binomial experiments. The process is controlled by a constant called the crossover ratio CR which can take on the values $0 \leq CR \leq 1$. For each parameter a uniformly distributed random number is generated within the interval from 0 to 1. The child vector takes a parameter from the original target vector (P_{target}) if the random number is greater than CR whereas it takes the parameter from the mutated parent vector if the random number is less than *CR*. The result is a new vector called the trial vector P_{trial} which constitutes another possible solution of the optimisation problem. By using *D-1* binomial experiments DE ensure that at least one parameter of the trial vector is always taken from the noisy mutated vector even when *CR*=0.

In the final Differential Evolution operation the fitness values of the target and trial vectors are compared and the best (in the case of the child model the one having the lowest error) survives to pass to the next generation held in the secondary array. This natural selection ensures progressive improvement of the population of parameter vectors from generation to generation. Operations for a single generation continue until all vectors of the primary array have been targeted and their corresponding positions in the secondary array filled. By then swapping the elements

of the secondary array for those of the primary array the process can be repeated any number of times. The process is halted when either a maximum number of iterations has been completed or a halting criteria such as an average fitness value for the population of the secondary array has been achieved. The operational sequence of the algorithm as applied to the child model is illustrated in Figure 3.22.

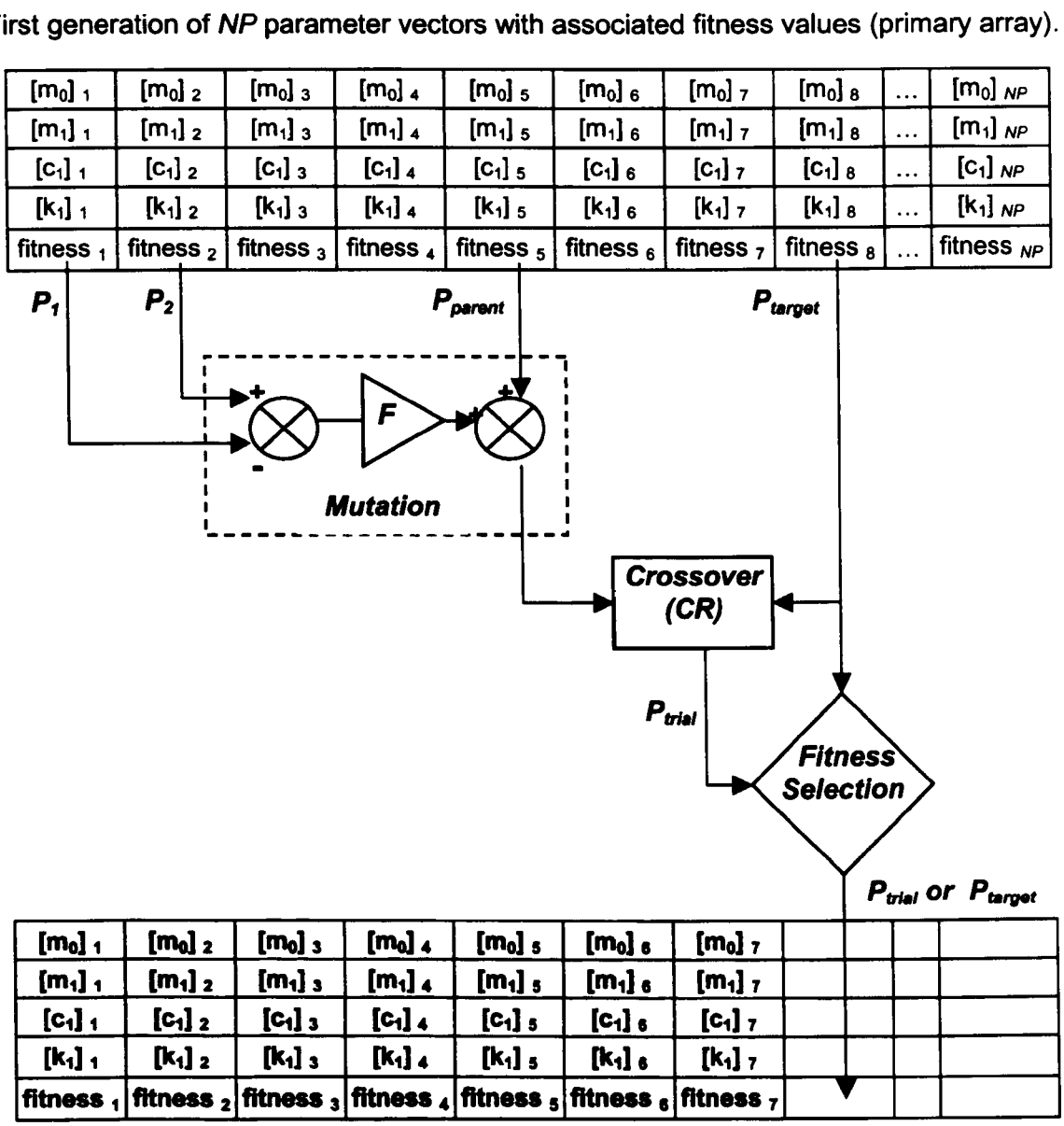

Figure 3.22 One trial of the Differential Evolution Algorithm as applied to the child model parameter estimation task.

Trial runs for the child mass-spring-damper model lead to the choice of Differential Evolution algorithm parameters NP=70, F=0.5 and CR=0.5 using 200 iterations.

Optimisation runs were performed for all children for the input amplitude of 1800 mV corresponding to 1.2 m/s^2 r.m.s. acceleration. The identified parameter values are presented along with the group average values and the m.s.e. in Table 3.6 below.

Child	m_{total} (kg)	m_o (kg)	m_1 (kg)	k_1 (N/m)	c_1 (Ns/m)	m.s.e (kg)
al	9.2	0.8	8.4	21187	350	0.11
im	10.8	1.2	9.6	19242	364	0.11
ja	10.5	0.9	9.6	27357	374	0.34
ju	6.3	1.3	5.0	18420	279	0.05
le	8.3	0.6	7.7	19211	298	0.17
ma	7.6	0.8	6.8	16618	232	0.23
mo	11.8	1.0	10.8	21162	431	0.33
sa	11.2	0.8	10.4	25853	305	0.29
Mean	**9.5**	**0.9**	**8.5**	**21131**	**329**	**0.20**
Std.	**1.9**	**0.2**	**2.0**	**3704**	**63**	**0.11**

Table 3.6 Parameter values of the optimal two-mass single degree of freedom model fit to the modulus function of each child data set.

It is of interest to compare the mean model parameters to models reported in the literature for primates and for adult humans. For a group of Rhesus monkeys Smith (1992) reported a mean mass of 6.67 kg, a mean stiffness of 15190 N/m and a mean damping coefficient of 231 Ns/m. For a group of older children and adults having a mean mass of 51.2 kg, Griffen and Wei (1998) reported a mean stiffness of 44130 N/m and a mean damping of 1485 Ns/m. The child model defined in the table above has mass, stiffness and damping parameters which are intermediate to the lighter primates and heavier adult humans, suggesting a simple scaling relationship. The nature of this scaling will be discussed further in the summary to this chapter. Figure 3.23 below provides a comparison between the apparent mass modulus and phase functions obtained experimentally and those predicted by the child models.

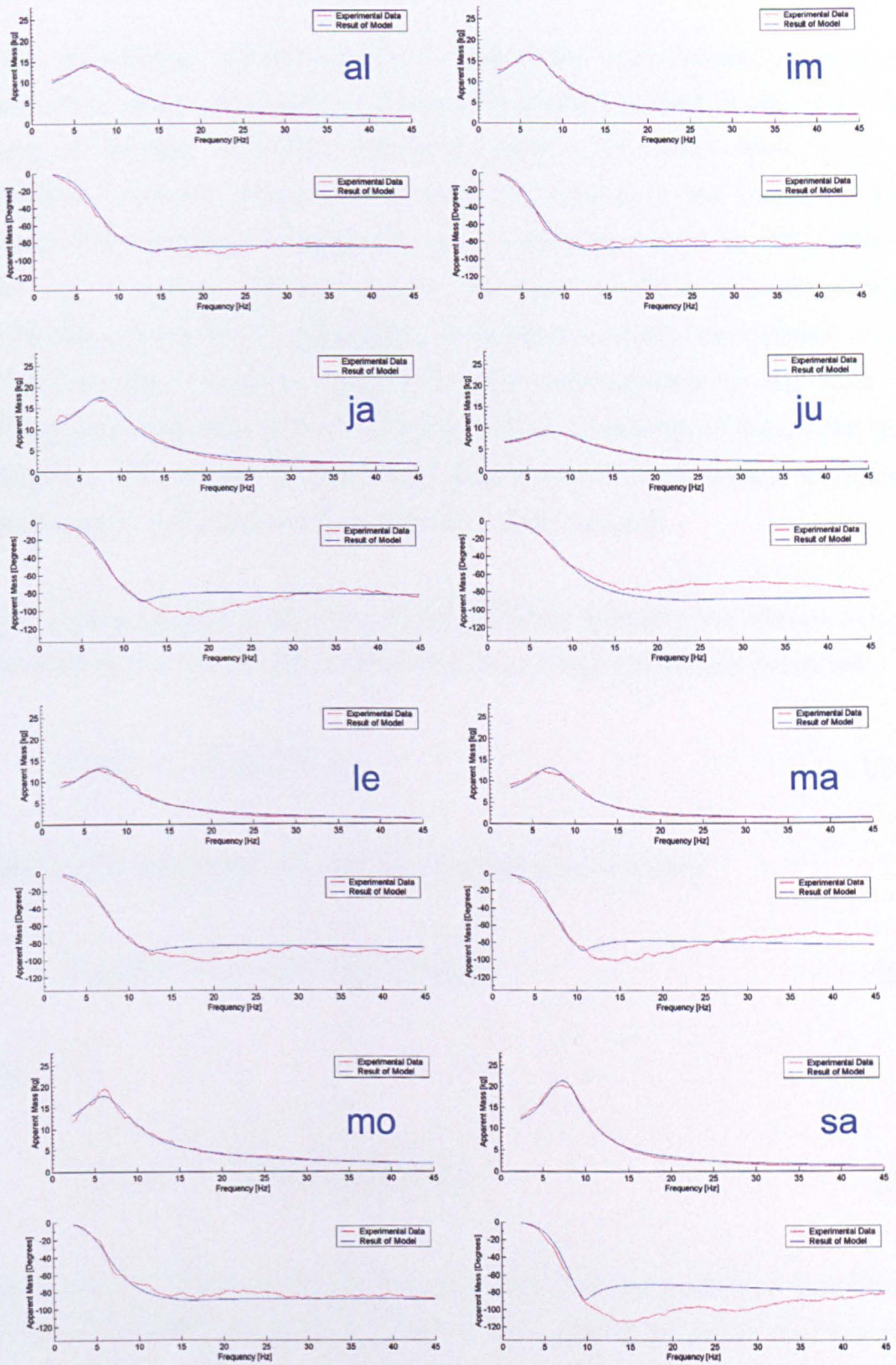

Figure 3.23 Single degree of freedom modelling results for 8 children.

3.5 Absorbed Power Analysis of Small children

In the whole-body vibration review it was noted that several researchers have performed studies which have measured for adults the mechanical power absorbed during a vibration exposure. Absorbed power has been seen as a possible alternative measure of exposure severity with respect to the frequency weightings derived from subjective responses used in standards such as ISO 2631 and BS 6841. As a metric, absorbed power has been found to provide different, and sometimes contradictory, indications of exposure severity with respect to the more commonly used frequency weightings. An understanding of the child vibration problem was expected to be incomplete without knowledge of the power absorption properties. This section presents absorbed power and normalised absorbed power determined from the force and acceleration data acquired.

If force and velocity are known at the interface between the human body and its environment the power can be determined by taking the product of the two

$$P(\omega) = F(\omega)V(\omega) \tag{3.17}$$

which can be separated into real and imaginary components

$$P_{\mathrm{Re}}(\omega) = F(\omega)V(\omega)Cos(\theta) \tag{3.18}$$

and

$$P_{\mathrm{Im}}(\omega) = F(\omega)V(\omega)Sin(\theta) \tag{3.19}$$

where θ is the phase angle between the force and the velocity. A question that can be asked regarding the power arriving at the human body is how much is returned to the source of the vibration, and thus how much is dissipated in the body. The motion of a pure mass element, which does not absorb energy, would be characterised by a velocity lag of 90 degrees with respect to the force. Likewise, the motion of a linear

spring which is also incapable of energy absorption would be characterised by a velocity which leads the force by 90 degrees. The motion of a linear (viscous) damper which dissipates energy is characterised by a velocity and force which are in phase. These observations suggest that only the real component of the power represents energy that is not returned to the vibrating surface from the body. The real part is therefore the power that is absorbed within the body and dissipated as heat. For convenience the absorbed power can be determined from the cross spectrum between velocity and force

$$P_{\mathrm{Re}}(\omega) = \left|G_{VF}(\omega)\right| Cos(\phi(\omega)) \tag{3.20}$$

where $\left|G_{VF}(\omega)\right|$ is the modulus and $\phi(\omega)$ the phase of the cross spectrum between the driving point input velocity and output force. Determined in this manner the absorbed power can be plotted in spectral density form which has units defined by the product of force and velocity divided by the spectral resolution, or (Nm/s)/Hz. Since absorbed power has been shown to increase with the square of the input acceleration authors such as Lee and Pradko (1968) and Mansfield and Griffin (1998) have also presented results in acceleration normalised form. In this form the absorbed power spectral density is divided by the square of the acceleration power spectral density leading to units of Ns^3/m. Authors such as Lunström et. al. (1998) have noted instead that the power absorbed by humans increases in proportion to body mass, leading them to normalise their data by the body mass in kilograms. These authors have presented results in units of Watts per kilogram in spectrum form or units of W/kgHz in spectral density form. In what follows the absorbed power is presented in both spectral density form in units of (Nm/s)/Hz and normalised spectral density form using units of Ns^3/m. Additionally, the effects of both test acceleration and subject mass have been simultaneously compensated by use of a double normalised measure having units of Ns^3/kgm.

The absorbed power was determined from the force and acceleration time histories recorded during the apparent mass tests of the child subjects. The acceleration time history was single integrated in the frequency domain and a 5^{th} order polynomial was applied to the data in the time domain to reduce low frequency trends caused by the

integration. The cross spectrum was then determined using the same processing parameters used previously for the apparent mass calculations. The sampling rate was 200 Hz, the window type was Hanning, the block size used was 512 points with an overlap of 97% which lead to a spectral resolution of 0.39 Hz between frequency lines and a total of 1541 averages for each 2 minute exposure signal.

Figure 3.24 presents the absorbed power determined for the eight subjects at 0.8 and 1.2 m/s^2. The absorbed power increased with both acceleration amplitude and subject mass. At 5.2 kg the smallest child (ju) absorbed the least energy while at 12.4 kg the largest (sa) absorbed the most. The frequency of peak power absorption suggested a single whole-body response resonance at approximately 7.4 Hz. All the individual absorbed power measurements are characterised by a noisy appearance, containing multiple peaks which at first inspection might suggest multiple body resonances. These variations in the absorbed power are largely due, however, to variations in the input acceleration spectra. Normalising each frequency line by the input acceleration spectra reduces this phenomena and leads to normalised absorbed power curves which are smoother and more easily interpretable in appearance.

All acceleration normalised absorbed power curves are presented in Figure 3.25. The curves confirm the single degree of freedom behaviour of the measured response data (no second peak) and also confirm a relatively high level of linearity (compared to results for other biological systems). Changes in the modulus peak for subjects le, ma, mo show some migration towards a lower anti-resonant frequency while the changes for subject ju show the opposite. Unfortunately, the number of subjects tested and the size of the changes did not result statistically significant for the two test acceleration amplitudes used (ANOVA $p>0.05$). It is thus not possible in this study to confirm or reject the hypothesis of nonlinear softening system behaviour often found for adult humans. It is nevertheless of interest to note that two of the heaviest children, mo and sa, showed possible evidence of softening system behaviour while the lightest (ju) was the only subject possibly showing hardening system behaviour.

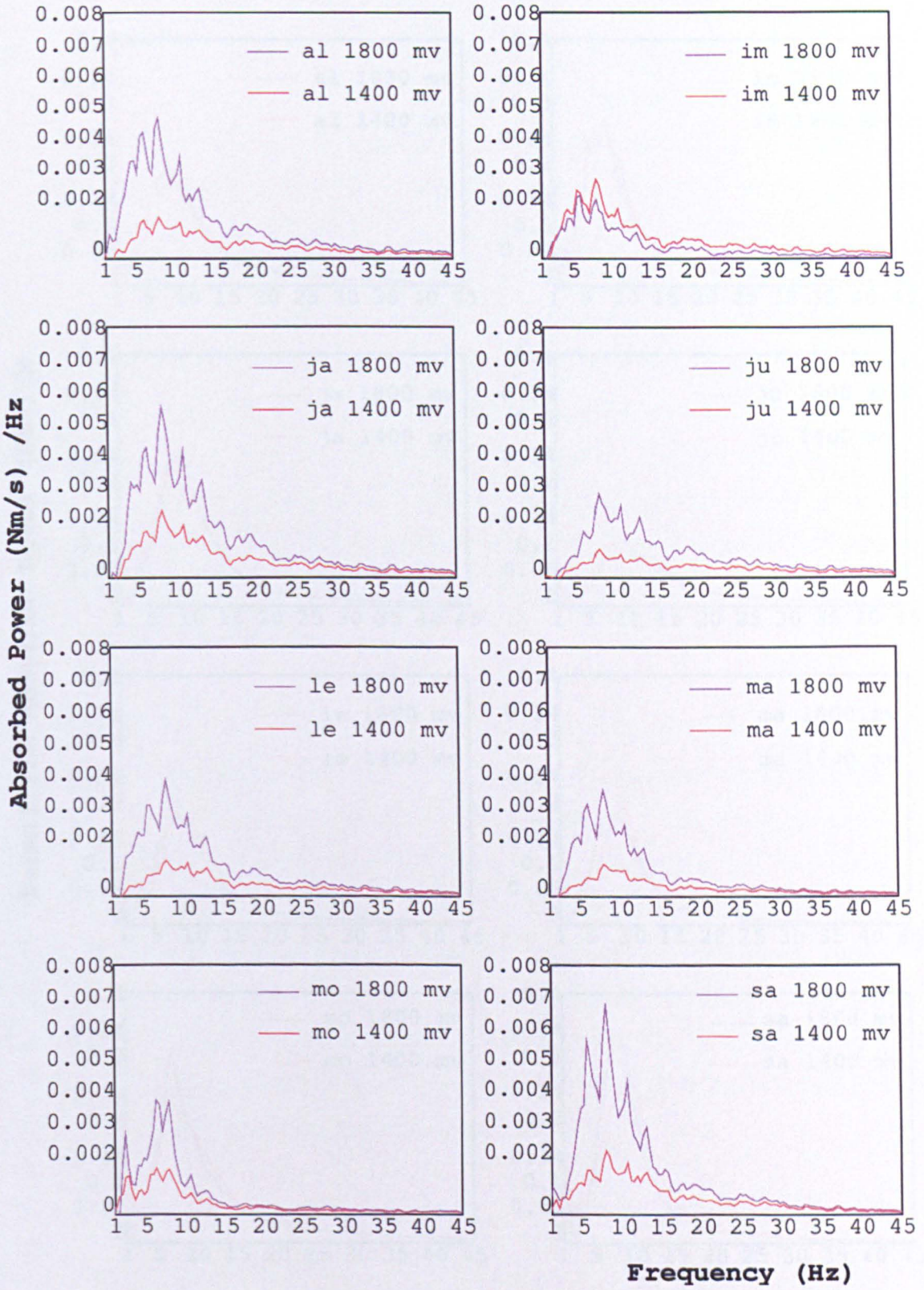

Figure 3.24 Absorbed power spectral density for 8 children tested at r.m.s. acceleration levels of 0.8 m/s^2 (1400mV) and 1.2 m/s^2 (1800 mV).

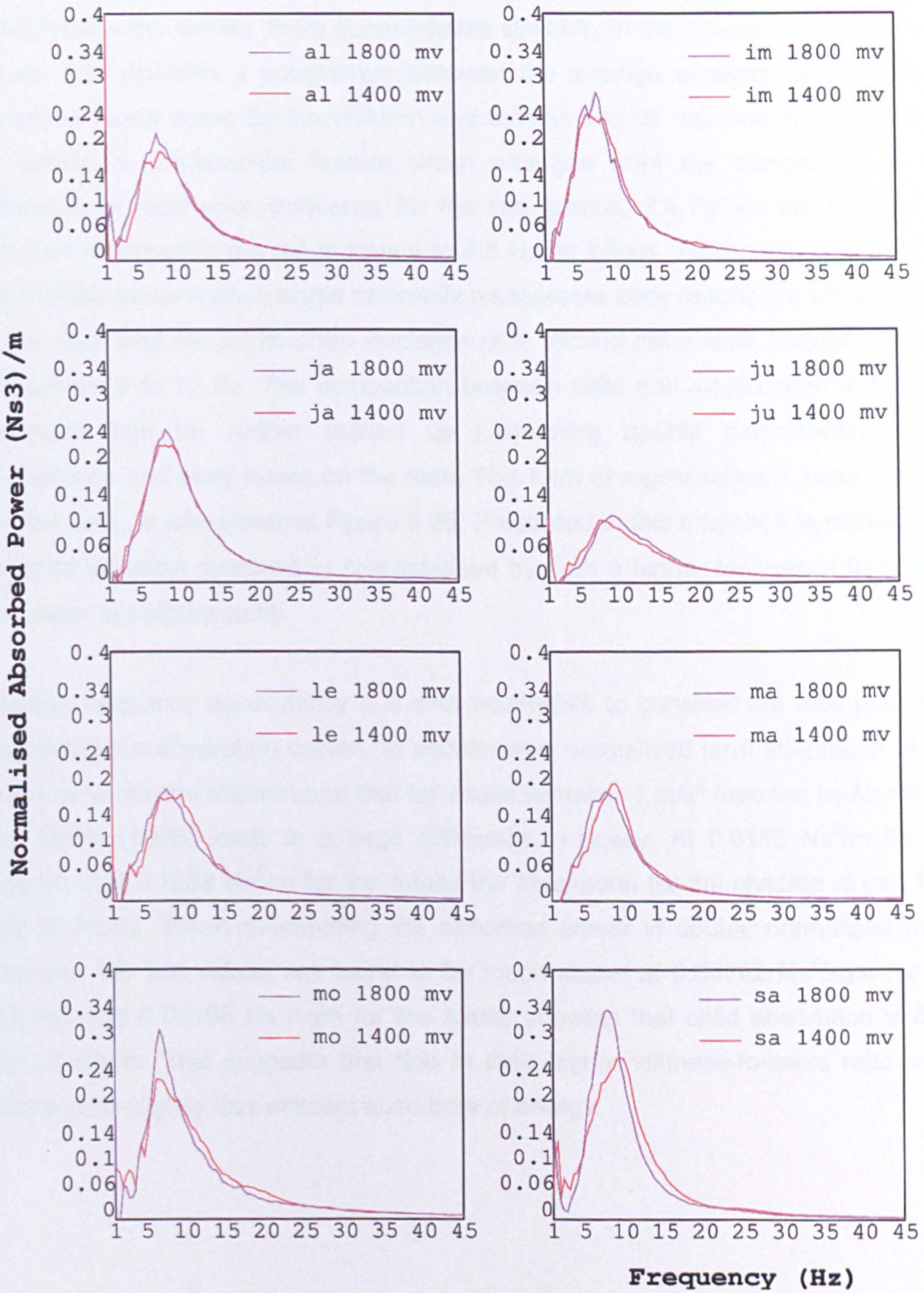

Figure 3.25 Normalised absorbed power for 8 children tested at r.m.s. acceleration levels of 0.8 m/s^2 (1400mV) and 1.2 m/s^2 (1800 mV).

Figure 3.26 presents the acceleration normalised absorbed power for each subject and the group average result obtained for the 1.2 m/s^2 tests. While body mass differentiates the curves, there is remarkable similarity in the frequency dependency. Figure 3.27 provides a comparison between the average acceleration normalised absorbed power curve for the children and measurements reported in the literature for adults. A fundamental feature which emerges from the comparison is the difference in resonance frequency for the two groups, 7.4 Hz for the children as opposed to values in the range from 4 to 4.5 Hz for adults. Additionally, the data for the children shows only a single externally measurable body resonance while several of the data sets for adults show evidence of a second resonance frequency in the range from 9 to 12 Hz. The comparison between child and adult power absorption behaviour can be further refined by performing double normalisation (both acceleration and body mass) on the data. This form of representation, used here for the first time, is presented as Figure 3.28. Presented in this manner it is evident that the child vibration response is characterised by both a higher resonance frequency and wider absorption peak.

Besides frequency dependency it is also worthwhile to consider the total power by integrating the absorption curves. In acceleration normalised form integration of the mean curve for the children and that for adults tested at 1 m/s^2 reported by Mansfield and Griffin (1998) leads to a large difference in power. At 0.0156 Ns^2/m for the children and 0.1289 Ns^2/m for the adults the absorption for the children is just 12% that of adults. When determining the absorbed power in double normalised form, however, the two values are found to be much closer at 0.00162 Ns^2/kgm for the children and 0.00188 Ns^2/kgm for the adults showing that child absorption is 86% that of adults. This suggests that due to their higher stiffness-to-mass ratio small children are slightly less efficient absorbers of energy.

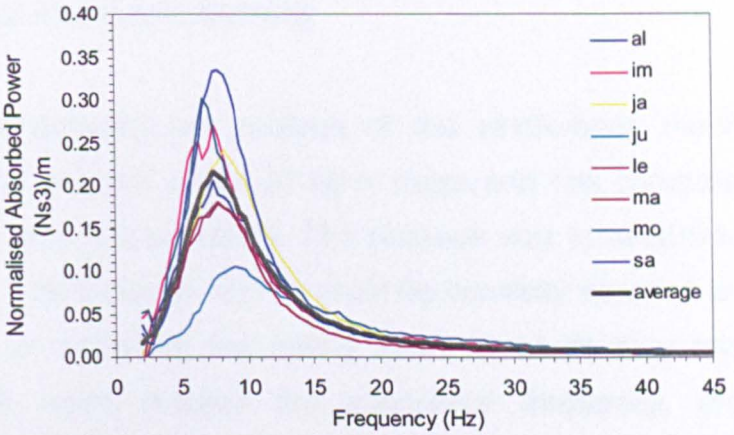

Figure 3.26 Individual and group average normalised absorbed power for 8 children tested at 1.2 m/s^2 (1800 mV).

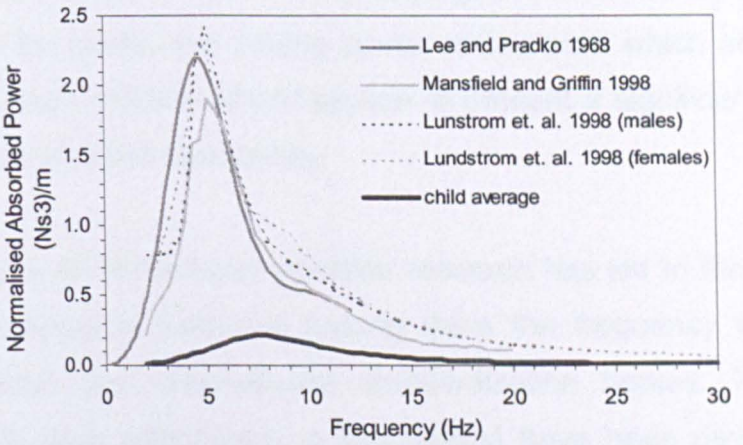

Figure 3.27 Comparison of acceleration normalised absorbed power for children and adults.

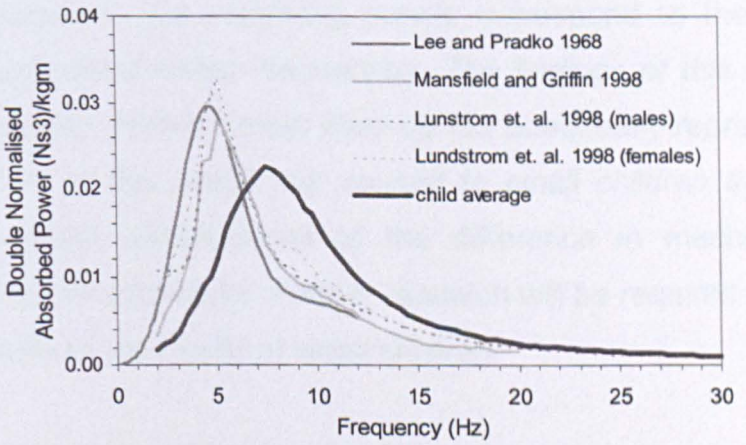

Figure 3.28 Comparison of double normalised absorbed power for children and for adults.

3.6 Summary and Allometric Scaling

This chapter has provided an analysis of the whole-body mechanical response properties of small children under 20 kg in mass and has compared the findings to data for primates and human adults. The purpose was to establish the dynamics of small children so that these dynamics could be correctly interpreted and represented when analysing or designing the safety seats in which they travel. *The findings suggest that for small children the resonance frequency, the anti-resonance frequency, the frequency dependence of both the apparent mass and the absorbed power, and the total absorbed power per kilogram are significantly different from what is currently known for adults.* Having average resonance frequencies which are 3 Hz higher than for adults and having power absorptions which are approximately 15 percent less, small children would appear to present a significant new challenge for the whole-body vibration community.

More than 60 years of whole-body vibration research has led to the development of numerous methodologies, foremost among them the frequency weighting curves defined by national and international standardisation bodies. These frequency weightings (W_b is used extensively in this thesis) have been developed from the subjective response of adult humans and their properties can be shown to strongly correlate with whole-body mechanical response. In general terms the frequencies with high gain values in the weighting curves correspond to the regions of the principal whole-body mechanical resonances. *The findings of this chapter suggest that existing evaluation methods most likely do not adequately represent the level of vibration discomfort or the health risk caused to small children by vibration.* This conclusion is a direct consequence of the difference in mechanical response between small children and adults. Further research will be required in order to adapt the existing methods to the needs of small children.

A possible aid to such developments may come from an analysis of the allometric scaling involved. Comparisons made in this chapter between primates, children and adult humans showed evidence of gradual changes across species and across body

mass. The dependence of a biological variable Y on body mass M is often described by means of an allometric scaling law (West, Brown and Enquist 1997) of the form

$$Y = Y_0 M^b \tag{3.21}$$

where Y_0 and b are constants. It was once thought that the scaling exponent b reflected geometric constraints on living organisms and that as such the values should be multiples of 1/3. More recently it has been shown that most biological phenomena have scaling exponents which are 1/4 powers of the mass. Examples include the metabolic rates of living organisms which scale with the +3/4 power of the mass, heartbeat which scales with the –1/4 power and blood circulation and life span which scale with the +1/4 power. West, Brown and Enquist (1997) have developed a general theory of 1/4 power scaling for biological organisms based on the transport of nutrients through fractal space-filling networks with branching tubes of finite size.

It is instructive to analyse the allometric relations for the principle parameters describing the vibration response of primates, children and adults. The basis for the analysis are the single degree of freedom (with base support) mass-spring-damper models reported for primates by Broderson and Von Gierke (1971), Slonim (1985) and Smith (1991), reported here for children under 20 kg in mass and reported for large children and adults by Wei and Griffin (1998). The parameters for each subject described by each author was entered into a table and used to determine the model natural frequency and damping ratio. With masses ranging from 5.98 to 108 kg (average 42.2 kg) the data set covers changes of more than one order of magnitude.

A first question of an allometric nature is the growth of the moving mass element with respect to the growth in total mass of the subject. Figure 3.29 presents the moving mass m_1 plotted against the total model mass m_{total} using logarithmic scales for both axis. A regression model of the data provides a scaling exponent of approximately unity, suggesting that moving mass grows linearly across body sizes. This represents an intuitive, but not guaranteed, result and is a 1/4 power exponent.

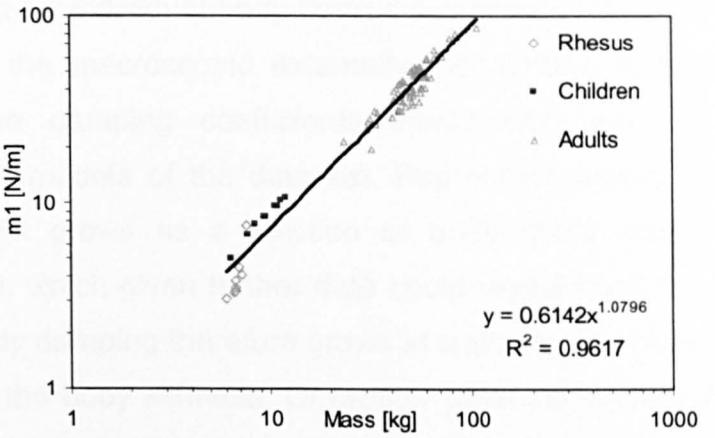

Figure 3.29 Allometric scaling of the moving mass of the upper body as a function of the total body mass determined from single degree of freedom models of primates, children and adult humans.

A second question of interest is the growth in the body spring stiffness with mass. Figure 3.30 presents the single degree of freedom spring constants plotted against body mass for the data set. The data and the regression model coefficients suggest that the stiffness grows with a power exponent of +1/2. Body mass therefore increases at a greater rate than tissue stiffness. This leads to body resonances which decrease in frequency with increasing size of the animal.

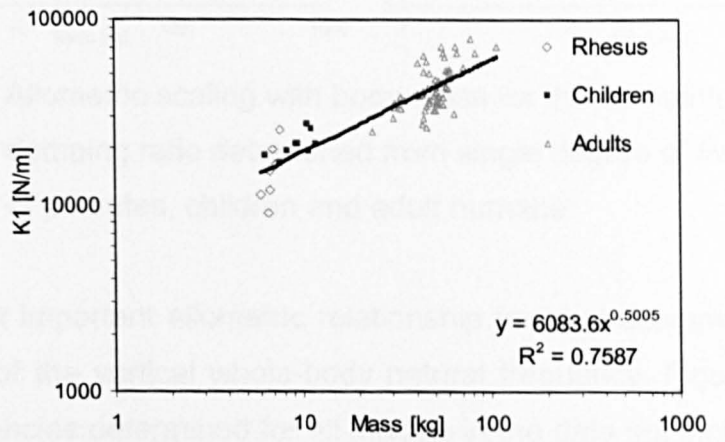

Figure 3.30 Allometric scaling of body stiffness with body mass determined from single degree of freedom models of primates, children and adult humans.

Of particular relevance to both the response amplitude and the absorbed power is the amount of damping exhibited. Given the complexities of measuring and

modelling damping for individual body tissues it is particularly important to obtain an understanding of the macroscopic externally measurable properties. Figure 3.31 presents both the damping coefficients themselves and the damping ratios determined for the models of the data set. Regression analysis suggests that the damping coefficient grows as a function of body mass according to a scaling exponent of +0.78, which given further data could reveal itself to be an exponent of +3/4 or +0.75. Body damping therefore grows at a slower rate than body mass, but at a faster rate than the body stiffness. Of greater potential interest than the growth in the damping coefficient itself is the relationship between the damping ratio and the body mass. The data in this case shows little or no change with mass, suggesting that evolutionary forces have lead to animals with nearly constant vibration decay rates and forced response magnification factors, possibly due to the elastic limits imposed by the load bearing tissues.

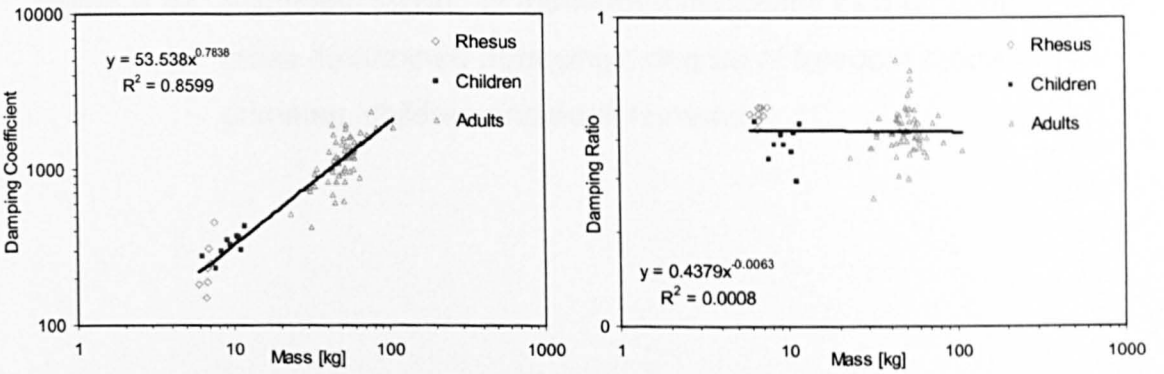

Figure 3.31 Allometric scaling with body mass for the damping coefficient and damping ratio determined from single degree of freedom models of primates, children and adult humans.

Perhaps the most important allometric relationship for seat designers is the change with body mass of the vertical whole-body natural frequency. Figure 3.32 presents the natural frequencies determined for all models in the data set plotted as a function of body mass. In this case the relationship is negative and regression analysis leads to an exponent of –0.289. As with the damping coefficients there is a possibility that given more data this relationship may result a quarter power with a value of –1/4. More importantly, with 83% of the variance accounted for there appears to be scope for estimating the most likely resonance frequency of a an individual from their body mass. Though the whole-body vibration literature identifies many factors which

influence the response frequency of a seated individual such as sitting posture and muscle tone, it does appear that an estimate of the response frequency for an "average" individual of given mass can be made. This result may be useful when attempting to adapt standard frequency weightings to the child vibration problem.

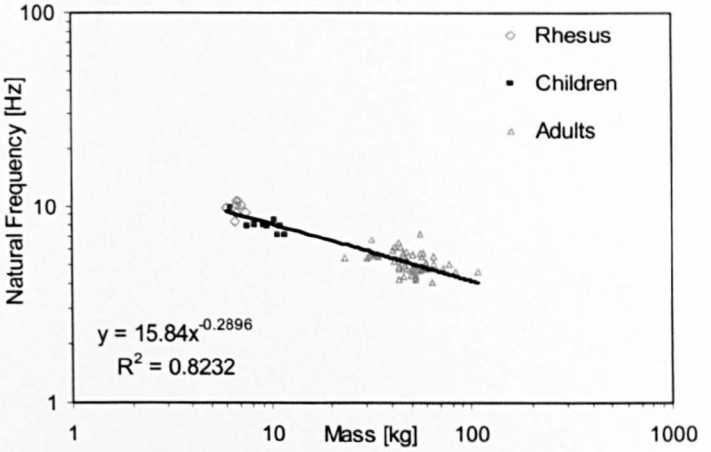

Figure 3.32 Allometric scaling of the natural frequency as a function of body mass determined from single degree of freedom models of primates, children and adult humans.

Chapter 4

Modal and Operational Deflection Properties of Child Seats

4.1 Introduction

Having investigated the vibration properties of the small children attention next focussed on the seat units. Given the lack of any literature for child seats several basic questions required answering:

- What resonant frequencies are typical of child seats ?
- What are the vibrating shapes of child seats ?
- Do vibrating frequencies or shapes change when carrying a child in a vehicle ?
- What is the damping level ?
- What properties can be altered to improve vibrational comfort ?

Any resonance frequencies in the whole-body vibration range from 0 to 100 Hz would be expected to affect child comfort. Both the frequency location and the vibrating shape are important since child mechanical response and child subjective response depend on both the frequency and direction of the movement. The nature and level of damping provided by child seats is also important since any efforts to reduce vibration by means of damping treatments or dynamic absorbers requires knowledge of the levels normally found in the units.

In order to answer some of these questions two forms of experimentation were used. A first set of tests applied Experimental Modal Analysis (EMA) methods to two child seats which were considered representative of a range of commercial products available in stores. The two seats were tested in isolation in the laboratory using a specially prepared test facility. The objective was to use linear frequency domain modal analysis techniques to determine the eigenvalues, eigenvectors and damping levels of the seats. In order to obtain the closest possible correspondence between the test results and the actual operating performance of the seats they were tested complete with all components and trim.

Since the vibration behaviour of a device can change greatly in its operational environment due to force coupling with other structures and due to kinematic constraints, a second set of tests was performed in an automobile using one child seat which was occupied by a child. After acquiring data from drives over a set of road surfaces an operational deflection shapes analysis (running modes analysis) was performed to identify the resonant frequencies and movement shapes occurring in practice. While not providing eigenvalues and eigenvectors as in the case of EMA, operational deflection shapes analysis provides an important check of the working dynamics of the test object.

This chapter presents the two experimental methodologies and the results obtained for the child seats tested. The objective of the research was to establish the vibrational behaviour of typical child seats and the possible differences occurring between seats of different design.

4.2 Child Seat Experimental Modal Analysis

4.2.1 Experimental Modal Analysis (EMA)

A linear undamped multiple degree of freedom system excited by a set of harmonic forces can be described by means of a *spatial model* of the form

$$\left[[K]-\omega^2[M]\right][X]e^{j\omega t}=[F]e^{j\omega t} \tag{4.1}$$

where $[M]$ is the mass matrix, $[K]$ is the stiffness matrix, $[F]$ is the vector of forcing amplitudes and $[X]$ is the matrix of response amplitudes. A spatial model of this type can be rearranged as

$$[X]=\left[[K]-\omega^2[M]\right]^{-1}[F]$$

which is of the general form

$$[X]=[\alpha(\omega)][F] \tag{4.2}$$

where [α(ω)] is the NxN receptance matrix. The receptance matrix consists of N^2 terms

$$\alpha_{ij}(\omega)=\left[\frac{x_i(\omega)}{F_j(\omega)}\right] \tag{4.3}$$

which quantify the relationship between the input force at each point j and the output displacement obtained at each point i. When a system is described by means of a frequency response function matrix such as the receptance matrix [α(ω)] we speak of a *response model*. It is also possible to express the receptance matrix in terms of the system's natural frequencies and mode shape vectors. This can be achieved by taking advantage of the orthogonality properties of the mode shape vectors starting with the definition of the receptance matrix.

$$\left[[K]-\omega^2[M]\right] = [\alpha(\omega)]^{-1}$$

The normalised modal shape matrix can be used to write

$$[\Phi]^T [[K] - \omega^2 [M]][\Phi] = [\Phi]^T [\alpha(\omega)]^{-1} [\Phi]$$

which can be further simplified by observing that normalising by the mode shape vector matrix [Φ] leads to

$$\begin{bmatrix} \ddots & & \\ & (\omega_r^2 - \omega^2) & \\ & & \ddots \end{bmatrix} = [\Phi]^T [\alpha(\omega)]^{-1} [\Phi]$$

or

$$[\alpha(\omega)] = [\Phi] \begin{bmatrix} \ddots & & \\ & (\omega_r^2 - \omega^2) & \\ & & \ddots \end{bmatrix}^{-1} [\Phi]^T$$

Which shows that any frequency response function of a linear system can be calculated from its mode shape vector matrix as

$$\alpha_{ij}(\omega) = \sum_{r=1}^{N} \frac{\phi_{ir} \phi_{jr}}{\omega_r^2 - \omega^2} = \sum_{r=1}^{N} \frac{R_{jk}}{\omega_r^2 - \omega^2} \qquad (4.4)$$

where the constant R is known as the modal constant or the residue, and each natural frequency ω_r is called a pole. The eigenvalues and mode shape vectors themselves therefore constitute a *modal model* of the system, and the formulation above shows how a response model can be determined from knowledge of the modal model. Texts such as those of Ewins (1984), Maia and Silva (1997) and He and Fu (2001) present various algorithms for analytically or experimentally determining modal models.

In the case of analytic development (Figure 4.1) a description is usually constructed by assembling the equations of the spatial model of the system. If correct, this model provides a compact and complete representation of the system that can be used to obtain the modal model or the response model as required. Analytic development necessitates, however, detailed and accurate a-priori knowledge of the system components.

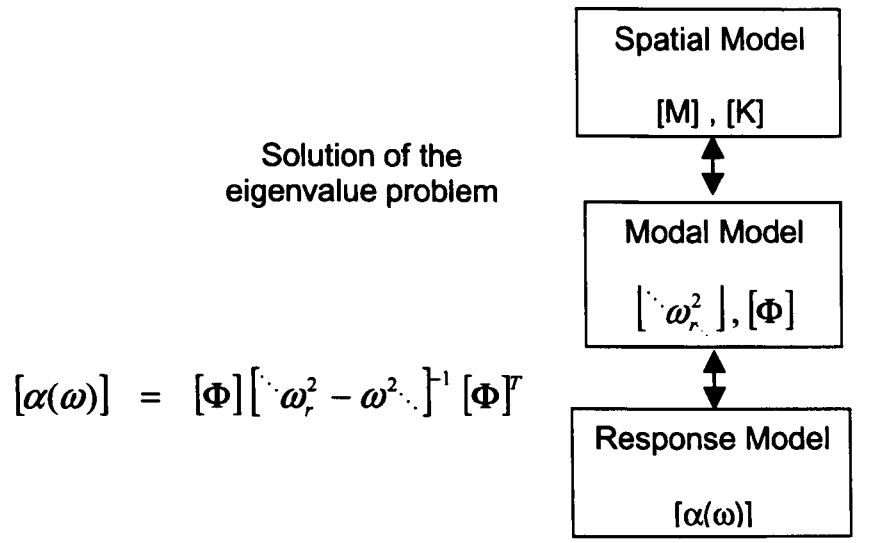

Figure 4.1 Analytic modelling approach.

The experimental approach (Figure 4.2), instead, starts with the measured response model then fits a modal model through a process of modal identification. Once a modal model is achieved it is then possible to directly write the spatial model from the mode shape vector and the natural frequency matrix. This approach can produce a very accurate representation of the system but can be difficult to obtain in practice due to problems such as noise in the data used during the modal identification stage.

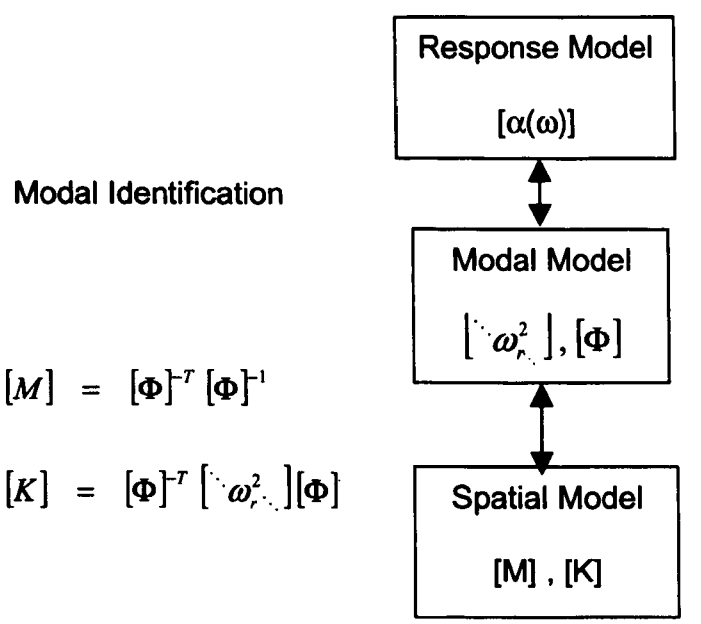

Figure 4.2 Experimental approach.

Due to the geometric complexity of child seats and uncertainties regarding the material property values, an experimental approach was chosen. Of the possible analysis methods the Frequency Domain Direct Parameter Identification method (FDPI) was chosen due to its robustness in the case of heavily damped systems. FDPI fits a spatial model directly to the experimentally measured frequency response functions then transforms the spatial model to obtain the modal model. A general model of the form

$$[M][\ddot{x}(t)]+[C][\dot{x}(t)]+[K][x(t)]=-[M][\ddot{z}(t)]+[F(t)] \qquad (4.5)$$

is assumed where [M], [C] and [K] are the mass, stiffness and damping matrices for the system of oscillators, [F] is a vector of external forces acting on the individual masses and [Z] is a vector of base excitation movements acting on the masses indirectly through springs and dampers. By assuming harmonic excitation and performing algebraic manipulation the matrix equation for a system with N_i inputs and N_o outputs can be written in the frequency domain as

$$\left[-\omega^2[I]+j\omega[A_1]+[A_0]\right][H(\omega)]=j\omega[B_1]+[B_0] \qquad (4.6)$$

where: $[A_1] = [M]^{-1}[C]$ is the mass modified damping matrix of order N_0 by N_o
$[A_0] = [M]^{-1}[K]$ is the mass modified stiffness matrix of order N_0 by N_o
$[H(\omega)]$ is the matrix of FRFs of order N_o by N_i
$[B_0]$ and $[B_1]$ are the force distribution matrices of order N_o by N_i

The equation above provides the basis for estimating the constant coefficients of the matrices $[A_1]$, $[A_0]$, $[B_1]$ and $[B_0]$. If during the experiment the power spectral densities and the frequency response functions are calculated for a total of L discrete frequency values then each term of $[H(\omega)]$ will contain 2L (both real and imaginary terms) values. Since in general the number of values (2L) in the $[H(\omega)]$ matrix will be far greater than the number of terms to estimate in the $[A_1]$, $[A_0]$, $[B_1]$ and $[B_0]$ matrices the problem is underconstrained and is therefore solved using regression analysis. Once $[A_1]$, $[A_0]$, $[B_0]$ and $[B_1]$ are estimated the natural frequencies and mode shape vectors of the modal model can be determined.

4.2.2 Child Seats Tested

Since experimental modal analysis is time consuming it had to be restricted to a limited number of child seats. Two selection criteria were adopted. The first was that each seat should be representative of a number of similar designs in terms of geometry, materials and cost. The second was that the seats should differ substantially between themselves in terms of their geometry, frame stiffness and carrying handle design. After inspecting a number of available products two seats were chosen. The first was a Mothercare Rock 'n' Go which used a plastic frame that was common to the products of several manufacturers. The frame was stiff, and the carrying handle could be folded down into a resting position against the frame. These properties suggested high resonance frequencies. The second seat, a Britax Rock-A-Bye, was representative of a class of products whose carrying handles remained exposed during use in the vehicle. The Rock-A-Bye also had the most flexible frame of the many seats inspected, a property would be expected to lead to low resonance frequencies. Three views of each seat are presented in Figure 4.3 below.

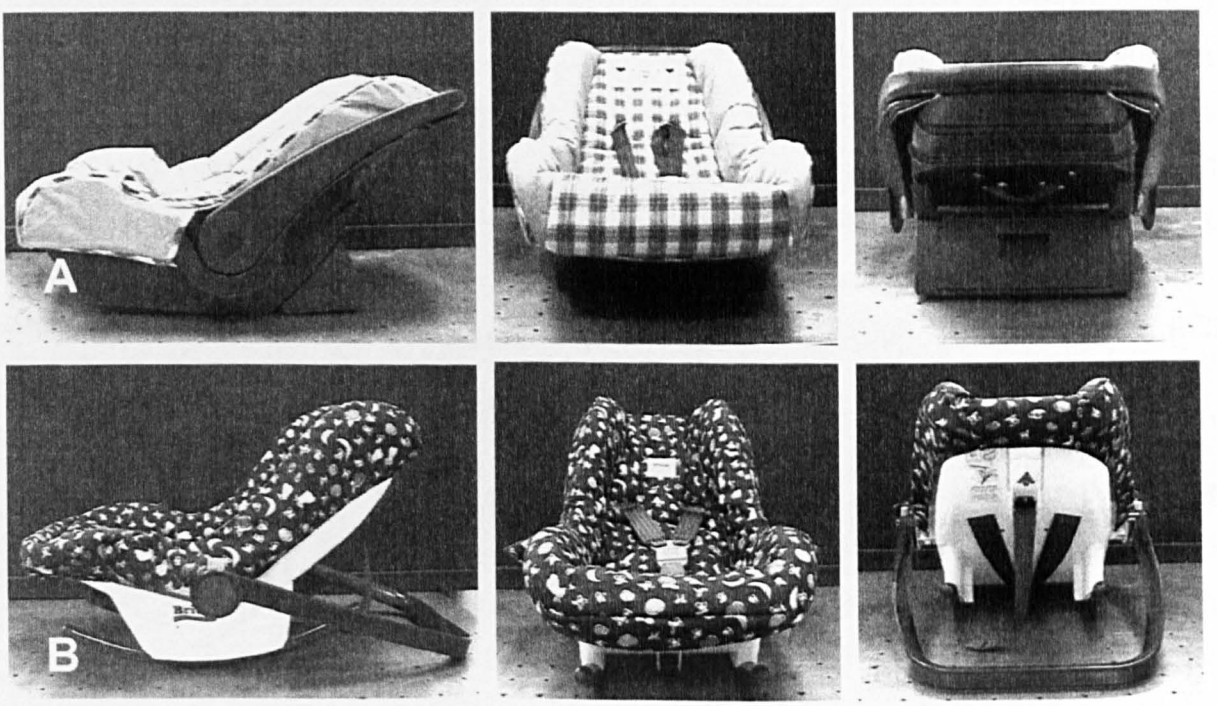

Figure 4.3 Three views of the Mothercare Rock 'n' Go (a) and Britax Rock-A-Bye (b)

4.2.3 Child Seat Vibration Testing Facility

A rig was built to perform the modal tests of the two child seats. A support frame held the child seat by means of elastic cords. The frame was centred over an LDS model 501 electrodynamic shaker (Ling Dynamic Systems 1977). The shaker was rated linear over the frequency range from 1.5 to 3000 Hz with a maximum force rating of 908 N and a maximum no-load acceleration of 40 g. Voltage drive signals were amplified by means of a Gearing & Watson SS300 power amplifier having a maximum current rating of 625 voltamps. The seat was connected to the shaker by means of a stinger-rod (Ewins 1984) which excited it from below in the vertical direction. The point of attachment of the stinger rod was chosen so as to be forward and to the left of the centre of gravity of the seat. This placement of the input avoided symmetry planes of the seat and thus guaranteed that both bending and torsional modes would be excited.

A PCB model 208B01 force transducer was attached to the child seat end of the stinger rod to measure the applied force. The transducer had a sensitivity of 122.1 mv/N and was rated linear from 0 to 90 Newtons, and from 1 to 50,000 Hz. It was hexagonal in shape and was 0.625 inch wide by 0.625 inch high. Twelve PCB model 336C04 piezoelectric accelerometers were fixed to the shell of each child seat to measure the motion response. The sensitivity values ranged from 94.3 to 100.8 $(m/s^2)/V$ as checked by means of a PCB model 394B06 calibration source. The linear range of the PCB 336C04 was ±50 g in amplitude and from 1 Hz (dependent on acceleration level) to 2000 Hz. The accelerometers were hexagonal in shape with a width of 0.625 inch and a height of 0.56 inch. Accelerometer charge output was amplified by means of a PCB model 483A DC power rack run from the mains supply.

Test signal generation, data acquisition and the experimental model analysis were performed using an LMS CADA-X revision 3.4 software system. The software was run on an HP model 715/64 workstation using a 24 channel Difa Systems SCADAS II front-end electronics unit. The frontend unit contained the multiplexers, A/D and D/A converters, conditioning circuits and a hardware DSP chip. Signal generation and data acquisition were performed using the Fourier Monitor [FMON] module while mode shape

vectors and loss factors were determined using the MODAL ANALYSIS module (LMS International 1999). Figure 4.4 presents a view of the test rig and associated hardware.

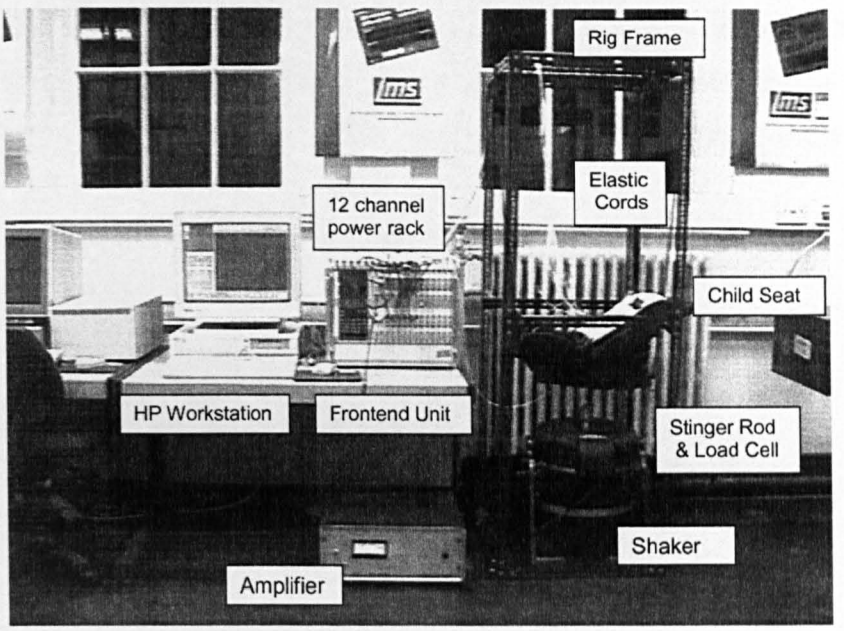

Figure 4.4 Child seat modal analysis test rig and instrumentation.

4.2.4 Measurement Points and Geometry Model

Restrictions in the number of available accelerometers and amplifiers limited the number of measurement points on the child seats to twelve. A sensor layout was sought which would provide an accurate representation of the first torsional and the first bending modes using 12 channels. Table 4.1 and Figure 4.5 present the accelerometer layout established for the Mothercare child seat, the layout for the Britax seat being similar. The axis system was taken such that the vertical direction of the child seat was Z, the fore-and-aft direction X and the lateral direction Y. Six accelerometers labeled n2, n3, n7, n8, n11 and n12 were placed along the inner surface of the seat with their measurement axis pointing in the direction normal to the surface. The accelerometers at positions n2 and n3 pointed in the vertical direction Z while those at n7, n8, n11 and n12 pointed normal to the backrest section of the child seat which made an angle of 120 degrees with respect to the X axis (i.e. reclined at 30 degrees with respect to the vertical). Six accelerometers numbered n1, n4, n5, n6, n9 and n10 were placed along the sides of the frame pointing normal to the surface in the lateral direction Y. Since a single-axis

accelerometer was used at each measurement point only one translational movement was measured per node rather than a full set of three. For nodes n1, n4, n5, n6, n9 and n10 only translations in the lateral (Y) direction were measured. Only vertical translations were measured for nodes n2 and n3, while n7, n8, n11 and n12 measured along an axis in the X-Z plane. The mode and deformation shapes presented therefore represent only deformations along the axis of the sensor, not a full 3 dimensional geometry.

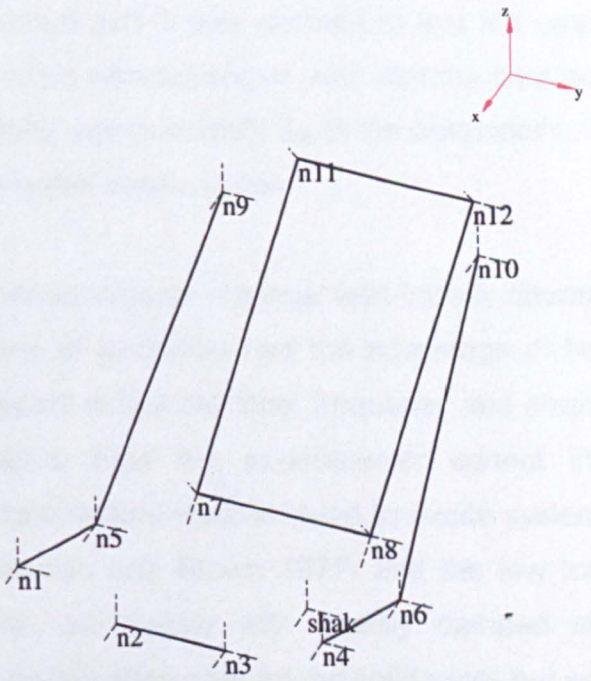

Figure 4.5 Child seat geometry model.

	Mothercare Rock 'n' Go			Britax Rock-A-Bye		
Measurement Point	**X (cm)**	**Y (cm)**	**Z (cm)**	**X (cm)**	**Y (cm)**	**Z (cm)**
Shaker	-18	5	-7.5	-21	6	-10.5
n1	0	-14	3.3	-5	-13.25	4
n2	0	-5	0	0	-9	0
n3	0	5	0	0	9	0
n4	0	14	3.3	-5	13.25	4
n5	-17	-14	-3.5	-19.5	-12.9	-6
n6	-17	14	-3.5	-19.5	12.9	-6
n7	-25	-8	-3.8	-28	-5	-5
n8	-25	8	-3.8	-28	5	-5
n9	-40.2	-11.7	16	-35.5	-12	21
n10	-40.2	11.7	16	-35.5	12	21
n11	-48	-8	15.4	-47	-5	23
n12	-48	8	15.4	-47	5	23

Table 4.1 Node coordinates of the child seat geometry model in cm.

4.2.5 Test Configuration and Test Excitation

As the modal analysis had the objective of establishing the dynamics of the child seats taken in isolation, and as no method of reproducing the impedance loading of a small child on the seat was identified (short of using an actual child but the necessary safety could not have been guaranteed), it was decided to test the empty devices suspended from elastic cords. The cords were arranged such that the seat remained with its bottom surface aligned horizontally, approximately as in the automobile. The seat was tested in full trim including covering and elastic straps.

Transient force input from an impulse hammer was initially attempted for performing the modal analysis. This form of excitation had the advantage of being rapid and easy to apply. A less positive aspect is that the time, frequency and amplitude characteristics of the force are interrelated, thus the experimenter cannot individually control the parameters. The high crest factors involved tend to excite system nonlinearities (Brown and Carbon 1977, Halvorsen and Brown 1977) and the low total energy can lead to signal-to-noise problems, particularly with heavily damped structures. An impulse hammer approach was initially attempted for the child seats but was soon discarded.

An LDS 501 electrodynamic shaker was used to produce 1 to 100 Hz band-limited Gaussian random force excitation to apply to the child seat. This excitation had the ability to measure the system response over a given frequency interval with a single test, thus reducing to a minimum the amount of time necessary for an analysis. Once random excitation was chosen a series of preliminary tests were performed to evaluate the achievable force levels at the input point (shaker), the resulting acceleration levels at the output measurement points (n1 to n12) and the amount of system nonlinearity. Since the shaker unit was large the necessary input forces were easily achieved. Preliminary inspection of the child seat frequency response functions showed that there were changes in some resonance frequencies with increasing levels of force, but that the movement of the resonance was not more than 1 Hz at excitation levels that were comparable to the vibration levels found in vehicles. Preliminary inspection of the

calculated mode shapes showed that there was also little qualitative change as a function of the input level. It was therefore decided to use only one force signal, chosen to have an amplitude which produced acceleration response levels at the output points of the child seat which were similar to those measured in automobiles. Table 4.2 below presents a summary of the input force signals used for each seat. The table provides the r.m.s. force levels at the input and the output acceleration levels produced at points n2 in the vertical direction and n9 in the lateral direction.

	Mothercare	**Britax**
r.m.s. force level	6.68 N	3.82 N
r.m.s acc. level at n2	0.806 m/s^2	0.341 m/s^2
r.m.s. acc. level at n9	0.071 m/s^2	0.236 m/s^2

Table 4.2 Summary of the test signals used.

4.2.6 Results for the Mothercare Child Seat

Since it is not convenient or informative to present all 12 measured frequency response functions for each seat only those relative to output locations n2 and n9 are presented. Additionally, all modulus curves indicate several resonances below 7 Hz which are not discussed further. These resonances were checked by visual inspection and found to be rigid body modes of the seat oscillating on the stinger rod and elastic cords. None were flexible body modes of the seat therefore they are not discussed further.

Figure 4.6 presents the accelerance and coherence functions measured from the shaker input point to output accelerometers n2 and n9 for the Mothercare seat. Several resonances are evident in the frequency range below 100 Hz, occurring at approximately 35, 73 and 92 Hz. All accelerance function peaks indicate relatively high levels of damping, with –3 dB points that were often separated by more than 3 Hz. Application of the half power method (Ewins 1984, Maia and Silva 1997, He and Fu 2001) to the resonances produced damping values which were in the range from 2 to 6

percent of critical. The high damping was assumed to be caused by the soft plastic material of the seat frame and the trim materials such as the polystyrene foam.

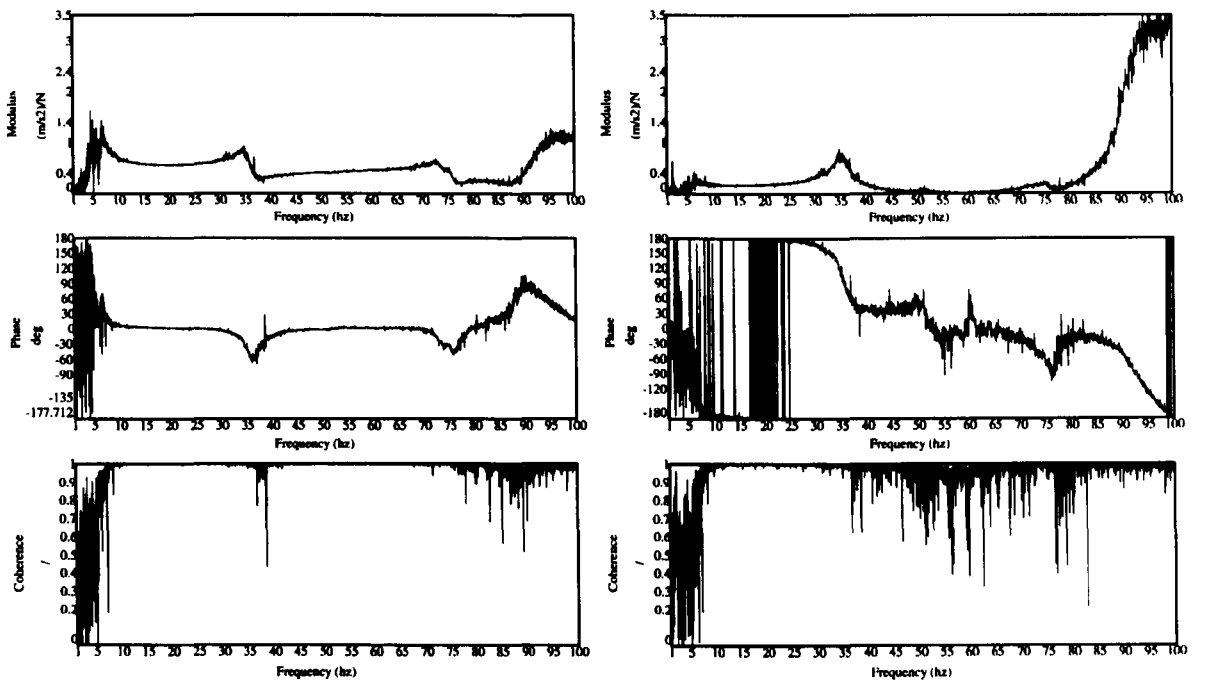

Figure 4.6 Accelerance and coherence functions from input to points n2 (left) and n9 (right) for the Mothercare seat.

Figures 4.7 to 4.9 present the mode shape vectors for the Mothercare child seat. The deformations have been amplified for visual clarity and all vectors have been plotted to the same scale. The first mode of vibration was a torsional mode. This was to be expected since the child seat shell resembles an elongated open U-section, with a bend in the middle. Open sections provide little resistance to torsion. The second mode of the Mothercare seat was a lateral bending mode which produced the highest movements at the centre near the handle mounting points. The small amplitude of vibration associated with this mode (compared to the first and third) suggested that it consisted of mainly handle movement which induced movement of the seat frame through the hinges. The third mode of vibration produced again large amplitudes and was principally an in-and-out flapping movement of the side panels.

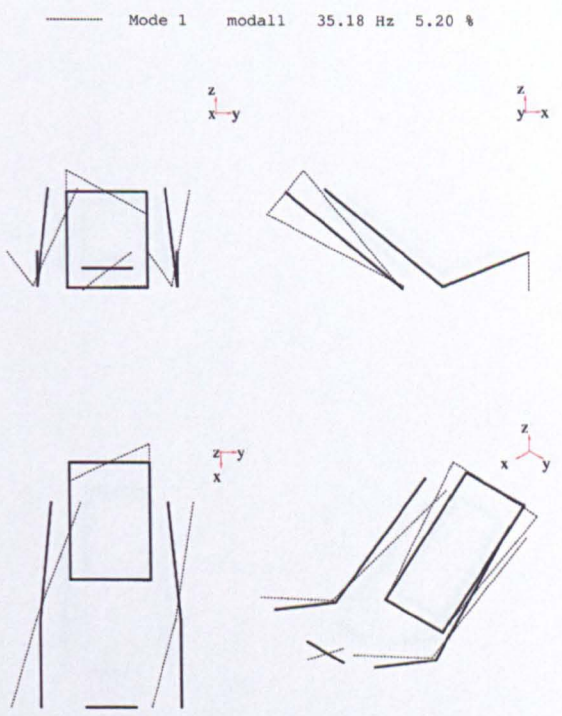

Figure 4.7 Mothercare child seat mode 1.

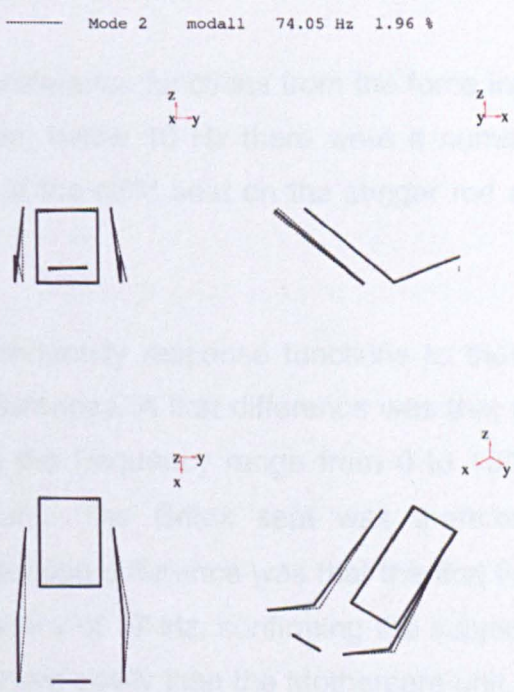

Figure 4.8 Mothercare child seat mode 2.

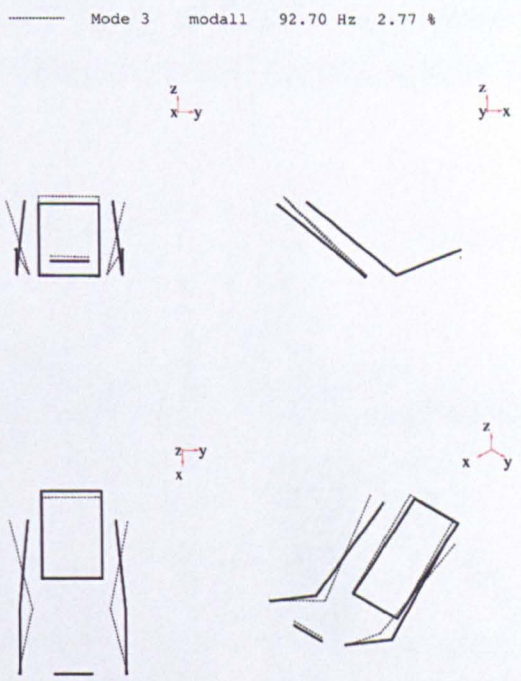

Figure 4.9 Mothercare child seat mode 3.

4.2.7 Results for the Britax Child Seat

Figure 4.10 presents the accelerance functions from the force input to the points n2 and n9 for the Britax seat. Again, below 10 Hz there were a number of rigid body modes associated with movement of the child seat on the stinger rod and elastic cords, these are not discussed further.

Comparison of the Britax frequency response functions to those from the Mothercare seat suggests important differences. A first difference was that there were eight flexible body modes of vibration in the frequency range from 0 to 100 Hz as opposed to the three of the Mothercare unit. The Britax seat was therefore a more challenging vibrational environment. A second difference was that the first flexible body mode of the seat was at the lower frequency of 17 Hz, confirming the subjective impression that the seat was softer and flexed more easily than the Mothercare unit. Inspection of any of the whole-body frequency weighting curves such as W_b suggests that vibration at a frequency as low as 17 Hz would be strongly perceived by a human occupant. A further

difference with respect to the Mothercare seat was the higher damping levels involved, the values being 2 to 8 percent critical. Finally, the accelerance modulus functions were generally higher than for the Mothercare seat, implying globally higher levels of vibration transmission.

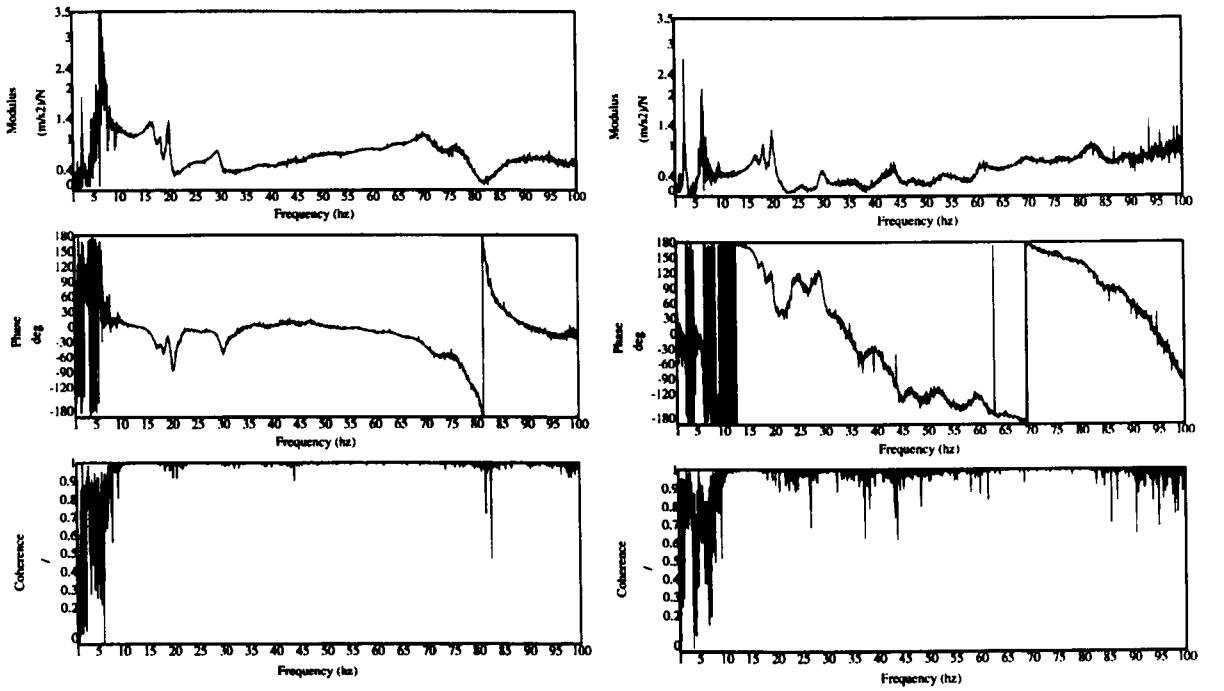

Figure 4.10 Accelerance and coherence functions from input to points n2 (left) and n9 (right) for the Britax seat.

Figures 4.11 through 4.14 present the mode shape vectors for the first four resonances of the Britax seat. The first two mode shapes consist of torsional movement of the frame, confirming again the weakness of the open U section currently used by all child seat designs. The third showed some torsion, but there was little movement of the frame generally. This resonance was inspected stroboscopically and found to be mainly movement of the handle. The fourth mode shape vector involved twisting and bending of the front part of the seat frame. Again, as with many resonances of the Britax seat, the handle was strongly vibrating at this frequency. All further mode shapes were impossible to resolve spatially given the 12 measurement accelerometers. Stroboscopic inspection was also unsuccessful in resolving the movements due to the small amplitudes involved.

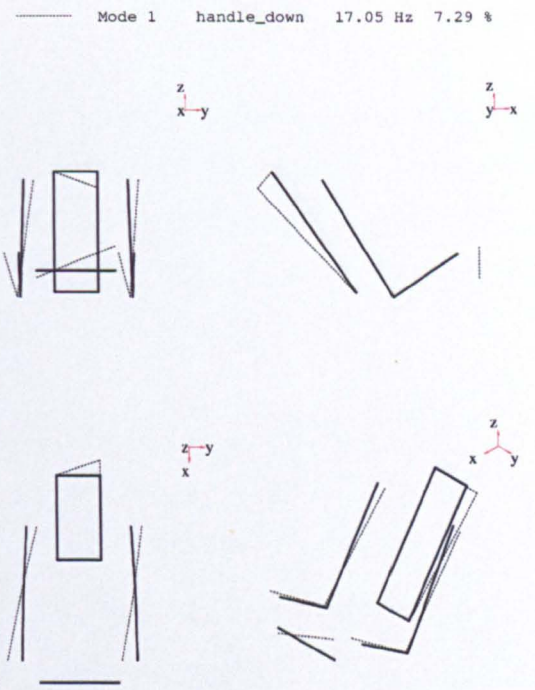

Figure 4.11 Britax child seat mode 1.

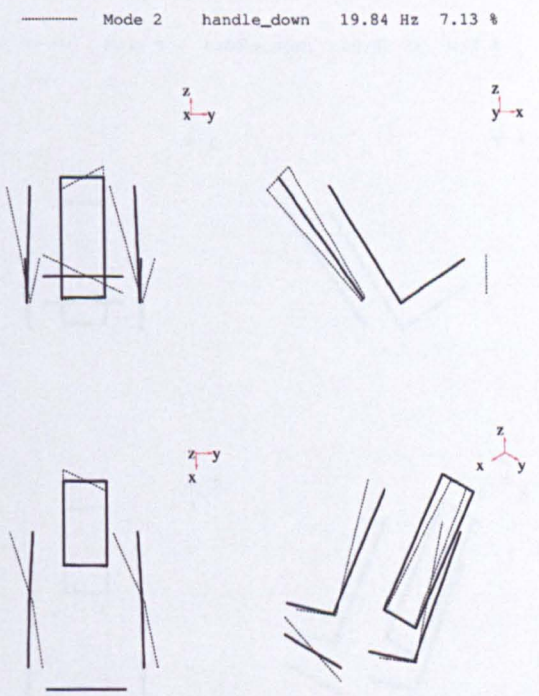

Figure 4.12 Britax child seat mode 2.

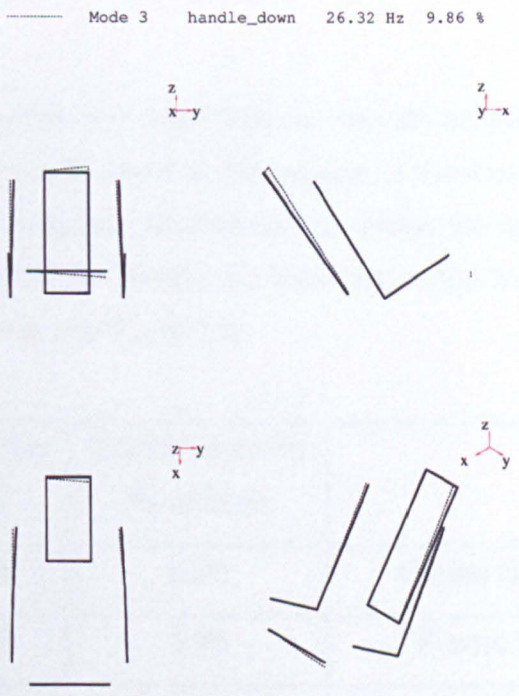

Figure 4.13 Britax child seat mode 3.

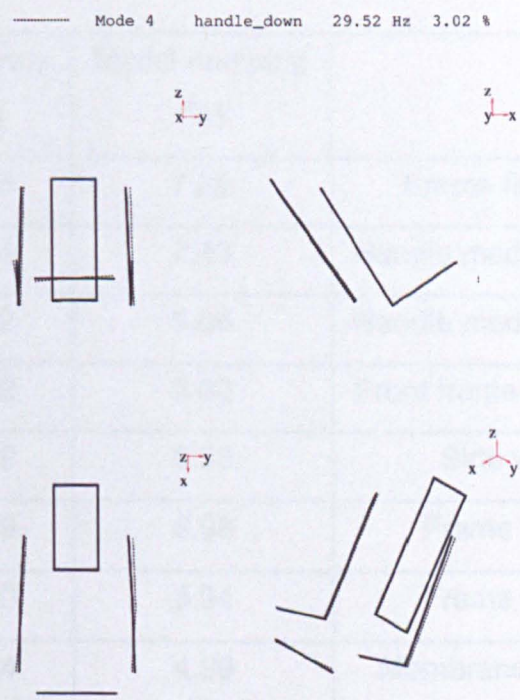

Figure 4.14 Britax child seat mode 4.

4.2.8 Discussion

Tables 4.3 and 4.4 summarise the experimental modal analysis results. Resonance frequencies, modal dampings and a verbal description of the mode shapes are provided. Question marks are used to indicate resonances for which the number of measurement accelerometers was insufficient to identify the movement due to spatial aliasing (Ewins 1984, Maia and Silva 1997, He and Fu 2001).

Mode Number	Frequency (Hz)	Modal Damping (% critical)	Shape
1	35.18	5.20	Frame first torsion mode
2	74.05	1.96	Frame lateral bending
3	92.70	2.77	Frame side flapping

Table 4.3 Vibrational modes of the Mothercare seat in the range from 0 to 100 Hz.

Mode Number	Frequency (Hz)	Modal damping (%)	Shape
1	17.05	7.29	Frame first torsion mode
2	19.84	7.13	Handle mode with frame torsion
3	26.32	9.86	Handle mode with frame torsion
4	29.52	3.02	Front frame twisting and handle
5	42.89	6.53	Side wings flapping
6	71.79	6.98	Frame torsion mode ?
7	83.40	3.94	Frame torsion mode ?
8	97.24	4.99	Membrane bulging of back ?

Table 4.4 Vibrational modes of the Britax seat in the range from 0 to 100 Hz.

It can be noted that both child seats had resonance frequencies in the range of human whole-body vibration comfort from 0.05 to 100 Hz. Current frequency weightings for vertical direction whole-body vibration such as W_b from national standard BS 6841 (1987) or W_k from ISO 2631 (2001) suggest that humans are sensitive to vibrations in the range from 0.5 to 100 Hz. For example, the asymptotic approximation of frequency weighting W_b of BS 6841 gives a value of 1.0 (the maximum) for the frequency range from 5 to 16 Hz and a value of 16/f for the frequencies from 16 to 80 Hz. At 17 Hz this gives a weighting value of 0.94 which is high. The Mothercare seat with a first resonance frequency of 35 Hz is better suited to isolating the child from road vibrations since the W_b value at 35 Hz is 0.45, less than half. Having flexible body mechanical resonances of the child seat unit at such low frequencies makes the task of vibration control difficult since the surfaces in contact with the child can be amplifying the vibration arriving from the vehicle. *It would therefore appear that the majority of the child restraint systems currently on the market are inappropriate vibrationally regardless of mounting system in the vehicle.*

A further interesting point is that the damping levels were found to be high for both child seats. *From the results it would not seem efficient to attempt to improve the vibrational behaviour of the seats by applying damping treatments.* The plastic and foam of the frame, together with the cloth and wadding of the trim materials, appear to be providing levels of damping similar to what can be achieved using constrained layer damping treatments (Beranek and Ver 1992). *It would seem probable that any further design improvements would need to originate from redesign of the structural elements to improve both handle and frame stiffness, and to reduce the free play which currently permits impact dynamics at the handle hinges.*

4.3 Child Seat Operational Deflection Shapes Analysis

4.3.1 Operational Deflection Shapes Analysis (ODS)

Modal analysis is normally performed on an object in the laboratory under controlled conditions using a reduced number of input excitations. Operational deflection shapes (ODS) analysis, on the other hand, normally involves identifying the response of a complete system during actual use. In operational deflection shapes analysis the measured quantities $XR_i(\omega)$ can be any forces and motions measured during a period of operation which represents either a specific mission (Giacomin, Steinwolf and Staszewski 2000) of the machine or a condition known to produce specific problems which are under investigation.

In operational deflection shape analysis (also known as running modes analysis) each measured signal is first transformed to the frequency domain by means of Fourier analysis. Once in the frequency domain a specific frequency value can be chosen and the amplitude and phase values used to animate a geometry model of the system. If a specific resonance frequency is chosen for analysis, such animation permits the movement shape to be clarified in a similar fashion to stroboscopic methods. In a given power spectrum a resonance peak which is widely separated from neighbouring resonances will have an operational deflection shape vector $[XR]$ which closely resembles the mode shape vector $[X_k]$ for the resonance. The reason is the low contribution, at that frequency, of other modes and resides due to the wide frequency separation. In such cases a running mode can be just as informative as a mode shape vector towards identifying the nature of the system response.

Some points must be remembered when working with operational deflection shapes. If, for example, a test of a given system measured *m* input forces and *N* output displacements then the running mode $[XR]$ could be described in terms of the mode shape vector $[X_k]$ by

$$[XR_i(\omega_p)] = [H_{i1}(\omega_p)]F_1(\omega_p) + [H_{i2}(\omega_p)]F_2(\omega_p) + \ldots [H_{im}(\omega_p)]F_m(\omega_p)$$

$$= \left[\sum_{k=1}^{N} \frac{X_{ik}\, X_{1k}}{j\omega_p - \lambda_k}\right] F_1(\omega_p) + \ldots + \left[\sum_{k=1}^{N} \frac{X_{ik}\, X_{mk}}{j\omega_p - \lambda_k}\right] F_m(\omega_p) \tag{4.7}$$

where i indicates the degree of freedom, ω_p is the frequency of the resonance being investigated and $F_j(\omega_p)$ is the force input at degree of freedom j. The above expression demonstrates several considerations. Firstly, a running mode can be identified for any measured frequency ω_p of the system whereas a normal mode vector has a fixed natural frequency. This suggests that the individual performing the analysis must decide a set of criteria external to the operational deflection shapes algorithm for choosing the frequencies which will be considered running modes. Secondly, it can also be seen that running modes depend on the level and nature of the forces acting on the system since the input excitation and the system frequency response are mixed together when determining a running mode. Care must be taken during selection and interpretation of the running modes since nonuniform system excitation (such as road input) can lead to assigning importance to a deflection shape which was simply the response of the system to a peak in the external excitation spectrum. Finally, running modes depend on the structural characteristics of the system since the measured frequency response functions are in the expansion. This implies that a well-chosen running mode will produce a deflection shape which closely matches the mode shape vector of the system at that resonance frequency.

4.3.2 Experiment

In order to measure the dynamic behaviour of a child seat during operation in a vehicle an experiment was organised in which an automobile was driven over several road surfaces. The test automobile used was a 1990 Fiat Uno with 145/SR14 radial tyres. The vehicle had 156,797 km on the odometer, suspensions were efficient, tyres were also efficient and inflated at the factory recommended pressure. During all tests there were two adults in the vehicle: one driving and one sitting on the rear seat operating a data recorder. The driver was female, weighed 55.0 kg and was 1.58 m

in height. The person operating the data recorder was male, weighed 88 kg and was 1.80 m in height.

The child seat used was a second Mothercare Rock 'n' Go identical to the one on which the modal testing was performed. As with the modal analysis twelve PCB model 336C04 piezoelectric accelerometers were fixed to the shell of the seat to measure the motion response. The sensitivity values ranged from 94.3 to 100.8 $(m/s^2)/V$. The linear range of the PCB 336C04 was ± 50 g in amplitude and from 1 Hz (dependent on acceleration level) to 2000 Hz. The accelerometers were hexagonal in shape with a width of 0.625 inch and a height of 0.56 inch. Accelerometer charge output was amplified by means of a PCB model 483A DC power rack run from an external 24 volt batery (so as to avoid noise from the vehicle's electrical system). The data was recorded by means of a 16 channel Sony PC216A DAT tape recorder. The PC216 recorder had a maximum throughput capacity of 5 kHz in 16 channel mode and a maximum recording time of 180 minutes.

A similar accelerometer layout to that used for the modal testing of the Mothercare Rock 'n' Go was adopted for the ODS tests. The vertical direction of the seat was taken to be Z, the fore-and-aft direction was labelled X and the lateral direction was labelled as Y. The origin of the reference system was fixed near the front edge along the centre-line of the seat midway between points n2 and n3. Six accelerometers were placed along the inner surface of the child seat with their measurement axis pointing in the direction normal to the surface. These accelerometers were labelled n2, n3, n7, n8, n10 and n11. The accelerometers at positions n2 and n3 pointed directly in the vertical direction Z while those at n7, n8, n10 and n11 pointed normal to the backrest section of the seat which made an angle of 120 degrees with respect to X axis (i.e. reclined at 30 degrees with respect to the vertical). Six accelerometers were placed along the sides of the frame pointing normal to the interior surface in the lateral direction Y. These were numbered n1, n4, n5, n6, n9 and n12. The coordinates (in cm) of each measurement point are given in Table 4.5 while the wire-frame representation of the geometry model is presented as Figure 4.15.

	Mothercare Rock 'n' Go		
Measurement Point	**X (cm)**	**Y (cm)**	**Z (cm)**
n1	0	-14.0	3.3
n2	0	-5.0	0
n3	0	5.0	0
n4	0	14.0	3.3
n5	-17.0	-14.0	-3.5
n6	-17.0	14.0	-3.5
n7	-25.0	-8.0	-3.8
n8	-25.0	8.0	-3.8
n9	-40.2	-11.7	16.0
n10	-50.0	-8.0	15.4
n11	-50.0	8.0	15.4
n12	-40.2	11.7	16.0

Table 4.5 Operational deflection shapes node coordinates in cm.

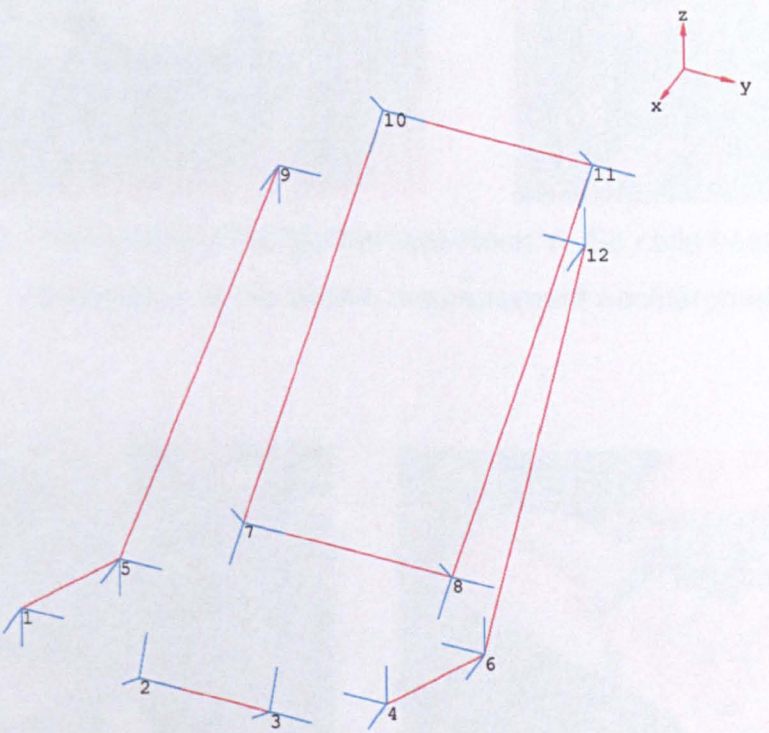

Figure 4.15 Geometry model for the Mothercare Rock 'n' Go used for the operational deflection shapes analysis.

As in the case of the modal analysis only one translational movement was measured at each node point rather than a full set of three. For nodes n1, n4, n5, n6, n9 and

n12 only translations in the lateral (Y) direction were measured while only vertical translations were measured for nodes n2 and n3. Nodes n7, n8, n10 and n11 measured along an axis in the X-Z plane reclined backwards at 30 degrees with respect to the vertical. Figure 4.16 presents two views of the instrumented child restraint with the covering cloth removed. The accelerometer cables exiting the sensors were passed under the covering cloth and gathered outside the seat into a harness. Figure 4.17 presents two views of the complete set of equipment as installed in the vehicle.

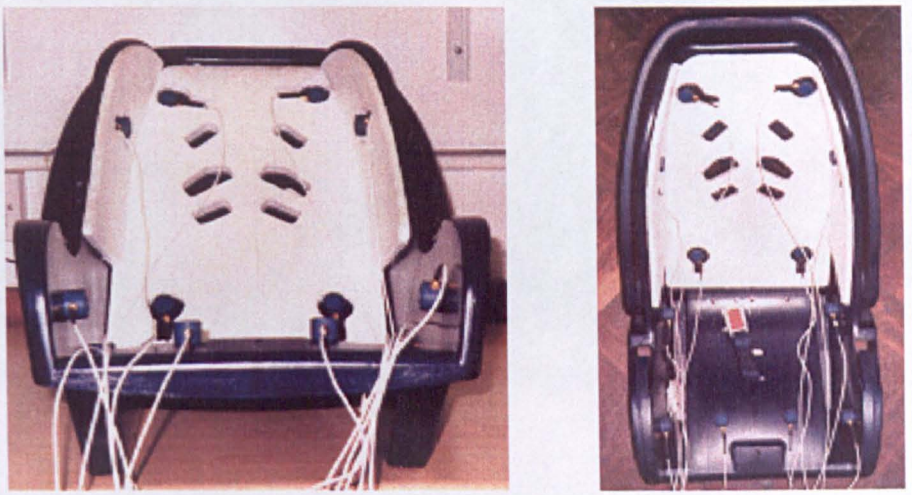

Figure 4.16 Two views of the Mothercare Rock 'n' Go child seat after installation of the twelve measurement accelerometers.

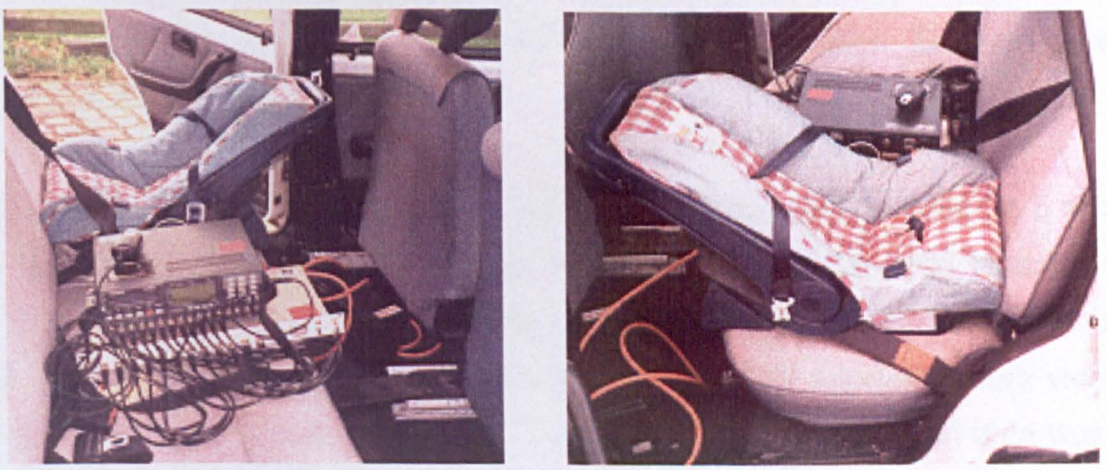

Figure 4.17 Two views of the Mothercare Rock 'n' Go seat and the measurement equipment after installation in the vehicle.

Three loading conditions were tested. The first loading was provided by a female child whose name was Lucy. At the time of the tests she was 10.5 months old and had a mass of 8.2 kg. The second loading condition was a sandbag filled to the same mass value of 8.2 kg as the child. The third was a no-loading condition, meaning an empty seat. Comparison of the results from the three conditions was expected to provide an indication of the sensitivity of the child seat dynamics to the loading.

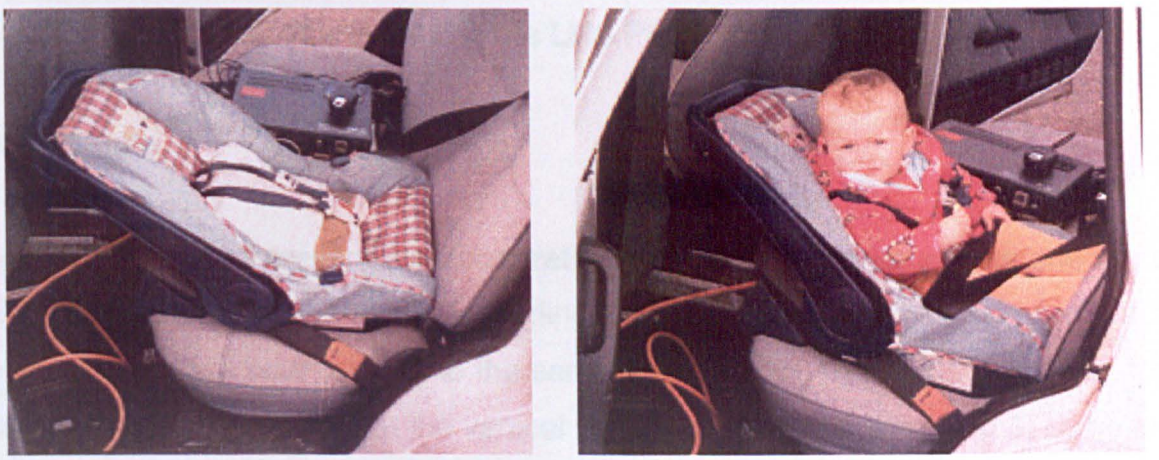

Figure 4.18 Sand bag installed in seat and child installed in seat.

The road surface chosen for performing the operational deflection shapes tests was the pave' (cobblestone) surface of Mary Street in Sheffield. It was chosen because of its ability to consistently generate significant amounts of random vibration at the floor of test vehicles for all frequencies up to 60 Hz (Giacomin 2000). Three runs were performed over the surface at 40 km/h for each loading condition. Each run provided approximately 20 seconds of data.

Data acquisition was performed using the Sony PC216A DAT recorder in 5 kHz, 16 channel, mode. Upon return to the laboratory the acceleration time histories were antialiase filtered at 250 Hz and sampled at 500 Hz using an LMS test and analysis system (LMS International 1999). Since the piezoelectric accelerometers were not accurate for frequencies below about 1.0 Hz all sampled acceleration data was high pass Butterworth filtered at 1 Hz with a 60 dB/oct slope. The acceleration was then single and double integrated by means of a Trapezium rule integrator so as to obtain velocity and displacement time histories for all twelve channels. All power spectral

densities and operational deflection shapes were determined using a block size of 4096 points which for the 500 Hz sampling used lead to a spectral resolution of 0.122 Hz. A 95% overlap was used which when applied to three runs with approximately 20 seconds of data each lead to a total of 150 averages.

Fourier analysis was performed using the LMS Time Data Processing software and the operational deflection shapes were determined using the LMS Running Modes software (LMS International 1999). All time histories, power spectral densities and deflection shapes were plotted using the LMS Plot Format Editor software.

4.3.3 Results

Figures 4.19 to 4.21 present the acceleration time histories measured for one run on Mary Street in each of the three loading conditions For ease of comparison all accelerations have been plotted to the same scale of ± 10 m/s^2 (approximately 1 g). The time histories confirm that the vertical direction (see channels 2 and 3) is the axis of greatest vibration and that the Mary Street surface is not purely random in nature. The high amplitude events such as the peaks at 2, 6, and 13 seconds on channels 2 and 3 of the child data confirm, along with the crest factor greater than 3.5, that the surface was not stationary. The Mary Street signal statistics actually place it in the category of Mildly Nonstationary road surfaces (Giacomin, Steinwolf and Staszewski 2001).

Figures 4.22 to 4.24 present the acceleration power spectral densities determined from the time histories. Inspection confirms that little if any vibrational energy was present in the child seat at frequencies greater than 60 Hz. An observation that can be made from the frequency domain data is that certain resonances are independent of the loading condition. For example, the vertical direction measurement channels 2 and 3 systematically contain resonance peaks at frequencies of approximately 1.7, 5.1, 6.6, 10.0, 21.2 and 30.0 Hz. From inspection it can also be noted that the resonances are not equally visible on all measurement channels. Whereas channels 2 and 3 measuring vertical acceleration at the front of the seat are strongly excited by the 1.7 Hz resonance, that resonance is almost completely missing from the date of channels 1, 4, 5, 6, 9 and 12 measuring the lateral (Y axis) acceleration.

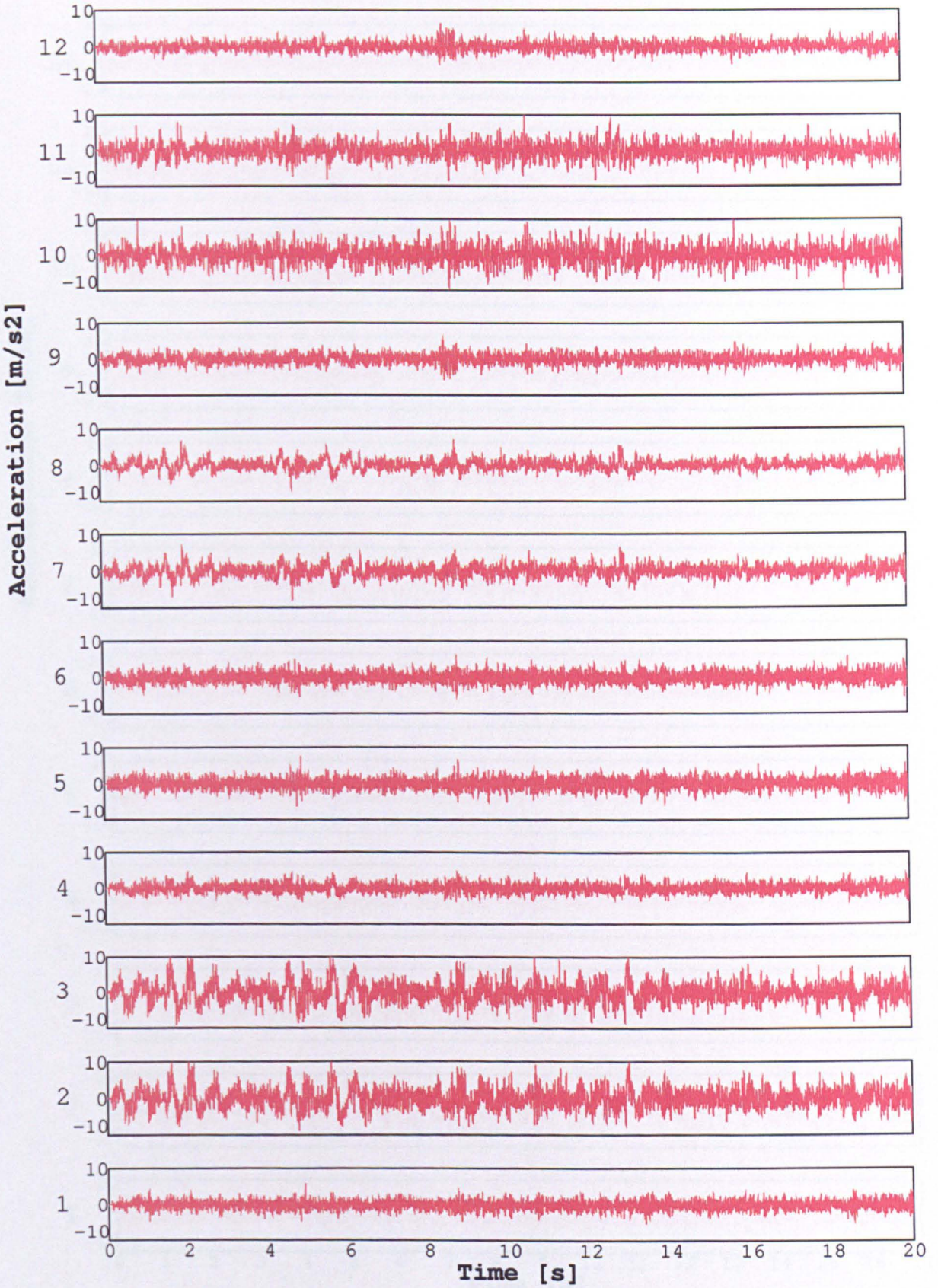

Figure 4.19 Acceleration time histories measured for one run with Lucy.

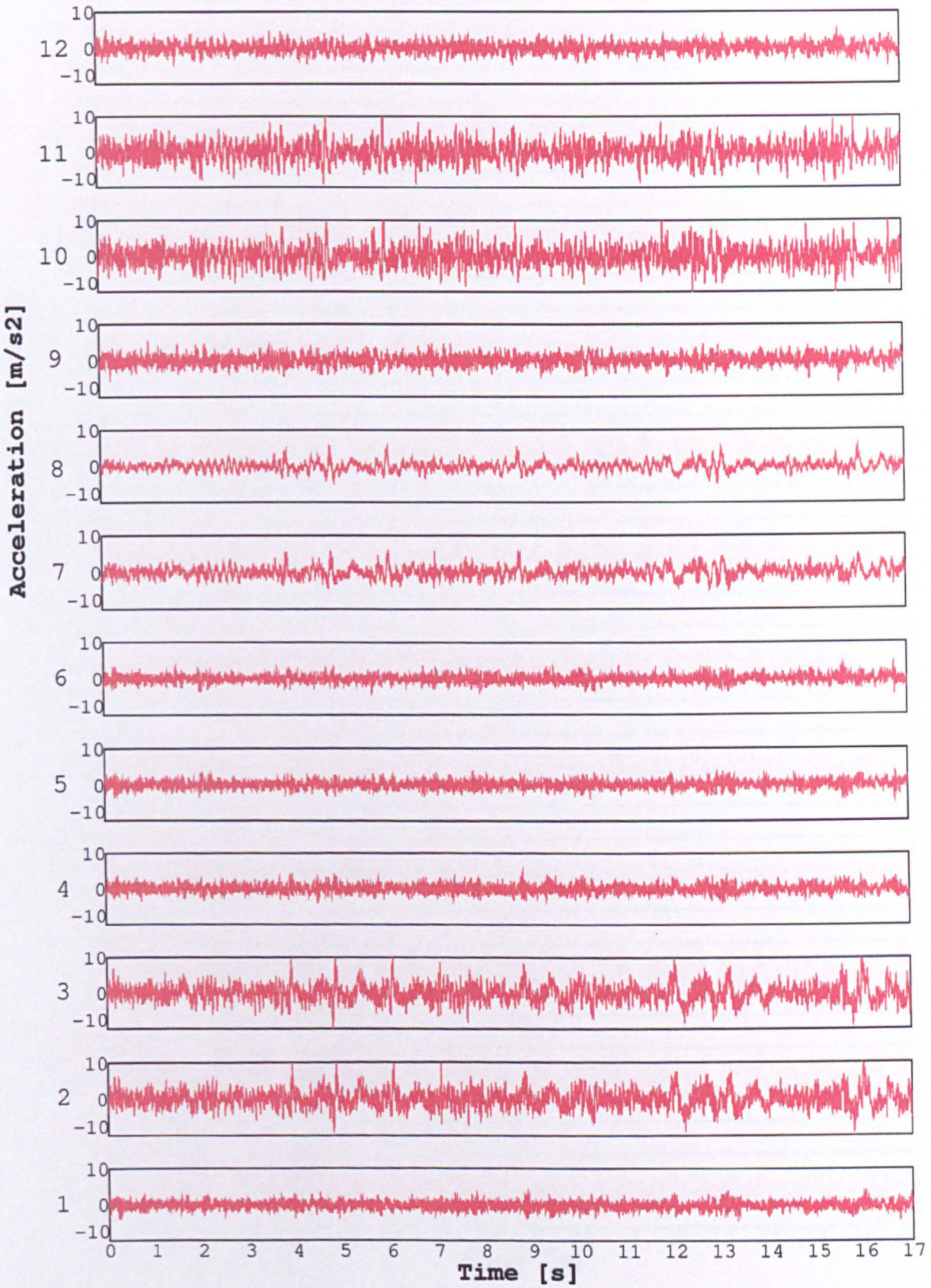

Figure 4.20 Acceleration time histories measured for one run with the sandbag.

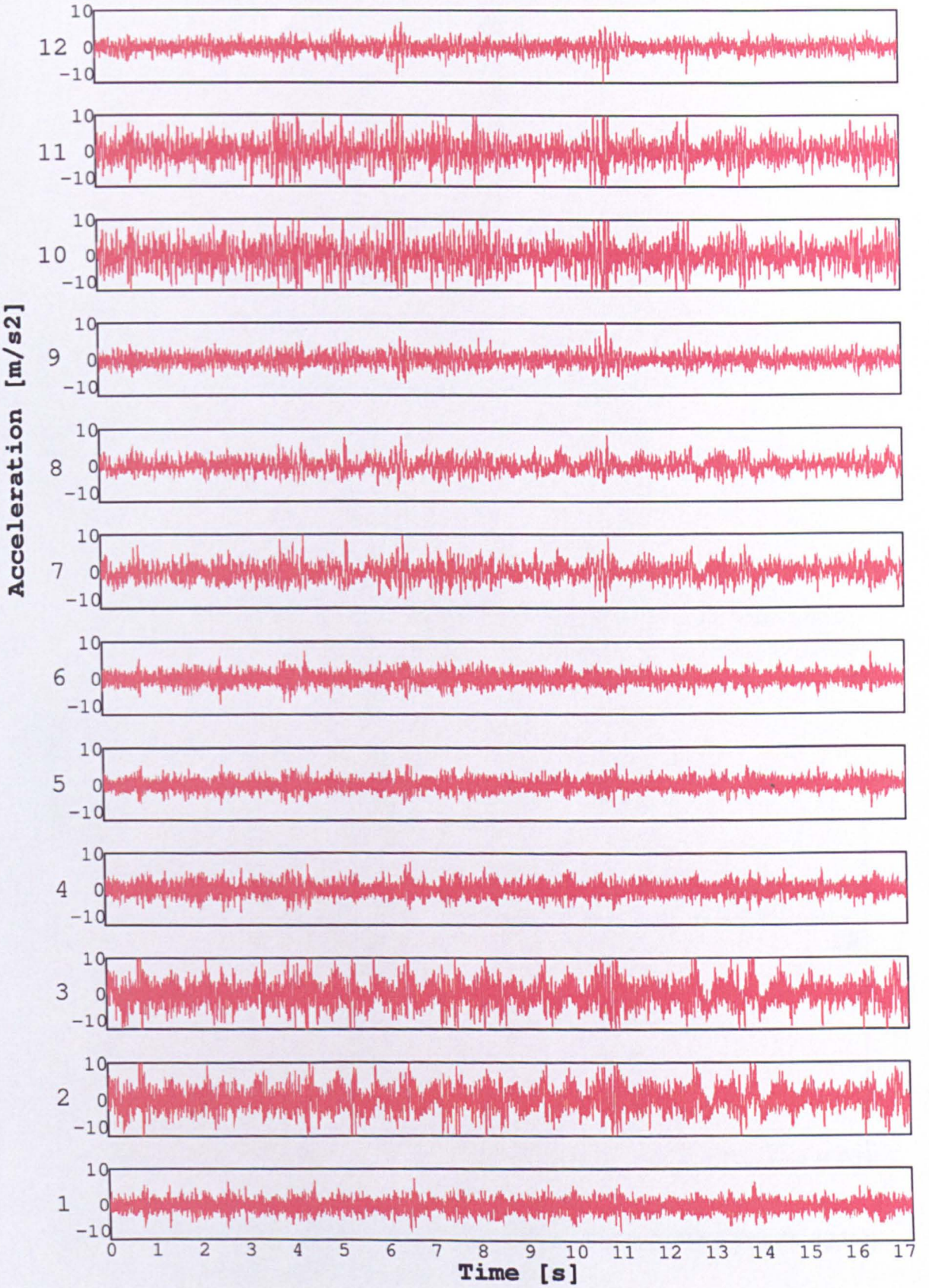

Figure 4.21 Acceleration time histories measured for one run with the empty seat.

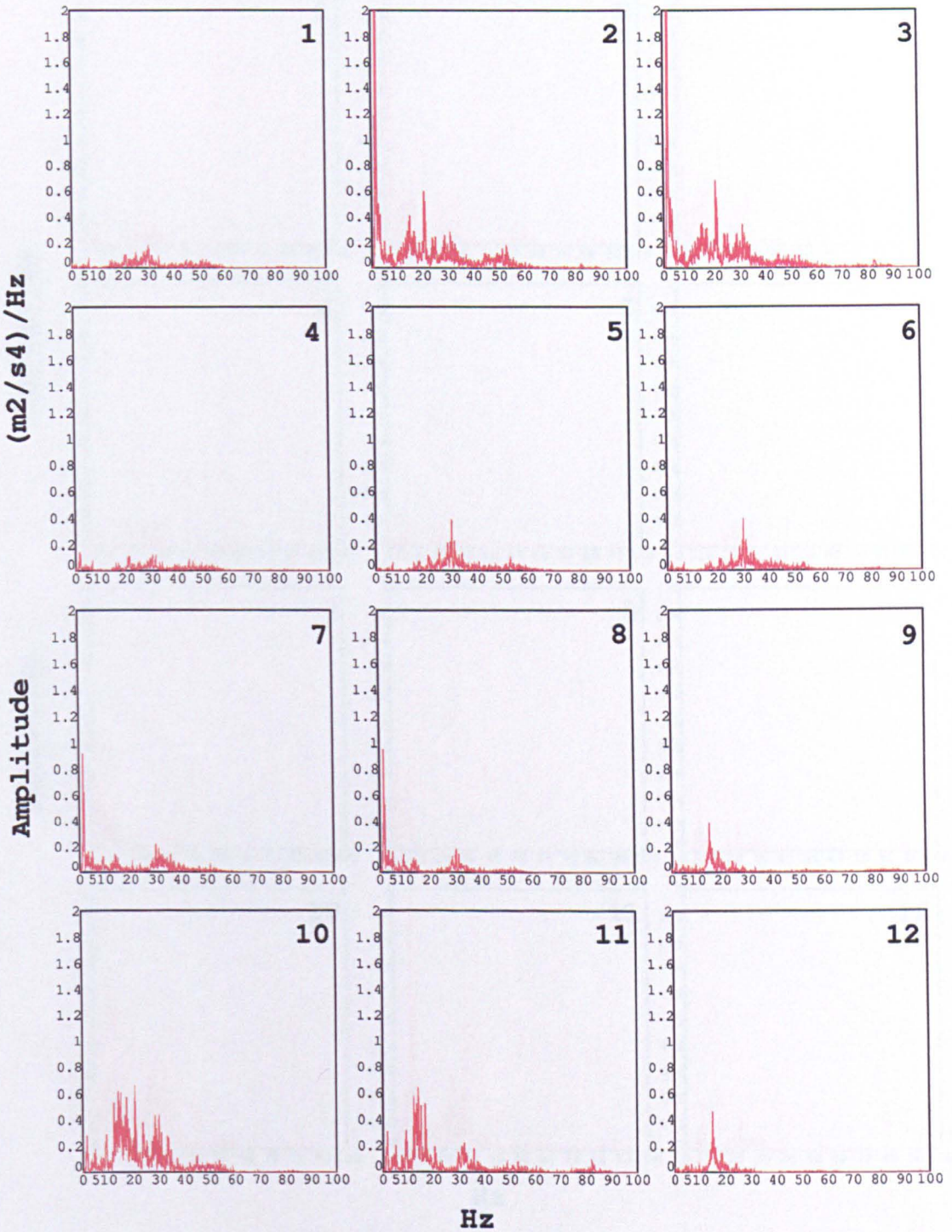

Figure 4.22 Acceleration PSDs for the twelve measurement points during one run with Lucy on Mary Street.

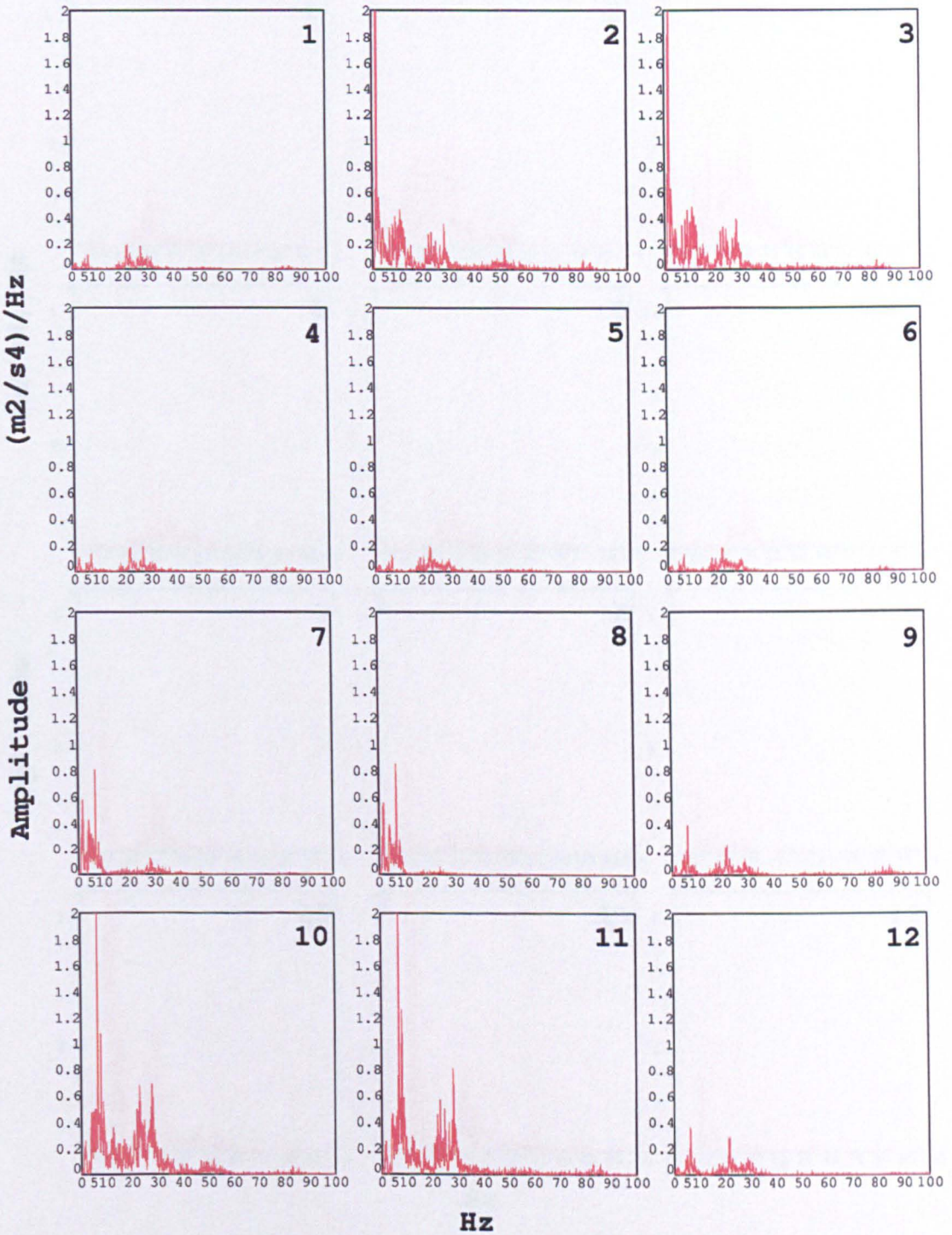

Figure 4.23 Acceleration PSDs for the twelve measurement points during one run with the sand bag on Mary Street.

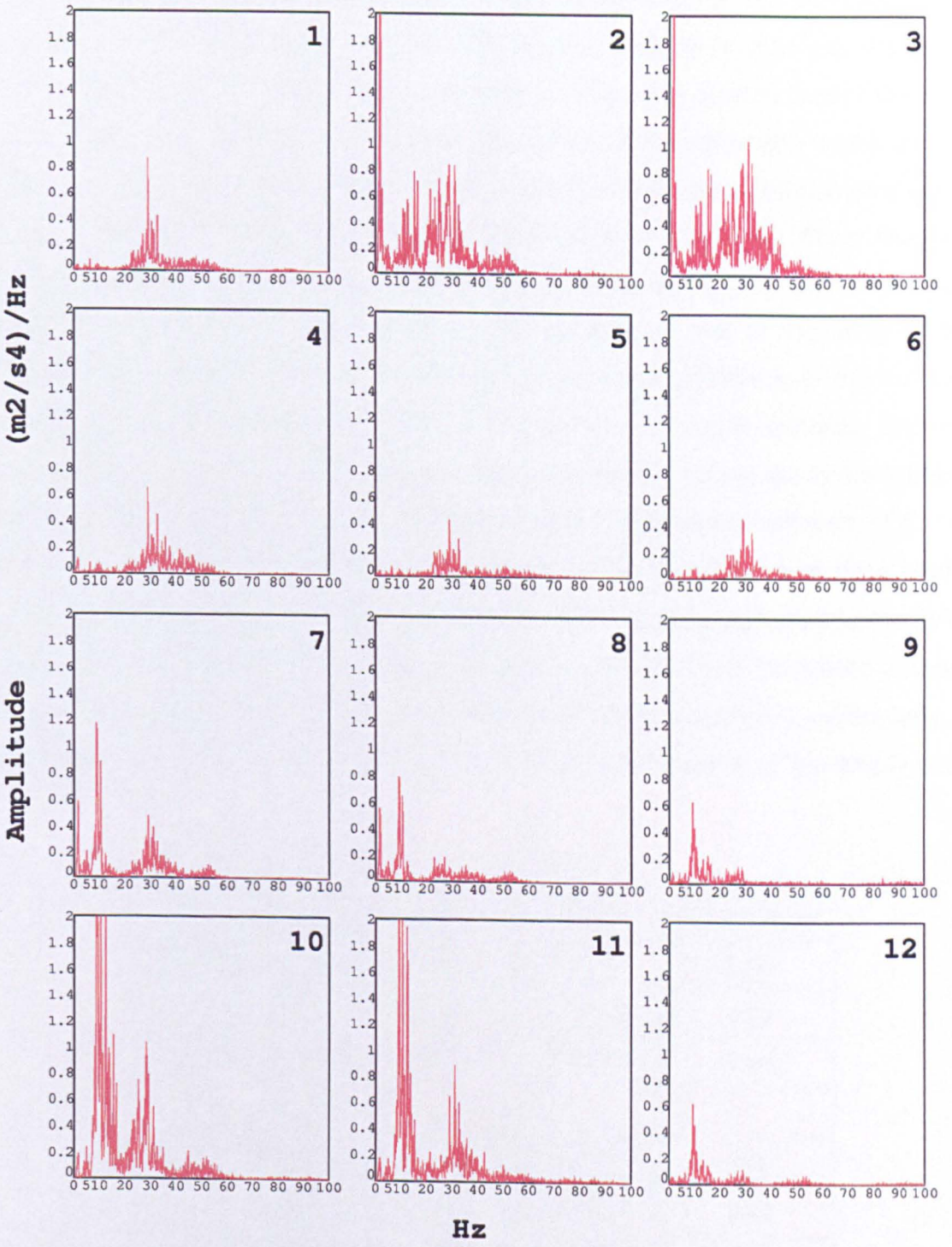

Figure 4.24 Acceleration PSDs for the twelve measurement points during one run with the empty seat on Mary Street.

Tables 4.6 to 4.8 present the root mean square, peak and crest factor statistics for each of the three loading conditions for measurement points 2 and 5. Point 2 was reported because it measured vertical vibration at the front of the child seat, thus it was sensitive to vertical input from the vehicle seat cushion and to any resonances involving vertical motion of the child. Grid point 2 was also directly under the legs of the child near the pressure points and thus one of the principle entry points of vibration into the body. Point 5 was chosen because it measured lateral vibration and because it was the closest point to the lower back of the child. From the power spectral densities of the twelve measurement channels it can be seen that all resonances identified as running modes were present on one or the other of these two channels (2 and 5). Table 4.6 contains the summary statistics of the measured accelerations, table 4.7 the velocities and table 4.8 the displacements. Given the nature of measurements performed using accelerometers the values in the tables are *absolute movements of the seat* as opposed to the *relative movements of the child seat with respect to the vehicle*. The magnitude of the displacement data confirms that the signals are relative to *the movement over the road* as opposed to the *relative movements within the vehicle*. An interesting point of note from the tables is that the levels are similar across the three very different loading conditions, particularly, and unexpectedly, between the test with the child (Lucy) and the test of the empty seat.

Test	r.m.s.	Peak	Crest Factor
Sand Bag (n2)	2.307	10.15	4.40
Lucy (n2)	2.621	10.30	3.93
Empty Seat (n2)	3.073	12.78	4.16
Sand Bag (n5)	1.002	4.073	4.06
Lucy (n5)	1.370	7.494	5.47
Empty Seat (n5)	1.480	5.896	3.98

Table 4.6 Summary of the acceleration signals measured at point 2 (vertical direction) and point 5 (lateral direction) on the pave' surface at 40 km/h. All values are in units of m/s^2.

Test	r.m.s.	Peak	Crest Factor
Sand Bag (n2)	0.108	0.401	3.71
Lucy (n2)	0.126	0.4663	3.70
Empty Seat (n2)	0.101	0.252	2.49
Sand Bag (n5)	0.02235	0.08621	3.86
Lucy (n5)	0.01628	0.05618	3.45
Empty Seat (n5)	0.01750	0.06978	3.99

Table 4.7 Summary of the velocity signals measured at point 2 (vertical direction) and point 5 (lateral direction) on the pave' surface at 40 km/h. All values are in units of m/s.

Test	r.m.s.	Peak	Crest Factor
Sand Bag (n2)	10.1	27.5	2.72
Lucy (n2)	11.67	32.0	2.74
Empty Seat (n2)	9.52	20.4	2.14
Sand Bag (n5)	2.31	6.14	2.66
Lucy (n5)	2.31	5.65	2.44
Empty Seat (n5)	1.90	4.98	2.62

Table 4.8 Summary of the displacement signals measured at point 2 (vertical direction) and point 5 (lateral direction) on the pave' surface at 40 km/h. All values are in units of mm.

Figures 4.25 and 4.26 present the average power spectral densities determined for points 2 and 5 using all the data from all runs in the three loading conditions. Peaks are found at 1.7, 5.1, 6.6, 10.0, 21.2 and 30.0 Hz. The data for the empty seat was remarkably similar to the data measured with the child, with most major resonances being the same. A possible explanation is that the measurement points chosen for the study were more sensitive to the dynamics of the seat unit than to those of the coupled system of child and seat. For the lateral direction this explanation is quite plausible since, unless the child is quite large, children do not actually touch the side panels of the seats unless they are leaning against them during a movement. This is

evident from visual inspection of seats in use. Also, for the tests described in this chapter, the sandbag was large enough to fit snugly into the Mothercare seat suggesting force exchange in the lateral direction. The contact, or lack of contact, might explain the similarity between the child and empty results and the differences between both of these sets and the data from the sandbag (particularly above 25 Hz). While in the lateral direction the dynamics of the child body may not play a large role given the low input levels present, the similarity between the child and empty loading results is remarkable in the vertical direction where child body dynamics have been shown (chapter 3) to be important and where input levels are high. *This single result, more than any other, suggests that measurements of acceleration performed on child seat frames actually measure mostly the frame response.* The data sets also suggest decoupling of child and seat frame at frequencies above the body resonance of the child. This can be seen in the vertical direction acceleration of measurement point n2 where the child and empty seat curves can be seen to separate starting from approximately 10 Hz. A further feature of all the data sets which is of particular interest is the similarity of response at 1.7 Hz.

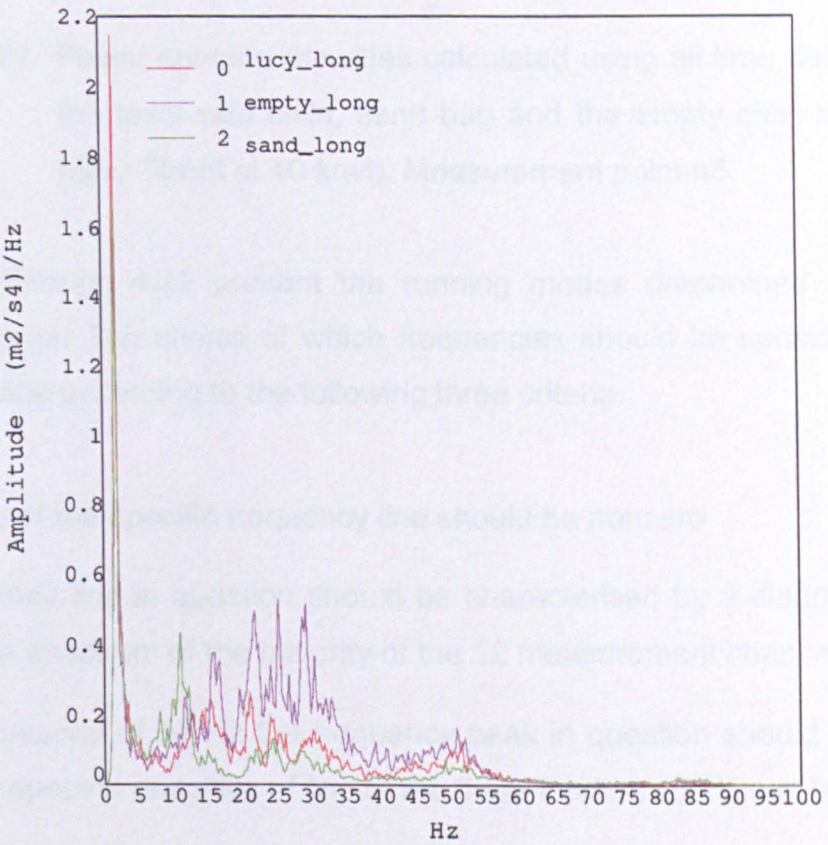

Figure 4.25 Power spectral densities calculated using all time data from the tests with child, sand bag and the empty seat on Mary Street at 40 km/h. Measurement point n2.

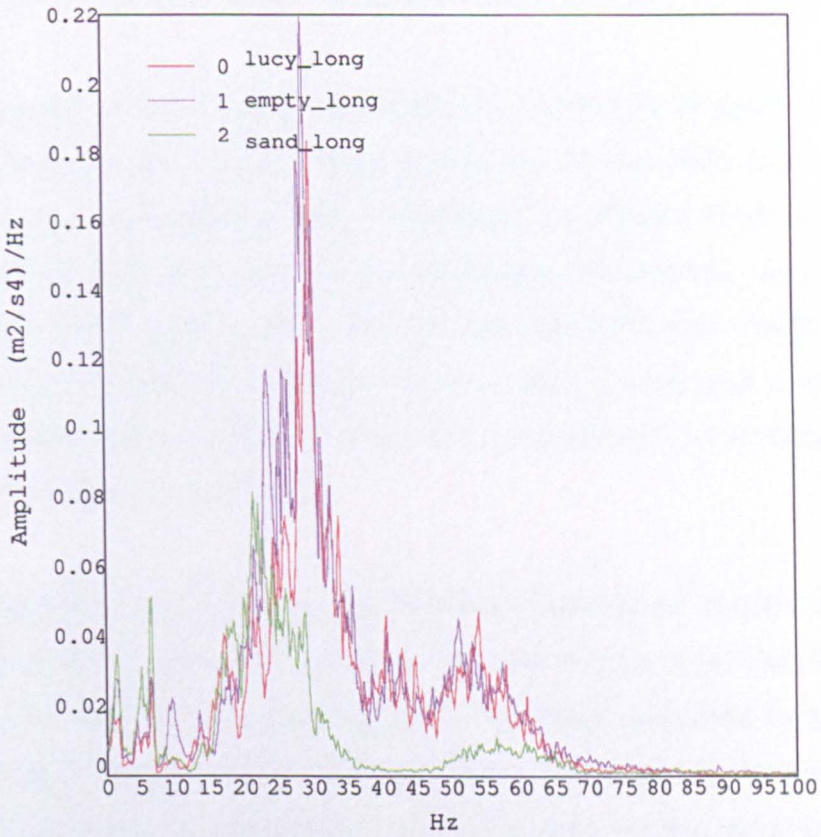

Figure 4.26 Power spectral densities calculated using all time data from the tests with child, sand bag and the empty child seat on Mary Street at 40 km/h. Measurement point n5.

Figures 4.27 through 4.29 present the running modes determined for the three loading conditions. The choice of which frequencies should be considered running modes was made according to the following three criteria:

- the energy of the specific frequency line should be nonzero
- the frequency line in question should be characterised by a clearly discernable peak in the spectrum of the majority of the 12 measurement channels
- within an interval of ±2 Hz the frequency peak in question should be present in the power spectral densities of two of the three loading conditions tested.

Applying the above criteria, 6 running modes were identified for the test with the child occupying the seat while 8 running modes were found for each of the other two loading conditions. The frequencies 1.7, 5.1, 6.6, 10.9, 21.7, 30.0 Hz were found to

be running modes of all three conditions while the frequencies 18.3 and 24.1 Hz were only present in the running modes of the sand bag and empty seat tests.

Several observations can be made regarding the deflection shapes. The first is that the 1.7 Hz resonance was a rigid body movement of the child seat in the vertical direction due to lack of coupling with the vehicle. Insufficient tension in the vehicle safety belts permits the child seat to produce large movements, and perhaps even bounce, on the vehicle seat cushion. The operational deflection shape indicates that while most of the movement is vertical, there is also a rotational component to the motion with instantaneous centre of rotation near to point of connection between the child seat and the vehicle safety belt.

A second observation is that the running modes determined at 24.1 and 30 Hz are manifestations of the first torsion mode of the seat frame, found at 35.18 Hz in the modal analysis of the freely suspended seat. The peak response frequency is lower than the resonance frequency found during the modal analysis for the same type of seat. There are several possible explanations for this but the most probable is that the running mode peaks were identified at 24.1 and 30 Hz rather than 35.18 because there was more energy present in the road input signal at those frequencies. A third observation is that the running mode at 18.3 Hz appeared to be the operational manifestation of the 20.46 Hz handle mode determined from the modal analysis of the Rock 'n' Go. Installation in the vehicle environment modified the frequency at which the motion most strongly manifested itself but comparison of the running mode to the normal mode suggests that the underlying dynamics are the same.

While more difficult to interpret than the operational deflection shapes discussed above, the running modes at 5.1, 6.6 and 10.9 Hz all involved a large amount of lateral movement and some amount of rotation about the for-aft axis of the child seat. The 5.1 Hz running mode appears to be a side-to-side rocking motion of the child seat over the cushion of the vehicle seat. While also possibly a rocking movement, the 6.6 Hz running mode contains more lateral than rotational movement, thus could perhaps better be described as side-to-side translation. The 10.9 Hz running mode was more complex to interpret and varied more in spatial distribution across the three loading conditions. From the animation sequences it was not clearly a rigid body

motion nor a flexible body motion. The behaviour at 10.9 Hz could not be resolved by means of the data measured.

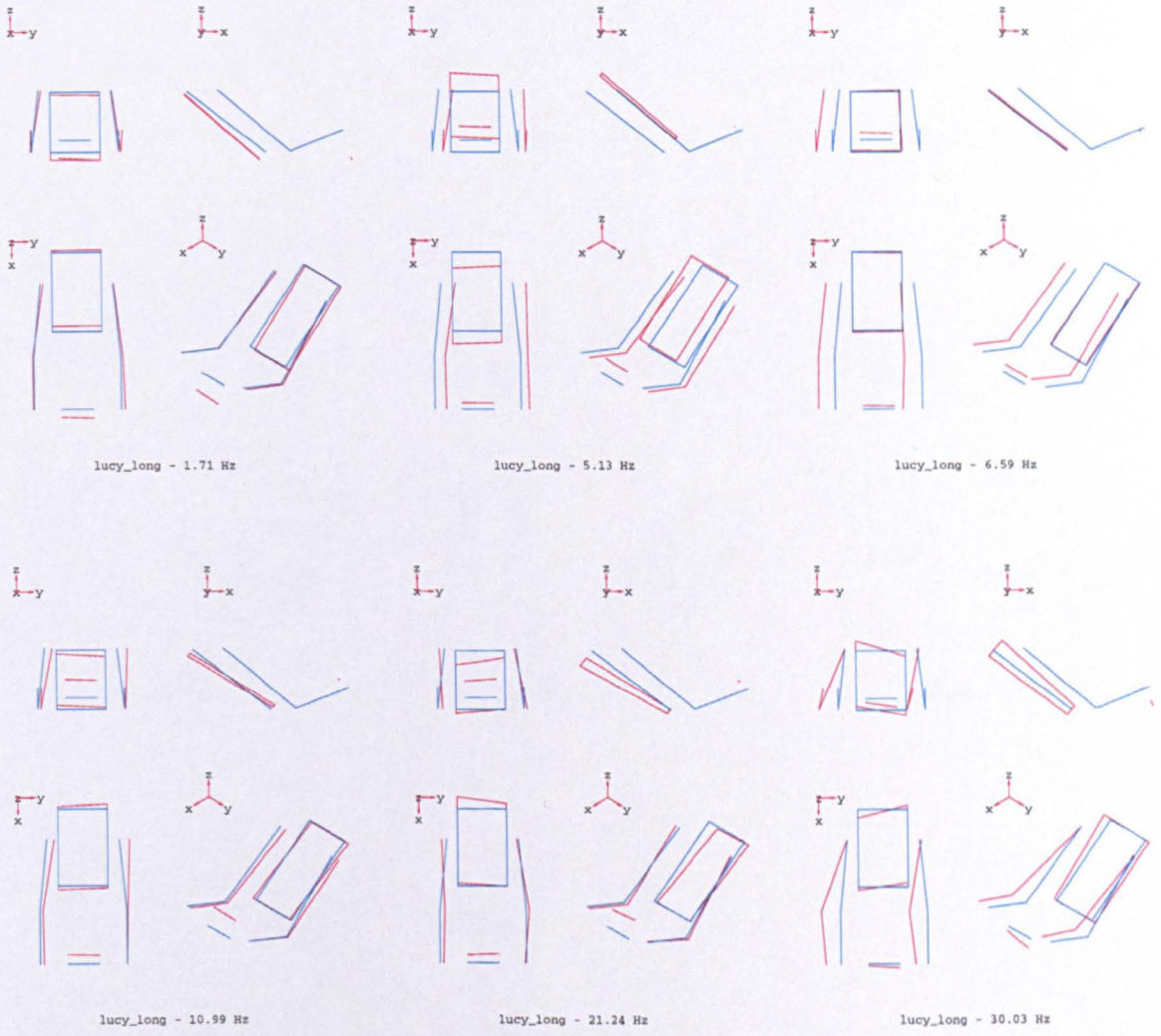

Figure 4.27 Running Modes of the Mothercare Rock 'n' Go on Mary Street when occupied by the child.

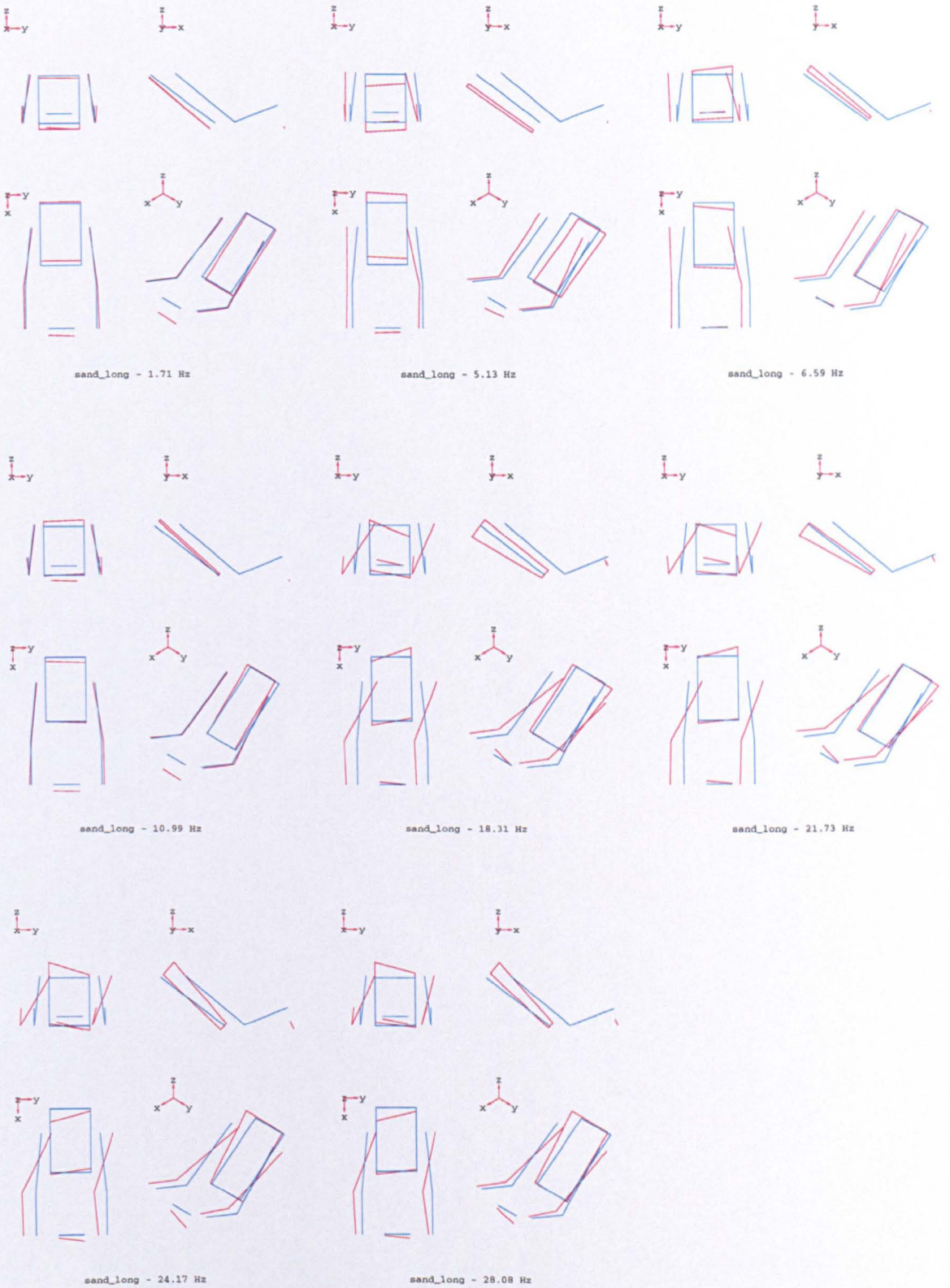

Figure 4.28 Running Modes of the Mothercare Rock 'n' Go on Mary Street when occupied by the sand bag.

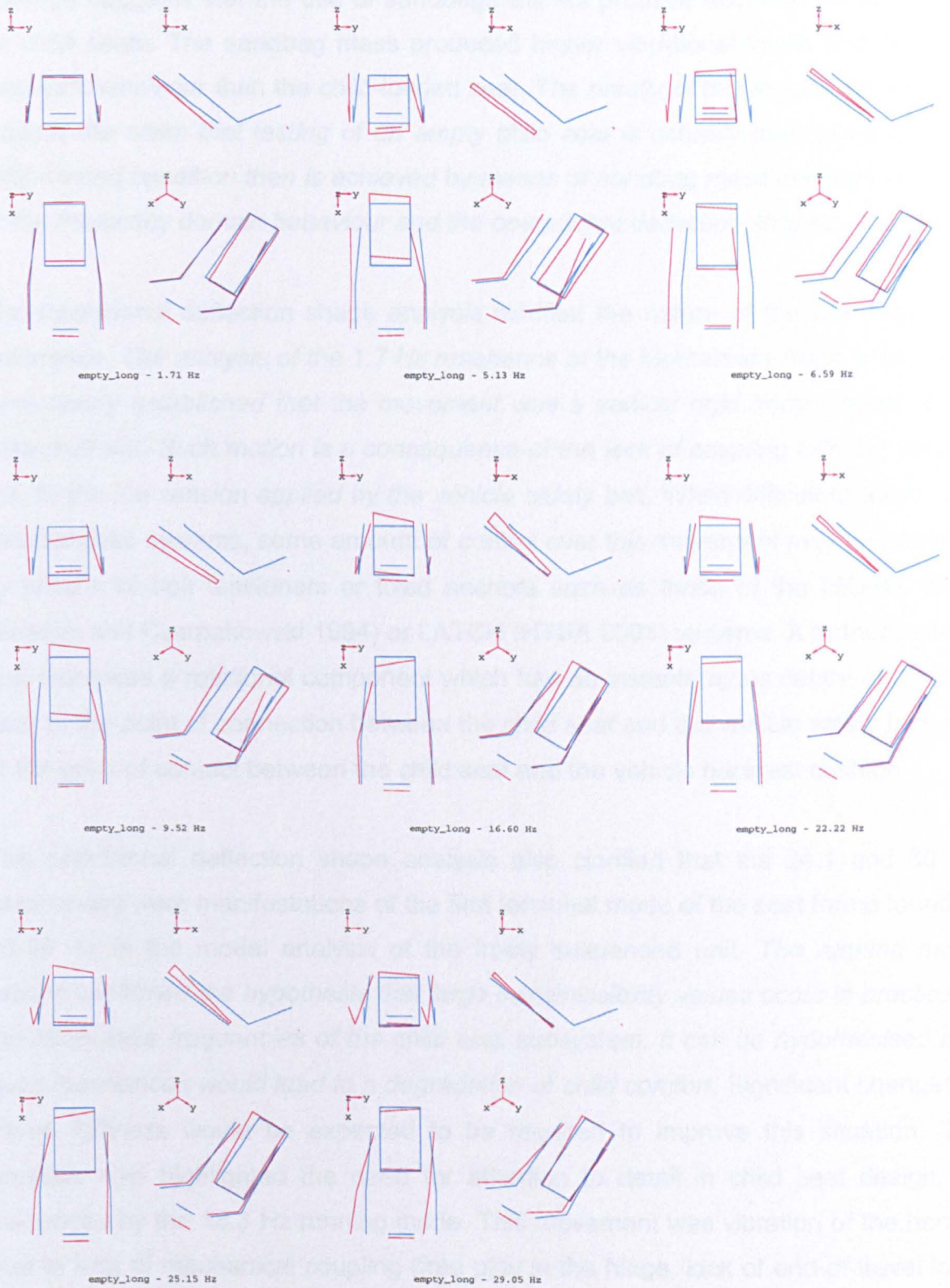

Figure 4.29 Running Modes of the Mothercare Rock 'n' Go on Mary Street when empty.

4.3.4 Discussion

Comparison of the vibration levels and of the power spectral densities for the three loadings suggests that the use of sandbags will not produce accurate vibration data for child seats. The sandbag mass produced higher vibrational levels and different resonant behaviour than the child-loaded seat. *The results of this investigation would support the claim that testing of an empty child seat is actually more similar to the child-loaded condition than is achieved by means of sandbag mass loadings in terms of the frequency domain behaviour and the operational deflection shapes.*

The operational deflection shape analysis clarified the nature of the low frequency resonance. *The analysis of the 1.7 Hz resonance of the Mothercare Rock 'n' Go child seat clearly established that the movement was a vertical rigid body motion of the child restraint. Such motion is a consequence of the lack of coupling with the vehicle due to the low tension applied by the vehicle safety belt.* While difficult to avoid with belt-fastened systems, some amount of control over this movement may be possible by means of belt tensioners or fixed anchors such as those of the ISOFIX (Bell, Burleigh and Czernakowski 1994) or LATCH (HTSA 2001) systems. A further point is that there was a rotational component which had an instantaneous centre of rotation near to the point of connection between the child seat and the vehicle safety belt, not at the point of contact between the child seat and the vehicle backrest cushion.

The operational deflection shape analysis also clarified that the 24.1 and 30 Hz resonances were manifestations of the first torsional mode of the seat frame found at 35.18 Hz in the modal analysis of the freely suspended unit. *The running mode results confirmed the hypothesis that large transmissibility values occur in practice at the resonance frequencies of the child seat subsystem. It can be hypothesised that such resonances would lead to a degradation of child comfort.* Significant changes in frame stiffness would be expected to be required to improve this situation. The analysis also highlighted the need for attention to detail in child seat design, as evidenced by the 18.3 Hz running mode. This movement was vibration of the handle due to lack of mechanical coupling (free play in the hinge, lack of end-of-travel lock) with the child seat frame when the handle was down in the travelling position. Such movement could be easily eliminated by means of small design changes to the hinge mechanism such that its free movement is limited when not in use.

Chapter 5

Transmissibility Properties of Child Seat Installations

5.1 Introduction

Having investigated the vibration properties of children and of child seat units individually, it was considered useful to perform field evaluations of the combined workings of the system composed of child, child seat and vehicle seat. The coupling of the three dynamic systems had the potential to introduce new dynamics which had not yet been identified. Additionally, it was considered important to widen the investigation by performing vibration measurements for several combinations of child, child seat and vehicle. In order to acquire realistic data it was decided to perform the experiments by driving over road surfaces. The measurement method chosen was acceleration transmissibility from a convenient input point on the floor of the test vehicle to the interface between the child and child seat. As in most previous

experiments described in this thesis the vertical direction was chosen for investigation as it represents the dominant vibrational axis in road vehicles.

A preliminary investigation was performed for two children in two seats in one vehicle in order to establish the instrumentation, the amplification settings and the dynamics of the in-vehicle environment. This investigation confirmed several findings from previous chapters regarding the child and child seat. Once sensors and methods had been perfected a survey was performed in which 8 combinations of child, child seat, and vehicle were tested. Ethical and safety considerations suggested that all tests be performed in the vehicles owned by the parents with the parents driving, thus reproducing a normal driving situation of the family involved. The test equipment and protocol was therefore developed to permit the investigator to enter the vehicle and establish the test arrangement within a few minutes. Once a family had arrived at the test road, all preparatory and testing activities could be performed within 10-15 minutes thus maximising safety and convenience for the families involved.

This chapter describes both the preliminary testing and the 8 system survey. The role of the material is to complete the understanding of child seat behaviour by providing an overview of the in-vehicle vibration transmission properties. The material helps to clarify the operational response characteristics of child seats and to quantify the level of vibration isolation offered by current systems.

5.2 Preliminary Investigation

5.2.1 Experiment

A search for suitable road surfaces in the city of Sheffield was performed following the testing practices of a major European automobile manufacturer (Giacomin and Lo Faso 1993). During the search a number of roads were evaluated in terms of two selection criteria: (1) the vibration intensity produced within the vehicle must be sufficiently strong to produce noticeable disturbance to passengers and (2) the road surface must carry low traffic volumes, at least at specific times of the day, so as to provide a safe testing environment. Two surfaces were selected, a speedbump (Rampton Road) and a pave' surface (Mary Street) which are shown in Figure 5.1.

The speedbump provided a low frequency and high amplitude transient input to the vehicle while the pave' (cobblestone) surface was selected to provide broadband random excitation to the vehicle. Preliminary tests on Mary street showed that the surface provided significant amounts of vibrational energy at the base of the vehicle seats for all frequencies up to 60 Hz. Vibrational energy was therefore provided over a significant portion of the frequency range associated with human whole-body vibration.

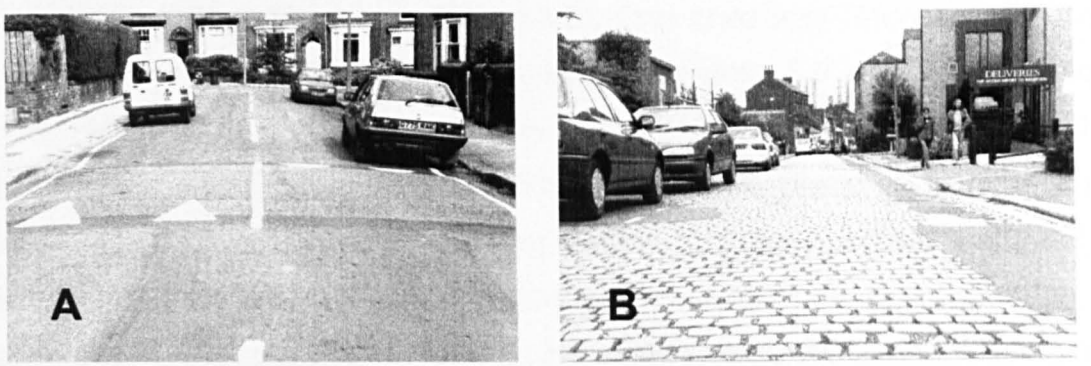

Figure 5.1 Surfaces used for the preliminary in-vehicle tests.
a) speedbump surface (Rampton Road)
b) pave' surface (Mary Street)

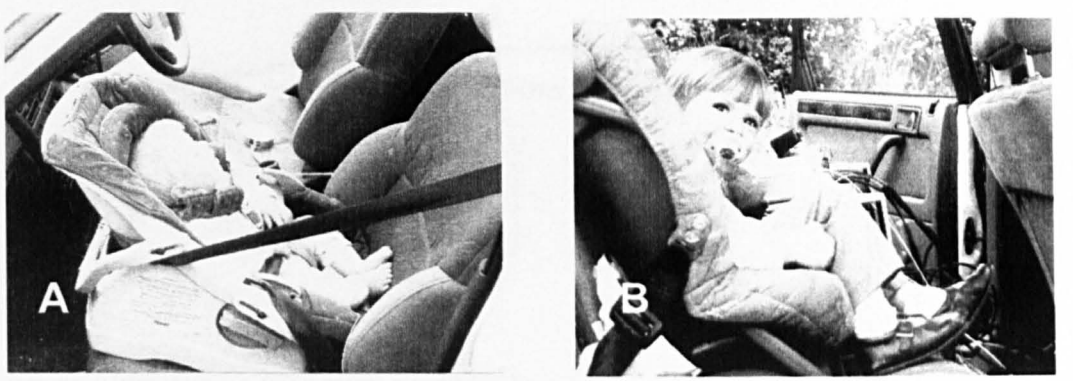

Figure 5.2 Children and child seats of the preliminary in-vehicle tests.
a) George in a seat manufactured by Tomy
b) Anna in a seat manufactured by Kwik-Fit.

The vehicle speeds selected for use were 20 km/h when driving over the speedbump and 40 km/h over the pave' surface. The choice of speeds was based again on the conditions used by European vehicle manufacturers when performing vibrational comfort investigations of whole vehicles or of only seats (Giacomin and Bracco

1995). The test automobile was a Rover 214 SLI with 175/SR14 radial tyres. The vehicle had 114,276 km on the odometer, suspensions were efficient, tyres were also efficient and inflated at the factory recommended pressure.

Two adults were seated in the vehicle during all tests, one driving and one in the rear operating an analogue tape recorder. The driver was female, weighed 62.3 kg and was 1.68 m in height. The passenger running the recorder was male, weighed 88 kg and was 1.80 m in height. During all tests there were also two children in the vehicle occupying two child safety seats (Figure 5.2). One child was George, who is male, and at the time of the tests was 74 cm in height, weighed 8.6 kg and was 7 months old. The second child was Anna who was 81 cm in height, weighed 9.9 kg and was 28 months old. George occupied a stage 0&1 seat manufactured by Tomy which was placed on the front passenger seat facing rearwards. Anna occupied a stage 1 seat manufactured by Kwik-Fit which was placed in the middle of the rear passenger seat facing forwards. Both seats were fixed to the vehicle using the automobile's belts as instructed by the accompanying documentation. Neither child seat was new, both had been used for several months prior to testing.

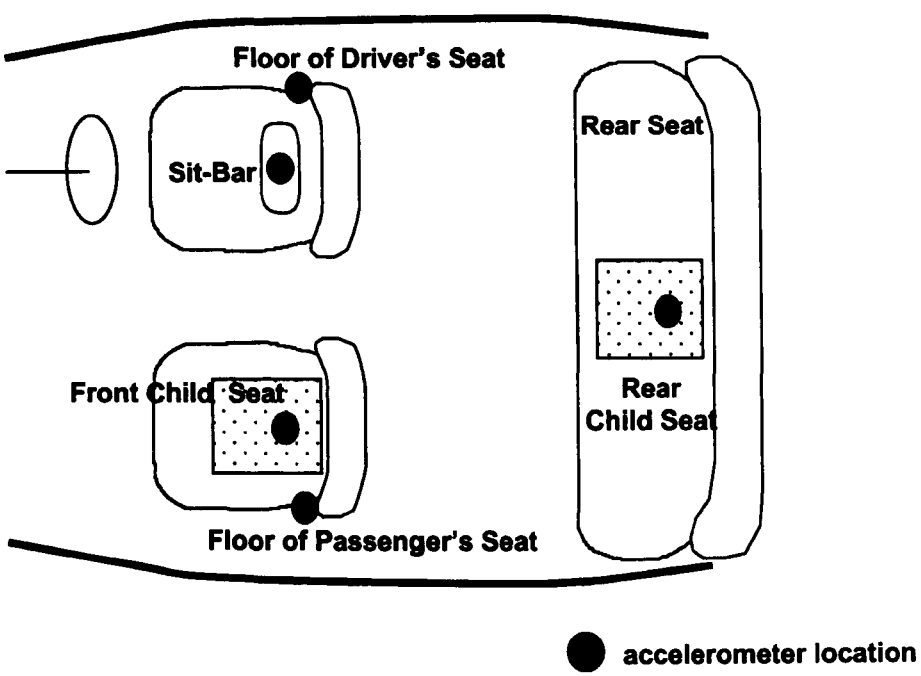

Figure 5.3 Seating arrangement and accelerometer measurement points.

Five PCB model 336C04 accelerometers were used as shown in Figure 5.3. The sensitivity values ranged from 97 to 102 $(m/s^2)/V$ as checked using a PCB model 394B06 calibration source. The useful amplitude range of the sensor was ± 50 g while the useful frequency range was from approximately 1 Hz to 2000 Hz. All accelerometers were oriented so as to measure the acceleration in approximately the vertical direction since that is the axis of greatest vibration in road vehicles (Pottinger and Yager 1986). The choice of mounting points to use as the vibration input to the seat was based on previous research performed for automobile seats (Giacomin, Giuliano and Giai Merlera 1994). For each front seat an accelerometer was mounted on the floor of the vehicle next to the rear mounting bolt of the outer guide a shown in Figure 5.4. These accelerometers were held to the floor by means of accelerometer wax since it guarantees adequate dynamic coupling to frequencies in excess of 2000 Hz. No accelerometer was placed under the rear seat since no information was available in the literature which established a reference point for the floor panel.

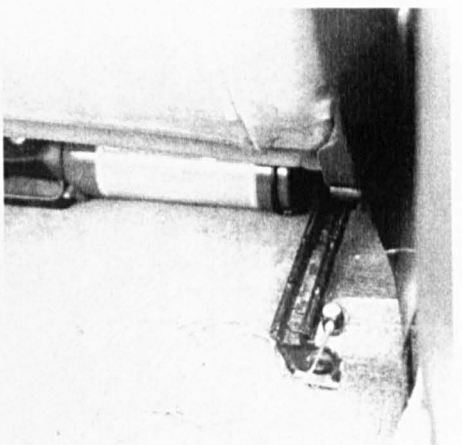

Figure 5.4 Front seat input accelerometer on the floor of the vehicle at the guide.

The vibration input to the driver was measured using a sit-bar (Griffin 1990) as shown in Figure 5.5. The sit-bar was constructed of aluminium and was 300 mm long, 180 mm wide and 18 mm thick and contained a centre-mounted accelerometer. The measurement of vibration at the interface between the child seat and child posed a problem since no measurement devices existed in the literature. For the preliminary investigation an aluminium child-bar was designed and built for use in the same manner as the sit-bar for adults. The child-bar (Figure 5.6) was 50 mm in

diameter and 15 mm in height and was manufactured from aluminium alloy. Simplified calculations suggested that the first resonance frequency of the sit-bar shell was in excess of 300 Hz. The weight of the child-bar shell was 38 grams, which became 44 grams when the PCB model 336C04 accelerometer was installed and 47 grams when measured with the micro dot cable connected and supported to one side. One child-bar was placed under the buttock region of each of the two children.

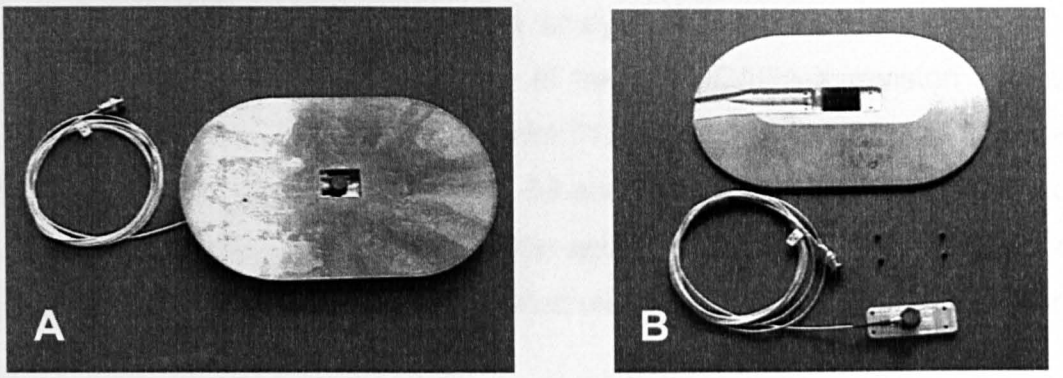

Figure 5.5 Sit-bar used at the interface between seat and driver.
a) Sit-bar viewed from top
b) Sit-bar viewed from bottom with accelerometer removed

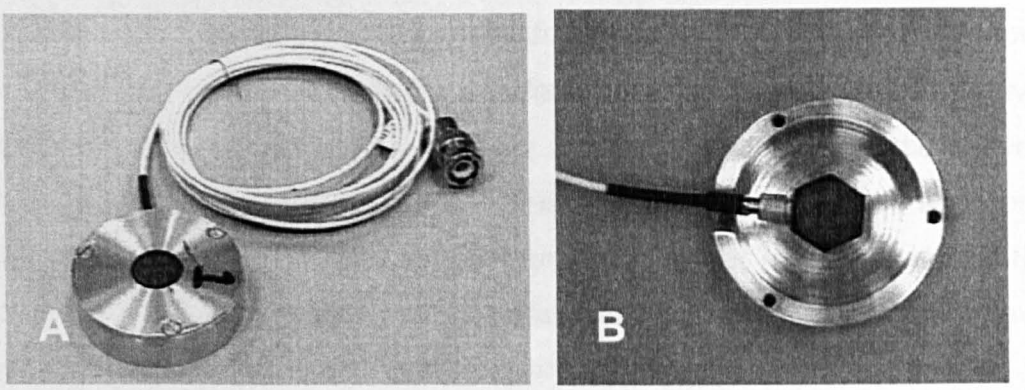

Figure 5.6 Child bar used at the interface between child seat and child.
a) Child-bar and connector cable.
b) View of the accelerometer inside the child-bar.

Charge amplification for all accelerometers was accomplished by means of each accelerometer's internal ICP circuit and an external 12 channel PCB model 483A DC power rack. The voltage signals from the accelerometers were recorded by means of a Kyowa RTP 610 analogue cassette data recorder which was located on the back seat of the automobile. Both the power rack and the tape recorder were run from an

independent 24V battery source so as to minimise noise from the automobile's electronic systems.

Five runs over the pave' surface (which produced approximately 20 seconds of vibration for each run) were performed at the fixed speed of 40 km/h and 7 passes over the speedbump were made at 20 km/h. The speed was controlled by the driver using the vehicle's instrumentation but some variation was unavoidable, particularly during impact with the speedbump. Data analysis was performed in the laboratory using the time data processing software of the LMS CADA-X revision 3.4 system. The LMS software was run on an HP model 715/64 workstation and 24 channel Difa Systems SCADAS II front-end was used. All acceleration signals were sampled from the recorder at 256 Hz and a low pass filter was applied which had a 120 Hz cut-off frequency. All plots of results were generated using the LMS Plot Format Editor.

5.2.2 Results

Figure 5.7 presents the acceleration time histories measured for one pass over the speedbump. All signals have high frequency components except the interface between the driver's seat and driver, which benefited from significant amounts of vibration isolation. For all test runs the interface between driver's seat and driver was the measurement channel which had the lowest overall acceleration level. The accelerations at the child interfaces were found to be higher in level, and contained more high frequency vibrational energy than at the driver interface. In addition, for the child in the front seat where a comparison could be made, the vibration level was everywhere as high or higher at the child than at the floor of the vehicle.

Figure 5.8 presents an acceleration time history obtained for the pave' surface by adding, front to back, the data from three individual runs. The lowest acceleration levels were again consistently found at the interface between the driver and the driver's seat. Direct comparison of the time histories suggests that the system composed of vehicle seat and driver provided better vibration isolation than the system composed of child seat and child in the vehicle tested. Tables 5.1 and 5.2 summarise the acceleration data measured for all channels.

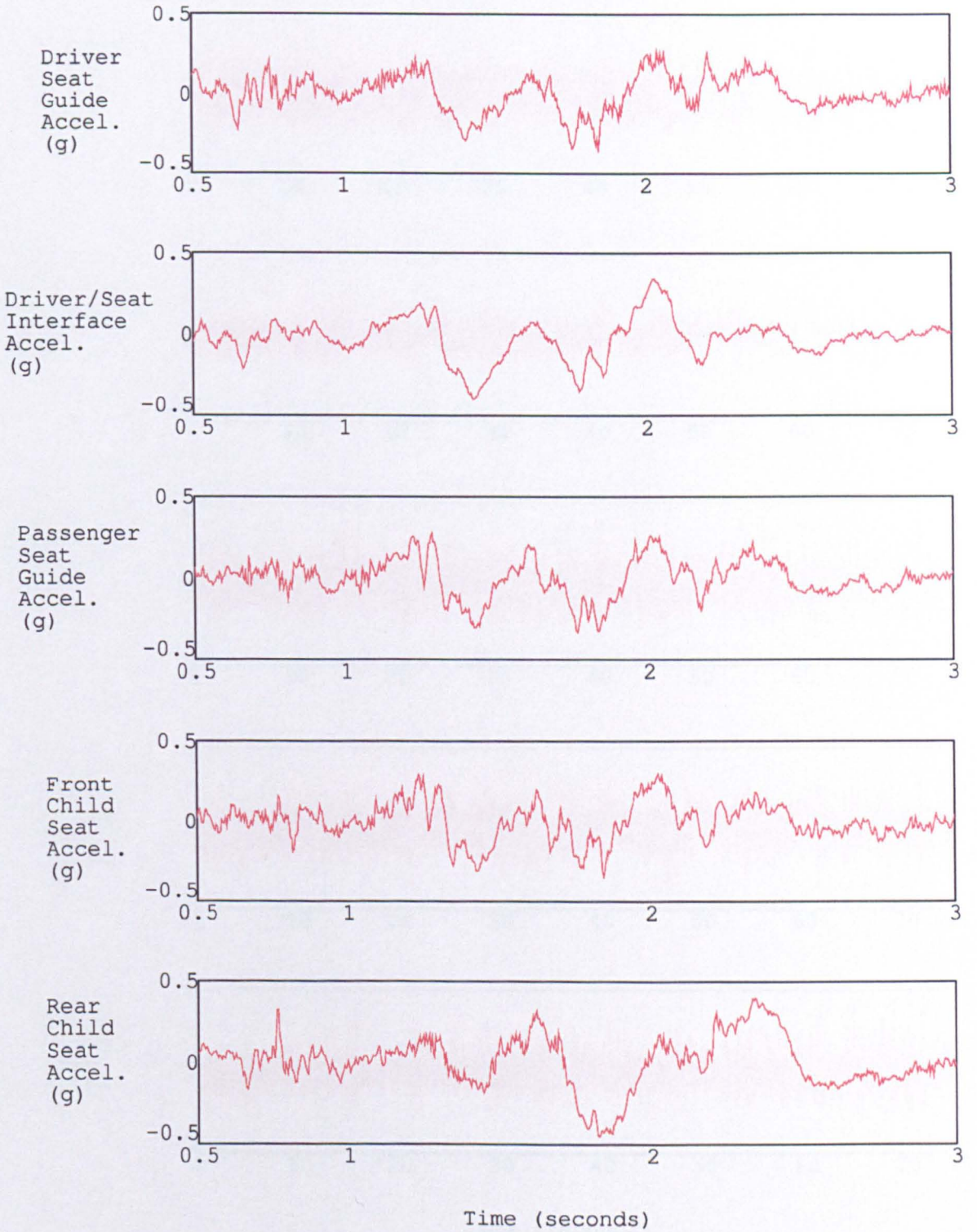

Figure 5.7 Time histories for one pass over the speedbump surface at 20 km/h.

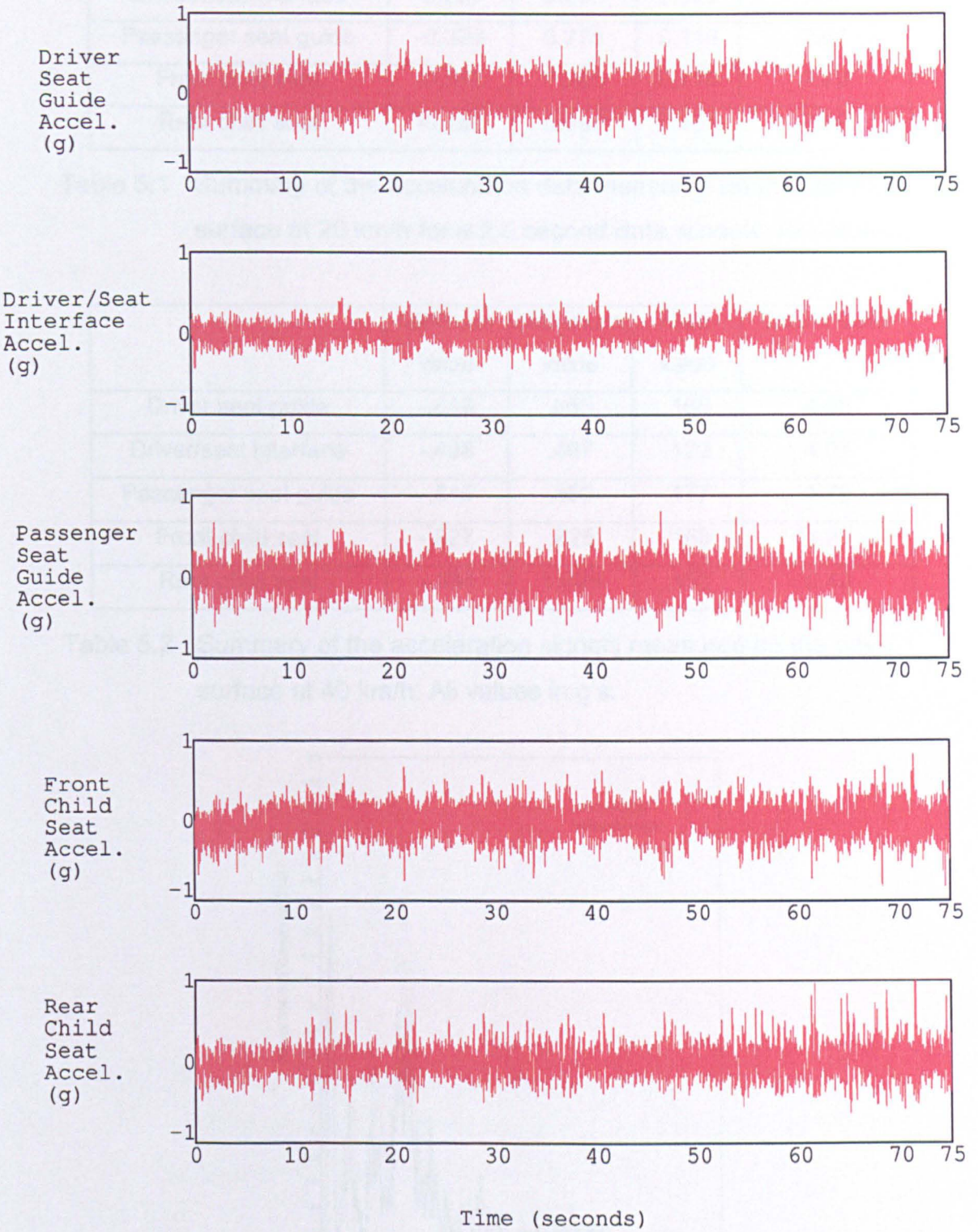

Figure 5.8 Time histories from three passes over the pave' surface at 40 km/h.

	Minimum value	Maximum value	RMS value	Crest Factor
Driver seat guide	-0.345	0.267	0.112	2.73
Driver/seat interface	-0.397	0.339	0.126	2.92
Passenger seat guide	-0.333	0.278	0.116	2.64
Front child seat	-0.346	0.299	0.115	2.79
Rear child seat	-0.452	0.396	0.158	2.69

Table 5.1 Summary of the acceleration data measured on the speedbump surface at 20 km/h for a 2.5 second data window. All values in g's.

	Minimum value	Maximum value	RMS value	Crest Factor
Driver seat guide	-.648	.855	.165	4.55
Driver/seat interface	-.498	.497	.122	4.07
Passenger seat guide	-.849	.850	.177	4.79
Front child seat	-.827	.825	.168	4.93
Rear child seat	-.634	1.025	.153	5.42

Table 5.2 Summary of the acceleration signals measured on the pave' surface at 40 km/h. All values in g's.

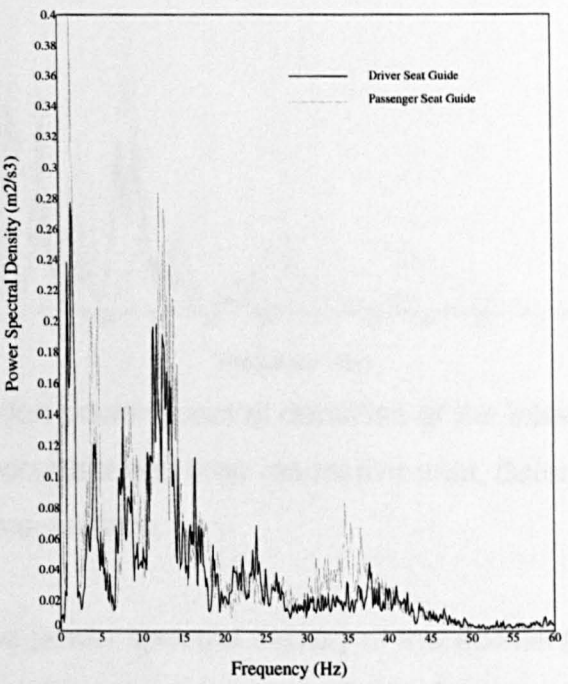

Figure 5.9 Acceleration power spectral densities at the two seat guides determined from the data of the pave' surface.

Figure 5.9 presents the power spectral densities determined from the acceleration data measured at the guide of the driver's seat and of the front passenger seat while driving over the pave' surface. The two spectral densities are similar but present small differences because the road inputs and the vehicle itself present asymmetries. The power spectral densities suggest that there was significant vibrational energy up to 60 Hz and that the energy level associated with each frequency line was mostly within one order of magnitude up to 45 Hz. These characteristics suggest that the vibration input to the seats was adequate to measure vibrational phenomena up to at least 45 Hz and possibly 60 Hz in frequency.

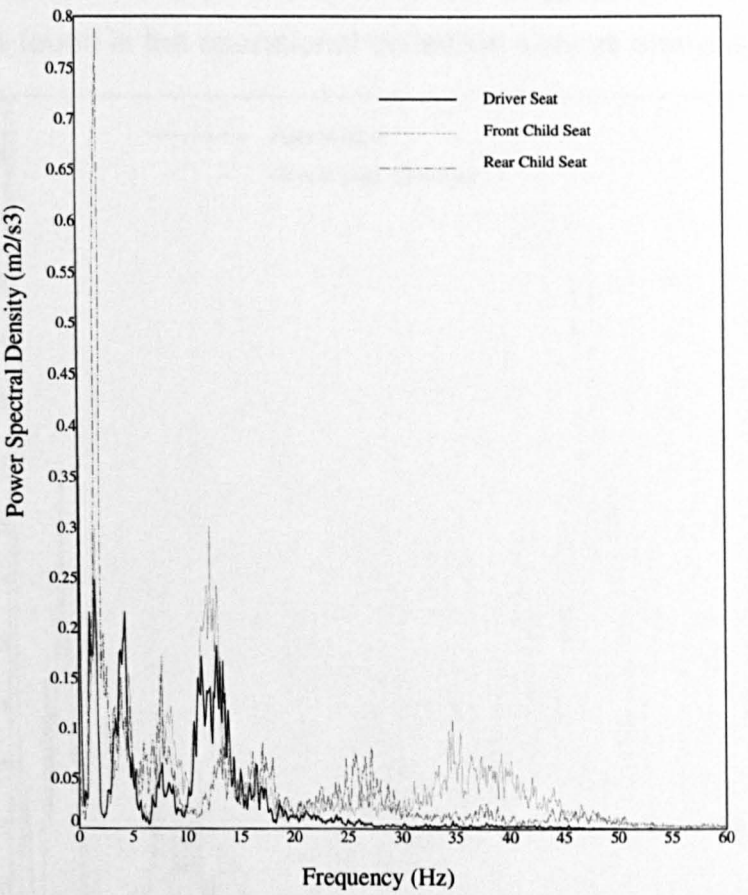

Figure 5.10 Acceleration power spectral densities at the interface between each vehicle occupant and their respective seat, determined from the data of the pave' surface.

Figure 5.10 presents the power spectral density of the acceleration signals measured at the interfaces between the human occupants and their seats for the pave' surface. As with the time histories, the frequency domain comparisons suggest that the

coupled system consisting of the driver and vehicle seat provided better isolation from road inputs than was the case for the children in the child seats. Both children were exposed to higher vibration levels than the driver, particularly at frequencies greater than 15 Hz.

Several interesting features were present in the data. One feature was the high level of vibration to which the child in the front seat (George) was exposed at frequencies greater than 10 Hz. The levels experienced by the child in the front seat were often more than two orders of magnitude greater than that experienced by the driver at the same frequency. A second interesting feature was the large resonance at 1.8 Hz experienced by the child in the rear seat (Anna), suggesting child seat rigid body motion of the type found in the operational deflection shapes analysis.

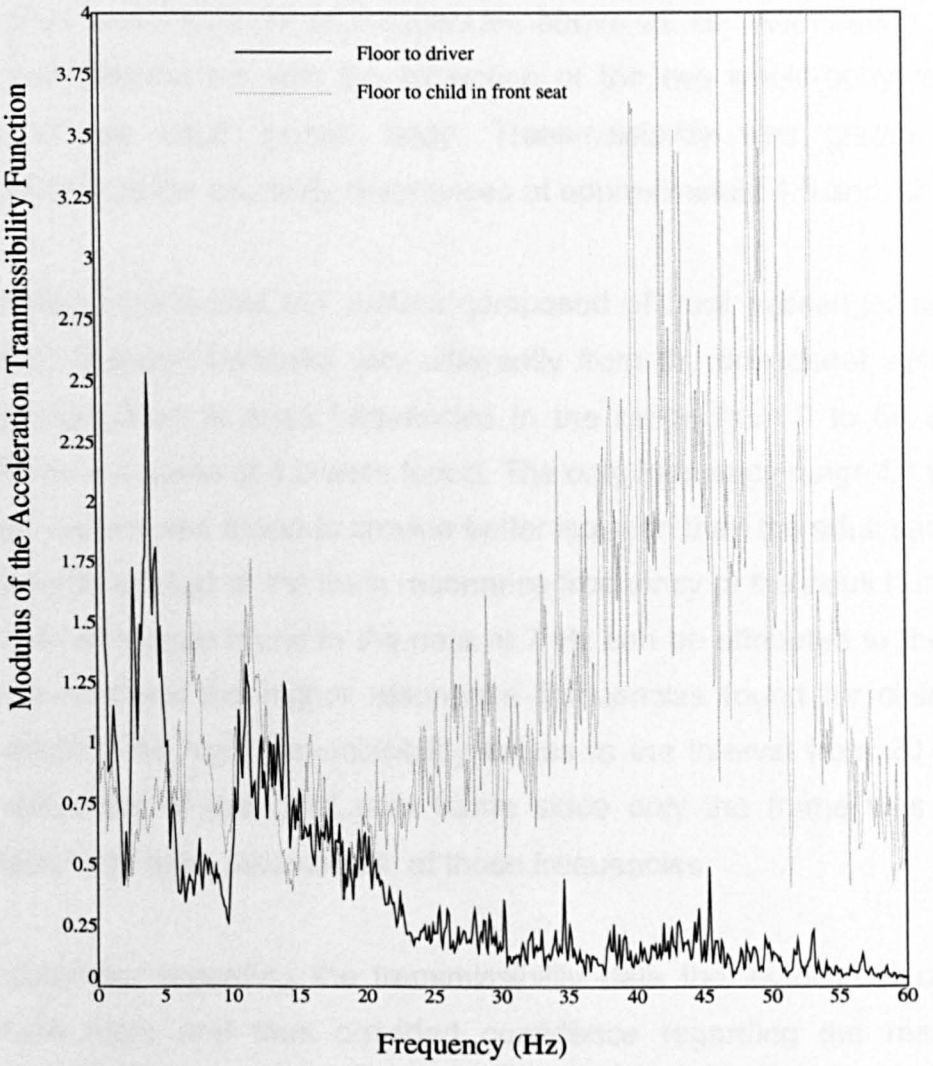

Figure 5.11 Acceleration transmissibility calculated from the floor to the driver, and from the floor to the child in the front seat, for the pave' test surface.

Figure 5.11 presents the vertical acceleration transmissibility functions (ATFs) from the floor of the automobile to the interface at the driver and to the interface at the child in the front seat (George). Due to the presence of energy in all 6 vibrational degrees of freedom in vehicles the transmissibility functions were evaluated using all three spectral estimators (H_1, H_2 and H_v) in order to check for differences. Only small differences less than 5 percent were found at any given frequency line using the three methods therefore the H_v estimator was used for all data presented in this chapter.

The transmissibility functions for the driver's seat and for the front child seat permit several observations. The first is that the driver's seat provided attenuation in line with data available in the general literature (Griffin 1990). Vibration attenuation of 75 percent or more was found for all frequencies above 22 Hz. Attenuation was also strong at lower frequencies with the exception of the two whole-body resonance frequencies of the adult human body. Transmissibility was greater than 1 (amplification) only at the two body resonances at approximately 4.5 and 12 Hz.

A second observation is that the system composed of front passenger seat, child seat and child (George) behaved very differently from the driver/seat system. The vibration was amplified at most frequencies in the range from 0 to 60 Hz. Peak transmissibilities in excess of 4.0 were found. The only frequency range for which the child restraint system was found to provide better isolation than the adult seat system was in the neighbourhood of the main resonance frequency of the adult human body at 4.5 Hz. The resonance found in the data at 7 Hz can be attributed to the body of the child and confirms the higher resonance frequencies found for children with respect to adults. The high transmissibility values in the interval from 20 to 60 Hz suggested dynamics of the child seat frame since only the frame was found in previous chapters to have resonances at those frequencies.

As a final comment regarding the transmissibility data the associated coherence functions were high, and thus provided confidence regarding the results. The coherence was greater than 0.94 in the region from 1 to 15 Hz and mostly in the neighbourhood of 0.7 for frequencies from 15 to 55 Hz. These values are to be considered good for road testing results in vehicles (Giacomin and LoFaso 1993).

5.2.3 Discussion

Several elements emerged from the preliminary study. The first was that the vibration isolation of the coupled system defined by the car seat, the child seat and the child was less effective than that of the automobile seat and driver in reducing the level of vibration. The calculated transmissibility functions showed that amplification of floor vibration was more than 400 percent at many frequencies in the interval from 0 to 60 Hz. A second point to emerge was that the child in the front seat (George) appeared to have a first resonance frequency at approximately 7 Hz, similar to that found for other children of his age in the child vibration study of this thesis. The presence of the body resonance in the transmissibility data confirmed the importance of considering the vibration characteristics of the child when analysing the coupled system. Additionally, as with the data for the driver, the child resonance response was found to be one of the largest peaks in the transmissibility curve.

A third point to emerge from the preliminary study was that the system composed of the automobile seat, child seat and child showed behaviours not typically found for the adult driver. The low frequency resonance condition of the child in the rear seat (Anna) suggested that there may have been problems due to a lack of coupling between the child restraint and the vehicle. The result appeared to confirm the rigid body motion identified in the operational deflection shapes analysis. Additionally, the high frequency amplification measured in the front child seat (George) in the interval from 20 to 60 Hz suggested that the child restraint frame structure played an important role vibrationally at the higher frequencies. The most probable cause of the high transmissibility values was a resonant response of the child seat frame. Additionally, the lack of soft interface material (for example foam padding) between the seat frame and child may have rendered the frame movement more evident in the measurement.

5.3 Vibration Survey

5.3.1 Introduction

The vibration measurements performed for two stage 0&1 seats in a vehicle while driving over two road surfaces were sufficient to highlight potential differences between child seats and adult passenger seats but not sufficiently representative to generalise the findings. A second study was therefore performed for the purpose of extending the statistical base of observation. As in the first investigation the vibrations measured at the interface between child seat and child were compared to those at the interface between the driver and the automobile primary seating system. In the vibrational survey 8 combinations of automobile, child seat and child were tested.

Safety and realism again suggested that road testing, as opposed to laboratory testing, would be the best approach for the study. In this investigation, however, the tests were limited to only the pave' (cobblestone) road surface of Mary Street. The random vibration signals generated by the pave' surface had proved the most repeatable and informative of the previous exercise therefore the decision was taken to limit the survey to that surface only.

5.3.2 Experiment

The intention to test several children meant involving several families. Working with such volunteers suggested that the testing time should be kept to a minimum so as to make the experience as quick and as pleasant as possible for the families. Working to strict time limits meant that a means of verifying, on-location, the quality of the acquired vibration data was required. Additionally, working with numerous and unfamiliar children meant that the equipment must be rugged and robust to support any possible treatment from children attempting to play with the equipment. These considerations resulted in a market survey of dual-channel FFT analysers which were hardened for field use, programmable, battery powered and equipped with a large amount of internal memory. After a lengthy survey a purchase was made of a Larson Davis Model 2900B dual channel spectrum analyser (Larson Davis Laboratories 1998). The 2900B performs dual channel FFT analysis with up to 400 frequency lines with an analysis range from 0 to a maximum of 20 kHz. The 2900B can run for up to 4 hours using its internal battery pack, which was more than sufficient for the planned road tests. Two Larson Davis model PRA950B power tubes

were also purchased for connection to the 2900B to provide the 2mA current required by the internal preamplifiers of the PCB accelerometers.

The other equipment used for the vibration survey consisted of three PCB model 336C04 ICP accelerometers and two accelerometer pads for human whole-body vibration testing. The accelerometer pads were used in substitution to the aluminium bars of the first road investigation because of their lighter weight and smaller size. One accelerometer pad was manufactured in the Mechanical Engineering Workshop to the specifications of SAE standard J1013 (Society of Automotive Engineers 1974) and was used for measuring the vibration at the driver's seat cushion. The SAE pad is a well known device used in vehicle comfort testing, thus guaranteeing compatibility with seat measurements performed by other researchers.

For performing acceleration measurements at the interface between child and child restraint system, however, no device was identified from the literature. A child pad was therefore designed and built by scaling the dimensions of the SAE pad to values appropriate for use with children of the age and weight group associated with stage 0&1 seats. Since the average inter ischial tuberosity distance for a 12 month old child is no more than 141 mm (Tilley 1993, Society of Automotive Engineers 1977) the outer diameter of the child pad was chosen to be 150 mm and the material was chosen to be 80 shore in hardness as in the case of the adult SAE pad J1013. The geometric dimensions of the child pad are shown in Figures 5.12 and 5.13. The weight of the pad was 224 grams, which increased to 230 when the PCB 336C04 accelerometer was installed. The device was fixed to a vibrating surface and found to measure the vibration without resonant amplification to frequencies in excess of 100 Hz.

One PCB model 336C04 ICP accelerometer was used to measure the input vibration at the base of the seat (either driver's seat or front passenger seat depending on the test). A second accelerometer was mounted inside the SAE J1013 pad for use in measuring the accelerations at the interface between the driver and driver's seat. A third accelerometer was mounted inside the child-pad to measure the acceleration at the interface between child restraint system and child.

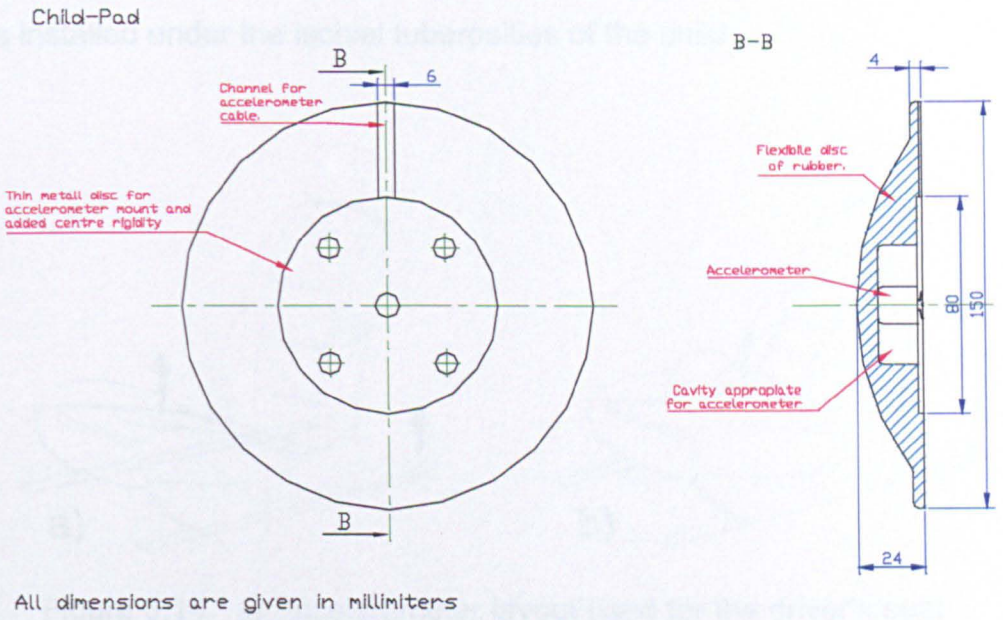

Figure 5.12 Child-pad used for measuring vibration at the interface between child and child seat.

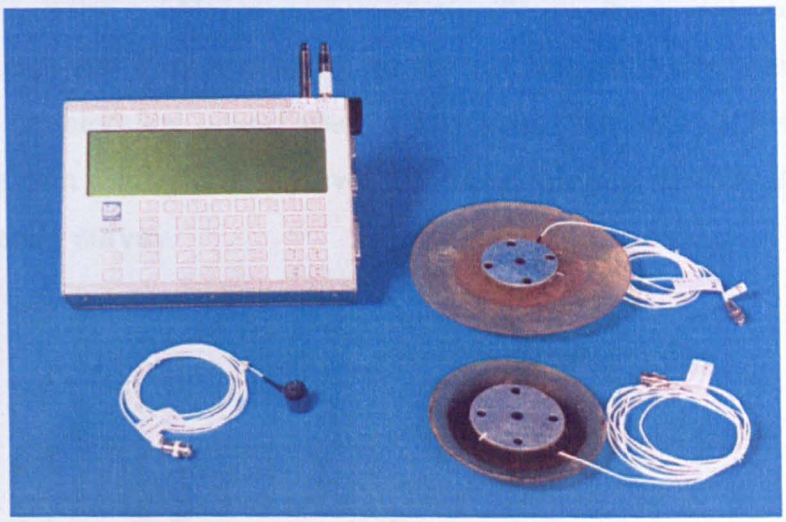

Figure 5.13 Equipment used for the vibration survey.

Each test vehicle was instrumented following to the accelerometer layout shown in Figure 5.14. An accelerometer was placed on the floor of either the driver's or the front passenger's seat by means of wax and was aligned as closely as possible to measure in the vertical direction. The floor accelerometer was placed next to the rear bolt of the outermost rail of the seat guide in question. The SAE pad was next

installed under the ischial tuberosities of the driver (the test participant) and the child pad was installed under the ischial tuberosities of the child.

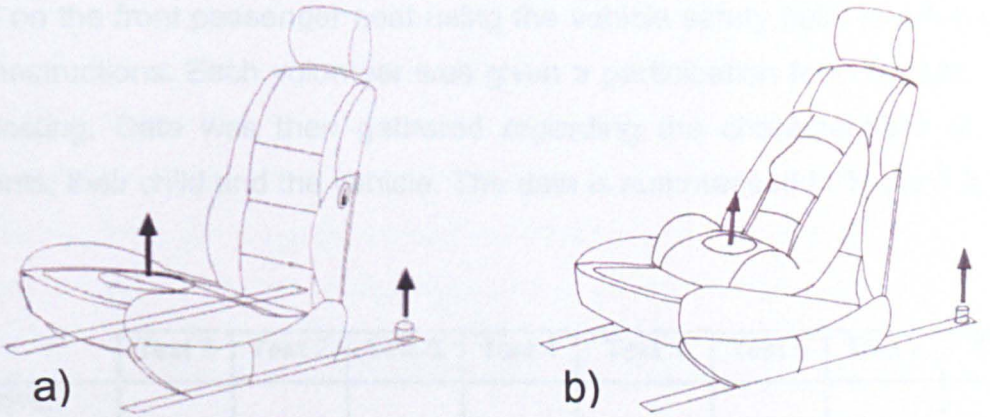

Figure 5.14 a) Accelerometer layout used for the driver's seat
b) Accelerometer layout used for the child seat

The road used was the pave' surface of Mary Street in Sheffield. It is straight and flat for 200 meters and the cobblestones furnish significant vibrational energy at the seat guides of vehicles for frequencies up to 60 Hz. Figure 5.15 below presents an example of the acceleration power spectral densities measured at the seat guides in the vertical direction during one run over the pave' surface at 40 km/h performed as part of the vibration survey.

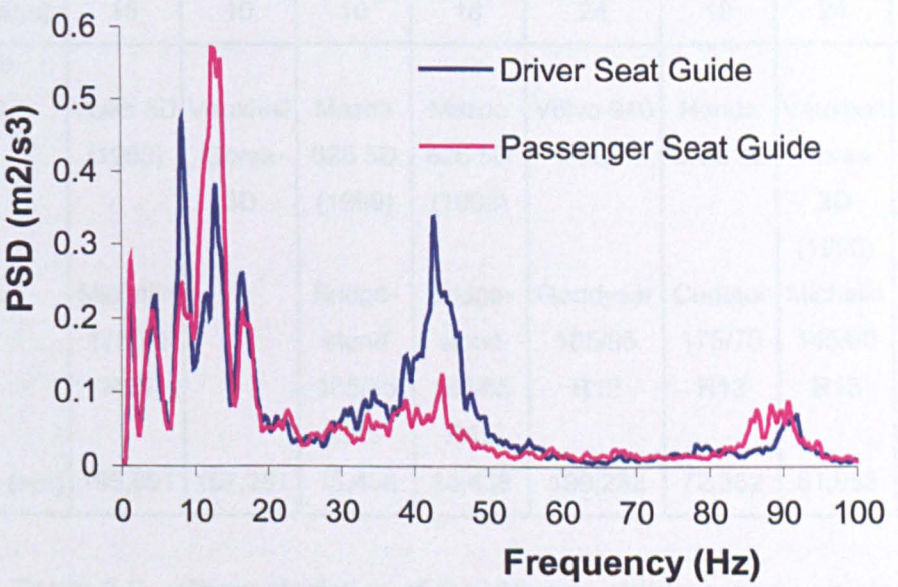

Figure 5.15 Vertical acceleration power spectral density measured at the seat guides during one run over Mary Street at 40 km/h.

Eight combinations of automobile, child seat and child were tested. Each participating family arrived at the test road with their own vehicle, their child seat and their child. All seats were belt-fastened stage 0&1 designs. Each restraint was installed on the front passenger seat using the vehicle safety belts and following the product instructions. Each volunteer was given a participation form to read and sign before testing. Data was then gathered regarding the characteristics of the test participants, their child and the vehicle. The data is summarised in Table 5.3 below.

	Test 1	Test 2	Test 3	Test 4	Test 5	Test 6	Test 7	Test 8
Driver								
Sex (M/F)	M	M	M	M	M	F	F	F
Age (years)	29	28	35	35	42	29	40	37
Height (m)	1.81	1.86	1.90	1.90	1.82	1.65	1.65	1.65
Mass (kg)	70.0	72.0	77.6	77.6	78.0	55.0	50.8	95.0
Child								
Sex (M/F)	M	M	M	F	F	M	M	M
Age (months)	8	8	9	24	30	10	36	9
Height (m)	0.68	0.60	0.65	0.85	-	0.70	0.91	0.70
Weight (kg)	7.5	7.2	10.0	14.5	13.0	12.0	13.6	8.0
Seat Manufacturer	-	Maxi	Britax	Britax	Mother-care	-	Britax	Klippan
Use (months)	15	10	10	18	24	10	24	9
Vehicle								
Model	Volks 5D (1983)	Vauxhall Corsa 3D	Mazda 626 5D (1999)	Mazda 626 5D (1999)	Volvo 940 5D	Honda Civic 3D	Vauxhall Corsa 3D (1996)	Mitsubishi Space Wagon
Tyres	Michelin 175/70 R13	-	Bridge-stone 185/65 R15	Bridge-stone 185/65 R15	Goodyear 185/65 R19	Centaur 175/70 R13	Michelin 145/80 R13	Indian GT70 185/70 R14
Odometer (km)	195,691	157,281	15,438	15,438	199,232	72,362	51,983	158,633

Table 5.3 Characteristics of the drivers, children and vehicles constituting the in-vehicle child seat vibration survey.

After installing the test instrumentation in the vehicle a series of runs were performed over the road surface. For each run the participant drove his or her vehicle maintaining the target speed by means of the vehicle's speedometer. The equipment operator sat in the rear of the vehicle using the 2900B and noting conditions. For the 40 km/h tests the spectrum analyser was set to perform an 18 second acquisition from trigger, while for the 20 km/h tests the acquisition time was set at 30 seconds. Since the analyser was a dual channel device the data for the driver (seat guide and SAE pad) and the child (seat guide and child pad) had to be acquired from separate runs over the surface. 16 runs were performed in total, 4 for each seat (driver's or child's) at each test speed (20 or 40 km/h).

The acceleration time histories were sampled at a rate of 400 Hz. Fourier analysis was performed using an FFT block size of 1024 points and a Hanning window. The combination of a 1024 point block size and 400 Hz sampling rate gave a total time window of 2.56 seconds and thus a spectral resolution of 0.391 Hz. All frequency domain results were saved as power spectral densities in units of m^2/s^3 and were downloaded from the analyser to a PC upon return to the laboratory.

5.3.3 Results

Figures 5.16 and 5.17 present the r.m.s. acceleration levels recorded at all four measurement points for all eight tests at 20 km/h and at 40 km/h. The levels measured at the child seat were higher than those measured at the driver's seat in all cases. Additionally, the vibration attenuation from floor to human occupant was lower for the child than for the driver in all cases. At 20 km/h tests 1 and 8 showed accelerations in the child seat which were nearly identical to those on the floor of the vehicle, confirming the findings of the preliminary tests. The 40 km/h tests, which produced higher vibration frequencies due to the increase in vehicle speed, still showed only a small reduction in vibration in the child seat for tests 1 and 8.

Table 5.4 summarises the average levels measured across the test ensemble. The ratio of the acceleration arriving at the human occupant to the acceleration present at the seat guide was 64% in the case of the driver and 80% in the case of the child for the 20 km/h tests. The same ratio was 59% for the driver and 74% for the child at 40

km/h. These results confirm the reduced effectiveness of the child seat system with respect to the vehicle primary seating.

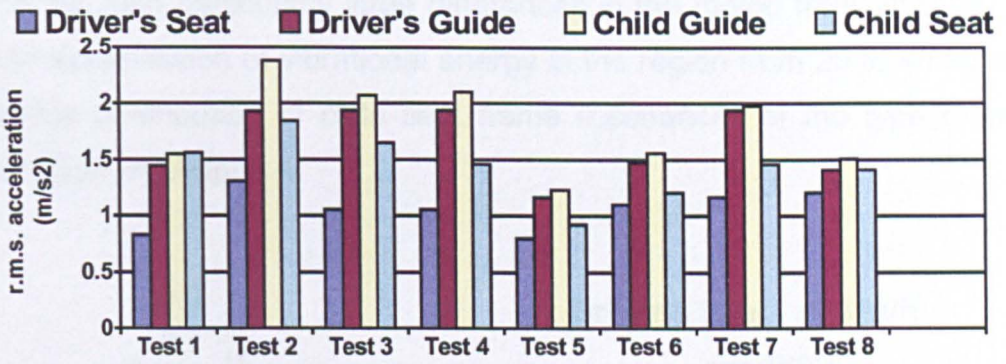

Figure 5.16 r.m.s. acceleration level at each measurement point for each of the eight in-vehicle tests performed at 20 km/h.

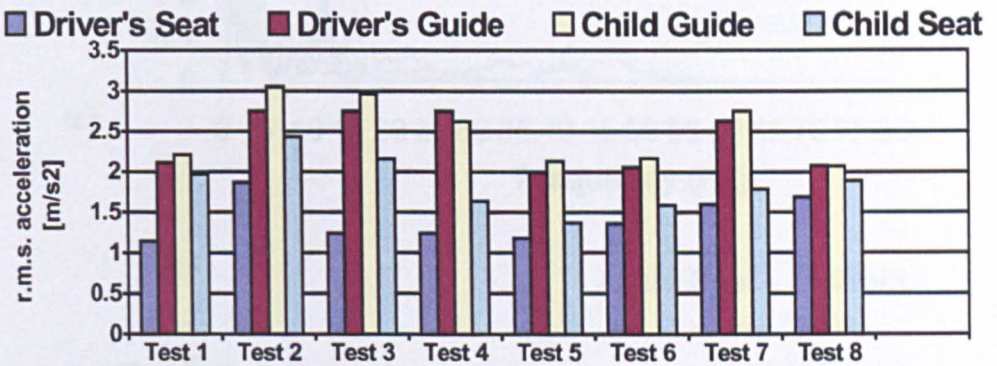

Figure 5.17 r.m.s. acceleration level at each measurement point for each of the eight in-vehicle tests performed at 40 km/h.

	20 km/h Tests		40 km/h Tests	
	Average Value	**Std.**	**Average Value**	**Std.**
Driver's Seat	1.07	0.18	1.41	0.27
Driver's Seat Guide	1.66	0.31	2.40	0.36
Child Seat's Guide	1.80	0.39	2.50	0.40
Child Seat	1.44	0.28	1.86	0.34

Table 5.4 Average and standard deviation of the r.m.s. acceleration levels determined from all tests. Units are m/s^2.

Figure 5.18 presents the average power spectral densities determined for the human interfaces for all eight tests. Comparison of the two sets of results suggests that the child seats transmitted more vibrational energy than the driver's seat at frequencies above 10 Hz, with particularly large differences in the region from 20 to 40 Hz. The increased transmission of vibrational energy in the region from 20 to 40 Hz suggests the possible contribution of child seat frame resonances of the type found in the modal analysis of chapter 4.

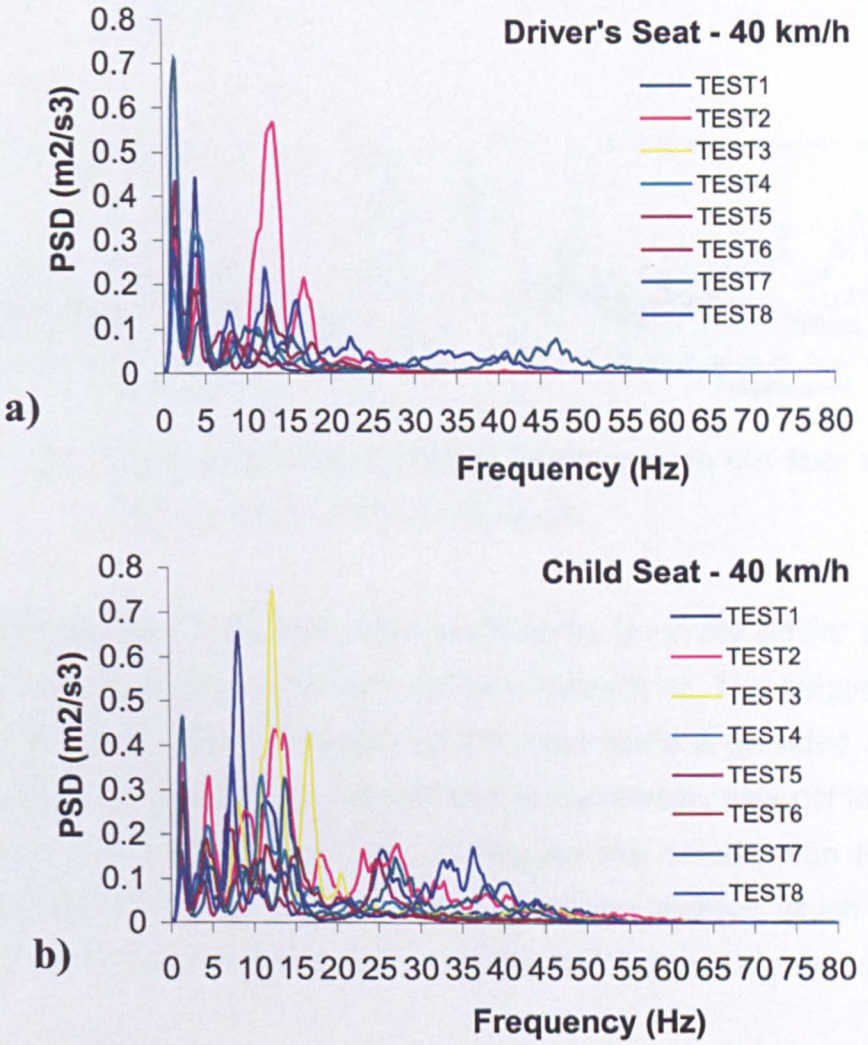

Figure 5.18 a) Acceleration PSDs measured at the driver's seat at 40 km/h
b) Acceleration PSDs measured at the child seat at 40 km/h

The average power spectral densities measured at the floor and at the human interfaces for each test were used to determine the acceleration transmissibility function (ATF) in the vertical direction. The 2900B analyser implementation of the transmissibility function consisted of an H_v estimator. Figure 5.19 presents the

acceleration transmissibility functions determined from all eight tests from the seat guides to the human interfaces at 20 and 40 km/h.

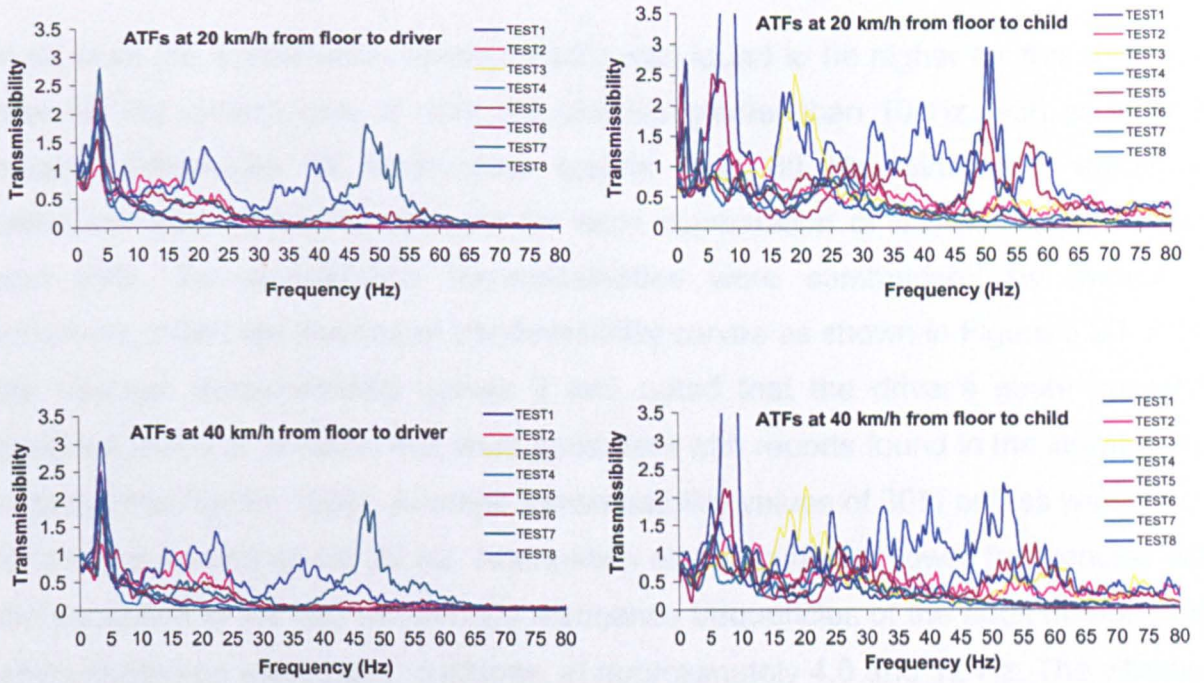

Figure 5.19 Acceleration transmissibility functions from the floor to the human interfaces at 20 km/h and 40 km/h.

The acceleration transmissibilities were found to be generally similar across the two test speeds except for the child measurements below 2 Hz. This suggests that above 2 Hz the vibrational energy provided by the road surface provided an acceptable signal-to-noise ratio and that the overall level of nonlinearity was not large enough to discourage the use of linear analysis techniques like acceleration transmissibility. These observations are supported by the coherence functions which were found to be greater than 0.7 in the range from 1 to 40 Hz and typically higher than 0.6 from 40 to 60 Hz.

The acceleration transmissibilities suggested that the main vertical adult whole-body resonance of the driver was strongly excited in all tests, as evidenced by the large peak in the transmissibility data in the region from 4 to 5 Hz for all subjects. Likewise, the first vertical resonance of the child body in the range from 5 to 10 Hz was excited in most tests, but the differences in body mass lead to greater dispersion in the frequency location of the resonance peaks than for the adults. The second vertical

adult whole-body resonance in the range from 9 to 15 Hz was found to be excited in a few cases but there was much variability from test to test due to differences in subject anthropometry and seat cushion design.

In all tests the acceleration transmissibility was found to be higher for the child seat than for the driver's seat at most frequencies greater than 10 Hz. with particularly evident differences for frequencies greater than 30 Hz. Since the vibrational behaviour was somewhat different for each combination of automobile, child seat and child, the acceleration transmissibilities were summarised by means of minimum, mean and maximum transmissibility curves as shown in Figure 5.20. From the average transmissibility curves it was noted that the driver's seats generally provided levels of isolation that were consistent with reports found in the literature for automobiles (Griffin 1990). Average transmissibility values of 30% or less were found for all frequencies above 20 Hz. Attenuation also occurred at lower frequencies with the exception of the two whole-body resonance frequencies of the adult human body when seated on elastic seat cushions, at approximately 4.0 and 12 Hz. The vibration attenuation was not as effective for the child seat systems, where the average transmissibility were rarely lower that 50% for frequencies up to 60 Hz.

The average transmissibility curves presented a main resonance peak for the children at 8.5 Hz, which was higher than the value of 4.0 Hz observed for the drivers. This finding confirmed the typical frequency of the principal vertical whole-body resonance of seated children, as found in chapter 3 of this thesis. This comparison can be further highlighted by taking the ratio of the acceleration transmissibility of the driver to that for the child, averaged across all tests, as shown in Figure 5.21. The average ratio for the eight systems suggested that the transmissibility to the child was greater than that to the adult at all frequencies except 4.0 Hz (where the ratio approached zero). Conversely, the transmissibility ratio produced a distinct peak at 8.5 Hz confirming the location of the principal seated whole-body resonance of the children. Additionally, the ratio suggests generally higher transmissibility at all frequencies greater than 20 Hz. A large peak in the average transmissibility ratio at approximately 32 Hz suggested the contribution of child seat frame resonances while the high values at frequencies greater than 50 Hz suggested suboptimal behaviour of any foam padding present in the child seats.

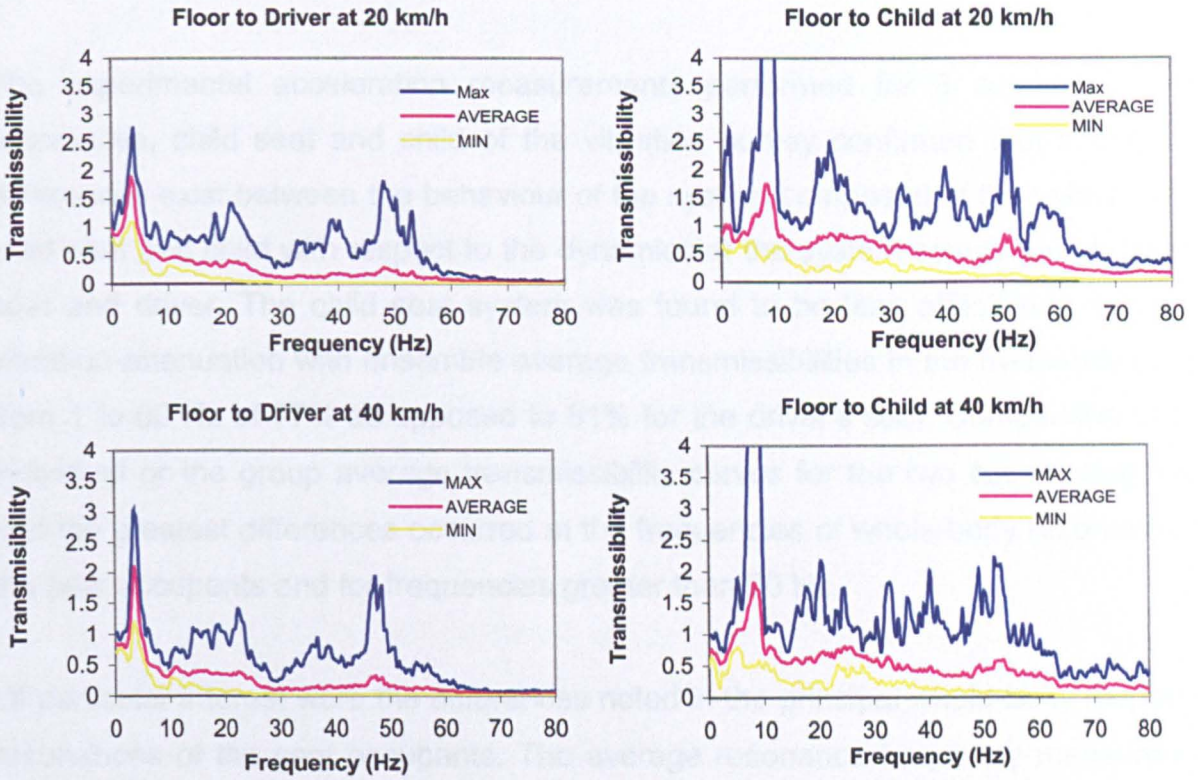

Figure 5.20 Miminum, Average and Maximum ATFs calculated from the floor to the human interfaces from all data.

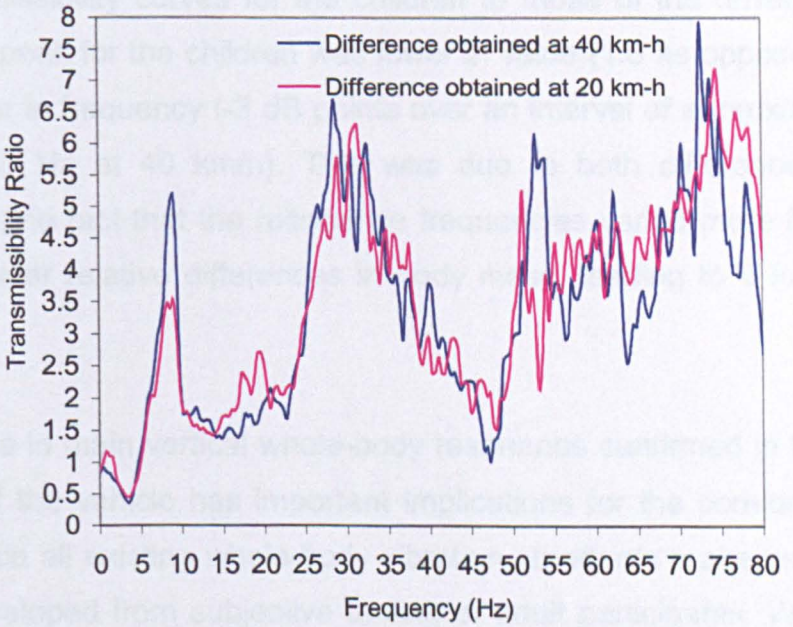

Figure 5.21 Ratio between the acceleration transmissibility to the driver and that to the child, averaged over all 8 tests.

5.3.4 Discussion

The experimental acceleration measurements performed for 8 combinations of automobile, child seat and child of the vibration survey confirmed that substantial differences exist between the behaviour of the system composed of the vehicle seat, child seat and child with respect to the dynamics of the system composed of driver's seat and driver. The child seat system was found to be less effective in terms of vibration attenuation with ensemble average transmissibilities in the frequency range from 1 to 60 Hz of 77% as opposed to 61% for the driver's seat. Comparison of the individual or the group average transmissibility curves for the two cases suggested that the greatest differences occurred at the frequencies of whole-body resonance of the seat occupants and for frequencies greater than 20 Hz.

Of particular interest were the differences noted in the principal whole-body response resonances of the seat occupants. The average resonance frequency measured in the child seats across the complete ensemble of tests was 8.5 Hz as opposed to the 4.0 Hz found for the seated adults. This provided a confirmation of the child apparent mass results of chapter 3 and showed that body response differences are important within the operational environment of the vehicle. In addition, comparison of the average transmissibility curves for the children to those of the drivers showed that the resonance peak for the children was lower in value (1.8 as opposed to 2.2 at 40 km/h) and wider in frequency (-3 dB points over an interval of approximately 4 Hz as opposed to 1.5 Hz at 40 km/h). This was due to both differences in damping characteristics and fact that the resonance frequencies varied more for the children due to the greater relative differences in body mass, leading to a lower and wider average curve.

This differences in main vertical whole-body resonance confirmed in the operational environment of the vehicle has important implications for the comfort evaluation of child seats since all existing whole-body vibration standards make use of frequency weightings developed from subjective testing of adult participants. Weightings such as the vertical direction W_b of BS 6841 (British Standards Institution 1987) or the vertical direction W_k of ISO 2631 (International Organisation for Standardisation

1997) have a shape which reflects the mechanical resonances of the seated adult body. As with the child apparent mass results, the transmissibilities presented here suggest that the existing weighting curves would not be expected to be applicable to children since the mechanical resonances occur at different frequencies. How comfort should be evaluated in the case of small children remains an open question.

A final point of note is that all eight seats considered were fastened to the vehicle by means of the vehicle's safety belts and that most showed evidence of a resonance response at a frequency of approximately 2 Hz. The resonance was more evident in the data from the 20 km/h tests than in the data from the 40 km/h tests, presumably due to a more favourable signal-to-noise ratio in the 40 km/h tests, but it was nonetheless present for most seats. The frequency value confirmed the presence of the rigid body child seat motion identified in the operational deflection shapes analysis of chapter 4. The results would suggest that the weak mechanical coupling produced by the untensioned belt attachment systems adopted in most current child seat designs is leading to large low frequency movements of the units in practice in the vehicle.

Chapter 6

Conclusions and Recommendations for Future Research

6.1 Summary of the Research Findings

The activities described in chapters 3 to 5 of this thesis were performed for the purpose of answering questions about the nature of the vibrations of small children and of child safety seats. Since no data treating the subject was available in the literature most of the activities consisted of experimental tests designed to shed light on one or more aspects of child or child seat behaviour. Taken as a whole the findings provide a first response to the questions posed in chapter 1, therefore it is useful to summarise the findings in light of the originally posed questions.

- *What are the vibrational characteristics of the seated child body ? Are the resonance frequencies, resonant amplitudes and energy dissipation properties similar to those of adults ?*

The testing and modelling activities of chapter 3 have shown that the resonance frequencies of small children are not the same as those of adults, they are instead higher. Depending on the children and adults being compared differences of 3 to 4 Hz appear common. The in-vehicle tests of chapter 5 suggested a mean principal resonance frequency of approximately 4.0 Hz for the adult drivers and 8.5 Hz for the children in the stage 0&1 seats. Additionally, since the damping ratio was found to be approximately constant across body sizes from small primates, to children to adults, the higher resonance frequencies of small children lead to frequency response curves with wider peaks. It can therefore be concluded that both the resonance frequency and the shape of the mechanical response curve are different for seated children. The data for the children also did not furnish any evidence of a second resonance peak similar to the 9 to 12 Hz movement of seated adults.

Absorbed power curves for small children were also found to be different from those of adults in terms of both the frequency of peak absorption and the width of the curve. Double normalising the absorbed power curves by both body mass and input acceleration highlighted this point and made it possible to determine that the energy dissipation per unit kilogram per unit acceleration for children was only 86% that of adults. With respect to adults small children differ therefore in terms of body mass, body mass distribution, body stiffness, resonant frequency and absorbed power. The nature and extent of the differences suggest that child seats should be designed following different criteria from those used for vehicle primary seating systems.

- *If the child vibrational response were different from that of adults how would it affect the use of the currently accepted methodologies for quantifying subjectively perceived vibrational comfort ?*

A basic element of all current methodologies used to evaluate the vibrational performance of seats is a weighting which quantifies the effect of frequency on the human mechanical and subjective response. The whole-body vibration weightings of BS 6841 or ISO 2631 (the two most widely applied standards) are conceptually similar to the familiar decibel A weighting used in the field of acoustics. As with the decibel A the weightings of BS 6841 and ISO 2631 are based on equal sensation

curves determined from the subjective response of test subjects. For whole-body vibration a high correlation exists between subjective response and the mechanical response since body resonances are characterised by relatively large movements and these movements produce sensation. The problem highlighted by the findings described in this thesis is that small children differ substantially in terms of their mechanical response behaviour, therefore their subjective response would be expected to be different and, as a consequence, any frequency weightings would also be different. Application of the vertical direction W_b or W_k weightings of BS 6841 and ISO 2631 to child vibration measurements would, based on the measurements presented in this thesis, be expected to produce misleading results. It therefore seems important to develop a weighting specifically for children. The development of an appropriate weighting will, however, require creativity since small children would not be expected to be able to provide accurate subjective data.

- *What are the vibration characteristics of child restraints as an individual unit ? And how are these modified by installation in the vehicle ?*

When tested in isolation the child seat response was found to be characterised by a series of flexible body resonances of the frame starting from frequencies as low as 15 to 20 Hz in the case of seats constructed from the softest plastic materials and 30 to 40 Hz for the strongest units. All available information points to the first mode of vibration being a torsional mode due to the open U-section design of current frames. Due to large gaps in the joints, components such as the carrying handle were found to add additional vibrational modes. A further effect caused by free play in hinges and fittings of the auxiliary components was a noise structure on the frequency response functions, similar to findings for vehicle seat frames having free play in the backrest hinges. The operational deflection shapes analysis of the Mothercare Rock 'n' Go seat confirmed that the flexible body resonances (the first at 35 Hz) remained largely unchanged in terms of frequency and mode shape when installed in the vehicle. One important new feature found only in the vehicle environment was, however, a resonance consisting of rigid body motion of the child seat and child at approximately 1.8 to 2.0 Hz. This behaviour, a result of the weak coupling between child seat and vehicle provided by the seat belts, was found to consist of vertical translation combined with rotation about the belt attachment point. The findings of

chapters 4 and 5 therefore suggest that child seat behaviour can be thought of in terms of frame flexible body resonances, movements of the auxiliary components, and rigid body motions of the complete unit over the seat cushion of the automobile in which it is travelling. Unfortunately, examples of each of these motions occurred within the frequency interval from 0.5 to 100 Hz normally considered when analysing human whole-body vibrational comfort.

- *What vibration levels and floor-to-child transmissibilities occur in current child restraint systems ? And how much can these characteristics vary from design to design ?*

The results of the vibration survey suggest that the environment in child safety seats was characterised by higher vibration amplitudes than commonly found for vehicle primary seating systems. The overall r.m.s. level was 30 percent higher in child seats than in the vehicle seats. Besides the differences in the body resonance frequencies of adults (4.0 Hz) and children (8.5 Hz), the frequency domain analysis also suggested that child seats have generally higher vibration transmissibility for all frequencies greater than about 20 Hz. Large differences were sometimes found between individual child seat units at a specific frequency value due to differences in design, but when averaged the results for the complete group confirmed a higher overall transmissibility than vehicle seats, with most of the additional energy being contributed by the low frequency rigid body resonance and the lack of high frequency attenuation.

- *How do the vibrational characteristics of current child seats compare to those of the vehicle primary seating systems used by adults ?*

The differences in geometric and material properties make it difficult to compare the behaviour of the two systems. Nevertheless, all data measured suggested that child seats have significantly higher vibration transmissibilities above 20 Hz. The frequency range in question and the materials used in current child seats suggest a lack of isolating and damping material placed in the vibration transmission path between the vehicle and the child. Few of the child seats tested had foam pads of other soft materials over the frame to cushion the contact with the child. There was

therefore no equivalent of the soft polyurethane foam material commonly found in vehicle seat cushions. In addition, unlike their vehicular counterparts, the child seats suffered from additional dynamics due to the lack of coupling with the vehicle. New child seat systems such as the LATCH or ISOFIX systems would be expected to provide greater and more controllable coupling to the vehicle frame, thus facilitating the control of low frequency movements. From the findings of this thesis it seems possible to state that child seat design is currently suffering from a lack of information regarding the behaviour of the child and of the seat unit, and that this lack of information, combined with cost pressures, has lead to less sophisticated and less performant designs than what is currently found in vehicle primary seating systems.

6.2 Further Research Regarding Child Safety Seats

Consideration of what currently constitutes an industrial vibrational comfort testing procedure for vehicle seats (see section 2.9) helps to suggest where more research is required before similar methods can be defined for child safety seats. In addition, the findings from the experiments performed in this thesis also suggest areas for further research. A few highly important areas are described below.

Child Impedance Loading Test Dummy: Since at least 1969 research has been underway to develop single or dual degree of freedom mechanical boxes capable of reproducing the vertical impedance loading of the adult human body. The research has been driven by the time and cost associated with the regular use of test subjects and by the desire for the greatest possible measurement repeatability. Examples of the research include the work of Suggs, Abrams and Stikeleather (1969), the work of Tomlinson and Kyle reported by Sandover (1970), Knoblauch, Wölfel and Buck (1995), Mansfield and Griffin (1996), Smith (1997), Huston, Johnson and Zhao (1998), Lewis (1998), Gu (1999), Towards (2000), Culmann and Wölfel (2001) and Lewis and Griffin (2002). From the number and quality of the papers found in the literature it appears that important and compelling motivations have driven the research. In the case of small children there is a further and overriding motivation for such research; ethical considerations. It would be difficult to justify the repeated and regular use of children for performing engineering measurements of child seats. Some of the knowledge needed to develop a loading device for performing child

safety seat vibration tests has been developed in this thesis. A first set of apparent mass curves has been produced for 8 children along with accompanying mass-spring-damper models. The models could serve as the basis for the development of mechanical devices which match the input impedance characteristics of the children. As in the research by the group of authors cited above, the development of an effective vibration dummy would be expected to involve many implementation issues from the fixing of the device in the seat to the susceptibility of the device to cross-axis motion. Research to develop such a device would be challenging, but such a technology might possibly be achievable within the limits of a 2-3 year study.

Child Frequency Weighting: A key element of any seat vibration testing procedure is the weighting curve which accounts for the frequency dependency of the whole-body mechanical and subjective response. The weightings defined in BS 6841 and ISO 2631 are used in numerous testing and simulation applications. The research described in this thesis has shown that the mechanical response of small children is different from that of adults, which would lead to significant differences in any frequency weighting defined for use with small children. This suggests a fundamental technical limitation that remains unresolved by the research presented in this thesis. Development of a frequency weighting for use with small children represents a significant technical and creative challenge for future researchers. Small children would not be expected to be capable of providing accurate subjective responses of the type normally used to define a frequency weighting, and many occupants of stage 0 & 1 seats are too young to even talk. Physiological measures such as heart rate have been used to estimate iso-comfort contours for animals such as piglets (Perremans et. al. 1996) but the vibration levels involved were higher than what would be considered ethical in child testing. Behavioural modifications have also been used as a response metric for the purpose of developing frequency weightings for animals such as chickens (Duggan et. al. 1996), but the level of conditioning required of the animals in order to obtain accurate results would probably not be acceptable with small children. The design of an observational study based on the influence of vibration on alertness or sleep/awake periods may provide a way of developing a weighting, but a thorough research investigation is required if a useful weighting curve is to be developed.

Mobile Child Apparent Mass Testing Unit: The practical difficulties encountered when attempting to identify test subjects and when organising the laboratory sessions during the research described in this thesis suggested that it would be very difficult to extend the statistical base from the current 8 children. The test equipment used was a fixed installation, located in a university laboratory, requiring families to bring their children to the university at a specifically arranged time. Given the nature of everyday life few people can afford the time required to participate in such as study, even with economic incentives. Despite possible difficulties, tests for as many as 30 or 40 children would be expected to be required before the statistical base was sufficiently wide to permit the definition of a standard, similar to ISO 5982 (2001) for seated adults, which specifies the apparent mass characteristics of small children. An obvious solution to the research requirement would be the development of a mobile child apparent mass testing device, capable of providing low intensity vibrations to seated children over the frequency range from 1 to 20 Hz. If such a device were safe, lightweight and portable, it would be expected to permit vibration testing to occur directly in a pediatric hospital once suitable agreements had been achieved with the hospital and consent given by the parents. Even if the mobile device was quite basic and limited to a single test amplitude, the scope for rapidly widening the test database would be promising.

Child Seat Coupling Dynamics: An important vibrational behaviour found in many of the tests performed in this thesis was a low frequency (1 to 2 Hz) rigid body movement of the child seat over the vehicle seat cushion. The cause appeared to be the weak mechanical coupling between child seat and vehicle due to the fastening method based on the use of the vehicle's safety belts. Changes in this behaviour could be achieved through the introduction of new fastening systems or of seat belt pretensioners. The dynamics of such systems could be effectively evaluated by means of numerical models such as Finite Element models which could include a simplified representation of the vehicle foam cushion, a simplified representation of the child seat frame and a detailed modelling of the belt and other coupling structures. Numerical simulation would permit rapid quantification of the effect of parameters such as belt tension, belt angle and child frame stiffness. In addition, it would permit rapid evaluation of the potential benefits and pitfalls of the recently introduced LATCH and ISOFIX attachment systems

Bibliography

Allen, G. 1978, A critical look at biodynamic modelling in relation to specification for human tolerance of vibration and shock, Paper A25-5, AGARD Conference Proceedings. No. 253, Paris, France, 6-10 Nov.

Allen, M.D. 1971, Mean square error of prediction as a criterion for selecting variables, Technometrics, Vol. 13, No. 3, pp 369-375

American Psychological Association (APA) 1992, Ethical principles of psychologists and code of conduct, American Psychologist, Vol. 47, No. 12, pp1597-1611

Amirouche, F.M.L.1987, Modeling of human reactions to whole-body vibration, Journal of Biomechanical Engineering, Trans. of the ASME, Vol. 109, pp 210-217

Amirouche, F.M.L.1987, Biodynamic analysis of the human body subjected to vibration, IEEE Engineering in Medicine and Biology Magazine, Sept., pp 22-26

Amirouche, F.M.L. and Ider, S.K. 1988, Simulation and analysis of a biodynamic human model subjected to low accelerations – a correlation study, Journal of Sound and Vibration, Vol. 123, No. 2, pp 281-292

Amirouche, F.M.L., Xie, M. and Patwardhan, A. 1994, Optimization of the contact damping and stiffness coefficients to minimise human body vibration, Journal of Biomedical Engineering, Vol. 116, pp 413-420

Arbogast, K.B., Moll, E.K., Morris, S.D. and Winston, F.K. 2001, Child occupant protection: a summary of current safety recommendations, Primary Care Update Ob/Gyns, Vol. 8, No. 4, pp 141-148

Arbogast, K.B., Moll, E.K., Morris, S.D., Anderko, R.L., Durbin, D.R. and Winston, F.K. 2001, Factors influencing pediatric injury in side impact collisions, Journal of Trauma Injury, Infection and Critical Care , Vol. 51, No. 3, pp 469-477

Arlt, F. and Marach, A. 1998, CAD modelling of a human 3D child body, Int. Journal of Industrial Ergonomics, Vol. 22, pp 333-341

Arvikar, R.J. and Seirig, A. 1978, Distribution of spinal disc pressures in the seated posture subjected to impact, Aviation and Space Environmental Medicine, Vol. 49, pp 166-169

Bakke, S.N. 1931, Rontgenologische beobachtungen uber die bewegungen der wirbelsaule, Acta Radiologica, Suppl. 13

Bartz, J.A. and Gianotti, C.R. 1975, Computer programme to generate dimensional and inertial properties of the human body, ASME Journal of Engineering for Industry, Vol. 97, pp 49-57

Bell, R., Burleigh, D. and Czernakowski, W. 1994, ISOFIX: The potential of a universal vehicle/child restraint interface for misuse reduction and performance enhancement, SAE paper 942220

Belytschko, T., Schwer, L. and Schultz, A. 1976, A model for analytic investigation of three dimensional head spine dynamics, Aerospace Medical Research Laboratory WPAFB Ohio, AMRL TR-76-10

Belytschko, T., Schwer, L. and Privitzer, E. 1978, Theory and application of a three dimensional model of the human spine, Aviation and Space Environmental Medicine, Vol. 49, No. 1, pp 158-165

Beranek, L.L. and Ver, I.L. 1992, Noise and vibration control engineering, John Wiley & Sons Inc., New York

Berg, M.D., Cook, L., Corneli, H.M., Vernon, D.D. and Dean, J.M. 2000, Effect of seat position and restraint use on injuries to children in motor vehicle crashes, Pediatrics, Vol. 105, No. 4, Part 1 of 2, pp 831-835

Berger, E. and Gilmore, B.J. 1993, Seat dynamic parameters for ride quality, SAE paper 930115

Berk, L.E. 1997, Child Development, Fourth Edition, Allyn and Bacon Publishers, Boston

Blevins, R.D. 1986, Formulas for natural frequency and mode shape, Robert E. Krieger Publishing Company, Malabar, Florida

Boileau, P.E. and Rakheja, S. 1998, Whole-body vertical biodynamic response characteristics of the seated vehicle driver: Measurement and model development, International Journal of Industrial Ergonomics, Vol. 22, pp 449-472

Boileau, P.E., Wu, X. and Rakheja, S. 1998, Definition of a range of idealised values to characterize the seated body biodynamic response under vertical vibration, Journal of Sound and Vibration, Vol. 215, No. 4, pp 841-862

Boileau, P.E., Rakheja, S. and Wu, X. 2002, A body mass dependent mechanical impedance model for applications in vibration seat testing, Journal of Sound and Vibration, Vol. 253, No. 1, pp 243-264

Bourke, G.J. 1996, Airbags and fatal injuries to children, The Lancet, Vol 347 (9001), March, pp 560

Brite-Euram Project 4186 2001, Final project report, Brite Euram project BE-97-4186 Seat Comfort Optimisation Procedure (SCOOP)

British Standards Institution 1987, Measurement and evaluation of human exposure to whole-body vibration and repeated shock, BS 6841

British Standards Institution 1989, Safety aspects of experiments in which people are exposed to mechanical vibration and shock, BS 7085

British Standards Institution 1992, Evaluation of human exposure to vibration in buildings (1 Hz to 80 Hz), BS 6472

British Standards Institution 1994, Mechanical vibration – Laboratory method for evaluating vehicle seat vibration, Part 1: Basic requirements, BS 30326-1

Broderson, A.B. and Von Gierke, H.E. 1971, Mechanical impedance and its variation in the restrained primate during prolonged vibration, ASME Paper 71-WA / BHF-8

Broman, H., Pope, M.H., Benda, M., Svensson, M., Ottosson, C. and Hansson, T. 1991, The impact response of the seated subject, Journal of Orthopaedic Research, Vol. 9, pp 150-154

Broman, H. , Pope, M. and Hanson, T. 1996, A mathematical model of the impact response of the seated subject, Medical Engineering Physics, Vol. 18, No. 5, pp 410-419

Brown, D. and Carbon, G. 1977, Survey of excitation techniques applicable to the testing of automotive structures, SAE paper 770029

Bruncassan, F., Cailleret, M.C. and Tarriere, C. 1992, Contribution of biomechanics to child safety in motor vehicles, Annales De Pediatrie, Vol. 39, No. 3, pp 165-173

Bull, M.J., Stroup, K.B., Everly, J.S., Weber, K. and Doll, J.P. 1994, Child safety seat use for infants with Pierre-robin sequence, Archives of Pediatrics & Adolescent Medicine, Vol. 148, No. 3, pp 301-305

Bull, M.J., Stroup, K.B. and Gerhart, S. 1988, Misuse of car safety seats, Pediatrics, Vol. 81, No. 98

Carlsson, G., Norin, H. and Ysander, L. 1991, Rearward-facing child seats: the safest car restraint for children ?, Accid. Anal. Prev., Vol. 23, No. 2-3, pp 175-182

Christ, W. and Dupuis,H. 1963, Der einfluß vertikaler schwingungen aud die wirbelsäule und magen (Röntgenkinematographische Studien), Zentralblatt für Arbeitsmedizin und Arbeitsschutz, Band 13, pp 3-9

Christ, W. and Dupuis,H. 1966, Über die beanspruchung der wirbelsäule unter dem einfluß sinusförmiger und stochastischer schwingungen, Int. Z. angew. Physiol. Einschl. Arbeitsphysiol., Vol. 22, pp 258-278

Clark, W.S., Lange, K.O. and Coermann, R.R. 1962, Deformation of the human body due to uni-directional forced sinusoidal vibration, Human Factors, Vol. 4, pp 255-274

Coermann, R.R. 1940, Untersuchungen über die einwirkung von schwingungen auf den menschlichen organismus, Luftfahrtmedizin 2, Bd. 4, pp 73-117

Coermann, R.R., Ziegenruecker, G.H., Wittwer, A.L. and von Gierke, H.E. 1960, The passive dynamic mechanical properties of the human thorax-abdomen system and of the whole body system, Aerospace Medicine, Vol. 31, No. 6, pp 443-455

Coermann, R.R. 1961, The mechanical impedance of the human body in sitting and standing position at low frequencies, ASD Technical Report No. 61-492, ASD-ASF, Wright-Patterson Air Force Base

Coermann, R.R. 1962, The mechanical impedance of the human body in sitting and standing position at low frequencies, Human Factors, Vol. 4, pp 227-253

Coermann, R.R., Magid, E.B. and Lange, K.O. 1962, Human performance under vibrational stress, Human Factors, Vol. 4, pp 315-324

Coemann, R.R. 1965, Physiologische schwingungsprobleme in fahrseugen, Zentralbl. Verk. Med. Verk. Psych. Luft. Raumf Med. 11: 3

Coermann, R.R. 1968, Mechanical impedance of the sitting human under sustained acceleration, Aerospace Medicine, Vol.39, pp 675-679

Cole, J.H. 1993, Developing a cost effective integrated structural seat, SAE paper 930108, Society of Automotive Engineers

Corbridge, C., Griffin, M.J. and Harborough, P.R. 1989, Seat dynamics and passenger comfort, Proc. Instn. Mech. Engrs., Vol. 203, pp 57-64

Coren, S. and Ward, L.M. 1989, Sensation & Perception,
Harcourt Brace Jovanovich Publishers, Fort Worth

Cramer, H.J., Liu, Y.K. and Von Rosenberg, D.U. 1976, A distributed parameter model of the inertially loaded human spine, Journal of Biomechanics, Vol. 9, pp 115-130

Cullmann, A. and Wölfel, H.P. 2001, Design of an active vibration dummy of sitting man, Clinical Biomechanics, Vol. 16, Suppl. No. 1, S64-S72

Cunningham, A., Huygens, E. and Leenslag, J.W. 1994, MDI foam cushioning for automotive applications, Cellular Polymers, Vol. 13, No. 6, pp 461-472

Dargenio, P., Binkin, N., Carrieri, M.P., Salamina, G., Salmaso, S., Taggi, F., Tozzi, A., Niccolini, A., Maestro, A., Cafaro, L., Lomonaco, R., Sodano, L., Pandolfi, P., Filipetti, F., Selvaggi, T.M. and Viviani, S. 1994, Child safety seat use in 7 Italian Regions, Rivista Italiana Di Pediatria, Vol. 20, No. 6, pp 671-676

Deboli, R. and Potecchi, S. 1986, Determinazione del comportamento dei sedili per macchine agricole mediante banco vibrante, Conference: Infortunistica, sicurezza e confort nella meccanizzazione agricola e forestale e nei fabbricarti di esercizio, Florence, 2-3 December

Decina, L.E. and Knoebel, K.Y.1997, Child safety seat misuse patterns in four states, Accident Analysis and Prevention, Vol. 29, No. 1, pp 125-132

Denninger, L. and Besnault, B. 2001, Development and validation of a finite element human body model, SCOOP Project Report, EU Brite Euram project BE-97-4186 Seat Comfort Optimisation Procedure (SCOOP)

Der Avanessian, H., Ridella, S.A., Mani, A. and Krishnaswamy, P. 1992, Analytical model to study the infant seat/airbag interaction, SAE paper 920126

DeSantis-Klinich, K., Pritz, H.B., Beebe, M.S. and Welty, K.E. 1994, Survey of older children in automotive restraints, SAE paper 942222

Deter, T. and Hellkamp, U. 1996, Development of MADYMO P6 child dummy model, ESV Conference paper 96-S10-W30, Melbourne, http://www.tu-berlin.de/fb10/ISS/FG7/studis/esvp6.html

Deutsches Insitut für Normung e.V. 1987, DIN 45 676 Mechanische eingangsimpedanz und übertragungsfunktion des menschlichen körpers, Sept.

Dieckmann, D. 1956, Die einwirkung mechanischer schwingungen bis 100 Hz auf den menschen, Ultraschall Med Grenzgebiete, Vol. 9, No. 3, pp 1-10

Dieckmann, D. 1957, A study of the influence of vibration on man, Ergonomics, Vol. 1, pp 347-355

Dieckmann, D. 1957, Einfluß vertikaler mechanischer schwingungen auf den menschen, Internat. Z angew. Physiol. Arbeitsphysiol, Bd., pp 519-564

Dieckmann, D. 1958, Einfluß horizontaler mechanischer schwingungen auf den menschen, Internat. Z angew. Physiol. Arbeitsphysiol., Bd. 17, S., pp 83-100

Dietrich, M., Kedzior, K. and Zagrajek, T. 1995, Three dimensional FEM model of man-operator under vibration, Proceedings of the 9th congress on the theory of machines and mechanisms, Vol 3., Politecnico di Milano, pp 2187-2190

Donkers, P.C.M., Toussaint, H.M., Molenbroek, J.F.M. and Steenbekkers, L.P.A. 1993, Recommendations for the assessment and design of young children's bicycles on the basis of anthropometric data, Applied Ergonomics, Vol. 24, No. 2, pp 109-118

Doolan, R.J. and Mannino, V.F. 1995, Comparison of seat system resonant frequency testing methods, SAE paper 951335

Dounis, D.V., Moreland, J.C., Wilkes, G.L., Dillard, D.A. and Turner, R.B. 1993, The mechano-sorptive behavior of flexible water-blown polyurethane foams, Journal of Applied Polymer Science, Vol. 50, pp 293-301

DuBois, A.B., Brody, A.W., Lewis, D.H. and Burgess, B.F 1956, Oscillation mechanics of lungs and chest in man, Journal of Applied Physiology, Vol. 8, pp 587-594

Duggan, J.A., Randall, J.M., White, R.P. and Nicol, C.J. 1996, Frequency weightings for aversion of broiler chickens to whole-body vertical vibration, UK Group Meeting on Human Response to Vibration, MIRA, Nuneaton, 18th-20th September

Dupuis, H. 1969, Zur physiologischen beanspruchung des menschen durch mechanische schwingungen, VDI Berlin, Vol. 11, No. 7, pp 1-168

Dupuis, H. 1980, Stand der arbeitsmedizinischen bewertung mechanischer schwingungen am arbeitsplatz, Arb. Med. Soz. Med. Prav. Med., Vol. 15, No. 10, pp 236-243

Dupuis, H. and Hartung, E. 1980, Einfluß von vibrationen auf die optische wahrnehmung, Research Report Wehrmedizin BMVg-FBWM 80-10, pp 1-141

Dupius, H. and Zerlett, G. 1986, The effects of whole-body vibration, Springer-Verlag, Berlin

Ebe, K. 1994, Effect of density of polyurethane foam on vibration transmission, United Kingdom Informal Group Meeting on Human Response to Vibration, Institute of Naval Medicine, Alverstoke, Gosport, Sept. 19-21

Ebe, K. 1994, The effect of polyurethane foam composition on dynamic comfort of automotive seats, Japan Informal Group Meeting on Human Response to Vibration, National Institute of Industrial Health, Nagao, Tamaku, Kawasaki, July 1-3

Eby, D.W. and Kostyniuk, L.P. 1999, A statewide analysis of child safety seat use and misuse in Michigan, Accident Analysis and Prevention, Vol. 31, pp 555-566

Edwards, R.G., Lafferty, J.F. and Knapp, C.F. 1976, Experimental and analytical determinations of the mechanical impedance response of animals to vertical vibration, Journal of Biomechanics, Vol. 9, pp 55-61

Edwards, R.G. and Lafferty, J.F. 1978, A model to predict the mechanical impedance of the sitting primate during sinusoidal vibration, ASME 73-DET-78

Ekman, R., Welander, G., Svanstrom, L. and Schelp, L. 2001, Long-term effects of legislation and local promotion of child restraint use in motor vehicles in Sweden, Accident Analysis and Prevention, Vol. 33, pp 793-797

El-Khatib, A., Guillon, F. and Dômont, A. 1998, Vertical vibration transmission through the lumbar spine of the seated - subject first results, Journal of Sound and Vibration, Vol. 215, No. 4, pp 763-773

European Parliament and the Council of the European Union 2002, Directive 2002/44/EC on the minimum health and safety requirements regarding the exposure of workers to the risks arising from physical agents (vibration), June 25th

Ewins, D.J. 1984, Modal Testing: Theory and Practice, Research Studies Press Ltd., Taunton, Somerset

Fairley, T.E. 1990, Predicting the transmissibility of a suspension seat, Ergonomics, Vol. 33, No. 2, pp 121-135

Fairley, T.E. and Griffin, M.J. 1986 A test method for the prediction of seat transmissibility, SAE paper 860046/860047

Fairley, T.E. and Griffin, M.J. 1989, The apparent mass of the seated human body: vertical vibration, Journal of Biomechanics, Vol. 22, No. 2, pp 81-94

Fairley, T.E. and Griffin, M.J. 1990, The apparent mass of seated human body in the fore-and-aft and lateral directions, Journal of Sound and Vibration, Vol. 139, pp 299-306

Fine, R. 1963, Correlation of vertical acceleration and human comfort in a passenger car, SAE Paper 630314, (733C), pp 1-4

Flaherty, L. and Snyder, J.A. 1999, An easier fit for child safety seats, Journal of Emergency Nursing, Vol. 25, No. 2, pp 138

French, M. 1997, Contact problems in modal analysis, Proc. of the 15th Int. Modal Analysis Conf., Orlando, Florida, USA

Garg, D.P. and Ross, M.A. 1976, Vertical mode human body vibration transmissibility, IEEE Transactions on Systems, Man and Cybernetics, SMC-6, No. 2, pp 102-112

Geiger,J. 1927, Mechanische schwingungen, Berlin, S., 250

Giacomin, J. 2000, Some observations regarding the vibrational environment in child safety seats, Applied Ergonomics, Vol. 31, pp 207-215

Giacomin, J. 1997, Modal properties of child safety seats, ATA 4th Int. Conf. On Comfort in the Automobile Industry, Bologna, Italy, October 2-3

Giacomin, J. 1997, In-vehicle measurement of the apparent mass of small children, UK Group Meeting on Human Response to Vibration, ISVR, University of Southampton, United Kingdom, September 17-19

Giacomin, J. and Bracco, R. 1995, An experimental approach for the vibration optimisation of automotive seats, ATA 3rd Int. Conf. on Vehicle Comfort and Ergonomics, Bologna, Italy, March 29-31, 199-208

Giacomin, J., Giuliano, F. and Giai Merlera, M. 1994, Survey of seat guide vibrations, Brite-Euram Project 5549 SED Progress Report, Centro Ricerche Fiat, Torino, Italy

Giacomin, J. and Lo Faso, G. 1993, Vibration survey of the Fiat Tempra and Fiat Tipo, Brite-Euram Project 5549 SED Progress Report, Centro Ricerche Fiat, Torino, Italy

Giacomin, J., Steinwolf, A. and Staszewski, W.J. 2000, An algorithm for mildly nonstationary mission synthesis [MNMS], Engineering Integrity, Vol. 7, January, pp 44-56

Gillespie, T.D. 1992, Fundamentals of vehicle dynamics, Society of Automotive Engineers, Warrendale, PA.

Glass, R.J., Segui-Gomez, M. and Graham, J.D. 2000, Child passenger safety: decisions about seating location, airbag exposure, and restraint use, Risk Analysis, Vol. 20, No. 4, pp 521-527

Goldman, D.E. and Von Gierke, H.E. 1960, The effect of shock and vibration on man, Naval Medical Research Institute Report No. 60-3, Bethesda

Graham, C.J., Kittredge, D. and Stuemky, J.H. 1992, Injuries associated with child safety seat misuse, Pediactric Emergency Care, Vol. 8, No. 6, pp 351-353

Grandjean, E. 1980, Sitting posture of car drivers from the point of view of ergonomics, Human factors in Transport Research (Edited by D.J. Osborne and J.A. Levis), Academic Press, London

Griffin, M.J. 1975, Vertical vibration of seated subjects: effects of posture, vibration level and frequency, Aviation, Space and Environmental Medicine, Vol. 46, No. 3, pp 269-276

Griffin, M.J. and Whitham, E.M. 1978, Individual variability and its effects on subjective and biodynamic response to whole-body vibration, Journal of Sound and Vibration, Vol. 58, No. 2, pp 239-250

Griffin, M.J., Lewis, C.H., Parsons, K.C. and Whitham, E.M. 1979, The biodynamic response of the human body and its application to standards, AGARD CP-253, Paper A28

Griffin, M.J. 1986, Evaluation of vibration with respect to human response, SAE paper 860047

Griffin, M.J. 1990, Handbook of human vibration, Academic Press, London

Griffin, M.J. 2001, The validation of biodynamic models, Clinical Biomechanics 16, Supplement 1, S81-S92

Gu, Y. 1999, A new dummy for vibration transmissibility measurement in improving ride comfort, SAE Publication 99B-14, Paper 1999-01-0629

Guignard, J.C. 1959, The physiological effects of mechanical vibration: a selected bibliography, R.A.F. Institute of Aviation Medicine, Report No. 124, August

Hagena, F.W., Wirth, C.J., Piehler, J., Plitz, W., Hofmann, G.O. and Zwingers, T.H. 1985, In-vivo experiments on the response of the human spine to sinusoidal Gz-vibration, AGARD Conference Proceedings, Backache and Back discomfort, No. 378, pp -12

Halvorsen, W.G. and Brown, D.L. 1977, Impulse technique for structural frequency response testing, Sound and Vibration, November, pp 8-21

Hayes, B.E. 1992, Measuring customer satisfaction: development and use of questionnaires, ASQC Quality Press, Milwaukee, Wisconsin

Harazin, B. and Grzesik, J. 1998, The transmission of vertical whole-body vibration to the body segments of standing subjects, Journal of Sound and Vibration, Vol. 215, No. 4, pp 775-787

He, J. and Fu, Z.F. 2001, Modal analysis, Butterworth Heinemann, Oxford

Helberg, W. and Sperling, E. 1941, Critical appraisal of the riding qualities of railway vehicles, Organ f.d. Fortschr d. Eisenbahnwesens, Vol. 96, (British Railways Board Research Department Translation Service, 743, 1967)

Hendey, G.W. and Votey, S.R. 1994, Injuries in restrained motor vehicle accident victims, Annals of Emergency Medicine,Vol. 24, No. 1, pp 77-84

Henzei, J.H., Mohr, G.C. and Von Gierke, H.E. 1968, Reappraisal of biodynamic implications of human ejections, Aerospace Medicine, Vol. 39, No. 3, March, pp231-240

Herterich, J. and Schnauber, H. 1992, The effects of vertical mechanical vibration on standing man, Journal of Low Frequency Noise and Vibration, Vol.11, No. 2, pp 52-61

Hess, J.L. and Lombard, C.F. 1958, Theoretical investigations of dynamic response of man to high vertical acceleration, Journal of Aviation Medicine, Vol. 29, pp 66-75

Hinz, B., Seidel, H., Brauer, D., Menzel, G., Bluthner, R. and Erdmann 1988, Bidimensional accelerations of lumbar vertebrae and estimation of internal spinal load during sinusoidal vertical whole-body vibration: a pilot study, Clinical Biomechanics, Vol. 3, pp 241-248

Hinz, B., Menzel, G., Blüthner, R. and Seidel, H. 2001, Transfer functions as a basis for the verification of models – variability and restraints, Clinical Biomechanics 16, Suppl. No. 1, S93-S100

Hodgson, V.R., Lissner, H.R. and Patrick, L.M. 1963, The effect of jerk on the human spine, ASME paper 63-WA-316, pp 1-8

Holmlund, P and Lunström, R. 1998, Mechanical impedance of the human body in the horizontal direction, Journal of Sound and Vibration, Vol. 215, No. 4, pp 801-812

Holmlund, P. and Lundström, R. 2001, Mechanical impedance of the sitting human body in single-axis compared to multi-axis whole-body vibration exposure, Clinical Biomechanics, Vol. 16, Supl. 1, S101-S110

Hopkins, G.R. 1970, Nonlinear lumped parameter mathematical model of dynamic response of the human body, Symposium on Biodynamic Models and Their Applications, Dayton, Ohio, 26-28 Oct., pp 105-122

Hornick, R.J. Vibration isolation in the human leg, Human Factors, Vol. 4, No. 5, October

Huston, D.R., Johnson, C.C. and Zhao, X.D. 1998, A human analog for testing vibration attenuating seating, Journal of Sound and Vibration, Vol. 214, No. 1, pp 195-200

International Organisation for Standardisation 1982, ISO 5007:1990 (E) Agricultural wheeled tractors – Operators seat - Laboratory measurement of Transmitted vibration, International Organisation for Standardisation.

International Organisation for Standardisation 1982, ISO 7096:1982 (E), Earth-moving machinery - Operators Seat - Transmitted Vibration, International Organisation for Standardisation.

International Organisation for Standardisation 1987, ISO 7962:1987 (E) Mechanical vibration and shock – mechanical transmissibility of the human body in the Z direction, International Organisation for Standardisation.

International Organisation for Standardisation 1992, ISO 10326-1 (E) Mechanical vibration – Laboratory method for evaluating vehicle seat vibration, Part 1: Basic requirements, International Organisation for Standardisation

International Organisation for Standardisation 1997, ISO 2631-1 (E) Mechanical vibration and shock – evaluation of human exposure to whole-body vibration, International Organisation for Standardisation.

International Organisation for Standardisation 2001, ISO 5982:2001 (E) Mechanical vibration and shock – range of idealised values to characterise seated-body biodynamic response under vertical vibration, International Organisation for Standardisation.

Ishihara, H., Tsuji, H., Hirano, N., Ohshima, H. and Terahata, N. 1992, Effects of continuous quantitative vibration on rheologic and biological behaviours of the intervertebral disc, Spine, Vol. 17, No. 3S, pp s7-s12

Jacklin, H.M. 1936, Human reactions to vibration, S.A.E. Journal (Transactions), Vol. 39, No. 4, Oct., pp 401-407

Janeway, R.N. 1948, Vehicle vibration limits to fit the passenger, Paper presented to the SAE, March 5, 1948

Janeway, R.N. 1975, Human vibration tolerance criteria and applications to ride evaluation, SAE paper 750166

Jex, H.R. and Magdaleno, R.E. 1978, Biomechanical models for vibration feedthrough to hands and head for a semi-supine pilot, Aviation and Space Environmental Medicine, pp 304-316

Ji. T. 1995, A continuous model for the vertical vibration of the human body in a standing position, Paper Presented at the United Kingdom Informal Group Meeting on Human Response to Vibration, Silsoe Research Institute, Silsoe, 18-20 Sept.

Johnston, C., Rivara, F.P. and Soderberg, R. 1994, Children in car crashes - analysis of data for injury and use of restraints, Pediatrics, Vol. 93, No. 6, pp 960-965

Joyce, J. and Dunn, W.H. 1992, Evaluation of seat design parameters for improved occupant ride, IMechE paper 925172

Kasra, M., Shirazi-Adl, A. and Drouin, G. 1992, Dynamics of human lumbar intervertebral joints: experimental and finite-element investigations, Spine, Vol. 17, No. 1, pp 93-102

Katcher, M.L., Bull, M.J., Palmer, S.D., Rodgers, G.C., Smith, B.L., Spivak, H.R. and Tully, S.B. 1996, Selecting and using the most appropriate car safety seats for growing children - guidelines for counseling parents, Pediatrics, Vol. 97, No. 5, pp 761-763

Kitazaki, S. and Griffin, M.J. 1995, A data correction method for surface measurement of vibration on the human body, Journal of Biomechanics, Vol. 28, No. 7, pp 885-890

Kitazaki, S. and Griffin, M.J. 1997, A modal analysis of whole-body vertical vibration, using a finite element model of the human body, Journal of Sound and Vibration, Vol. 200, No. 1, pp 83-103

Kitazaki, S. and Griffin, M.J. 1998, Resonance behaviour of the seated human body and effects of posture, Journal of Biomechanics, Vol. 31, pp 143-149

Knoblauch, J., Wölfel, H.P. and Buck, B. 1995, Ein schwingungsdummy des sitzenden menchen, ATZ Automobiltechnische Zeitschrift, Vol. 97, No 10, pp668-671

Kobayashi, F., Nakagawa, T., Kanada, S., Sakakibara, H., Miyao, M., Yamanaka, K. and Yamada, S. 1981, Measurement of human head vibration, Industrial health, Vol. 19, pp 191-201

Koizumi, T., Tsujiuchi, N. and Kawamura, R. 2001, Dynamic analysis of child in misused CRS during car accident, Proceedings of the IMAC XIX Conference on Structural Dynamics, Kissimmee, Florida, USA

Holmlund, P. 1999, Absorbed power and mechanical impedance of the seated human measured within a real vehicle environment compared with single axis laboratory data, Journal of Low Frequency Noise, Vibration and Active Control, Vol. 8, No. 3, pp 97-110

Kryter, K.D. 1985, The effects of noise on man, Academic Press, Orlando, Florida

Kubo, M., Terauchi, F., Aoki, H. and Matsuoka, Y. 2001, An investigation into a synthetic vibration model for humans: an investigation into a mechanical vibration model constructed according to the relations between the physical, psychological and physiological reactions of humans exposed to vibration, Int. Journal of Industrial Ergonomics, Vol. 27, pp 219-232

Kuboki, N., Okamura, H., Enomonto, T., Nishimoto, T., Ohue, T. and Ando, K. 2001, An occupant sensing system for automobiles using a flexible tactile force sensor, Furukawa Review, No. 20, April 2001, pp 89-94

Kuhane, C.J. 1986, An evaluation of child passenger safety: the effectiveness and benefits of safety seats, DOT-HS-806-890, National Highway Traffic Safety Administration, Washington D.C.

Kyprianou, A., Giacomin, J., Heidrich, M. and Böcking, J. 2000, Differential evolution based identification of automotive hydraulic engine mount model parameters, Proceeding of the Institution of Mechanical Engineers, Part D Automotive, Vol. 214, pp 249-264

Lanthan, F.A. 1957, A study in body ballistics: seat ejection, Proceedings of the Royal Society, Ser. B., Vol. 147, pp 121-139

Larson Davis Laboratories 1998, Model 2900B User Manual, Larson Davis Laboratories, Provo, Utah

Lee, R.A. and Pradko, F. 1968, Analytical analysis of human vibration, SAE paper 680091

Lee, R.A. and King, A.I. 1970, Visual vibration response, ASME Biomechanical and Human Factors Conference, 70-BHF-16, May 31st - June 3rd , pp 1-8

Lehmann, G. and Dieckmann, D. 1956, Die wirkung mechanischer schwingungen (0.5-100 Hz) auf den menschen, Research Report Wirtschafts-und-Verkehrsministerium, NRW 362

Lewis, C.H. and Griffin, M.J. 1996, The transmission of vibration to the occupants of a car seat with a suspended backrest, Proc. Instn. Mech. Engrs, Vol. 210, pp 199-207

Lewis, C.H. 1998, The implementation of an improved anthropodynamic dummy for testing the vibration isolation of vehicle seats, UK Group Meeting on Human Response to Vibration, Health and Safety Executive, Buxton, Derbyshire, Sept. 16-18

Lewis, C.H. and Griffin, M.J. 2002, Evaluating the vibration isolation of soft seat cushions using an active anthropodynamic dummy, Journal of Sound and Vibration, Vol. 253, No. 1, pp 295-311

Ling Dynamic Systems Ltd 1977, Vibrator Model 501 Instruction Manual, Ling Dynamics Systems Ltd, Royston, Hertfordshire

Liu, Y.K. and Murray, J.D. 1966, A theoretical study of the effect of impulses on the human torso, Proceedings of the ASME, Symposium on Biomechanics, Fung Y.C. Editor, New York, pp 167-186

Lizee, E., Robin, S., Song, E., Bertholon, N., LeCoz,, J.Y., Besnault, B. and Lavaste, F. 1998, Development of a 3D finite element model of the human body, SAE paper 983152

LMS International 1999, LMS CADA-X Endurance Monitor Manual, Revision 3.5B, LMS International, Leuvan

LMS International 1999, LMS CADA-X Fourier Monitor Manual, Revision 3.5B, LMS International, Leuvan

LMS International 1999, LMS CADA-X Modal Manual, Revision 3.5B, LMS International, Leuvan

LMS International 1999, LMS CADA-X Running Modes Manual, Revision 3.5B, LMS International, Leuvan

LMS International 1999, LMS CADA-X Time Data Processing Manual, Revision 3.5B, LMS International, Leuvan

Lundström, R. and Holmlund, P. 1998, Absorption of energy during whole-body vibration exposure, Journal of Sound and Vibration, Vol. 215, No. 4, pp 789-799

Lundström, R., Holmlund, P. and Lindberg, L. 1998, Absorption of energy during vertical whole-body vibration exposure, Journal of Biomechanics, Vol. 31, pp 317-326

Magid, E.B., Coermann, R.R. and Ziegenruecker, G.H. 1960, Journal of Aerospace Medicine, Vol. 31, pp 915

Magnusson, M., Pope, M., Rostedt, M. and Hansson, T. 1993, Effect of backrest inclination on the transmission of vertical vibrations through the lumbar spine, Clinical Biomechanics, Vol. 8, No. 1, pp 5-12

Maia, N.M.M. and Silva, J.M.M.1997, Theoretical and experimental modal analysis, Research Studies Press Ltd., Taunton, Somerset, England

Mandel, M.J. and Lowry, R.D. 1962, One-minute tolerance in man to vertical sinusoidal vibration in the sitting position, DDC No. AD 292704, October

Mansfield, N.J. and Griffin, M.J. 1996, Vehicle seat dynamics measured with an anthropodynamic dummy and human subjects, Inter-Noise 96, Proceedings of the 25th Anniversary Congress, Liverpool, Book 4, pp 1725-1730

Mansfield, N.J. and Griffin, M.J. 1998, Effect of magnitude of vertical whole-body vibration on absorbed power for the seated human body, Journal of Sound and Vibration, Vol. 215, No. 4, pp 813-825

Mansfield, N.J. and Lundström, R. 1999, The apparent mass of the human body exposed to non-orthogonal horizontal vibration, Journal of Biomechanics, Vol. 32, pp 1269-1278

Mansfield, N.J. and Lundström, R. 1999, Models of the apparent mass of the seated human body exposed to horizontal whole-body vibration, Aviation, Space and Environmental Medicine, Vol. 70, No. 12, pp 1166-1172

Mansfield, N.J. and Griffin, M.J. 2000, Non-linearities in apparent mass and transmissibility during exposure to whole-body vertical vibration, Journal of Biomechanics, Vol. 33, pp 933-941

Mansfield, N.J., Holmlund, P. and Lundström, R. 2001, Apparent mass and absorbed power during exposure to whole-body vibration and repeated shocks, Journal of Sound and Vibration, Vol. 248, No. 3, pp 427-440

Mansfield, N.J. and Griffin, M.J. 2002, Effects of posture and vibration magnitude on apparent mass and pelvis rotation during exposure to whole-body vertical vibration, Journal of Sound and Vibration, Vol. 253, No. 1, pp 93-107

Margolis, L.H., Wagenaar, A.C. and Molnar, L.J. 1992, Use and misuse of automobile child restraint devices, American Journal of Diseases of Children, Vol. 146, No. 3, pp 361-366

Matsumoto, Y. and Griffin, M.J. 1998, Movement of the upper-body of seated subjects exposed to vertical whole-body vibration at the principal resonance frequency, Journal of Sound and Vibration, Vol. 215, No. 4, pp 743-762

Matsumoto, Y. and Griffin, M.J. 2001, Modelling the dynamic mechanisms associated with the principal resonance of the seated human body, Clinical Biomechanics 16, Suppl. No. 1, S31-S44

Matsumoto, Y. and Griffin, M.J. 2002, Effect of phase on human responses to vertical whole-body vibration and shock – analytical investigation, Journal of Sound and Vibration, Vol. 250, No. 5, pp 813-834

Matsumoto, Y. and Griffin, M.J. 2002, Effect of muscle tension on non-linearities in the apparent masses of seated subjects exposed to vertical whole-body vibration, Journal of Sound and Vibration, Vol. 253, No. 1, pp 77-92

McConnell, K.G. 1995, Vibration testing: theory and practice, John Wiley & Sons, New York

McLain, R.F. and Weinstein, J.N. 1994, Effects of whole body vibration on dorsal root ganglion neurons, Spine, Vol. 19, No. 13, pp 1455-1461

McLeod, R.W. and Griffin, M.J. 1993, Effects of duration and vibration on performance of a continuous manual control task, Ergonomics, Vol. 36, No. 6, pp 645-659

Medical Research Council, Natural Sciences and Engineering Research Council and Social Sciences and Humanities Research Council of Canada 1998, Tri-council policy statement on ethical conduct for research involving humans, August

Mehlman, C.T., Scott, K.A., Koch, B.L. and Garcia, V.F. 2000, Orthopaedic injuries in children secondary to airbag deployment, The Journal of Bone and Joint Surgery, Vol. 82-A, No. 6, pp 895-898

Melvin, J.W., Stalnaker, R.L. and Mohan, D. 1978, Protection of child occupants in automotive crashes, Proceedings of the 22nd Stapp Car Crash Conference, Oct. 24-26, Ann Arbor, Michigan, USA

Mertens, H. 1978, Nonlinear behaviour of sitting humans under increasing gravity, Aviation, Space and Environmental Medicine, Vol. 49, No. 1, pp 287-298

Mitchell, L.D. and Elliot, K.B. 1984, How to design stingers for vibration testing of structures, Sound and Vibration, April, pp 14-18

Miwa, T. 1967, Evaluation methods for vibration effect: Part 1 Measurements of threshold and equal sensation contours of whole body for vertical and horizontal vibrations, Industrial Health, Vol. 5, pp 183-205

Miwa, T. 1967, Evaluation methods for vibration effects: Part 2 Measurement of equal sensation level for whole body between vertical and horizontal sinusoidal vibrations, Industrial Health, Vol. 5, pp 206-212

Miwa, T. 1967, Evaluation methods for vibration effect: Part 3 Measurements of threshold and equal contours on hand for vertical and horizontal sinusoidal vibrations, Industrial Health, Vol. 5, pp 213-220

Miwa, T. 1968, Evaluation methods for vibration effect: Part 4 Measurements of vibration greatness for whole body and hand in vertical and horizontal vibrations, Industrial Health, Vol. 6, pp 1-10

Miwa, T. 1968, Evaluation methods for vibration effect: Part 5 Calculation method of vibration greatness level on compound vibrations, Industrial Health, Vol. 6, pp 11-17

Miwa, T. 1968, Evaluation methods for vibration effect: Part 6 Measurements of unpleasant and tolerance limit levels for sinusoidal vibrations, Industrial Health, Vol. 6, pp 18-27

Miwa, T. 1969, Evaluation methods for vibration effect: Part 8 The vibration greatness of random waves, Industrial Health, Vol. 7, pp 89-115

Miwa, T. 1975, Mechanical impedance of human body in various postures, Industrial Health, Vol. 13, No. 1, pp 1-22

Morris, S.D., Arbogast, K.B. and Winston, F.K. 1999, Injury mechanisms of children in side impact collisions, Pediatrics, Vol. 104, No. 3, Supplement to Pediatrics Part 3 of 3, pp 697-698

Mueller, E.A. 1939, Die wirkung sinusförmiger vertikalschwingungen auf den sitzenden und stehenden menschen, Arbeitsphysiologie 10, No. 5, pp 459-476

Muksian, R. and Nash, C.D. 1974, A model for the response of seated humans to sinusoidal displacements of the seat, Journal of Biomechanics, Vol. 7, pp 209-215

Muksian, R. and Nash, C.D. 1976, On frequency-dependent damping coefficients in lumped-parameter models of human beings, Journal of Biomechanics, Vol. 9, pp 339-342

National Safe Kids Campaign 2001, Campaign Research, www.safekids.org

Necking, L.E., Dahlin, L.B., Friden, J., Lundborg, G., Lundström, R. and Thornell, L.E. 1992, Vibration induced muscle injury, The Journal of Hand Surgery, Vol. 17B, No. 3, June, pp 270-274

NHTSA 2001, Dictionary of child safety seat terms, US Department of Transportation National Highway Traffic Safety Administration, http://www.nhtsa.dot.gov/people/injury/childps/csr2001/csrhtml/glossary.html

NHTSA 2001, One minute safety seat checklist, US Department of Transportation National Highway Traffic Safety Administration, http://www.nhtsa.dot.gov/people/injury/childps/ChildSS/OneMinuteChecklist/Index.html

NHTSA 2001, Types of child safety seats, US Department of Transportation National Highway Traffic Safety Administration, http://www.nhtsa.dot.gov/people/injury/childps/ChildSS/TypesOfSeats/Index.html

Nigam, S.P. and Malik, M. 1987, A study on vibratory model of a human body, Transactions of the ASME, Journal of Biomechanical Engineering, Vol. 109, pp 148-153

Olley, M. 1934, Independent wheel suspension - Its whys and wherefores, S.A.E. Journal (Transactions), Vol. 34, No. 3, pp 73-81

Nishiyama, S., Uesugi, N., Takeshima, T. and Kano, Y. 2000, Experimental investigation of the effects of seat position on human dynamic behaviour, JSME International Journal, Series C, Vol. 43, No. 2, pp 283-292

Nishiyama, S., Uesugi, N., Takeshima, T., Kano, Y. and Togii, H. 2000, Research on vibration characteristics between human body and seat, steering wheel, and pedals (effects of seat position on ride comfort), Journal of Sound and Vibration, Vol. 236, No. 1, pp 1-21

Oggero, E., Pipino, M., Deweese, R., Mugnai, A., Aljundi, B. and Pagnacco, G. 2000, Numerical simulation of a child restraint system in an aircraft crash-test, Biomedical Sciences Instrumentation, Vol. 36, pp 257-262

Orne, D. and Liu, Y.K. 1971, A mathematical model of spinal impact, Journal of Biomechanics, Vol. 4, pp 49-71

Paddan, G.S. and Griffin, M.J. 1988, The transmission of translational seat vibration to the head – I. Vertical seat vibration, Journal of Biomechanics, Vol. 21, No. 3, pp 191-197

Paddan, G.S. and Griffin, M.J. 1988, The transmission of translational seat vibration to the head – II. Horizontal seat vibration, Journal of Biomechanics, Vol. 21, No. 3, pp 199-206

Paddan, G.S. and Griffin, M.J. 1992, The transmission of translational seat vibration to the head: the effect of measurement position at the head, Proc. Instn. Mech. Engrs., Vol. 206, pp 159-168

Paddan, G.S. and Griffin, M.J. 1993, The transmission of translational floor vibration to the heads of standing subjects, Journal of Sound and Vibration, Vol. 160, No. 3, pp 503-521

Paddan, G.S. and Griffin, M.J. 1998, A review of the transmission of translational seat vibration to the head, Journal of Sound and Vibration, Vol. 215, No. 4, pp 863-882

Paddan, G.S. and Griffin, M.J. 2000, Transmission of yaw seat vibration to the head, Journal of Sound and Vibration, Vol. 229, No. 5, pp 1077-1095

Paddan, G.S. and Griffin, M.J. 2002, Evaluation of whole-body vibration in vehicles, Journal of Sound and vibration, Vol. 253, No. 1, pp 195-213

Panjabi, M.M. and White, A.G. 1971, A mathematical approach for three-dimensional analysis of the mechanics of the spine, Journal of Biomechanics, Vol. 4, pp 203-211

Panjabi, M.M. 1973, Three dimensional mathematical model of the human spine structure, Journal of Biomechanics, Vol. 6, pp 671-680

Panjabi, M.M., Andersson, G.B.J., Jorneus, L., Hult, E. and Mattsson, L. 1986, In Vivo measurements of spinal column vibrations, The Journal of Bone and Joint Surgery, Vol. 68-A, No. 5, pp695-702

Pankoke, S., Buck, B. and Woelfel, H.P. 1998, Dynamic FE model of sitting man adjustable to body height, body mass and posture used for calculating internal forces in the lumbar vertebral disks, Journal of sound and Vibration, Vol. 215, No. 4, pp 827-839

Parsons, K.C. and Griffin, M.J. 1978, The effect of the position of the axis of rotation on the discomfort caused by whole-body roll and pitch vibration of seated persons, Journal of Sound and Vibration, 58, 1, pp 127-141

Partners for Child Safety 2000, Partners for child safety interim report 2000, Philadelphia, Pennsylvania, The Children's Hospital of Philadelphia and State Farm Insurance Company

Payne, P.R. 1961, The dynamics of human restraint systems in impact acceleration stress, National Academy of Science, Washington D.C., National Research Council Publication No. 977, pp 195-257

Payne, P.R. 1978, Method to quantify ride comfort and allowable accelerations, Aviation, Space and Environmental Medicine, Vol. 49, No. 1, January, pp 262-269

Payne, P.R. and Band, E.G.U. 1971, A four degree of freedom lumped parameter model of the seated human body, AMRL TR-76-10 (AMRL TR-70-35)

Pedder, J., Legault, F., Salcudean, G., Hillebrandt, D., Gardner, W. and Labrecque, M. 1994, Development of the CANFIX infant and child restraint/vehicle interface system, SAE paper 942221

Perremans, S. Randall, J.M., Allegaert, L., Stiles, M.A. and Geers, R. 1996, Influence of vibration on piglets' heart rate during vertical motion, UK Group Meeting on Human Response to Vibration, MIRA, Nuneaton, 18th-20th September

Pheasant, S. 1988, Bodyspace: anthropometry, ergonomics and design Taylor and Francis, London

Pope, M.H., Broman, H. and Hansson, T. 1989, The dynamic response of a subject seated on various cushions, Ergonomics, Vol. 32, No. 10, pp 1155-1166

Pope, M.H., Kaigle, A.M., Magnusson, M., Broman, H. and Hansson, T. 1991, Intervertebral motion during vibration, Proc. Instn. Mech. Engrs., Vol. 205, pp 39-44

Pope, M.H., Magnusson, M. and Hansson, T. 1996, The upper extremity attenuates intermediate frequency vibrations, Journal of Biomechanics, Vol. 30, No. 2, pp 103-108

Potemkin, B.A. and Frolov, K.V. 1971, O model'nykh predstavleniyakh biomekhanicheskoi sistemy "chelovek-operator" pri sluchainom vibratsionnom vozdeistvii, DAN, SSSR, 197, 6, 1284-1287 (Royal Aircraft Establishment Library Translation 1651, 22/6/1972, Representation by models of the biomechanical system "man-operator" under the action of random vibration)

Pottinger, M.G. and Yager, T.J. 1986, The tire pavement interface, ASTM Special Publication 929, American Society for Testing and Materials, Philadelphia

Pradko, F. 1965, Human response to random vibration, Shock and Vibration Bulletin, 34, Part 4, pp 173-190

Pradko, F., Orr., T.R. and Lee, R.A. 1965, Human vibration analysis, SAE paper 650426, pp 1-9

Pradko, F., Lee, R. and Greene, J.D. 1967, Human vibration response theory, ASME Biomechanics Monograph, pp 205-222

Prasad, P., King, A.I. and Ewing, C.L. 1974, The role of articular facets during +Gz acceleration, ASME Journal of Applied Mechanics, Vol. 41, No. 2, pp 321-326

Prasad, P. and King, A.I. 1974, An experimentally validated dynamic model of the spine, Journal of Applied Mechanics, Transactions of the ASME, September, pp 546-550

Price, K. and Storn, R. 1997, Differential evolution: a simple evolution strategy for fast optimisation, Dr. Dobb's Journal, Vol. 264, April

Qassem, W. 1996, Model prediction of vibration effects on human subject seated on various cushions, Medical Engineering Physics, Vol. 18, No. 5, pp 350-358

Quandieu, P. and Pellieux, L. 1982, Study in situ et in vivo of the acceleration of lumbar vertebrae of a primate exposed to vibration in the Z-axis, Journal of Biomechanics, Vol. 15, No. 12, pp 985-1006

Rainford, J.A., Page, M. and Porter, J.M. 1993, How and why child safety restraints in cars are misused, Proc. of the Ergonomics Society's 1993 Annual Meeting, Edinburgh, Scotland, April 13-16

Rakheja, S., Afework, Y. and Sankar, S. 1994, An analytical investigation of the driver-seat-suspension system, Vehicle System Dynamics, 23, pp 501-524

Rakheja, S., Stiharu, I. and Boileau, P.E. 2002, Seated occupant apparent mass characteristics under automotive postures and vertical vibration, Journal of Sound and Vibration, Vol. 253, No. 1, pp 57-75

Randall, J.M., Matthews, R.Y. and Stiles, M.A. 1997, Resonant frequencies of standing humans, Ergonomics, Vol. 40, No. 9, pp 879-886

Rao, B.K.N., Ashley, C. and Jones, B. 1975, Effects of postural changes on the head responses of standing subjects subjected to low frequency constant velocity spectral inputs, Journal of the Society of Environmental Engineers, Vol. 14., March, pp 27-30

Rao, S.S. 1997, Engineering optimisation: theory and practice, Wiley Interscience, New York

Reiher, H and Meister, F.J. 1931, Die empfindlichkeit des menschen gegen erschütterungen, Forschung auf dem Gebiete des Ingenieurwesens, Band. 2., Nr. 11, pp 381-386

Rowlands, G.F. 1977, The transmission of vertical vibration to the heads and shoulders of seated men, Technical Report 77068, Royal Aircraft Establishment, pp 1-79

Ruff, S. 1950, Brief accelerations: less than one second, German Aviation Medicine in World War II, Vol. 1, Ch. VI-C, pp 584-597

Ruffell, C.M. and Griffin, M.J. 1995, Effects of 1-Hz and 2-Hz transient vibration on discomfort, J. Acoustical Soc. Am., 98, 4 October, 99 2157-2164

Ruta, D., Beattie, T. and Narayan, V. 1993, A prospective study of nonfatal childhood road traffic accidents - what can seat restraint achieve, Journal of Public Health Medicine, Vol. 15, No. 1, pp 88-92

Sandover, J. 1970, Some current biomechanical research in the United Kingdom as related to the effects of impact and vibration on man, Symposium on Biodynamic Models and Their Applications, Dayton, Ohio, 26-28 Oct., pp 105-122

Sandover, J. 1978, Modelling human responses to vibration, Aviation, Space and Environmental Medicine, Vol. 49, No. 1, pp 335-339

Sandover, J. and Dupuis, H. 1987, A reanalysis of spinal motion during vibration, Ergonomics, Vol. 30, No. 6, pp 975-985

Sandover, J. 1988, Behaviour of the spine under shock and vibration: a review, Clinical Biomechanics, Vol. 3, pp 249-256

Schmitz, M.A. 1959, Man's response to low-frequency vibration, ASME Publication 59-A-20, pp 1-11

Schneider, L.W. and Bowman, B.M. 1978, Prediction of head/neck dynamic response of selected military subjects to –Gx acceleration, Aviation, Space and Environmental Medicine, Vol. 49, No. 1, pp 211-223

Schultz, A.B. and Galante, J.O. 1970, A mathematical model for the study of the mechanics of the human vertebral column, Journal of Biomechanics, Vol. 3, pp 405-416

Segui-Gomez, M. 1998, Evaluating interventions that promote the use of rear seats for children, American Journal of Preventive Medicine, Vol. 16, No. 1S, pp 23-29

Seidel, H. 1995, Belastung der lendenwirbelsäule durch stoßhaltige ganzkörperschwingungen, Schriftenreihe der bundesanstadlt für arbeitsmedizin, Berlin

Seidel, H., Blüthner, R. and Hinz, B. 2001, Application of finite-element models to predict forces acting on the lumbar spine during whole-body vibration, Clinical Biomechanics 16, Suppl. No. 1, S57-S63

Shanon, A., Bashaw, B., Lewis, J. and Feldman, W. 1992, Nonfatal childhood injuires – a survey at the childrens hospital of Eastern Ontario, Canadian Medical Association Journal, Vol. 146, No. 3, pp 361-365

Shoenberger, R.W. 1972, Human response to whole-body vibration, Perceptual and Motor Skills, Vol. 34, pp 127-160

Slonim, A.R. 1983, Some vibration data on primates implanted with accelerometers on the upper and lower spine: methodology and results in Rhesus monkeys, Air Force Aerospace Medical Research Laboratory Report, AFAMRL-TR-81-153

Slonim, A.R. 1985, Comparative biodynamic response of two primate species to the same vibrational environment, Aviation, Space and Environmental Medicine, Vol. 56, Oct., pp 945-955

Slonim, A.R. 1987, Biodynamic response of subhuman primates to vibration, The Physiologist, Vol. 30, No. 1, S19-S22

Smeathers, J.E. 1985, Scrutiny of the classical model for intervertebral disc function, British Journal of Rheumatology, Vol. 24, pp 219

Smeathers, J.E. 1989, Measurement of transmissibility for the human spine during walking and running, Clinical Biomechanics, Vol. 4, pp 34-40

Smeathers, J.E. 1989, Transient vibrations caused by heel strike, Proc. Instn. Mech. Engrs., Part H: Journal of Engineering in Medicine, Vol. 203 pp 181-186

Smith, S.D. 1992, Impedance response characteristics of the primate mucaca mulatta exposed to seated whole-body g_z vibration, Journal of Biomechanics, Vol. 25, pp 839-847

Smith, S.D. and Kazarian, L.E. 1994, The effects of acceleration on the mechanical impedance response of a primate model exposed to sinusoidal vibration, Annals of Biomedical Engineering, Vol. 22, pp 78-87

Smith, S.D. 1994, Nonlinear resonance behaviour in the human exposed to whole-body vibration, Shock and Vibration, Vol. 1, No. 5, pp 439-450

Smith, S.D. 1997, Limitations in predicting human vibration response characteristics from manikin and rigid body masses, SAE paper 970598, Society of Automotive Engineers

Smith, S.D. 2000, modelling differences in the vibration response characteristics of the human body, Journal of Biomechanics, Vol. 33, pp 1513-1516

Snijders, C.J., Bakker, M.P., Vleeming, A., Stoeckart, R. and Stam, H.J. 1995, Oblique abdominal muscle activity in standing and in sitting on hard and soft seats, Clinical Biomechanics, Vol. 10, No. 2, pp 73-78

Society of Automotive Engineers 1974, Measurement of whole body vibration of the seated operator of agricultural equipment, SAE J1013 Handbook Part II, Society of Automotive Engineers, Detroit, Michigan

Society of Automotive Engineers 1977, Anthropometry of infants, children and youths to age 18 for product safety and design, Society of Automotive Engineers, Detroit, Michigan

Soechting, J.F. and Paslay, P.R. 1973, A model for the human spine during impact including musculature influence, Journal of Biomechanics, Vol. 6, pp 195-203

Stikleather, L.F. and Foutz, T. L. 1989, Simulation of seat ride performance as influenced by the mechanical impedance of the test load, SAE paper 891161

Stoner Halpern, J. 1990, How safe are child safety seats ? Journal of Emergency Nursing, Vol. 16, No. 3, pp151-155

Storn, R. and Price, K. 1997, Differential evolution – a simple and efficient heuristic for global optimisation over continuous spaces, Journal of Global Optimization, Vol. 11, pp 341-359

Stout, J.D., Bandy, P., Feller, N., Stroup, K.B. and Bull, M.J. 1992, Transportation resources for pediatric orthopaedic clients, Orthopaedic Nursing, Vol. 11, No. 4, pp 26-30

Suggs, C.W., Abrams, L.F. and Stikeleather, L.F. 1969, Application of a damped spring-mass human vibration simulator in vibration testing of vehicle seats, Ergonomics, Vol. 12, pp 79-90

Terry, C.T. and Roberts, V.L. 1968, A viscoelastic model of the human spine subjected to $+g_z$ accelerations, Journal of Biomechanics, Vol. 1, pp 161-168

Thomas, R.E., Congleton, J.J., Huchingson, R.D., Whiteley, J.R. and Rodrigues, C.C. 1991, An investigation of relationships between driver comfort, performance and automobile seat type during short term driving tasks, Int. Journal of Industrial Ergonomics, Vol. 8, pp 103-114

Tilley, A.R. 1993, The measure of man and woman, Henry Dreyfuss Associates, New York

Toth, R. 1966, Multiple degree-of-freedom nonlinear spinal model, Proceedings of the 19th Annual Conference on Engineering in Medicine and Biology, San Francisco, CA, Vol. 8, pp 102

Tregoubov, V.P. 2000, Problems of mechanical model identification for human body under vibration, Mechanism and Machine Theory, Vol. 35, pp 491-504

Ueno, K. and Liu, Y.K. 1987, A three-dimensional nonlinear finite element model of lumbar intervertebral joint in torsion, Journal of Biomechanical Engineering, Transactions of the ASME, Vol. 109, pp 200-209

Uphold, R., Harvey, R., Misselbeck, W. and Hill, S. 1991, Bilateral tibial fractures in properly restrained toddlers involved in motor vehicle collisions: Case reports, The Journal of Trauma, Vol. 31, No. 10, pp 1411-1414

Varterasian, J.H. On measuring automobile seat ride comfort, SAE paper 820309

Varterasian, J.H. and Thompson, R.R. 1977, The dynamic characteristics of automobile seats with human occupants, SAE paper 770249

Versace, J. 1963, Measurement of ride comfort, SAE Paper 638 A, pp 1-13

Vogt, L.H., Coermann, R.R. and Fust, H.D. 1968, Mechanical impedance of the sitting human under sustained acceleration, Aerospace Medicine, Vol. 39, No. 7, pp 675-679

Vogt, L.H., Krause, H.E., Hohlweck, H. and May, E. 1973, Mechanical impedance of supine humans under sustained acceleration, Aerospace Medicine, Vol. 44, No. 2, pp 123-128

Vogt, L.H., Mertens, H. and Krause, H.E. 1978, Model of the supine human body and its reactions to external forces, Aviation, Space and Environmental Medicine, Vol. 49, No. 1, pp 270-278

Vold, H., Crowley, J. and Rocklin, G.T. 1984, New ways of estimating frequency response functions, Sound and Vibration, November, pp 34-38

Von Bekésy, G 1939, Über die vibrationsemfindung, Akustische Zeitschrift, 4, September, pp 316-334

Von Bekésy, G 1939, Über die empfindlichkeit des stehenden und sitzenden menschen gegen sinusförmige erschütterungen, Akustische Zeitschrift, 4, November, pp 360-369

Von Gierke, H.E. 1962, Biomechanics of impact injury, National Academy of Sciences, National Research Council Publication 977, pp 121- 122

Von Gierke, H.E. 1964, Biodynamic response of the human body, Applied Mechanics Reviews, Vol. 17, No. 12, pp 951-958

Von Gierke, H.E. and Goldman, D.E. 1988, Chapter 44: Effects of shock and vibration on man, Shock and Vibration Handbook, Third Edition, Cyril M. Harris Editor, McGraw-Hill, New York

Von Wimmersperg, H.F. and Czernakowski, W.J. 1976, Safe deceleration of infants in car crashes, Proceedings of the 20th Stapp car crash conference, Oct. 18-20, Dearborne, Michigan, USA

Walsh, M.J., Kelleher-Walsh, B. and McCullough, C. 1996, Study of motor vehicle accidents involving children, Proceedings of the 40th Stapp Car Crash Conference, Nov. 4-6, Albuquerque, New Mexico, USA

Vykukal, H.C. 1968, Dynamic response of the human body to vibration when combined with various magnitudes of linear acceleration, Aerospace Medicine, Vol. 39, Nov., pp 1163-1166

Wilder, D.G., Frymoyer, J.W. and Pope, M.H. 1985, The effect of vibration on the spine of the seated individual, Automedica, Vol. 6, pp 5-35

Weis, E.B., Clarke, N.P., Brinkley, J.W. and Martin, P.J. 1964, Mechanical impedance as a tool in research on human response to acceleration, Aerospace Medicine, Vol. 35, pp 945-950

Weis, E.B. and Primiano, F.P. 1966, The motion of the human canter of mass and its relationship to mechanical impedance, Human Factors, Vol. 8, pp 399-405

Weis, E.B. and Mohr, G.C. 1967, Cineradiographic analysis of human visceral responses to short duration impact, Aerospace Medicine, Vol. 38, pp 1041-1044

Wei, L. and Griffin, M.J. 1998, Mathematical models for the apparent mass of the seated human body exposed to vertical vibration, Journal of Sound and Vibration, Vol. 212, No. 5, pp 855-874

West, G.B., Brown, J.H. and Enquist, B.J. 1997, A general model for the origin of allometric scaling laws in biology, Science, Vol. 276, April, pp 122-126

Wilder, D.G., Woodworth, B.B., Frymoyer, J.W. and Pope, M.H. 1982, Vibration and the human spine, Spine, Vol. 7, No. 3, pp 243-254

Wilder, D., Magnusson, M.L., Fenwick, J. and Pope, M. 1994, The effect of posture and seat suspension design on discomfort and back muscle fatigue during simulated truck driving, Applied Ergonomics, 25, 2, pp 66-76

Winston, F. and Durbin,. D. 1999, Buckle up ! is not enough: enhancing protection of the restrained child, Journal of the American Medical Association, Vol. 281, pp 2070-2072

Wittmann, T.J. and Phillips, N.S. 1969, Human body nonlinearity and mechanical impedance analyses, Journal of Biomechanics, Vol. 2, pp 281-288

Woods, A.G. 1967, Human response to low frequency sinusoidal and random vibration, Aircraft Engineering, July, pp 6-14

Wu, X., Rakheja, S. and Boileau, P.E. 1999, Analysis of relationships between biodynamic response functions, Journal of Sound and Vibration, Vol. 226, No. 3, pp 595-606

Yu-Hallada, L.C., Kuczynski, E.T. and Weierstall, M. 1998, Polyurethane: the material of choice for occupant protection and energy management, Journal of Cellular Plastics, Vol. 34, No. 3, pp 272

Zagorski, J., Jakubowski, R., Solecki, L., Sadlo, A., and Kasperek, W. 1976, Studies on the transmission of vibrations in human organism exposed to low-frequency Whole-body Vibration, ACTA Physiol. Pol., Vol. 27, No. 4, pp 347-354

Zaza, S., Sleet, D.A., Thompson, R.S., Sosin, D.M. and Bolen, J.C. 2001, Reviews of evidence regarding interventions to increase use of child safety seats, American Journal of Preventive Medicine, Vol. 21, No. 4S, pp31-47

Zimmermann, C.L. and Cook, T.M. 1997, Effects of vibration frequency and postural changes on human responses to seated whole-body vibration exposure, Int. Arch. Occupational Health, Vol. 69, pp 165-179

BS 7085 Suggested Practice for Experiments in Which People are Exposed to Mechanical Vibration and Shock	**Child Vibration Facility Safety Features**
3.4.1 Equipment should be designed so that no failure could result in magnitudes of mechanical vibration or shock producing vibration dose values in excess of 15 $m/s^{1.75}$, unless the experiment is designed to study effects of higher magnitudes.	The shelf assembly mass of 12.8 kg, rigid seat mass of 3 kg and average child mass of 9 kg sum to a total 24.8 kg. For this mass the maximum force output of the V406 shaker of 98 N implies a maximum acceleration of 4 m/s^2 which for exposures lasting 1-2 minutes is less than 15 $m/s^{1.75}$.
3.4.2 Safeguards should be used to avoid the following three physical hazards: a) the experimenter or another person in the vicinity of the equipment may receive a blow through inadvertent contact with the moving parts; b) the subject on a moving part may receive a blow through inadvertent contact with a fixed object; c) anyone on the equipment or in the vicinity may be at risk from pinching or shearing between fixed and moving parts.	The maximum peak-to-peak stroke of the V406 shaker is 14mm, thus the limited travel provides few opportunities for entrapment or impacting. The moving shelf assembly has a large surface area of 760 mm x 405 mm. The rigid seat is centred on this platform thus the child cannot reach rig components when seated and restrained.
3.4.3 In experiments where subjects are restrained, special care should be taken to ensure that during normal operation or malfunction any restraint does not present a hazard.	The child restraining straps are standard items from a commercial safety seat and are fitted in the same physical location and in the same manner as in the original unit.
4.2 The attendance of a medical officer is not essential for experiments in which the subjects are exposed to magnitudes of mechanical vibration and shock comparable to those found in common forms of transportation and in any but the most severe of civilian working environments. These are defined as experiments in which the total daily exposure for any subject does not exceed a vibration dose value of 15 $m/s^{1.75}$.	The shelf assembly mass of 12.8 kg, rigid seat mass of 3 kg and average child mass of 9 kg sum to a total 24.8 kg. For this mass the maximum force output of the V406 shaker of 98 N implies a maximum acceleration of 4 m/s^2 which for exposures lasting 1-2 minutes is less than 15 $m/s^{1.75}$.
5.1 Mechanical and electrical components should be chosen for high reliability and should be conservatively rated.	All components are standard commercial equipment. The DIFA SCADAS frontend unit is certified for human testing by the manufacturer.

5.1 The subject should be adequately restrained, particularly where malfunction would jeopardize the safety of an unrestrained subject.	The child restraining straps are standard items from a commercial safety seat and are fitted in the same physical location and in the same manner as in the original unit.
5.1 The device and any electrical equipment used in conjunction with the machine should be adequately earthed so that the subject and operator are protected from electrical shock.	All system components are earthed according to manufacturer's instructions. No electrical components were made or modified for the child test bench.
5.1 Emergency stop and shut-down procedures should render the device safe so that the subject can escape from the equipment with the minimum delay in the event of an emergency.	The DIFA SCADAS electronic frontend unit incorporates a condenser-based soft shutdown circuit for bringing the shaker to rest in the case of failure of either the mains supply or the controller software.
5.1 Safety and control wire and fluid power lines should be positioned and secured in such a manner that accidental disconnection or breakage does not occur.	All cables are out of the reach of the children and of the parents.
5.2.2 Start-up and shut-down procedures should follow a logical sequences and be sequence interlocked to prevent improper operation.	The EMON test control software operates front-end arming and test initiation as separate, independent, functions. The EMON test control software was programmed with a fixed operational sequence of 2 tests, each consisting of a signal ramp-up, two minutes of vibration exposure, and signal ramp-down.
5.2.3 The operator should be provided with displays which unambiguously indicate the following: (a) the status of the safety circuits and the nature of a malfunction if this is detected by a safety circuit; (b) when the device is in safe mode in order that the subject may safely be positioned on, or leave, the motion platform; (c) the intensity of the motion stimuli being generated by the device (i.e. displacement, velocity, acceleration of the platen).	The EMON software interface was configured to continuously display underload, operational load or overload ratings for all acquisition and control channels. The EMON software interface was configured to continuously display the frequency response function between seat acceleration and control voltage (bench transfer function). The EMON software interface was configured to continuously display the frequency response function measured for the child (child apparent mass).
5.2.4 It is recommended that the operator should have sight, either directly or by closed circuit television, of the subject and relevant equipment so that normal or abnormal operation can be visually assessed.	Child subject, parents and all bench components are visible without obstruction from the operator's position.

5.2.5 The operator should have ready access to the subject in the event of his/her distress or equipment malfunction.	The operator's station is within 2 meters of the test bench.
5.2.6 The design of the controls and displays should be such that the intensity of the motion stimuli and the levels at which any pre-set limit circuits will operate are clear to the operator.	The EMON software interface was configured to continuously display underload, operational load or overload ratings for all acquisition and control channels. The EMON software interface was configured to continuously display the frequency response function between seat acceleration and control voltage (bench transfer function).
5.2.7 The operator should have immediate and ready access to a clearly labelled control which initiates the emergency stop.	The child vibration bench incorporates a DIFA SCADAS Shutdown Control Unit which includes a large red emergency stop button attached to a cable for easy positioning.
5.2.8 The operator should have control of a scaled input attenuator which determines the magnitude of the demand signal fed to the control system. This should be designed to avoid the sudden application of an excessive demand function.	Not implemented.
5.3 The subjects should be able to stop the motion stimulus by the operation of an emergency stop control, usually a push-button switch, which can be held in the hand or is placed in a position to which he/she has immediate and ready access.	Not implemented for child subjects.
5.3 Communication between the subject and the operator also allows him/her to request the termination of exposure to the motion stimulus.	Not implemented for child subjects.
5.4.2 Input monitor. This circuit monitors the demand function to the control system and, if pre-set limits are exceeded, the demand function is modified. In its most basic form, this circuit may act as a simple limiting device, which may be acceptable if the platen acceleration follows the input signal.	Software limits of 1.0 m/s^2 peak seat acceleration amplitude and 100 N transmitted force were set in the EMON test control environment.

5.4.3 Platen motion monitor. An input monitor does not protect the subject from aberrant motion stimuli generated by failures within the control system. Consequently, it is highly desirable that the motion of the platen is monitored by circuitry which stops the motion if this exceeds pre-set limits. Whether the withdrawal of the motion stimulus is achieved through the control system, or the control system is disabled and an emergency stop sequence is initiated, is dependent upon the detailed design of the equipment.	Not implemented electronically. Achieved physically through the maximum force rating of the V406 shaker unit.
5.4.4 System monitor. This circuit monitors parameters within the control system which are indicative of normal operation, such as supply and rail voltages, amplifier current, servo-valve operation, integrity of transducers circuits, etc. If any of these parameters exceeds limits which are preset but not operator-adjustable, then a shut down procedure is initiated with an emergency stop of the platen.	The PA100E electronic power amplifier driving the V406 shaker incorporates a core overheating and an overvoltage interrupt which shuts down the voltage supply in the case of a failure condition.
5.4.5 In those situations in which it is not necessary to achieve the maximum performance of the device, it is desirable to restrict performance by means which are not dependent upon input or output monitoring circuits...In electro-hydraulic mechanical vibration machines, peak platen velocity can be limited by restricting flow.... In electrodynamic machines, accelerations can be controlled by limiting the peak current available to the actuator.	Not implemented due to the low force rating of the V406 shaker.
5.5 Provision should be made for the motion of the platen to be limited to the equivalent of a vibration dose values of 15 $m/s^{1.75}$,in the event of failure of the monitoring circuits and the platen being driven into the end-stops at the maximum velocity achievable.	Not implemented due to the low force rating of the V406 shaker.

5.6 The equipment should be tested before it is used with any subjects, to ensure that under any predictable fault condition or with any predictable operator error the resulting motion has a total vibration dose value of less than 15 $m/s^{1.75}$.	The system has been tested for a range of operating and failure conditions including: test loads from 0 kg to 20 kg; incorrect settings of the PA100E electronic power amplifier; constant offset voltages and incorrect voltage gains of the MSC conditioning unit; acceleration or force sensor disconnect; incorrect setting of the shelf assembly suspension system (shaker end-of-travel impact); controller software failure.
6.2 In some circumstance it may be desirable for a second person to be present as an observer.	The parents are asked monitor and assist.
6.2.2 The observer should have a good understanding of the experiment being conducted and be familiar with emergency procedures for the equipment.	A detailed explanation of the test objectives and procedure is provided to the parents.
6.3.3 Normal operating sequence. The normal operating sequence for each trail should follow a predetermined routine which is familiar to the operator and to any observer. This should include the sequence of stimuli and their durations, the sequence of any activities in which the subject is to be engaged, and the times at which responses are required of him/her.	The EMON test control software was programmed with a fixed operational sequence of 2 tests, each consisting of a signal ramp-up, two minutes of vibration exposure, and signal ramp-down.
6.3.3 The operator should check that the subject is fit to take part.	Not implemented, based on parental consent.
6.3.3 The operator should check that the subject is familiar with the experimental procedure and in particular that for the emergency shut-down.	Not implemented for the child subject.
6.3.3 The operator should check that the subject is adequately supported and, when necessary, restrained.	After being seated in the device the operator adjusts the safety belts to restrain the child.
6.3.3 The equipment should be brought to rest and made safe before the subject leaves or dismounts.	Upon completion of the test sequence the EMON test control software automatically deactivates the frontend unit bringing voltage production to a halt.

6.3.3 The subject should be provided with an opportunity to report any adverse reaction to the mechanical vibration and shock.	Not implemented for the child subject.
6.4.1 Documentation associated with mechanical vibration and shock experiments on subjects should include: a) an operational record of the use of mechanical vibration and shock equipment: durations of use and characteristics of mechanical vibration and shock used, results of start-up and pre-trial checks, servicing and maintenance; b) a record of each exposure to mechanical vibration and shock of any subject; c) check lists for start-up and operational sequence for current trials; d) a list of people authorised to operate the mechanical vibration and shock equipment; e) copies of the consent forms as a record that each subject has been questioned or examined with regard to fitness to participate.	Point A is not implemented. Points B and E are incorporated in the consent form. Point C is incorporated in a checklist used by the operator. Point D is not implemented as the bench is currently only operated by one individual.
6.4.2 The record of exposure of each subject to mechanical vibration and shock should include the following: a) purpose of the experiment; b) date of the experiment; c) identification of the subject; d) any medical certification provided; e) nature of the mechanical vibration and shock exposure; f) any unusual reactions of after-effects noticed; g) name of the experimenter; h) name of the operator in charge of the experimental run; i) name of the observer (if present); j) name of medical officer (if present); k) name of chaperone/parent/guardian (if present).	Points A, B, C, E, I and K are implemented by means of the consent form. Points D, F, G, H and J have not been implemented.